Ontario Geological Survey
Miscellaneous Paper 120

Exploration Technology Development Program of the Board of Industrial Leadership and Development

Summary of Research 1983 - 1984

edited by
V.G. Milne and R.B. Barlow

Program funded by the Board of Industrial Leadership and Development

1984

Ontario
Ministry of Natural Resources
Hon. Alan W. Pope
Minister
John R. Sloan
Deputy Minister

©1984 Government of Ontario
Printed in Ontario, Canada
ISSN (Series) 0704-2752
ISSN (Sub-series) 0826-791X

Publications of the Ontario Ministry of Natural Resources are available from the following sources. Orders for publications should be accompanied by cheque or money order payable to the *Treasurer of Ontario.*

Reports, maps, and price lists (personal shopping or mail order):
Public Service Centre, Ministry of Natural Resources
Room 1640, Whitney Block, Queen's Park
Toronto, Ontario M7A 1W3

Reports and accompanying maps only (personal shopping):
Ontario Government Bookstore
Main Floor, 880 Bay Street
Toronto, Ontario

Reports and accompanying maps (mail order or telephone orders):
Publications Services Section, Ministry of Government Services
5th Floor, 880 Bay Street
Toronto, Ontario M7A 1N8
Telephone (local calls), 965-6015
Toll-free long distance, 1-800-268-7540
Toll-free from area code 807, 0-ZENITH-67200

A project funded by the Board of Industrial Leadership and Development of the Government of Ontario.

Every possible effort is made to ensure the accuracy of the information contained in this report, but the Ministry of Natural Resources does not assume any liability for errors that may occur. Source references are included in the report and users may wish to verify critical information.

Parts of this publication may be quoted if credit is given. It is recommended that reference to this report be made in the following form for each individual paper:

Lazenby, P.G., and Becker, A.
1984: Grant 003 Redefinition of the INPUT® System: Part B -Signal Processing and Field Results; p.5-16 *in* Exploration Technology Development Program of the Board of Industrial Leadership and Development, Summary of Research 1983-1984, edited by V.G. Milne and R.B. Barlow, Ontario Geological Survey, Miscellaneous Paper 120, 176p. Accompanied by 1 chart (coloured).

Scientific Editor: Murthy Ghandikota
800-84-CSG

Contents

Introductory Remarks 2

Grant 003. Redefinition of the INPUT® System: Part B - Signal Processing and Field Results, *P.G. Lazenby and A. Becker* 5

Grant 010. Advanced Hardware and Software Development for Ground EM Prospecting, *J.C. Macnae et al.* 17

Grant 011. Development of Computer Software for Geophysical Interpretation, *S.W. Reford, N.R. Paterson, and D.J. Misener* .. 44

Grant 012. A) Determination of Short-Lived Isotopes by Neutron Activation Analysis and B) Investigation of Commerical Viability of Prompt Gamma Analysis, *E.L. Hoffman et al.* 52

Grant 014. The Design of a New Digital Pulse EM Receiver, *G.J. Bogden and H.P. Grunenberg* 57

Grant 039. Single Receiver, Frequency Scanning Fixed Source Electromagnetic System, *Andrew Rogozinski* 61

Grant 048. Portable Intelligent Digital Graphic Recorder, *Onorio Rocca* 66

Grant 050. The Application of Reflectance Radiometry to Semiquantitative Alteration Mineral Determination in Geological Materials, *D.R. Gladwell* 69

Grant 051. Development of Field Portable Apparatus for the Analysis of the Magnetite, Hematite, and Ilmenite Content of Basal Tills, *W.A. Morris* 77

Grant 052. Production of a 7-Frequency Helicopter Electromagnetic System, *P.E. Wessler* 84

Grant 053. Improvements to Geochemical Analysis, *J.D. Kinrade, W. Kostiak, and J.C. Robbins* 95

Grant 058. Portable Broadband Multiple Geometry HEM System, *R.L.S. Hogg, M.S. Granovsky, and A.B. Routledge* 108

Grant 059. Development of a Borehole Magnetic Properties Logging System, *W.R. Thuma, Detlef Blohm, and M.T. Hamalainen* 115

Grant 061. The Development of a Geochemical Analytical Method for Simultaneous Determination of Gold, Antimony, Arsenic, Tellurium and Mercury, *R. Jackson and R.E. Lett* 120

Grant 065. Development and Adaptation of Geochemical Techniques to Gold Exploration in Glacial Drift, *C.F. Gleeson et al.* 129

Grant 066. Luminescent Mineral Analyzer/Data Acquisition System, *T.B. Nagel* 150

Grant 068. Isotope Ratios and Trace Elements in Gold and Base Metal Occurrences in Ontario: An Application of Plasma/Mass Spectrometry, *E.J. Brooker* 160

Grant 072. Microprocessor-Based Digital Receiver Console for the Dighem$^{III/IV}$ Helicopter Airborne Electromagnetic System, *S.J. Kilty* 173

CHART (Back Pocket)

Figure 5; Grant 011; (coloured) — Ternary colour diagram and the assignment of radioelements to ink colours.

Figure 6; Grant 011; (coloured) — Map of corrected uranium intensity, Hearne Lake area.

Figure 7; Grant 011; (coloured) — Map of corrected thorium

intensity, Hearne Lake area.
Figure 8; Grant 011; (coloured) — Map of corrected potassium intensity, Hearne Lake area.
Figure 9; Grant 011; (coloured) — Map of radioelement distribution with simplified geology, Hearne Lake area.
Figure 10; Grant 11; (coloured) — Map of radioelement distribution and intensity with radiometric zoning, Hearne Lake area.

CONVERSION FACTORS FOR MEASUREMENTS IN ONTARIO GEOLOGICAL SURVEY PUBLICATIONS.

CONVERSION FROM SI TO IMPERIAL			CONVERSION FROM IMPERIAL TO SI		
SI Unit	*Multiplied by*	*Gives*	*Imperial Unit*	*Multiplied by*	*Gives*
			LENGTH		
1 mm	0.039 37	inches	1 inch	**25.4**	mm
1 cm	0.393 70	inches	1 inch	**2.54**	cm
1 m	3.280 84	feet	1 foot	**0.304 8**	m
1 m	0.049 709 7	chains	1 chain	20.116 8	m
1 km	0.521 371	miles (statute)	1 mile (statute)	**1.609 344**	km
			AREA		
1 cm^2	0.155 0	square inches	1 square inch	**6.451 6**	cm^2
1 m^2	10.763 9	square feet	1 square foot	**0.092 903 04**	m^2
1 km^2	0.386 10	square miles	1 square mile	2.589 988	km^2
1 ha	2.471 054	acres	1 acre	0.404 685 6	ha
			VOLUME		
1 cm^3	0.061 02	cubic inches	1 cubic inch	**16.387 064**	cm^3
1 m^3	35.314 7	cubic feet	1 cubic foot	0.028 316 85	m^3
1 m^3	1.308 0	cubic yards	1 cubic yard	0.764 555	m^3
			CAPACITY		
1 l	1.759 755	pints	1 pint	0.568 261	L
1 L	0.879 877	quarts	1 quart	1.136 522	L
1 L	0.219 969	gallons	1 gallon	**4.546 090**	L
			MASS		
1 g	0.035 273 96	ounces (avdp)	1 ounce (avdp)	28.349 523	g
1 g	0.032 150 75	ounces (troy)	1 ounce (troy)	**31.103 476 8**	g
1 kg	2.204 62	pounds (avdp)	1 pound (avdp)	**0.453 592 37**	kg
1 t	1.102 311	tons (short)	1 ton (short)	**907.184 74**	kg
1 kg	0.000 984 21	tons (long)	1 ton (short)	**0.907 184 74**	t
1 t	0.984 206 5	tons (long)	1 ton (long)	**1016.046 908 8**	kg
			1 ton (long)	**1.016 046 908 8**	t
			CONCENTRATION		
1 g/t	0.029 166 6	ounce (troy)/ton (short)	1 ounce (troy)/ton (short)	34.285 714 2	g/t
1 g/t	0.583 333 33	pennyweights/ton (short)	1 pennyweights/ton (short)	1.714 285 7	g/t

OTHER USEFUL CONVERSION FACTORS

1 ounce (troy) per ton (short)	20.0	pennyweights per ton (short)
1 pennyweight per ton (short)	0.05	ounces (troy) per ton (short)

Note. Conversion factors which are in bold type are exact. The conversion factors have been taken from or have been derived from factors given in the Metric Practice Guide for the Canadian Mining and Metallurgical Industries, published by the Mining Association of Canada in cooperation with the Coal Association of Canada.

Exploration Technology Development Program of the Board of Industrial Leadership and Development

Summary of Research 1983-1984

edited by
V.G. Milne[1] and R.B. Barlow[2]

[1]Director, Ontario Geological Survey.
[2]Chief, Geophysics/Geochemistry Section, Ontario Geological Survey.

EXPLORATION TECHNOLOGY DEVELOPMENT PROGRAM

Exploration in Ontario has reached a point where most mineral deposits located at or near the surface have been detected and tested for their economic viability. Therefore, future exploration must concentrate on locating mineral deposits at some depths below the surface. In order to resolve deeper deposits more effectively, new instrumentation must be developed. The Exploration Technology Development Program was created in late 1981 to facilitate this need for more precise instrumentation and techniques required in modern exploration programs.

With the establishment of the Ontario Geoscience Research Grants Program in the late 1970s, the Ontario Geological Survey developed a program to encourage geoscience research at Ontario universities. This program was viewed as the first step towards defining geological parameters and determining possible areas of high mineral potential in Ontario. The Exploration Technology Development Program was conceived as an important second step towards bringing these ideas and concepts to the private sector and ensuring the development of new technology through them.

The Exploration Technology Development Program was initiated to encourage the advancement of exploration geophysics and geochemistry by providing joint venture funding to Ontario companies leading to the development of innovative technology, specifically in those areas which support the mineral exploration industry in Ontario. The program supports applied research and development to 7 areas of exploration activity.

1. mineral deposit and overburden, physical and chemical characterization studies
2. development of new or modified airborne systems for improved detection of mineral deposits
3. development of new ground portable systems or modification of existing ground equipment for better detection and dissemination of mineral deposits
4. development of concepts and techniques in exploration geochemistry
5. development of borehole logging systems and related drilling techniques
6. development or implementation of laboratory support equipment not presently available in Ontario for the purpose of offering improved analytical service to mineral exploration companies
7. development of data acquisition and signal processing hardware and software for real-time and part-time collection and interpretation of field data

Companies are eligible to receive grants for any one project for up to 3 years in duration, with the Ontario Government financing 60% of all activities to a maximum contribution for an individual project of $150 000 per year.

In order to receive funding support from the Program, companies are asked to submit project proposals to the Ontario Geological Survey by January 15. These proposals are reviewed

and ranked by a Review Committee according to their scientific merit and relevance to the Program.

The members of the 1983-1984 Committee included:

L.S. Collett, Chairman	Geological Survey of Canada
Dr. A.P. Annan	A-Cubed Incorporated
Dr. R.B. Band	Falconbridge Limited
R.B. Barlow	Ontario Geological Survey
Dr. W.B. Coker	Kidd Creek Mines Limited
Dr. W.O Karvinen	Karvinen and Associates
Dr. J.P. Lalonde	Government of Quebec
R.S. Middleton	R.S. Middleton Exploration Services Limited
R.H. Pemberton	Noranda Mines Limited
Dr. D.H. Watkinson	Carleton University
Dr. G.W. West	University of Toronto

During the 1983-84 year, 22 proposals were funded under this program. Of these, 9 were renewals to multiyear projects. Grant allocations in support of these 22 projects totaled $1 133 000. The Exploration Technology Development Program receives financial support from the Board of Industrial Leadership and Development (BILD) and is administered by the Ontario Geological Survey of the Ministry of Natural Resources. BILD is the Cabinet Committee responsible for directing the province's economic development policies.

The following research projects funded during 1983-84, will be published as Ontario Geological Survey Open File Reports by May 1985:

Grant 003: Redefinition of the INPUT® Airborne Electromagnetic Exploration System; P.G. Lazenby, Questor Surveys Limited.

Grant 010: Advance Hardware and Software Development for Ground EM Prospecting; Y. Lamontagne, Lamontagne Geophysics Limited.

Grant 011: Development of Computer Software for Geophysical Interpretation; N.R. Paterson, Paterson, Grant and Watson Limited.

Grant 012: Determination of Short-lived Isotopes by Neutron Activation Analysis and the Analysis of Trace Elements by Prompt Gamma Analysis; E.L. Hoffman, Nuclear Activation Services Limited.

Grant 050: The Application of Reflectance Radiometry to Semi-quantitative Alteration Mineral Determination in Geological Materials; D.R. Gladwell, Barringer Magenta Limited.

Grant 053: Improvements to Geochemical Analysis; Dr. J.D. Kinrade, Scintrex Limited.

Grant 058: Portable Broadband Multiple Geometry HEM System; R.L.S. Hogg, Aerodat Limited.

Grant 061: The Development of a Geochemical Analytical Method for Simultaneous Determination of Au, Sb, As, Te, and Hg; R.E. Lett, Barringer Magenta Limited.

Grant 065: Development and the Adaptation of Geochemical Techniques to Gold Exploration in Glacial Drift; C.F. Gleeson, Gleeson and Associates Limited, and V.N. Rampton, Terrain Analysis and Mapping Services Limited.

Grant 066: Luminescent Mineral Analyzer/Data Acquisition System; T.B. Nagel, Scintrex Limited.

The undersigned would like to thank L.S. (Len) Collett, Chairman of the Program Review Committee, and the rest of the members and participating companies who gave freely of their time and made the whole program possible. As well, the efforts of the researchers are acknowledged. Thanks are also due to R.B. Watson who acted as Grants Administrator and Secretary to the Committee.

V.G. Milne
Director
Ontario Geological Survey

Grant 003 Redefinition of the INPUT® System: Part B - Signal Processing and Field Results

P.G. Lazenby and A. Becker

Questor Surveys Limited, Mississauga

ABSTRACT

High speed digital data acquisition affords unprecedented opportunities for enhancing the signal-to-noise ratio for airborne electromagnetic exploration data. Although digital signal processing techniques have been used for some time for improving target detection with sonar or radar, their use in airborne electromagnetics (AEM) is relatively new. The fundamental principles of digital signal processing however, are reasonably well understood and optimal filtering can be applied to the acquired data once the nature of the noise that must be eliminated is known.

The redefined INPUT® system is centred on a high speed digital detector that acquires data over a 9 Khz bandwidth. Field tests carried out over Lake Ontario, the Cavendish test range, and the Night Hawk test range conclusively show that this type of detector can produce superior data by allowing real-time processing that compensates for sensor motion, rejects atmospheric spikes, and improves the overall signal-to-noise ratio. Post-flight processing can be used to further amplify the signal. Because of the relatively high density of the digitally recorded data, many different signal enhancement options may be exercised. In fact, once the type of anomaly sought is defined, one may devise an optimal enhancement process for it.

INTRODUCTION

The INduced PUlse Transient (INPUT®) airborne electromagnetic exploration system (Barringer 1962) has now served the world's mining industry for over 20 years. It owes its unprecedented longevity to the foresight that was shown by the inventor, A.R. Barringer, and to the extended series of technical improvements that have been made to the apparatus throughout its years of service. At present, the INPUT system produces more than half of the world's airborne electromagnetic exploration data. It was directly implicated in the discovery of about 15 economical ore deposits with an aggregate worth in excess of $6 billion. About a third of these are located in the province of Ontario.

The research program described here was undertaken in order to improve on the very high performance standards that have been set by the commercial INPUT apparatus. The program objectives have been described at some length in a previous report (Lazenby and Becker 1983). In brief, however, the system was redesigned to include a long duration, high power, primary field pulse transmitter and a sophisticated digital signal detector. In addition to this, the receiver sensor was modified to allow the simultaneous measurement of both the vertical and horizontal components of the pulsed electromagnetic fields.

PREVIOUS WORK - INSTRUMENTATION AND TEST FACILITY

The first phase of our research program (October 1981 to March 1983) was fully reported on by Lazenby and Becker (1983). In summary, it can be said that most of that effort was dedicated to the equipping of an appropriate airborne test facility (aircraft CF-YED) and to the acquisition of some fundamental data needed for the design of the new sensors and the digital detector. The end product for the 1982-83 fiscal year was a DC-3 aircraft (Figure 1) equipped with a high power pulse transmitter of novel design and fully digital signal detector. The elements of the digital detector are shown in Figure 2. Included are a signal conditioning and digitizer unit, the microprocessor based digital signal conditioning unit, the tape drive controller unit, and the digital magnetic drive. The synoptic diagram of a 2-channel detector is shown in Figure 3. The digital signal processor has an internal clock that provides trigger pulses for the transmitter and the timing for the coherent sampling of the sensed electromagnetic signals. Besides acquiring, digitizing, and recording the signal, the digital detector is programmed to execute linear filtering, to reject atmospheric transients, to compensate for bird motion effects, and to compile a "real-time" monitor record which confirms its own proper functioning. Figure 4 illustrates in detail the analog to digital converter which is central to the data acquisition process. The assembly consists of the usual buffer amplifier and anti-alias filter. At this point the signal is fed to a binary gain ranging amplifier (BGA) which scales the signal.

The analog output of the BGA is connected to an analog signal multiplexer for transmission to the "sample and hold" amplifier while the digital signal representative of the amplifier's gain is passed on to

a digital multiplexer. This signal is then combined with the digitized analog output to form the floating point number that corresponds to a given digitized sample. The analog to digital converter is a 16 bit ZELTEX device. At present, the analog to digital conversion module has 2 signal channels, one for the vertical axis sensor and one for the horizontal axis device.

In addition to the digital detector, the aircraft also carries a conventional analog MK VI INPUT receiver. Data from both devices can be simultaneously recorded on an RMS graphic recorder. Thus data quality for both systems can be compared and evaluated in flight. Finally, the aircraft carries the usual complement of ancillary survey equipment. This includes a Sperry radio altimeter and a 35 mm frame camera for flight path recovery. Provision is made for the installation of a proton magnetometer and, if necessary, auxiliary Doppler or Loran C navigational aids. It should also be noted that the aircraft is equipped with large hatch doors which allow the in-flight retrieval of the towed sensors. This feature, more than any other, contributed to our rapid development of a 2-component electromagnetic sensor.

SIGNAL PROCESSING

PRINCIPLES OF NOISE REDUCTION

The principles of noise reduction by stacking the signal for a number of repetitions of the primary field pulse have been recently described by San Filipo and Hohmann (1983). In the time-domain, the process consists of sampling the analog data stream coherently at a given time after the onset of each primary field pulse. Because of the alternating polarity of the primary field, corresponding alternate samples are also made to alternate in sign. This process effectively removes any low frequency noise and DC drift from the data stream. If desired, a number of contiguous samples (i.e. those that are adjacent to each other) may be averaged to remove very high frequency noise. Figure 5 illustrates the sampling process and the formation of data windows by the summation of adjacent data samples to form data windows of width "s". The sampled data (either window averaged or not) are then usually averaged (stacked) for a number of repetitions of the primary field signal. This process reduces the noise by a factor proportional to the square root of the number of samples stacked while maintaining a

Figure 1. Flying laboratory, DC-3 CF-YED.

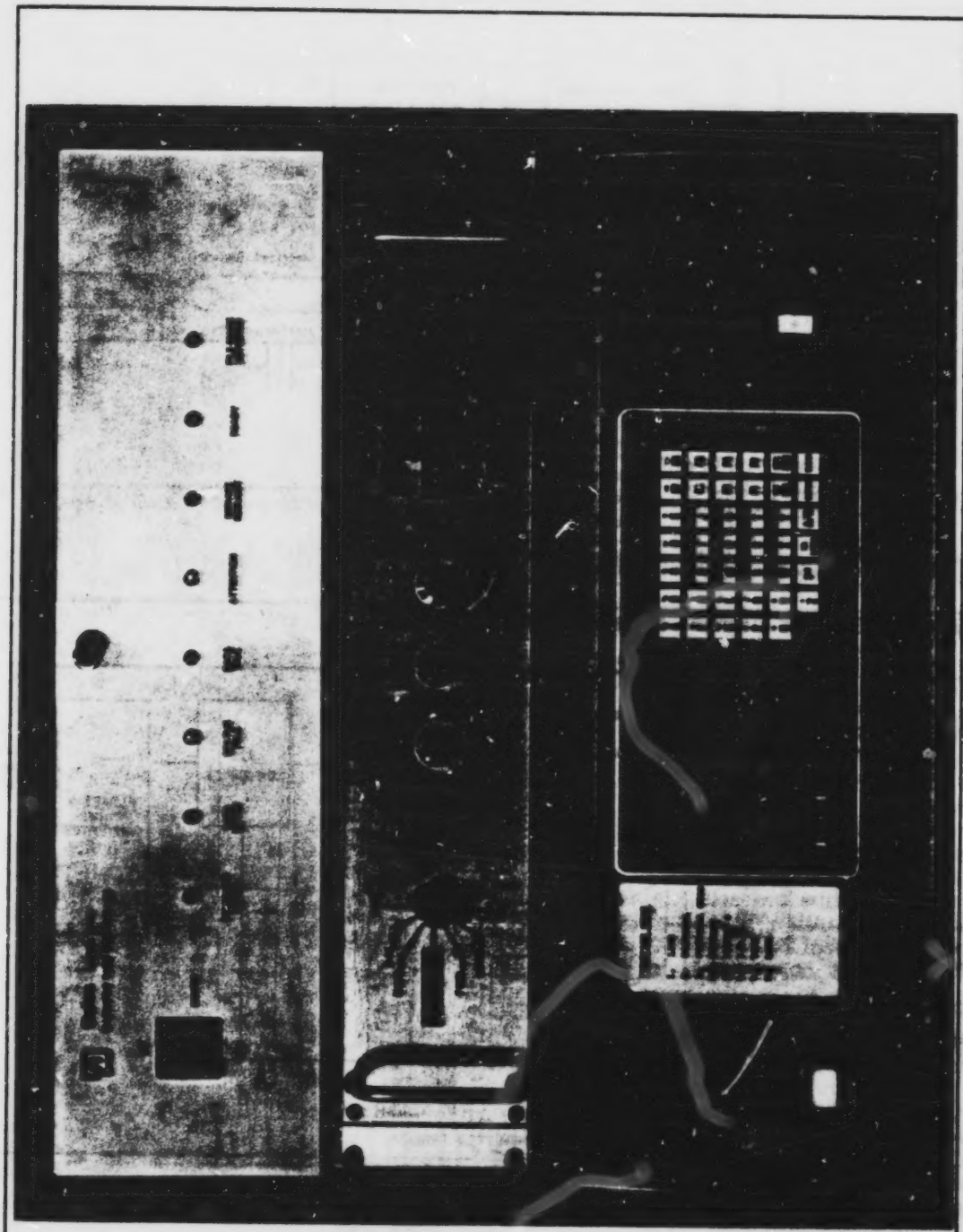

Figure 2. Digital signal detector.

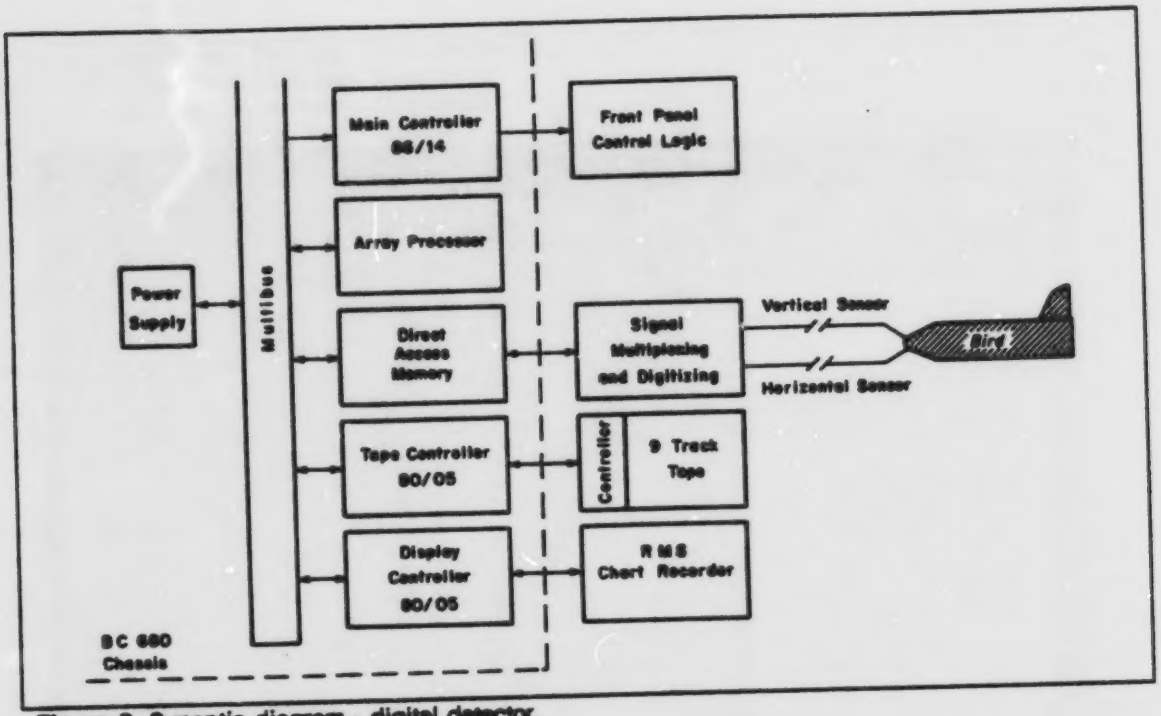

Figure 3. Synoptic diagram - digital detector.

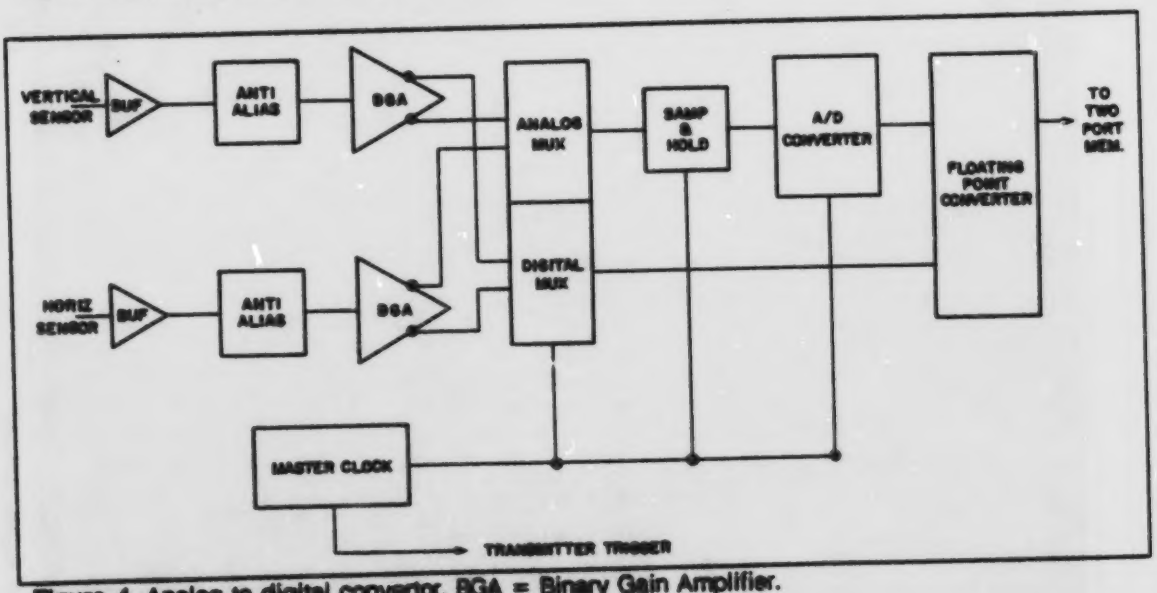

Figure 4. Analog to digital convertor. BGA = Binary Gain Amplifier.

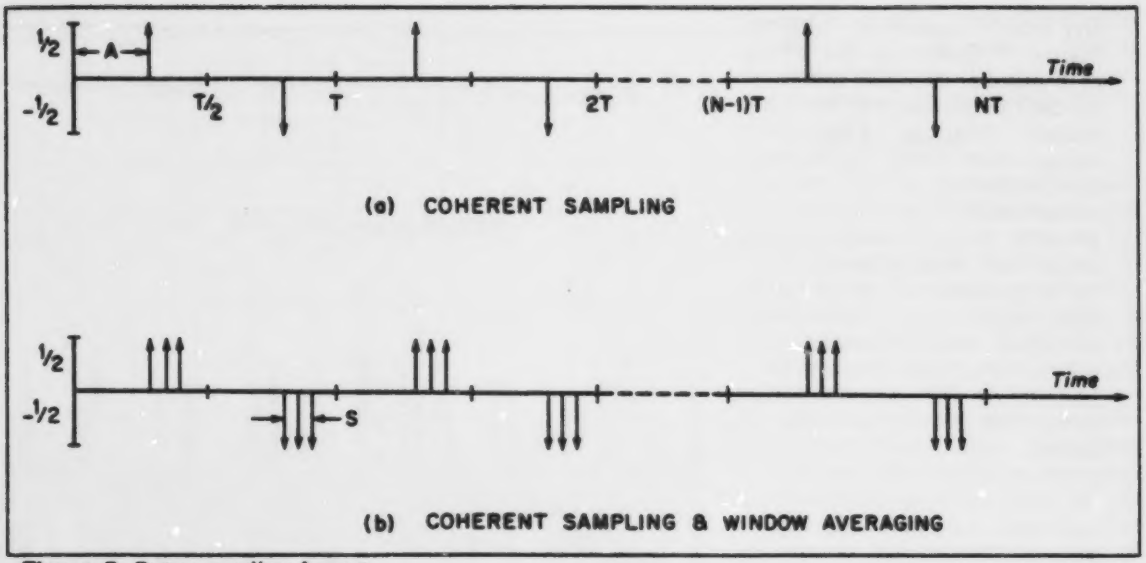

Figure 5. Data sampling format.

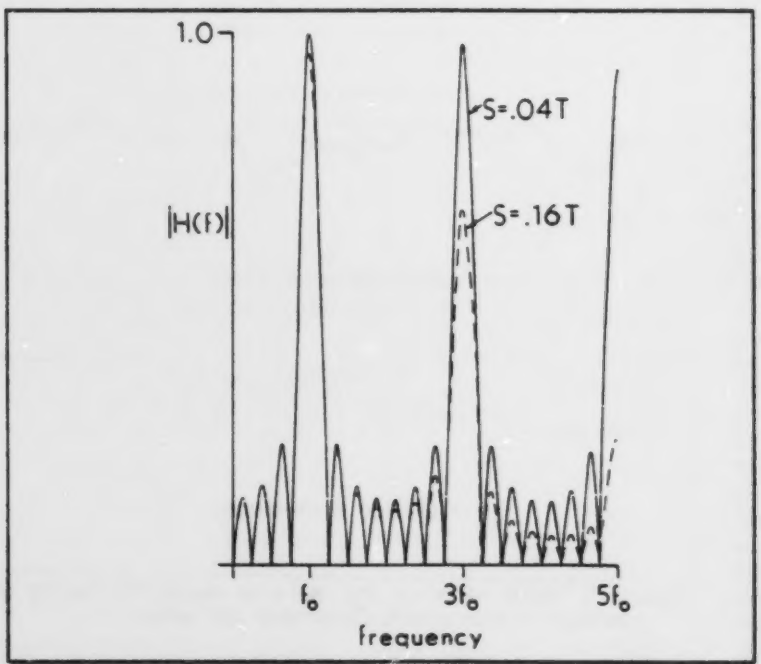

Figure 6. Frequency domain transfer function for coherent time-domain sampling (after San Filipo and Hohmann 1983).

constant level for the signal. In the frequency domain, the stacking process forms a comb filter with acceptance windows at all the odd harmonics of the fundamental frequency for the primary field waveform. Figure 6 illustrates the transfer function for the stacking process when 4 cycles of data are stacked with 2 different window widths, corresponding to 4% and 16% of the fundamental period. It appears that the effects of window averaging are minor for window widths of less than 10%. While the dominant features of the transfer function are the acceptance windows at the odd harmonics, we should also note the regular zeros of this function. These may be located at will to reject any particularly troublesome signals.

In addition to stacking and windowing, the data can then be filtered further using recur-

sive and/or nonlinear filtering. Figure 7 illustrates the effect of a number of these processes on data obtained over the Cavendish (Macnae 1980) test range. This data corresponds to Channel 3 in the conventional INPUT systems. It represents a signal sample taken some 800 microseconds after the termination of the primary field pulse. The data were averaged over a window of 440 microseconds and stacked for 9 periods of the primary wave form. While the anomaly is unobservable in the raw stacked and windowed data, it becomes clearly visible once real-time recursive filtering is applied. Post-flight smoothing further improves the signal-to-noise ratio.

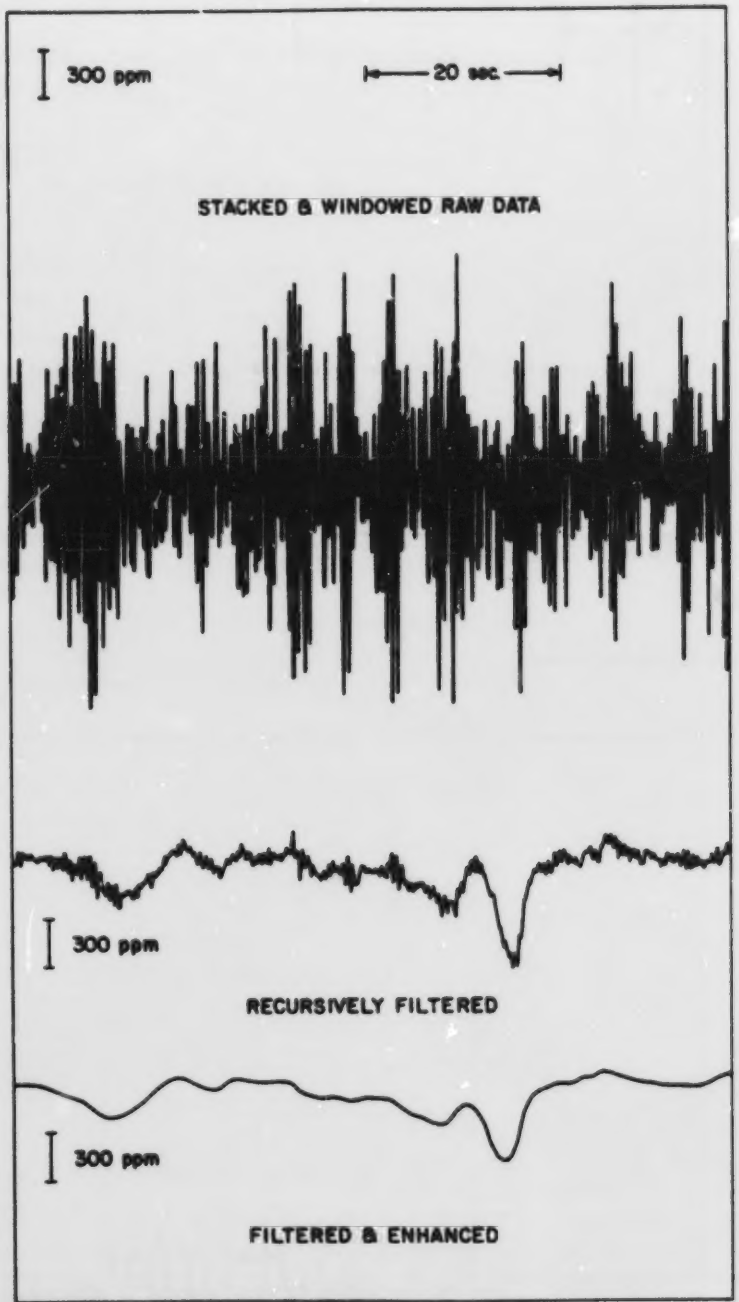

Figure 7. Noise reduction by real-time recursive filtering and post-flight enhancement, Cavendish test range.

COMPENSATION

One of the more serious problems that must be overcome in the production of acceptable airborne electromagnetic data is the effect of the motion of the sensor coils located in the towed bird. Motion of this device with respect to the aircraft can be compensated for by using a linear filtering process similar to that applied in the conventional analog system. The consequences of poor compensation can be immediately appreciated by examining Figure 8 which compares uncompensated and compensated data acquired over Line "E" on the Cavendish test range. The test results are presented in the conventional format for displaying INPUT data. In the worst case, the lack of compensation can result in trace movements, such as at points A and E, which are quite similar to the bonafide anomaly recorded at point D. At point B, we note the confusion of compensation effects with a small anomaly. As shown in the

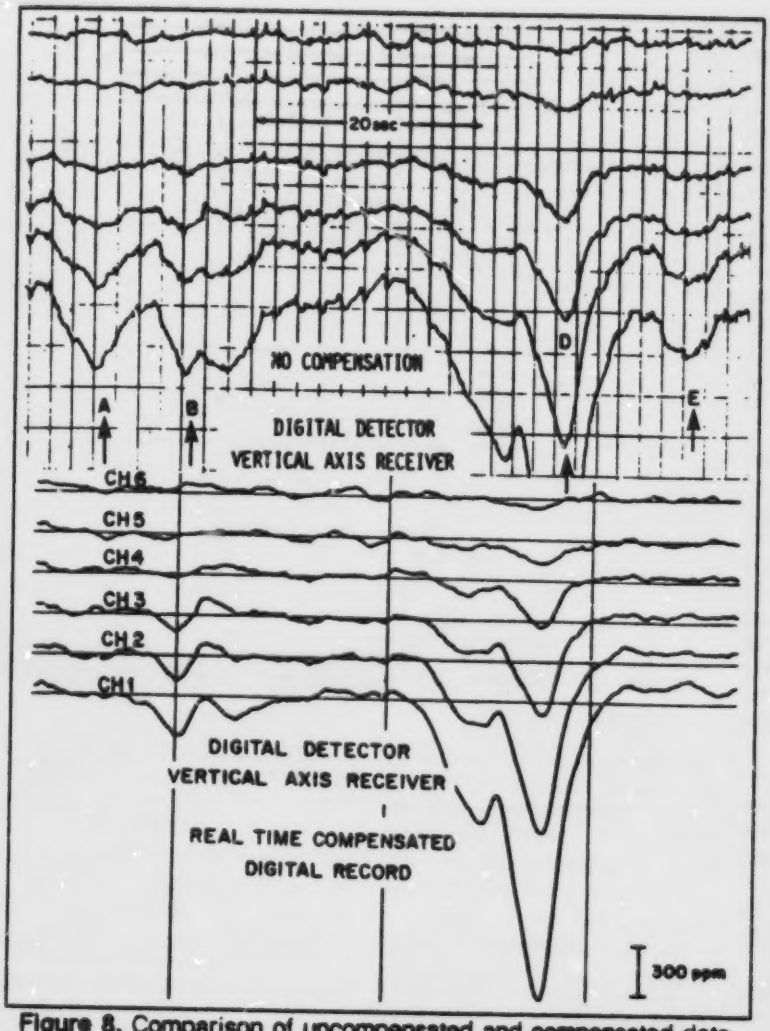

Figure 8. Comparison of uncompensated and compensated data, Line "E", Cavendish test range.

lower part of this illustration the effects of sensor motion with respect to the aircraft can be almost entirely removed.

REPROCESSING

One of the principal advantages of digital recording is the fact that the data may be reprocessed a number of times to optimize the signal-to-noise ratio. An example of this is shown in Figure 9 where we have enhanced data obtained over Line "E" of the Cavendish test range. Here, the upper part of the illustration shows the real-time compensated digital record that can be produced in the aircraft. The lower part illustrates one of our post-flight data enhancement techniques.

FIELD RESULTS

LAKE ONTARIO

During the 1983-84 fiscal year we performed about 100 hours of airborne testing. Most of the flights took place over Lake Ontario, as well as some over the Cavendish test range. A substantial testing exercise was carried out over the more recently established Night Hawk (Barlow 1981) test range near Timmins, Ontario. The performance of the digital detector was proven to meet all the requirements set out in the objectives of this research and development program. To illustrate the high fidelity of the digital data, Figure 10 shows a comparison between real-time digital data as displayed on the monitor in the aircraft and conventional analog data. The fidelity of the 2 data sets attests to the quality of the compensation procedures while the removal of spherics from the digital record is clearly evident. The test was flown over Lake Ontario with a horizontal axis

detector at a mean altitude of about 115 m above the water surface.

NIGHT HAWK TEST

The Night Hawk geophysical test range is located 40 km east of Timmins, close to operating base metal and gold mines. Since the site was established by the Ontario Geological Survey, many universities, contractors, and government agencies have surveyed the area with various types of equipment.

The survey site is underlain by Abitibi "greenstone" rocks of Precambrian age. These consist of acidic and intermediate to mafic volcanic flows and pyroclastic rocks with intercalated metasedimentary rocks. A prominent magnetic anomaly which can be observed on the profiles results from a diabase dike.

Even though the Night Hawk conductor has been designated as a test target, in reality very little is known about its true configuration. What is known or surmised, based on drilling and various geophysical surveys, is as follows:

1. it is a wide graphitic body of limited depth extent encompassed by schistose rocks in a rhyolitic host (from drilling results)
2. it is covered by 85 m of glacial unconsolidated sediments (from drilling results)
3. it is a south-dipping conductor, 200 m wide and of 200 m depth extent (University of Toronto UTEM Time-domain system)
4. it is a flat lying conductor 200 m wide (MaxMin horizontal-loop electromagnetic system)

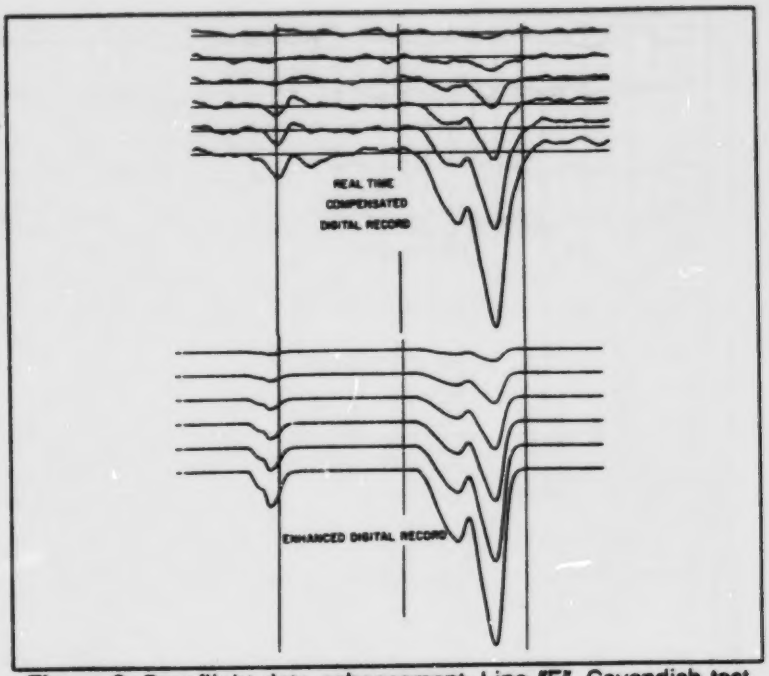

Figure 9. Post-flight data enhancement, Line "E", Cavendish test range.

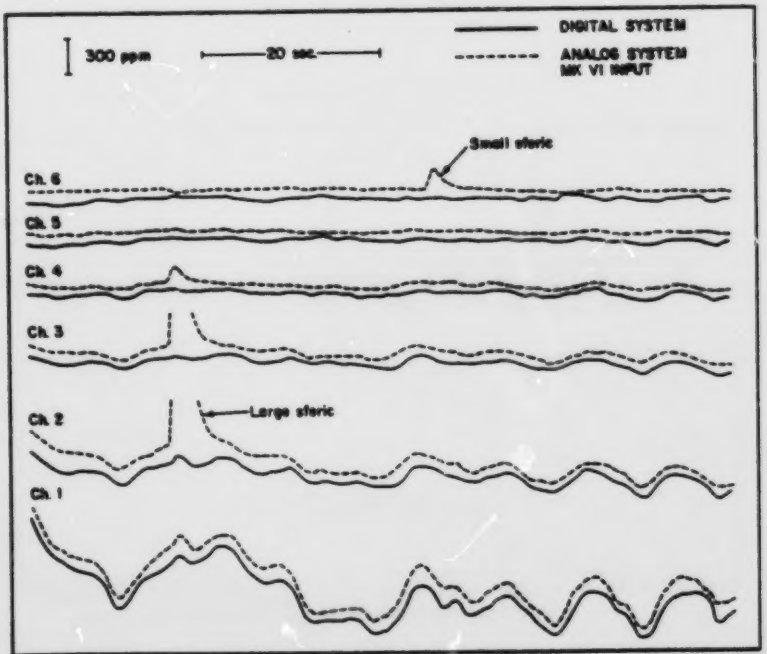

Figure 10. Comparison of analog and digital data, 115 m over Lake Ontario.

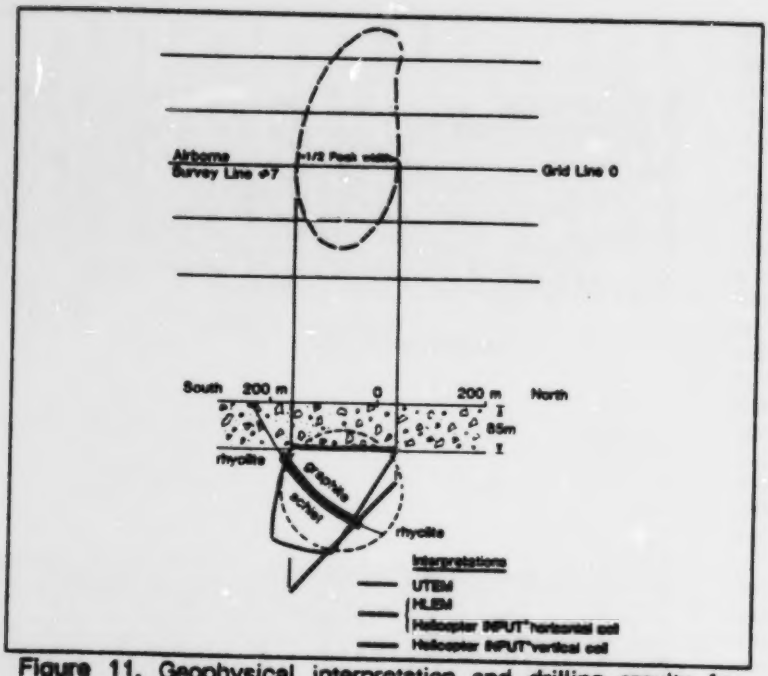

Figure 11. Geophysical interpretation and drilling results for Night Hawk conductor.

5. it is a plate-like body of limited depth extent dipping at 45°S (helicopter vertical-axis INPUT)
6. it is a spherical conductor of 100 m diameter or a flat lying ribbon of 100 m width (helicopter horizontal-axis INPUT and horizontal-loop electromagnetics)

These various interpretations and drilling results are shown in the lower half of Figure 11. The upper half of this figure depicts in plan view the outline of the conductor interpreted from the half-peak width amplitude data recorded with a conventional INPUT helicopter system using a vertical-axis receiver coil at normal survey height. Probably the best description of the target would be a potato-shaped body with a slice taken off the top. Unfortunately, this type of target does not lend itself well to theoretical, mathematical, or scale model studies and interpretation. It is too wide, too limited in depth extent, or too complex to realize an accurate interpretation.

Tests of the digital INPUT system were carried out by flying Grid Line 0, airborne Line 7, in a southerly direction at an average altitude of 122 m (400 feet) above ground level. On this test the weather was somewhat inclement causing a considerable amount of turbulence which resulted in an unusual quantity of motion noise. The data obtained in this test are shown in Figures 12 to 14. The conventional format for displaying INPUT results was chosen in order to facilitate the presentation. Figure 12 shows the raw data as they are recorded on the digital tape. The data are displayed at the rate of 10 points per second. It is obtained by coherently detecting the ambient electromagnetic signal, and filtering it in real-time to reduce noise and bandwidth. The data are also summed laterally to form the channel windows in a manner entirely analogous to the conventional INPUT detector. Although the raw data are evidently very noisy, the principal anomaly is visible and its fidelity (true shape) has been unaffected by the acquisition process. Figure 13 shows the analog monitor record that is produced onboard the aircraft during the survey flight. The computing process involved here emulates the functioning of the conventional analog INPUT receiver. The fidelity of the anomaly is reduced by the filtering process with the consequence that the recorded anomaly displayed here is smaller and broader than that detectable in the raw data. Although the signal-to-noise ratio is considerably improved by the filtering process, the record is still unusually noisy because of air turbulence during acquisition. Finally, Figure 14 shows the improvement in data quality that can be gained by post-flight data enhancement. Here, the input to the process is again the raw data shown in Figure 12. The filtering however, can be optimized to retrieve the anomaly with full fidelity, as evidenced by the small sidelobe immediately to the south of the main peak, while achieving a substantial improvement in the signal-to-noise ratio. It can be noted by comparing Figures 12 and 14 that the anomaly is recovered at nearly full amplitude.

CONCLUSIONS

Between 1960 and 1980, many improvements were made to the INPUT airborne electro-

magnetic system. These were related to, and took advantage of new developments in electronic and aviation technology. The research program described here was carried out in this very tradition. We have successfully adapted state-of-the-art digital equipment and processing techniques to a classic airborne electromagnetic system and were able to achieve the improvements sought. Although this research program was centred on the design, development, and construction of a microprocessor-controlled digital detector, which is vital to its successful completion, the work could not have been done without the availability of our flying electromagnetic laboratory complete with a redesigned transmitter loop, high power transmitter, and hatch for in-flight sensor retrieval.

There is no doubt that significant improvements to AEM system performance can be made with the aid of high speed data acquisition. Data acquired every 55 microseconds can be pruned, windowed, filtered, and interrogated on a virtually instantaneous basis. The result is superior equipment performance which includes the ability to reject atmospheric noise and to compensate for sensor motion in real-time. Thus already we can produce, in flight, a digital data record that equals in quality the conventional data acquired with an analog detector. The raw data which is stored on tape can, of course, be optimally reprocessed and enhanced at the computing centre. This procedure can result in a very substantial increase in the signal-to-noise ratio.

Although the objectives of the research program have

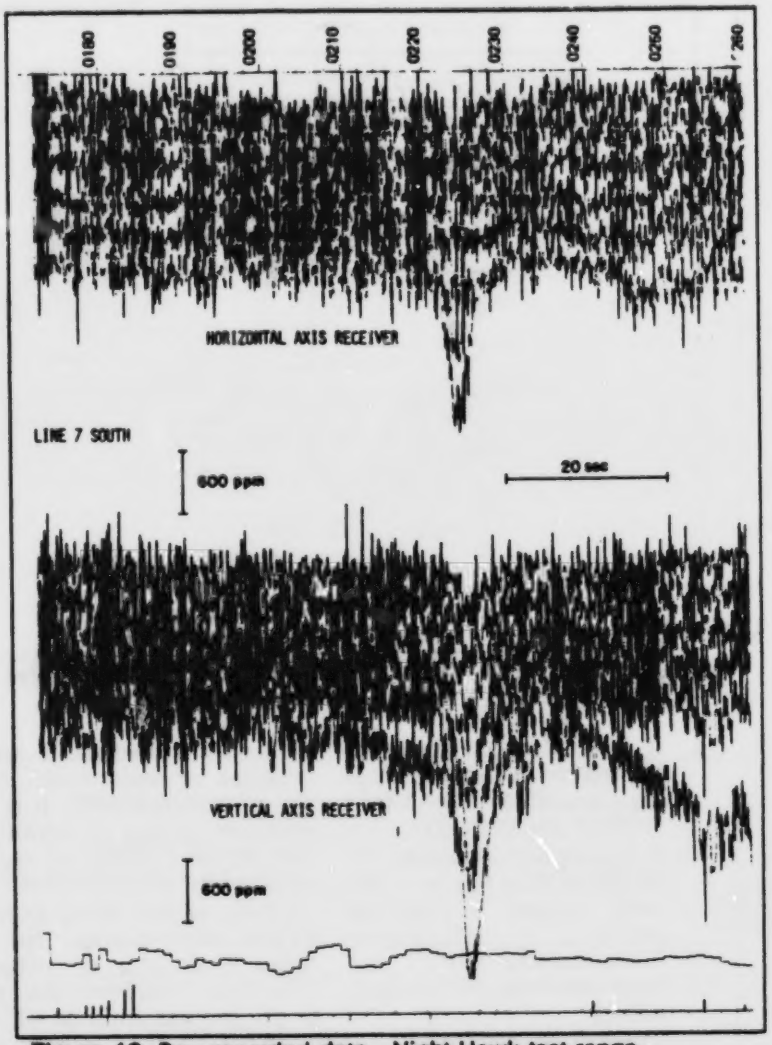

Figure 12. Raw recorded data - Night Hawk test range.

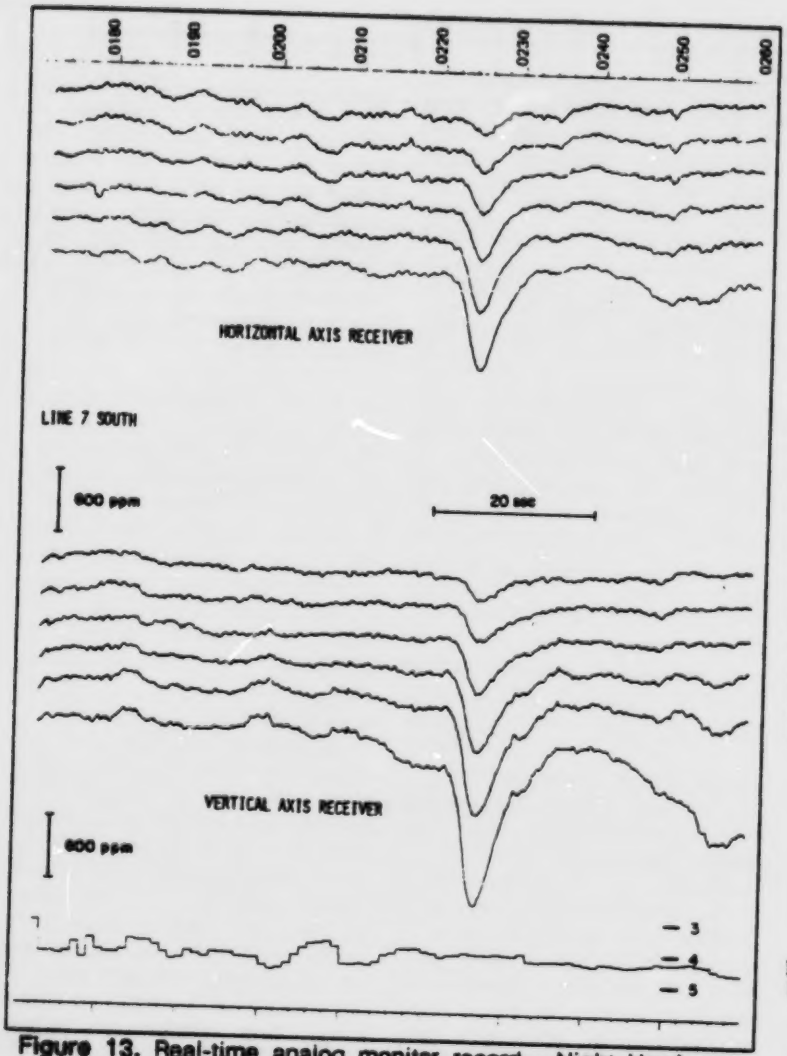

Figure 13. Real-time analog monitor record - Night Hawk test range.

been attained in that we have redefined the classical INPUT system by replacing the conventional analog detector which is the heart of the apparatus with its modern digital counterpart, much work remains to be done. Once we are even more familiar with the opportunities presented to us by the high speed digital data, we will surely be able to redesign our software to take advantage of these opportunities and once again improve the data quality. In geophysical terms, we are convinced that the new digital system will allow a greater depth of penetration to economic targets and a better degree of data fidelity which can be exploited for the purpose of geological-electromagnetic mapping.

REFERENCES

Barlow, R.B.
1981: Night Hawk Geophysical Test Range Results Using Two Electromagnetic Systems, District of Cochrane; p.152-159 *in* Summary of Field Work, 1981, by the Ontario Geological Survey, edited by John Wood, O.L. White, R.B. Barlow, and A.C. Colvine, Ontario Geological Survey, Miscellaneous Paper 100, 255p.

Barringer, A.R.
1962: The INPUT Airborne Electromagnetic Pulse Prospecting System; Mining Congress Journal, Volume 48, p.49-52.

Lazenby, P.G., and Becker, A.
1983: Redefinition of the INPUT® System: Part A - Instrumentation; p.1-9 *in* Exploration Technology Development Program of the Board of Industrial Leadership and Devlopment, Summary of Research 1981-1983, edited by E.G. Pye and R.B. Barlow, Ontario Geological Survey, Miscellaneous Paper 115, 135p. Accompanied by 2 charts.

Macnae, J.C.
1980: The Cavendish Test Site: A UTEM Survey Plus a Compilation of Other Ground Geophysical Data; Research in Applied Geophysics Laboratory, University of Toronto.

San Filipo, W.A., and Hohmann, G.W.
1983: Computer Simulation of Low Frequency Electromagnetic Data Acquisition; Geophysics, Volume 48, p.1219-1232.

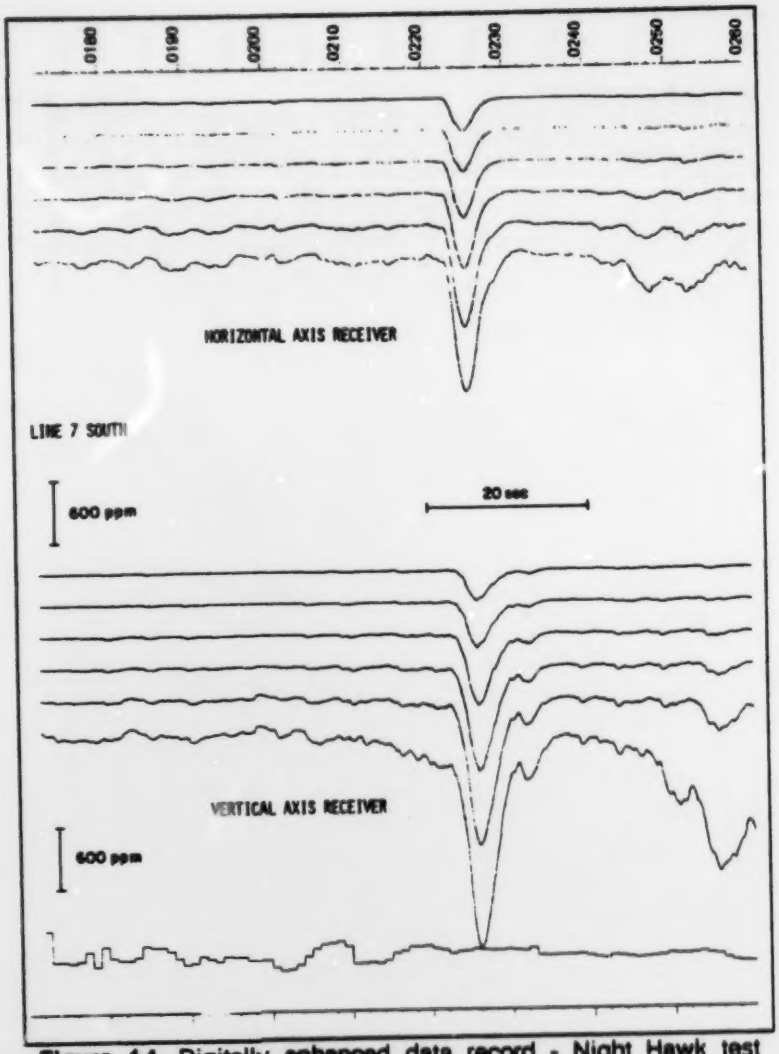

Figure 14. Digitally enhanced data record - Night Hawk test range.

Grant 010 Advanced Hardware and Software Development for Ground EM Prospecting

J.C. Macnae, Y. Lamontagne, H. Urbanski, and R. Huxter

Lamontagne Geophysics Limited, Toronto

ABSTRACT

A borehole system using a fibre optic data link was designed, constructed, and tested in the field. This project had 2 distinct aspects, instrumentation and field surveys, which are both reported separately. Electromagnetic (EM) interpretation aids, developed to make full use of EM measurements, are also reported separately. These aids consist of scale model data including more complex models, such as conductors under overburden, irregular overburden, and syncline-anticline structures. A computer program was also developed to make it possible to use the model data and a model data bank to fit field anomalies on a microcomputer.

In this system, a large loop on the surface generates a magnetic field and the down-hole sensor detects the field distorted by the ground. It was decided that a fibre optic link would best suit the system because of the problems associated with conventional electrical cables in down-hole applications, particularly with respect to common mode signals, cable channeling, and signal degradation. Although these problems can be overcome with difficulty in electrical cables, fibre optic cable does not have any potential for similar problems. As well, fibre optic cable has an additional advantage in that it is lighter in weight and lower in cost than conventional shielded electrical cable. These advantages must be balanced against the cost of additional down-hole electronics and battery operation however, leading to a more expensive probe than is usual for borehole systems. Our results show that a fibre optic cable of this design can be used in many borehole applications, particularly where the data rate is high and where signal degradation can be a problem.

INTRODUCTION

Improvements in exploration techniques can now be separated into 2 broad fields: hardware improvements resulting from developments in electronic instrumentation and mechanical systems, and software improvements dealing mostly with data processing and presentation. There is also the indistinct zone of firmware development involving hardware-oriented microprogramming in microprocessor controlled systems. The UTEM developments include all 3 of these aspects.

In hardware development, the largest project was the design and construction of the borehole UTEM system using a fibre optic link and an automatic servo-winch system. Part 1 is a report on this project. The field testing of the system (the development of the software tools to reduce and display the data, to display the primary field in the plane of the borehole, and to adjust the borehole position) and the use of the prototype hardware are reported in Part 2 of this report. To assist in the interpretation effort, a comprehensive series of model type curves were generated using a scale modeling apparatus as well as numerical modeling. The models and their use in the interpretation and fitting of field data are discussed in Part 3.

PART 1 — FIBRE OPTIC DATA LINKS FOR BOREHOLE EM APPLICATION

With the success of the UTEM system in surface applications (West *et al.* 1984; Lamontagne 1975), it became clear that there was a need for an EM sensor which could be lowered into boreholes. Some of the unique characteristics of the system made adaptation to a borehole system perhaps more difficult than for other systems. These difficulties arise from the unusually large bandwidth of the UTEM system and the unique fact that the transmitter is always on during measurements. An additional problem posed by a borehole system is the spurious response likely to be caused by the long cable connecting the sensor to the surface equipment. This proolem was solved by the use of a fibre optic cable, and the additional advantages and drawbacks of this technology, are discussed below.

CONVENTIONAL ELECTRICAL CABLE PROBLEMS

Initial analysis of existing borehole systems indicated that the task of supressing stray coupling effects to the required accuracy over the desired bandwidth was almost impossible using conventional electrical cable. Some initial tests by Dyck (1981) using a conventional borehole probe confirmed this suspicion. Three main areas of difficulty detected in this analysis are summarized in Table 1.

Common Mode Interference

With a transmitter loop excited by several hundred volts

at the surface, it is difficult to achieve a sufficiently high common mode rejection ratio, and a complete system balance is needed to avoid spurious responses where conductive zones provide an electrical link to parts of the loop by capacitive or resistive coupling. Some of the very sharp responses, often seen even on late channels when crossing minor conductive zones, are probably caused by these effects.

TABLE 1: DIFFICULTIES DETECTED IN CONVENTIONAL ELECTRICAL CABLE

PROBLEM	EFFECT	MEASUREMENTS AFFECTED	SOLUTIONS
1-Common Mode	-Systematic Error	-'On' time worse	-Balanced differential transmission
	-Noise	-Wideband	-Shielding
			-Electrical isolation
2-Signal Degradation	-Distortion	-HF worse	-Encoding
	-Gain variation	-'On' time	-Controlled impedance line
3-Cable Channeling	-Artificial response	-HF H field	-Electrical isolation
		-All E field	

Cable Related Signal Degradation

In a long electrical cable, mechanical and/or environmental effects caused by motion of the cable, flowing water, mechanical stress, temperature differences, etc., can introduce noise signals or change the electrical characteristics of the line (e.g. resistance) thus affecting any critical adjustment of common mode rejection.

Current Channeling in the Cable

When the probe depth is very large, a long shielded cable acts as a long antenna which can channel appreciable currents which are capacitively coupled to it. This disturbance in the induced current flow is more acute for early sampling times, where, depending on the symmetry of the channeled current flow in the vicinity of the probe, a variety of artificial responses may result.

These effects can not only introduce stray responses, but can also affect the system gain and fidelity, which would be interpreted as long time constant responses in UTEM.

THE NEED FOR AN ALL–DIELECTRIC LINK

From the start, the possibility of using fibre optic transmission was considered as a way around all of these problems. Since an optical link can be all-dielectric, complete electrical isolation can be realized, thus avoiding common mode problems and cable channeling effects. Also, one way to avoid signal degradation is signal encoding which is not only necessary for an optical link, but also can be done without introducing much noise in driving the long transmission line, as would be the case for electrical transmission (Hewlitt Packard 1978).

When the possibility was studied further, there appeared a number of further advantages in the use of an optical link. A good number of disadvantages were also discovered, mostly having to do with the use of a new technology. Both are summarized below:

Advantages—

1. no long cable effects
2. no mechanical effects
3. high throughput
4. low weight
5. low cost
6. lighter winch

Disadvantages—

1. more down-hole electronics
2. bending radius limit
3. termination problems
4. new technology

Design Problems Associated With the Use of a Fibre Optic Cable

Once the decision to use a fibre optic cable had been taken, it became necessary to find satisfactory solutions for various aspects of system design. These can be summarized as follows:

1. incompatibility of presently available standard fibre optic cable with high hydrostatic pressure

tolerance and tensile strength needed in logging operations

2. method of digital data encoding to be used
3. modifications required to a conventional winch to accommodate the special requirements of a fibre optic cable
4. types of electro-optical transducers required to modulate and demodulate the optical carrier used to transmit the 'H' field signal from the borehole sensor

The first 2 of these are discussed below, and the third is addressed in the subsequent section which describes the overall system.

Cable Construction

It was found that fibre optic cables can be considerably cheaper than electrical cables for a comparable data handling capability. They are also much lighter because no metallic members are needed. The effective density of a fibre optic cable is near 1.0, so it has almost no weight in a water filled borehole. This means that the winch system must only support the weight of the probe. One of the main difficulties encountered at the beginning was that there existed no fibre optic cable capable of withstanding a sufficiently high pressure without damage. This was due to the fact that in normal construction the cables are made to resist crushing rather than hydrostatic pressure. It was necessary to specify a special cable which could withstand high pressures and also have a greater tensile strength-to-weight ratio than usual. After several attempts, we arrived at a construction which could be made by our supplier and had the required properties. The normal fibre optic cable construction is shown in Figure 1 and consists of:

A—tough outer jacket (high density polyethylene)

B—soft plastic inner jacket to help cushion crushing loads

C—strength member (usually braided Kevlar)

D—rigid buffer tube (air filled)

E—optical fibre

The special fibre optic cable custom designed for borehole/high pressure work has a modified construction:

A—tough outer jacket as above

C—heavier Kevlar strength member

D—semirigid buffer tube

F—freeze-proof gel-filling with density of 1.0

G—optical fibre spiraling in buffer tube

The overall cable diameter and weight is reduced and the tensile strength/weight ratio is greater than for a standard cable. The physical properties are:

Overall diameter—3.8 mm

Attenuation—5 db/km

Weight—14 kg/km

Structural strength—3390 N (760 lbs)

Damage free loading—1160 N (260 lbs)

Bending radius—75 mm

Density—1 g/cm^3

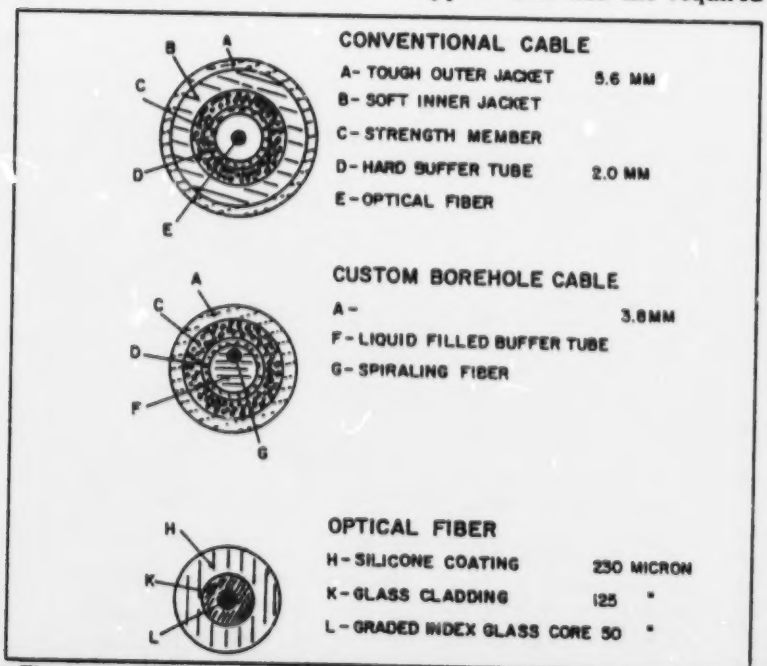
CONVENTIONAL CABLE
A- TOUGH OUTER JACKET 5.6 MM
B- SOFT INNER JACKET
C- STRENGTH MEMBER
D- HARD BUFFER TUBE 2.0 MM
E- OPTICAL FIBER
CUSTOM BOREHOLE CABLE
A- 3.8MM
F- LIQUID FILLED BUFFER TUBE
G- SPIRALING FIBER
OPTICAL FIBER
H- SILICONE COATING 230 MICRON
K- GLASS CLADDING 125 "
L- GRADED INDEX GLASS CORE 50 "

Figure 1. Sections showing the construction of fibre optic cables and the layering of the optical fibre.

OVERALL SYSTEM

The system consists of the following functional blocks: down-hole probe, optical link, winch assembly, and winch controller.

Probe

The sensor is physically distinct from the other down-hole electronics, as shown in Figure 2. Only an axial magnetic sen-

sor has been constructed so far, but an electric field sensor and transverse magnetic sensors will be implemented in the future.

Optical Link

The analog-digital-analog data link (Figure 3) contains a signal encoder, optical transmitter, fibre optic cable, optical receiver, and decoder. Physically, the encoder is in the borehole probe, as is the optical transmitter. The optical receiver is in the hub of the removable winch spool and the decoder is in the controller box. The signal going through the slip-rings is thus a digital pulse-coded electrical signal. The decoder reproduces the analog signal for normal sampling by the receiver. The analog signal at the surface lags that down-hole by 20 ms; this time delay is caused by encoding, decoding, and transmission through the 2 km of fibre optic cable.

Winch Assembly

The winch system was designed to include all components necessary for complete automation of the system (Figure 4). The winch is driven by a servo motor and brake system. Optical shaft encoders are used to measure the probe position and the tension on the cable. The rack-and-pinion tensiometer also acts as a shock absorber. It is comprised of a pulley mounted on a spring-loaded arm. The spool and pulleys were made reasonably large in diameter to avoid undue bending of the fibre optic cable. The winch has a maximum torque limit set by the hardware, but this corresponds to actual cable tensions varying over a range of 2.7:1, depending on how full the spool is. For this reason, a ten-

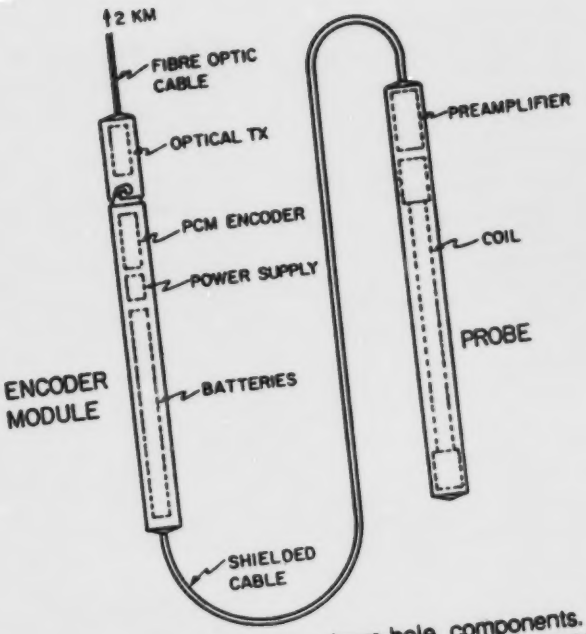

Figure 2. Schematic of the down-hole components. The magnetic sensor (PROBE) is separated from the encoder module by a 5 m cable. The optical transmitter housing which terminates the fibre optic cable is detachable from the encoder module.

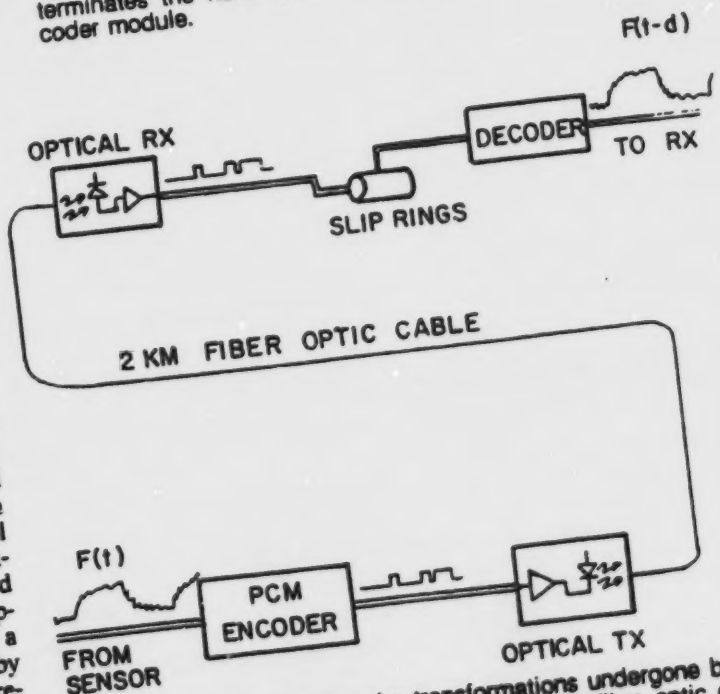

Figure 3. Sketch showing the transformations undergone by the signal from the sensor output, through the fibre optic cable, to the UTEM 3 receiver input.

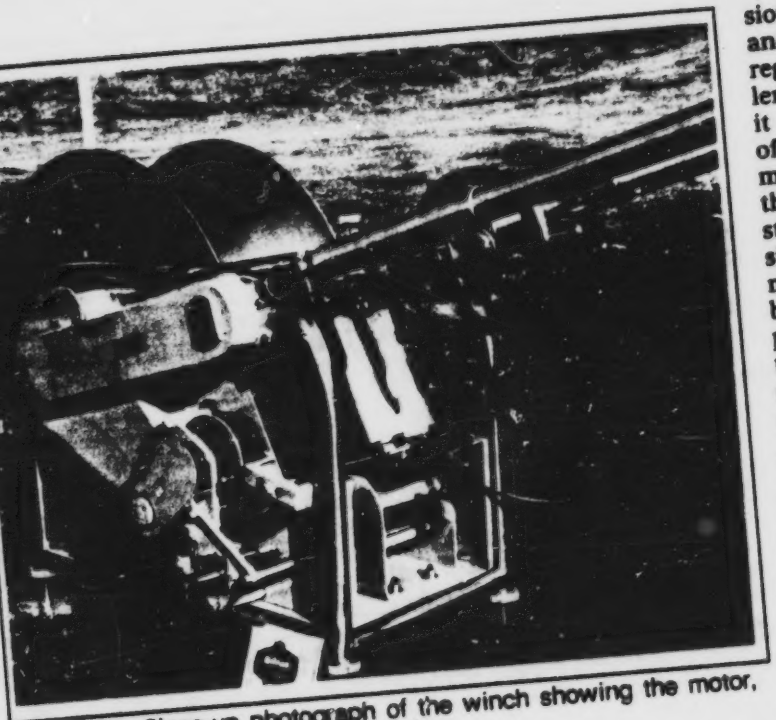

Figure 4. Close-up photograph of the winch showing the motor, gearbox, brake, and level winder.

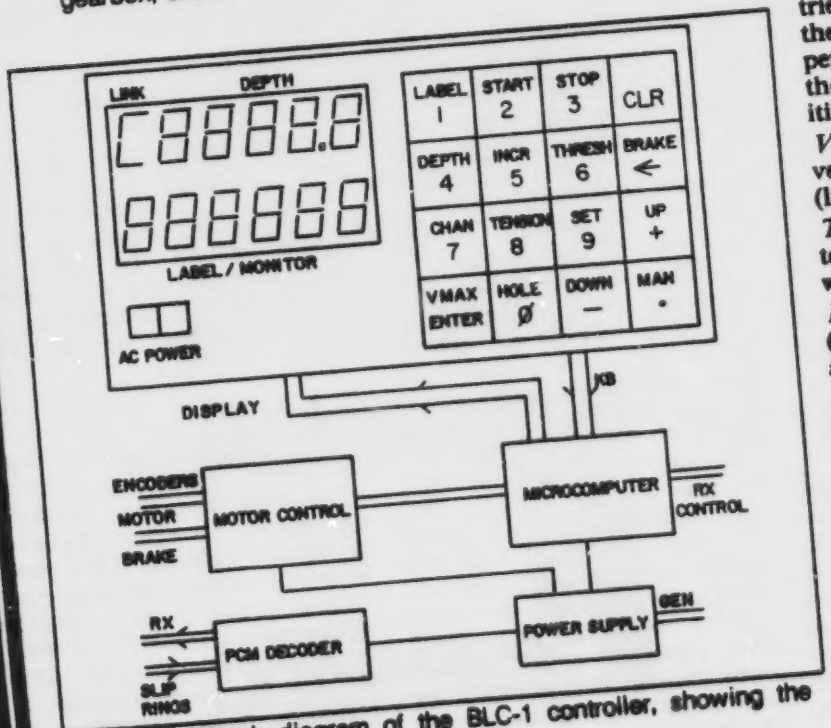

Figure 5. Block diagram of the BLC-1 controller, showing the front panel functions.

siometer is needed. The speed and braking of the winch is regulated by the winch controller unit. An upper tension limit is entered on the keyboard of the controller which determines the threshold at which the winch will slow down or stop to reduce the actual tension on the cable. This normally occurs when the probe is being pulled up. While the probe is being lowered, the tension is maintained by the controller above a fixed 5% minimum limit.

Winch Controller

This unit provides intelligence for the whole system, although its main purpose is to control the winch. The controller can be operated manually from the keyboard or set automatically. The keyboard layout, shown schematically in Figure 5, illustrates the controller operation functions. One set of entries is necessary to initialize the controller, and a second set permits on-line intervention by the operator. Entries which initiallize the controller are:

VMAX—sets the maximum velocity of the probe in cm/sec (limit of 150)

TENSION—sets the maximum tension in percent of probe weight in air

HOLE—sets the hole depth (controller will refuse to go to any greater depth)

SET—initializes the depth register from the keyboard

Entries which permit on-line intervention by the operator are:

DEPTH—enters the probe target depth (initiates movement of the probe upon entry)

STOP—controlled stop (gradually slows the winch to a complete stop)

MAN—emergency manual stop

START—re-initiates movement of the probe towards the current target depth (used after STOP or MAN or automatic stoppage)

In addition to the essential functions outlined above, the following functions are provided for convenience in routine keyboard operation:

INCR—sets the depth increment

UP—moves the probe up by the depth increment (INCR)

DOWN—moves the probe down by the depth increment (INCR)

THRESH—sets an anomaly threshold depth above which automatic detailing is performed

The probe speed is limited to the value specified by VMAX and by the tension monitoring system. During descent the tension is maintained above 5% of the probe's weight in air, whereas during ascent the tension limit is entered by the operator. When approaching these limits the winch is slowed by the controller, which regulates the rate of descent or ascent of the probe to keep the tension on the cable within the specified limits. Thus, the winch acts as a slip clutch during probe ascent and prevents cable spillage during probe descent. The controller digital loop characteristics are such that the speed is regulated steadily when the drag is viscous in nature.

A conservative hole depth limit is usually entered before logging a hole. Once the probe reaches that depth the controller warns the operator. The hole depth is then increased and the maximum velocity reduced until the controller detects the bottom of the hole by means of the tensiometer and stops the winch. In a greasy hole the same mechanism slows down the probe during probe descent in order to keep a slight tension on the cable. The whole cable retains some tension in such cases since the fibre optic cable itself has a null buoyancy in water.

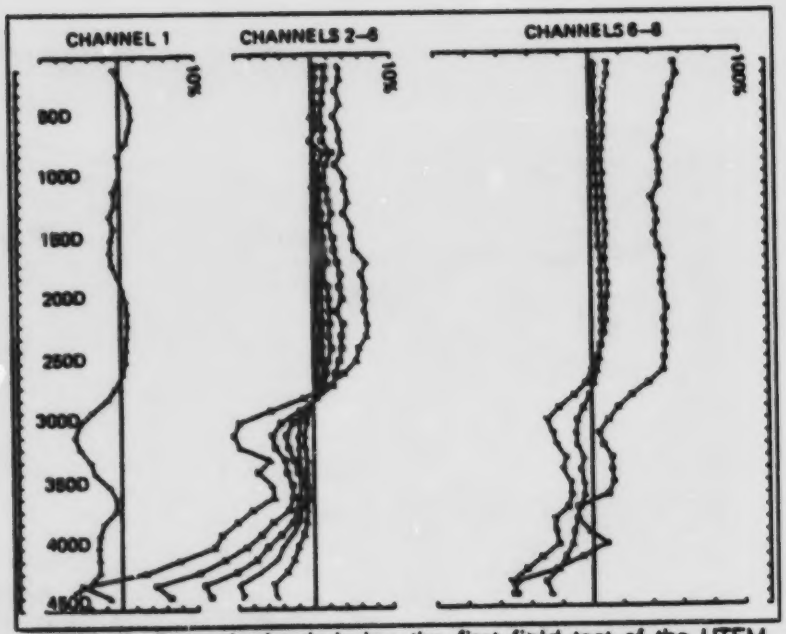

Figure 6. Data obtained during the first field test of the UTEM borehole system at Gertrude.

The signal connection from the down-hole coil to the UTEM 3 receiver is identical to that from the UTEM 3 surface coil. There is also an interface for automatic logging in which the winch controller unit can signal the UTEM 3 receiver to start reading and, upon completion of the reading, move the probe to a new depth. In both keyboard and automatic operation, the usual UTEM response and depth data (together with the standard header information) are stored on magnetic cassette in the receiver.

FIELD TESTING

Figure 6 shows the results from the first hole logged with the UTEM borehole system. The data collected in this hole did not include any compensation for the 20 second delay of the analog-digital-analog link, which caused the large response on channel 8. A subsequent receiver program modification corrects for this time delay.

CONCLUSIONS

The development of a fibre optic data link proved to be more of a challenge than initially anticipated. However, the technological problems have now been solved and the data link should prove to be a cheap, lightweight alternative to electrical wire data links with none of the usual problems of common mode rejection, capacitive pickup, or grounding. Many other applications for

the data link such as borehole induced polarization (IP) measurements are likely developments in the near future.

PART 2 — FIELD TESTING OF THE PROTOTYPE UTEM 3 BOREHOLE SYSTEM

A series of test borehole surveys was carried out as a comprehensive test of the new prototype UTEM 3 borehole system. These tests allowed us to first test the functionality of the system and also its capabilities in a variety of field situations. Some of the boreholes were surveyed at the Gertrude site near Sudbury from which there exists comparative data from other borehole systems (Dyck 1981), whereas other areas were surveyed to test the deep hole capability of the system. These tests also provided us with the field data necessary for the development of data reduction software for use with our field computer.

FIELD OPERATION

Transport to Site

The UTEM borehole system was carried to the test site by means of a 4-wheel-drive vehicle. It was necessary in some instances, however, to backpack the equipment for several hundred metres when road access was not available. The winch, including loaded cable spool, can be carried over such distances using simple carrying poles which are attached to the winch frame. Over longer distances it may be preferable to transport the winch assembly (22 kg) and full cable spool (30 kg) separately. The system can be easily installed by 2 persons, but, at the expense of more individual trips, a single person could also carry the system over short distances and operate it. The heaviest component of the system used in the test surveys was the 1500 W motor generator, required to operate the winch and UTEM 3 transmitter.

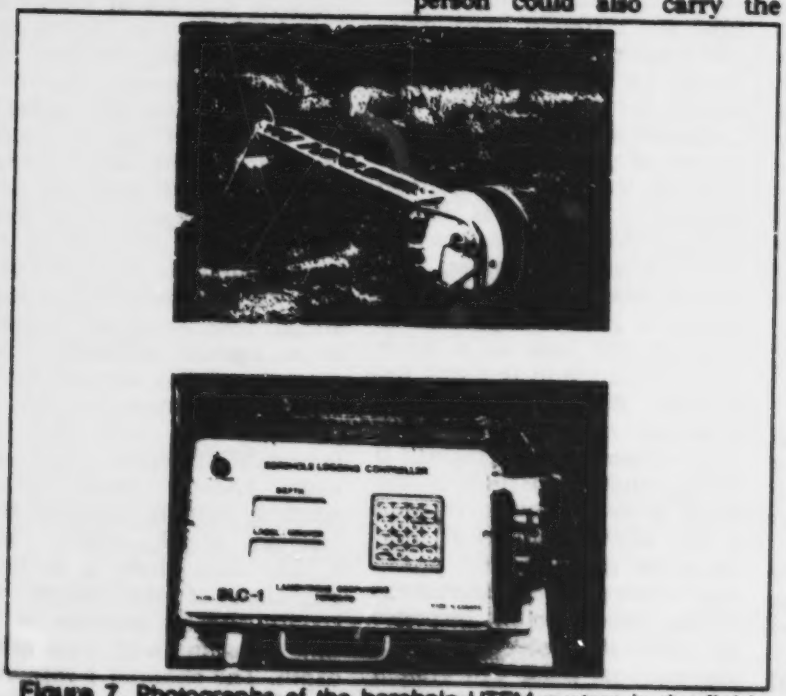

Figure 7. Photographs of the borehole UTEM system in the field and of the controller front panel.

Installation

The components of the borehole system necessary for field surveys are:

1. the winch assembly
2. the cable spool (which includes the optical decoder, located in the hub of the spool, and the optical transmitter housing)
3. the down-hole components (which includes the separate optical encoder tube and sensor)
4. the boom assembly (which disassembles into 2 sections for transport)
5. the controller unit
6. a 115 volt, 1500 W motor generator

Installation of the system requires roughly 15 minutes. As the last step in the installation procedure, 2 sections of the encoder tube (encoder and optical transmitter) are connected, providing power for the probe. An 'O' ring seals the 2 threaded sections of the connector, but this is not critical as both the encoder and transmitter housings are themselves pressure sealed from the connector compartment. Figure 7 shows the system ready for measurement and a close-up of the controller unit keyboard.

Start Up Procedure

The winch is connected to the controller unit, powered, and the brake applied before the down-hole components are placed into the hole. When the top of the optical transmitter housing (the uppermost part of

the down-hole probe) is flush with the borehole collar, the current depth of the probe is entered on the controller keyboard as 7.00 m. This is the distance between the centre of the sensor coil and the top of the optical transmitter housing and is mostly made up of a 5.0 m section of shielded cable linking the sensor coil and optical encoder/transmitter tube.

Measuring Mode Operation

After the controller has been initialized and the header information recorded, the normal UTEM measuring procedure is followed. Once the desired number of cycles has been stacked and the data recorded, the probe is lowered by a selected increment using the 2 controller keyboard functions 'DOWN' and 'ENTER', or to a selected depth using the controller keyboard functions 'DEPTH' nnnnn 'ENTER', where nnnnn is a number. At each new depth the measuring procedure is repeated. The depth increment and target depth may be selected at any time to a resolution of 1 cm. For moderate speeds of operation, the depth closure after the probe is raised is about 0.5% of the hole depth. This makes it practical to relog the hole on the way up with a different transmitter loop configuration.

DATA PRESENTATION

Since the UTEM system measures during the transmitter 'on' time, a special normalization procedure is necessary. The data are normalized by dividing by the total primary field which would exist at the measurement location in free air. Usually this total primary field is not strongly dependent on the borehole trajectory. For secondary field presentation, the calculated primary field along the borehole, as a percentage of the total primary field, is also subtracted. Usually, however, only channel 1 (the latest channel) is reduced in this manner. There may be anomalies caused by orientation/location errors if the borehole trajectory is unknown. This problem may be corrected by normalizing all earlier channels with respect to channel 1 rather than the calculated axial primary field since, in the absence of long time constant anomalies, the channel 1 response is a good approximation of the primary field.

By comparing the data from more than 1 transmitter loop the trajectory of the borehole may be estimated. The estimated trajectory may then be incorporated into the reduction data using an interactive feature of the program, and the resulting adjusted data from the different loops compared again. The process is repeated until the response appears to be corrected. Of course, it is still left to the discretion of the interpreting geophysicist whether the observed channel 1 anomaly is due to orientation/location errors or a real channel 1 response. If a real channel 1 response is suspected, it is always possible to resurvey the hole at a lower base frequency to test this hypothesis. With 3 or more loop locations, however, it can almost certainly be determined if the borehole trajectory is the cause of the anomaly. In spite of the added geometrical complications involved, this procedure allows the measurement of long time constant response not generally detectable by a conventional pulse EM system and possibly help determine the position of the borehole.

"VECPLOT" PRIMARY FIELD DISPLAY

As an aid to survey layout and understanding borehole trajectory effects, a microcomputer program (VECPLOT) was developed which can plot the direction (as vectors) and amplitude (as contours) of the primary field in any plane around the borehole. The transmitter loop location and borehole trajectory are plotted on the output to help orient the section. Figure 8 is an example of the output of VECPLOT.

EXAMPLES OF BOREHOLE DATA

The field data examples will be presented with only preliminary comments since the final interpretation has not yet been completed.

Gertrude Site

The first example is from borehole BH9266 at Gertrude. The borehole was logged several times during the field trials of the system. Figure 9 shows the borehole location and transmitter loop positions. In Figure 10 the data obtained using the north loop are presented. The legend of symbols used to label the channel response curves is given in Table 2. In the convention used here an off-hole response appears as a positive anomaly. The most prominent features are 2 off-hole responses at 315 m (anomaly A) and 435 m (anomaly B) depths which are well known from other borehole logging done at this location (Dyck 1981). The UTEM data show a definite migration of the deeper response and an increase in its time constant with increasing depth. The channel 1 response correlates well to responses of

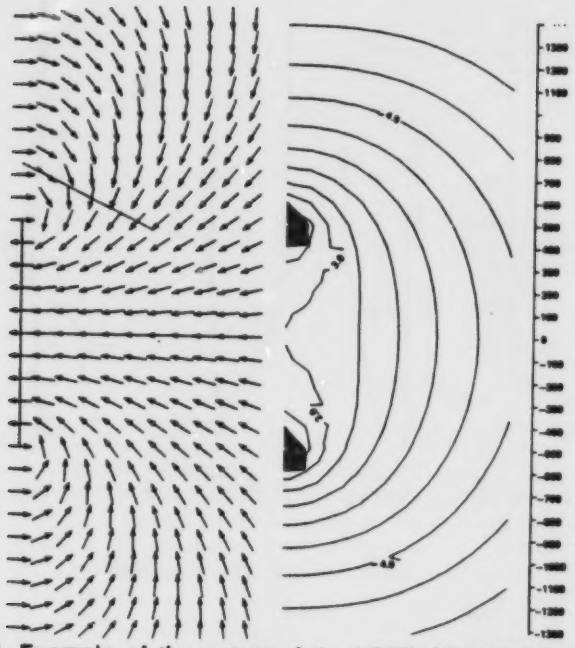

Figure 8. Example of the output of the VECPLOT program. This program maps the primary field in the section of the borehole for any loop position or size as an aid in survey layout.

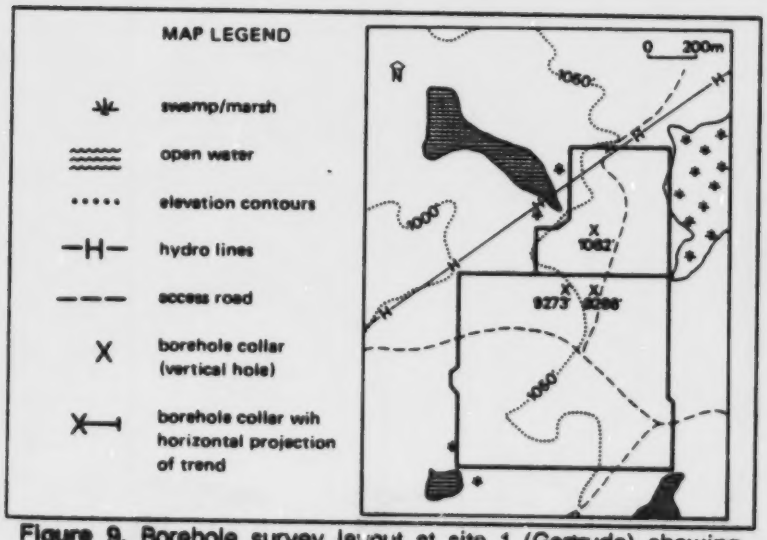

Figure 9. Borehole survey layout at site 1 (Gertrude) showing the positions of the boreholes and transmitter loops.

channels 2 through 6. If the channel 1 response is added back onto the channel 6 response (recall that it was subtracted during reduction), it would account for roughly half of the amplitude of the true anomaly of channel 6 of anomaly A. The decay also displays a definite bimodal character in the shallower anomaly with a plateau in the channel 4-5-6 responses. The data obtained using the south transmitter loop (Figure 11) show a much reduced anomaly at A and the coupling with the conductor causing anomaly B has even been reversed. But most notable is the channel 1 response over both A and B which has changed character and been reversed. Figure 12 is an expanded plot of the deepest part of the data of Figure 10 where the measurements were made every 2 m.

Figure 13 shows the data from the neighbouring borehole (BH9273) using the south transmitter loop. Basically, the response is a narrow in-hole anomaly which indicates the presence of a conductor of small effective size. The data from the same borehole, but using the north transmitter loop, show that this loop configuration couples with a much larger conductive zone (Figure 14). Particularly intriguing is the channel 1 response which suggests the presence of a long time constant, off-hole conductor above the in-hole intersection.

In another borehole at the site, the north loop data (Figure 15) have a more neutral response except for a tight in-hole anomaly over a known intersection. Data obtained using the south transmitter loop (Figure 16) are in complete agreement with the north loop data. Judging from the small

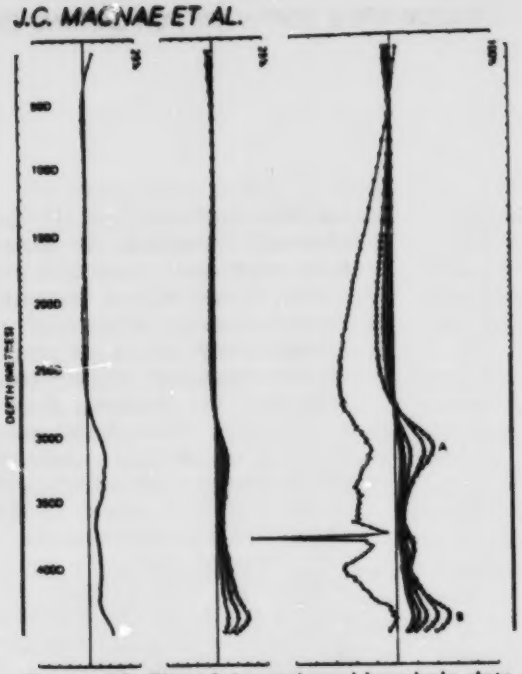

Figure 10. Plot of the reduced borehole data of BH9266 measured with the north loop. Refer to Table 2 for a legend of the plotting symbols. Channel 1 data, reduced by subtracting the calculated axial primary field component is plotted on the left scale. On the middle scale are channels 2 to 4, "channel 1 reduced", and on the right scale are channels 4 to 9 and "channel 1 reduced" at a reduced scale. The station spacings are 10, 5, and 2 m from the top to the bottom of the hole.

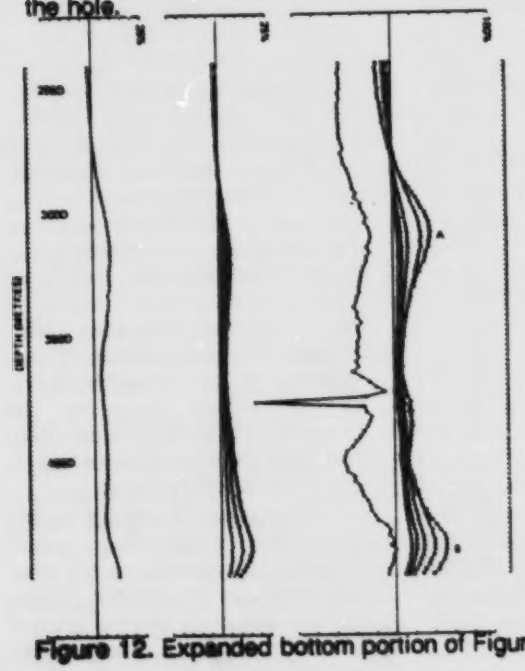

Figure 12. Expanded bottom portion of Figure 10.

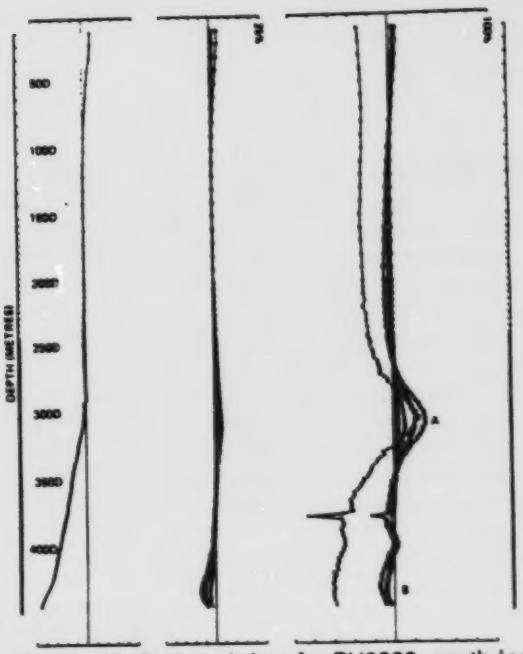

Figure 11. Reduced data for BH9266, south loop.

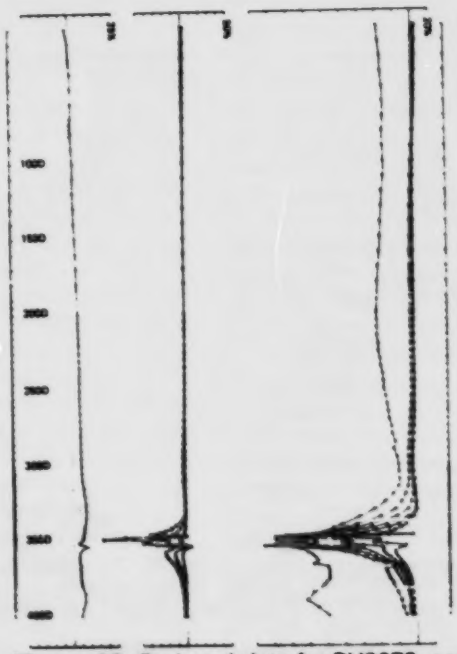

Figure 13. Reduced data for BH9273, south loop. The scales of the middle and top axes are reduced because of the large anomaly amplitude.

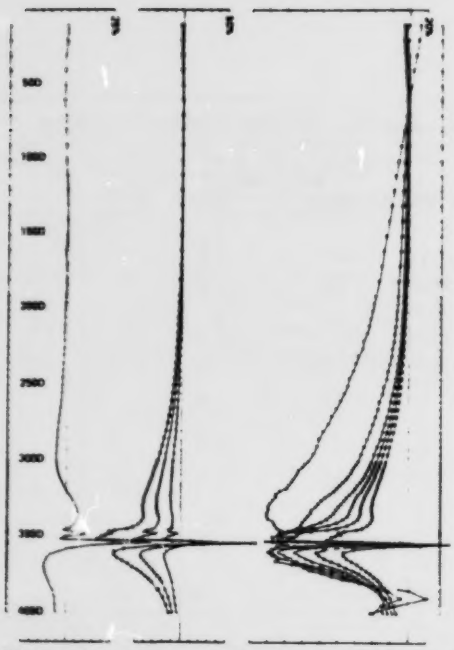

Figure 14. Reduced data for BH9273, north loop, with reduced scales.

Figure 15. Reduced data from BH10621, north loop.

Figure 16. Reduced data from BH10621, south loop.

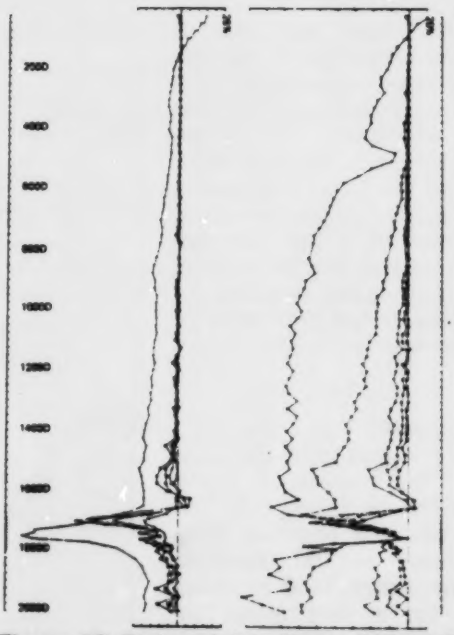

Figure 17. Reduced data from a 2000 m hole at site 2. Note the -100% anomaly on channel 1. The channel 1 reduction has removed this response from the other channels; this is why the early channels are near 0 at this point. The mirror image anomaly is caused by the subtraction of channel 1.

channel 1 response in the BH10621 data, it is apparent that it's time constant is much shorter than in the channel 1 responses of the previous examples, but this cannot be easily determined without first inspecting the primary field reduced channel 1 data.

Site 2

The measurements at this site were made early in the field trial period, before final adjustments were made to the instrument, and was primarily intended to test the 2 km depth capability of the system. For this reason, short stacking times were used resulting in a larger degree of scatter in the data than is usual (Figure 17). The most interesting feature of the data is the very large negative (-100%) channel 1 anomaly at a depth of 1760 m where there is a known sulphide intersection. The anomaly was so large that when it was first encountered, the operators were convinced that the effect was due to a transmitter shutdown. The transmitter had not stopped, however, and the effect was caused by a highly conductive zone, the centre of which the primary field was unable to penetrate. The time constant of this anomaly has been estimated to be more than 100 ms.

Site 3

The location of the first borehole logged, and the location of the transmitter loops, are shown in Figure 18. The data from this borehole show an almost neutral response over the entire 1600 m depth except for a very minor in-hole anomaly which appears in various forms in the responses for each of the 2 loop positions (Figures 19 and 20).

TABLE 2: SYMBOLS USED TO LABEL THE CHANNEL RESPONSE CURVES FOR THE UTEM

CHANNEL	SYMBOL	MEAN DELAY (ms) 30Hz	16.5Hz
1		12.8	25.6
2		6.4	12.8
3		3.2	6.4
4		1.6	3.2
5		0.8	1.6
6		0.4	0.8
7		0.2	0.4
8		0.1	0.2
9		0.05	0.1
10		0.025	0.05

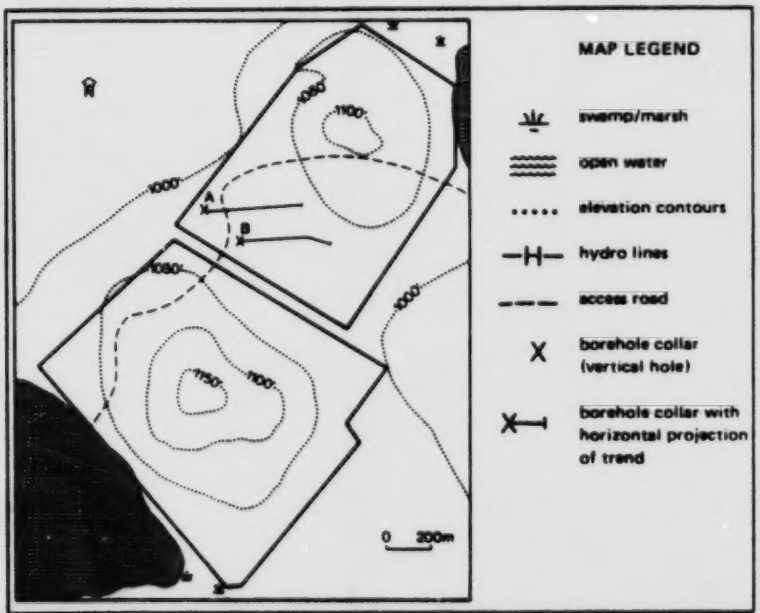

Figure 18. Survey layout at site 3 showing the 2 borehole locations and the loop positions. The projection of borehole B shown on the layout is only approximate.

In the last example, the borehole strays considerably from the south loop as a result of the great number of wedges (Figures 21 and 22). The effect of the wedges is clearly noticeable in the channel 1 response from the south loop data. It is obvious that the borehole position is poorly determined, but a minor deep, off-hole response is still detectable.

Conclusions

The field trials of the prototype model of the UTEM 3 borehole system provided the down-hole UTEM data necessary for the design of effective reduction and interpretation software and demonstrated the depth capability of the system. The data illustrated several aspects of the types of response obtained from a UTEM-style survey (i.e. an EM system which measures during 'transmitter on' time) when used in a down-hole environment.

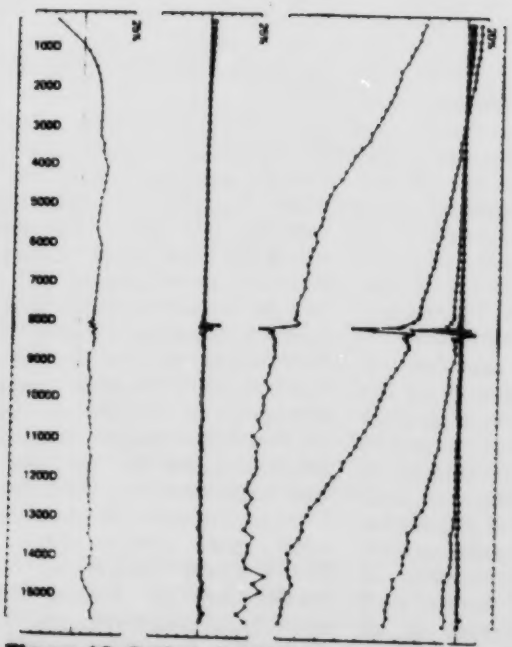

Figure 19. Reduced data from borehole A, north loop, showing only a weak conductor and the conductive overburden response. The near surface response is caused by the uninsulated wire of the south loop touching the ground.

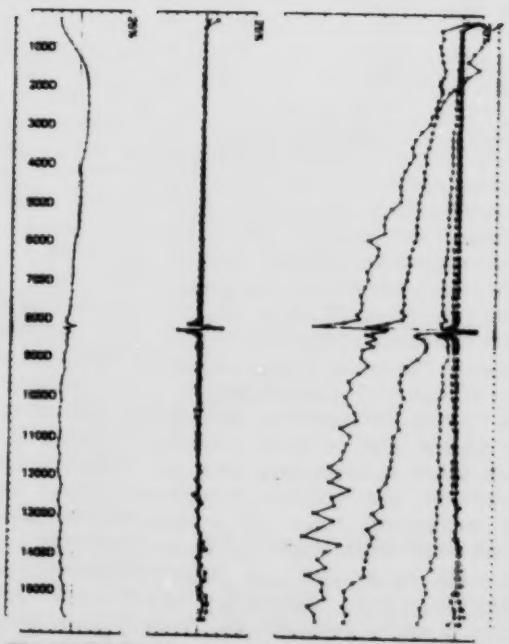

Figure 20. Reduced data from borehole B, south loop.

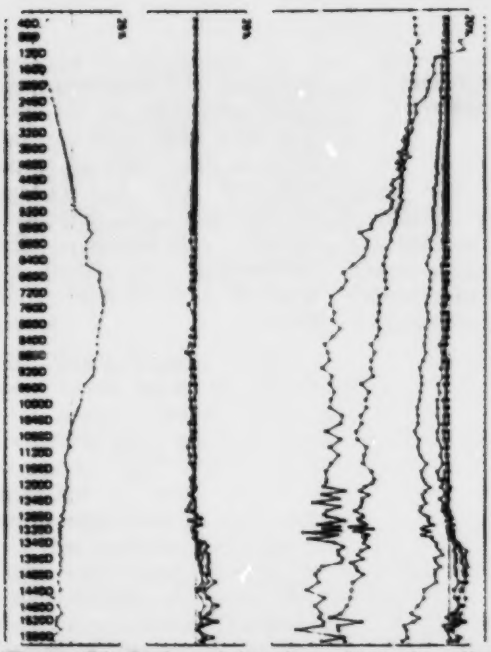

Figure 21. Reduced data loop. Note the effect of multiple wedges on channel 1. The jumps are caused by hole direction changes at the wedges. There is a small off-hole response at the bottom of the hole.

Figure 22. Reduced data from borehole B, north loop. The deep off-hole response is smaller and the wedges show differently.

PART 3 — INTERPRETATION AIDS FOR EM EXPLORATION

In the absence of economically reliable EM modeling programs for most of the 3-dimensional models which are relevant to EM interpretation, the most effective way to build a wide base of model data is to use a scale model apparatus and some ingenuity in finding and making models of varied shapes and properties. Once a large data base is available, the problem is one of extracting some rules or quasirules from these volumes of data to be used in interpreation, and ultimately to have it easily available for fitting field data.

SCALE MODEL PROGRAM

The scale model program was devised to complement the generally available numerical solutions, such as the 'Plate' and 'Sphere' programs available from the University of Toronto. Figures 23a, 23b, and 23c show an overview of the model shapes used. The modeling apparatus simulated a large loop system and the system response was that of the UTEM system. For each type and size of model, a variety of positions and depth relative to the loop were measured. Both vertical and in-line horizontal magnetic components were measured and presented. In all, 1800 types of curves were produced. In the case of an infinite half plane model, a numerical solution was used to compute the inductive limit (i.e. early amplitude) of the response.

Selected Examples of Model Data

The Infinite Half-Plane. A large number of infinite half-plane models were measured over a wide range of positions, depths, and dips. The half-plane is of particular relevance since it approximates the effect of large stratigraphic conductors truncated below the overburden, at a fault, or at an unconformity. Shallow dipping stratigraphic conductors give particularly complex responses depending on the position of the edge relative to the loop. Figures 24a and 24b compare 2 such cases (PH:A (24a) vs. PH:G (24b) continuous normalization) for vertical magnetic field measurements. The anomalies were normalized to the primary field at each point of measurement, which is usually referred to as 'continuous normalization'. Normalization to the primary field at a fixed

point is the basis of an alternate presentation called 'point normalization'. All model data are presented in both formats, but the examples here are of continuous normalization only. Figure 24b illustrates a more complex response because the model's conductor extends under the transmitter loop at shallow depth. Other models in this series, such as large slabs and wedges, show the characteristic response of thick tabular, or pinched-out conductors.

Laminated Conductors. As examples from the block/face series, the response between inductively interacting, but isolated, parallel plate conductors can be of significant relevance in areas of steeply dipping geology. A particularly intriguing case occurs when the laminations run perpendicular to the loop edge (Figure 25a). The broad positive response of similar shape on all channels can be mistaken for a deep horizontal conductor unless the decay characteristic is studied carefully. If the lamination runs parallel to the loop edge (Figure 25b), the response can be mistaken for a horizontal half-plane or a wedge dipping away from the loop unless, again, the decay is examined over a sufficiently long time range. This type of model is instructive in studying the response of large strongly interacting conductors.

Syncline/Anticline. This series of models is taken from the series pictured in Figure 23c, but contains a selection of more complex models. Figure 26a shows the response measured on a traverse over a large plunging syncline measured near the nose of the fold. The presence of the larger width of the structure down-plunge is obvious from the positive response lasting to the end of the line. The response of a broad anticline (Figure 26b) by comparison has a predominantly negative lobe and is much smoother than for most other models of the same depth to top.

Conversion to Other System Responses

It is possible to convert the UTEM responses to those of pulse EM system or frequency domain systems of the same geometry. This is possible because the large bandwidth of the UTEM system is generally wider than that of the other large loop systems. Some care had to be taken to obtain sufficient precision at the early channels, particularly since the model apparatus does not use high frequency pre-emphasis (prewhitening) as does the field UTEM 3 system. Figure 27 shows examples of data converted to the Crone PEM system response and frequency responses for the particular half-plane model of Figure 24a.

Model Data as a Direct Interpretation Aid

The first use of the model data is in training the EM interpreter. Even for the relatively restricted class of models covered, the responses obtained frequently have unexpected shapes over the time spectrum considered, which can call attention to the diagnostic features of the data. Very often the interpreter will find a response which matches his field data well in the model data. If the response of an EM system can be freely scaled in time (this is possible with frequency domain data and UTEM data), each of the model data sets can be used to interpret data from a similar model with different conductivity or measured with a different system base frequency. In general, the models were scaled in such a way that the time range measured includes as much of the range of response variation over time, or frequency, as possible.

For example, Figure 28 illustrates the response of irregular overburden with a step decrease in conductivity. It was found sufficient to include only 8 channels to cover the whole response variation (covering a time range of 1:256), but in fact the response of the step is undetectable in channels 1 and 2 (12.8 ms and 6.4 ms sampling times, respectively). The overburden conductance was chosen as 8.1 and 3.9 S to obtain a response over most of the channels. If, in fact, the likely situation is that of a step variation between 1 and 0.5 S, then the same model curves can be used, but would be scaled in time by a factor of 8 (i.e. 3 binary spaced channels). In this case, channels 1 to 5 would show no anomaly on the step instead of 1 and 2 only, and channel 8 would show an anomaly similar to channel 5 of the model curves. Furthermore, channel 10 of the field system would show the response of channel 7 of the model curves.

Interpretation Manual

To gain the maximum benefit from this arduous laboratory work, a preliminary interpretation manual was drafted which uses the model data as a base for simple interpretation. The manual was oriented towards the UTEM system, but most of it can be applied to

frequency domain data with minor adaptations. Charts and formulae are provided to interpret the location, depth, conductivity, and size of simple conductors based on converging evidence from profile anomaly shapes, absolute amplitude information, and time decay shape. Figure 29, for example, shows a chart used in the interpretation of dip from anomaly shape.

"LIGHT TABLE" FITTING PROGRAM ON A MICROCOMPUTER

A core computer program was derived to aid EM interpretation by comparing the field response to a selected model response. This program was made for the GFC-1 microcomputer using its dual page screen graphics capabilities. The program simulates the fitting of data on a light table, with the added advantage of instant scale changes and model scaling. The field data written on one graphics plane remain fixed, whereas on the other plane, data from the disc stored bank of model data can be scanned until a suitable set of data is found to attempt more specific fitting. The model data can be translated to be coincident with the field data. The reference position of the conductor is continuously updated during this process on the alphanumeric screen in the same coordinate system as the field data. If the horizontal scale of the model data must be changed to fit the field data, this can also be done continuously. In this case, all dimensional information of the model data are also scaled (as displayed on the alphanumeric screen) in proportion and the drawing of the model cross-section is similarly scaled. Also, the conductivity or conductance of the model is properly scaled. Time scaling is also allowed in 2 ways:

1. in changing the system base frequency to agree with the field frequency
2. channel interpolation without a frequency change, which has the effect of changing the model conductivity

Amplitude scaling of the profile data is permitted over a limited range. In this case the empirical relationship between depth, conductor size, and initial amplitude is used to alter the model depth and size, such as to produce the desired amplitude. The conductivity was also adjusted to reflect the change in conductor size. Fitting the time decays is similarly done by vertical and horizontal translations, and the anomaly decay time and inductive limit are determined.

The light-table program also has the capability of rotation, which could be useful for fitting data in contour form, but no model database exists for this yet. A list of the interactive graphics commands available to the program user is as follows:

c—locates the centre of transformation on the profile
o—plots the original data
a—uses graphics screen a
b—uses graphics screen b
O—overlays screen a and screen b
r—solid body translation right by the input increment
l—solid body translation left by the input increment
u—solid body translation up by the input increment
d—solid body translation down by the input increment
h—horizontal compression about a point picked by c
H—horizontal expansion about a point picked by c
v—vertical compression about a point picked by c
V—vertical expansion about a point picked by c
m—mirrors the profile about the x axis
M—mirrors the profile about the y axis
e—erases the present screen
F—keeps all of the preplotted images on the screen
f—refreshes the screen for every plot
p—clockwise rotation about a point picked by c
n—counterclockwise rotation about a point picked by c

Options:

—continuous alpha display of readjusted parameters
—many channels per use of program, each with a hard plot copy
—choice of automatic scaling or standard UTEM scaling
—choice of plotting symbols and line type
—autorepeat on any command key

The main requirement for this program is for fast vector graphics and computer arithmetic, such that the changes occur almost in real-time on the graphics screen. The interpreter can then judge the best fit by eye. This is done on the GFC-1 through the use of a dedicated graphics controller and dual processor organization of the computer.

Since the development of a computerized model database was beyond the scope of this research project, only a few test model data sets are presently accessible to the program. The building of the necessary disc-based model data catalogue has now been undertaken by Lamontagne Geo-

physics to make this program commercially useable.

CONCLUSIONS

With the availability of a large suite of scale model data curves, EM interpretation can be made easier and more reliable in providing an education for the interpreter, forming a base for interpretation rules, and quantitatively fitting field data with the aid of a computer which automatically uses scaling rules and empirically derived relationships.

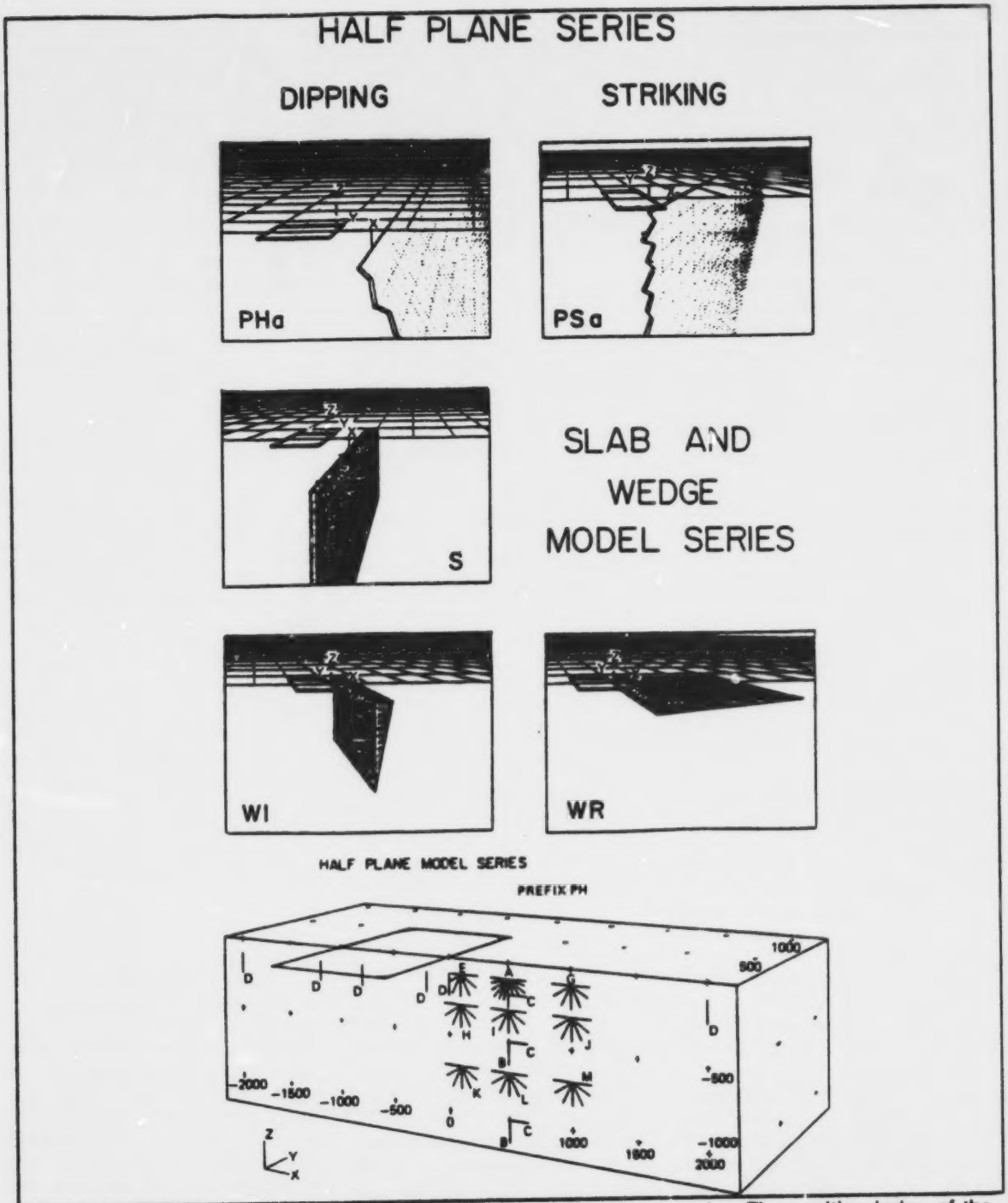

Figure 23a. Models included in the half-plane, slabs, and wedges series. The position index of the half-plane models shows all of the positions and dips of these models. The slab and wedge models were also measured for a variety of sizes, positions, and depths.

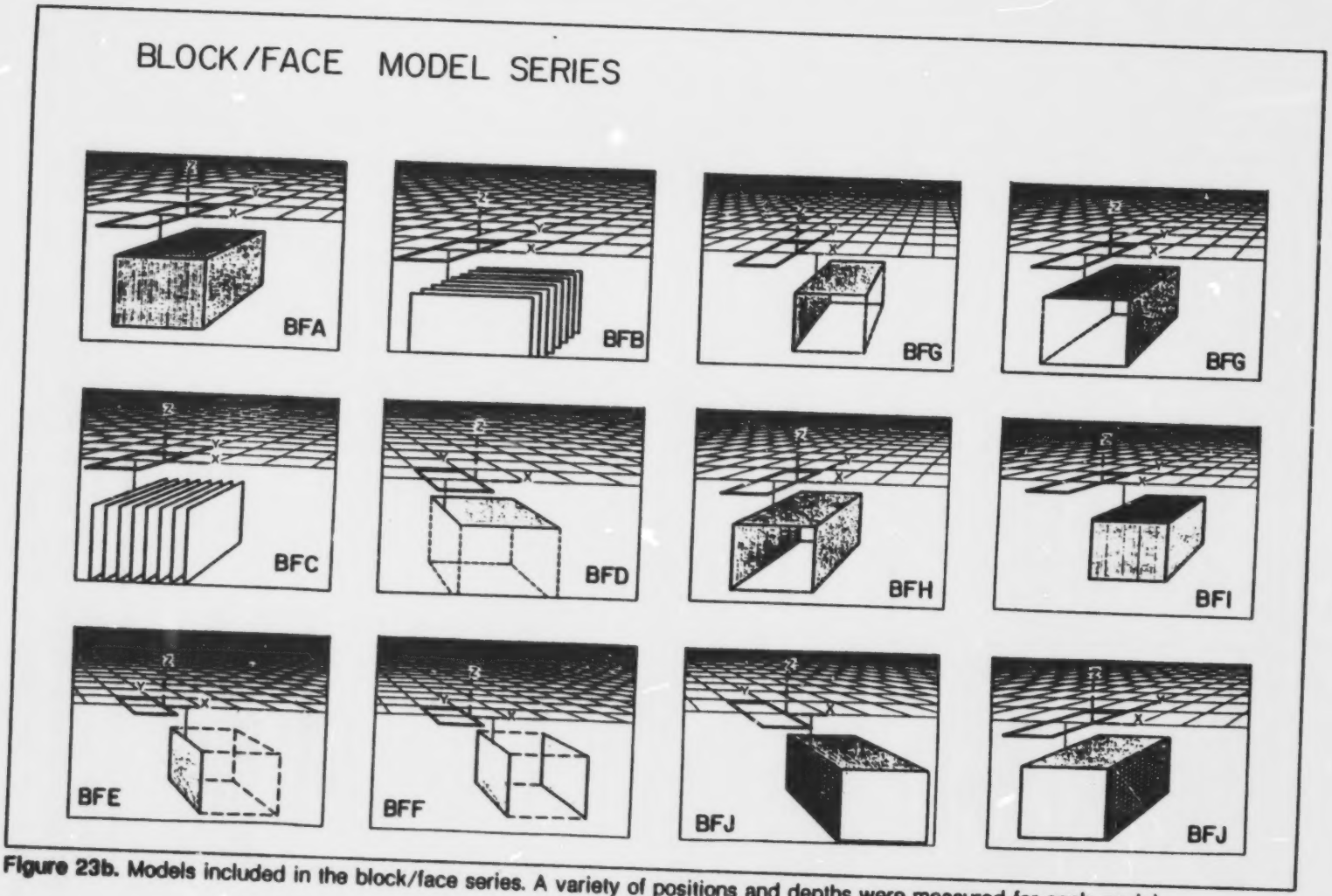

Figure 23b. Models included in the block/face series. A variety of positions and depths were measured for each model.

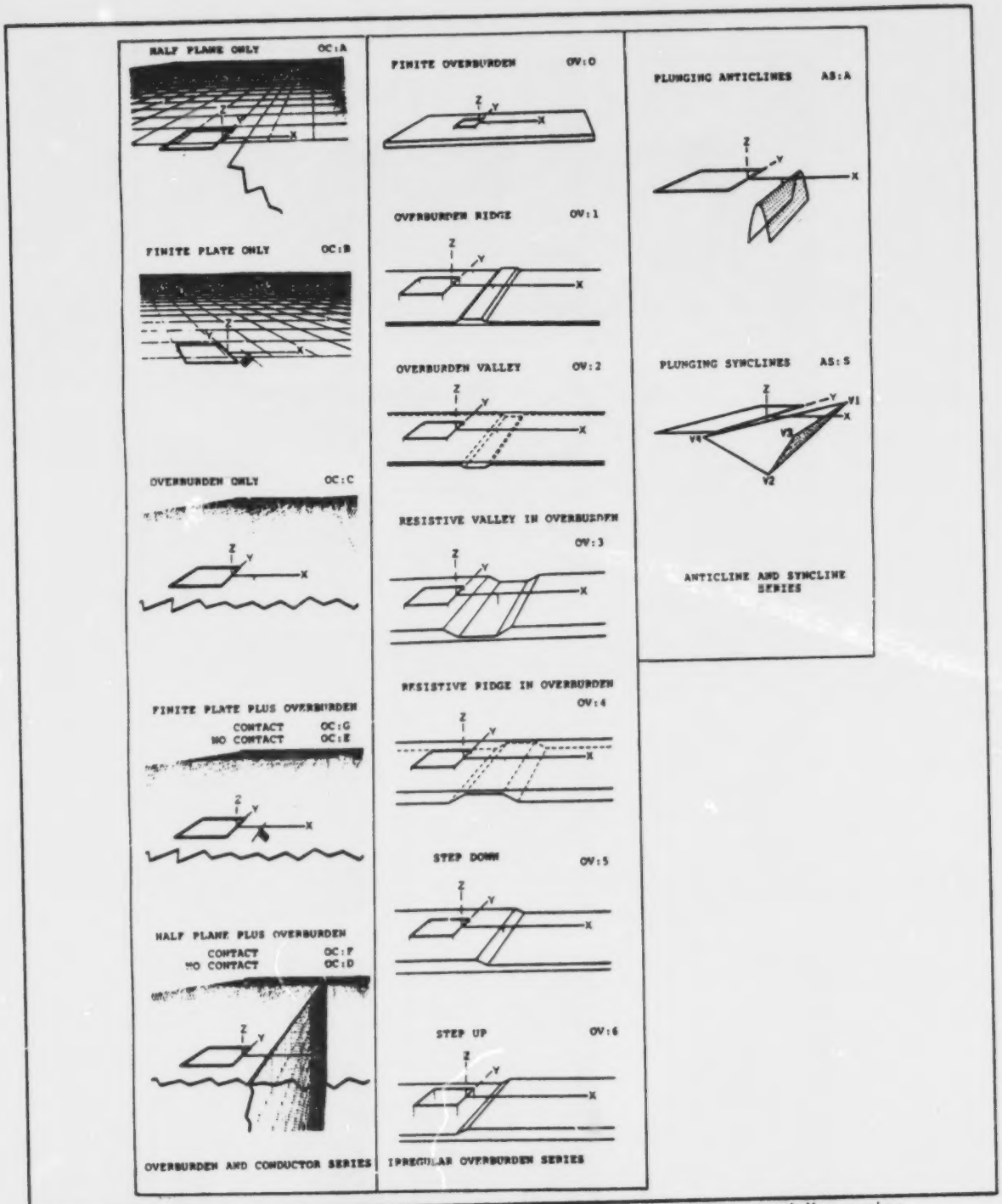

Figure 23c. Models in the overburden/plate, irregular overburden, syncline/anticline series.

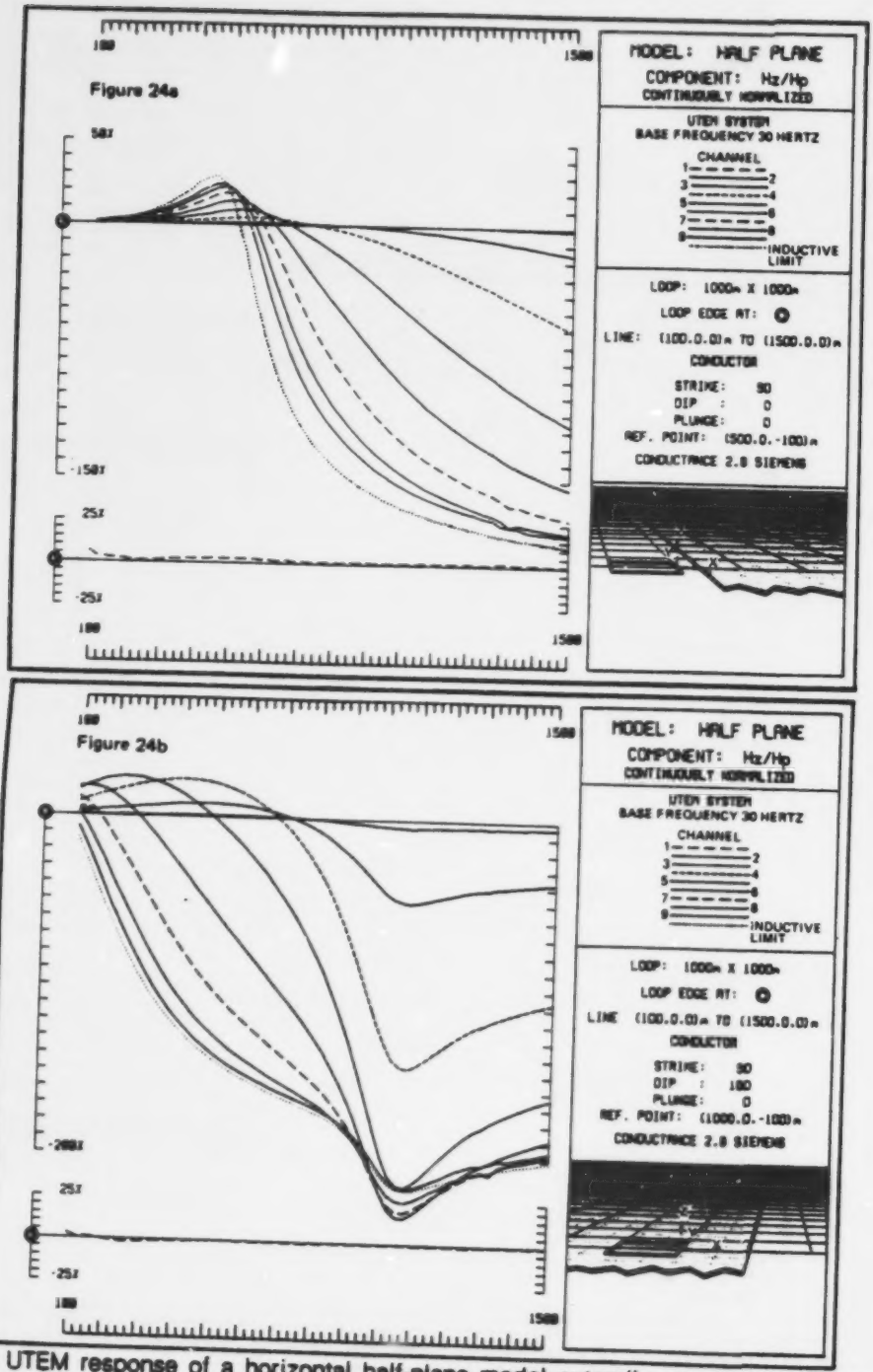

Figure 24a. UTEM response of a horizontal half-plane model extending away from the transmitter loop.

Figure 24b. UTEM response of a horizontal half-plane model extending under the transmitter loop.

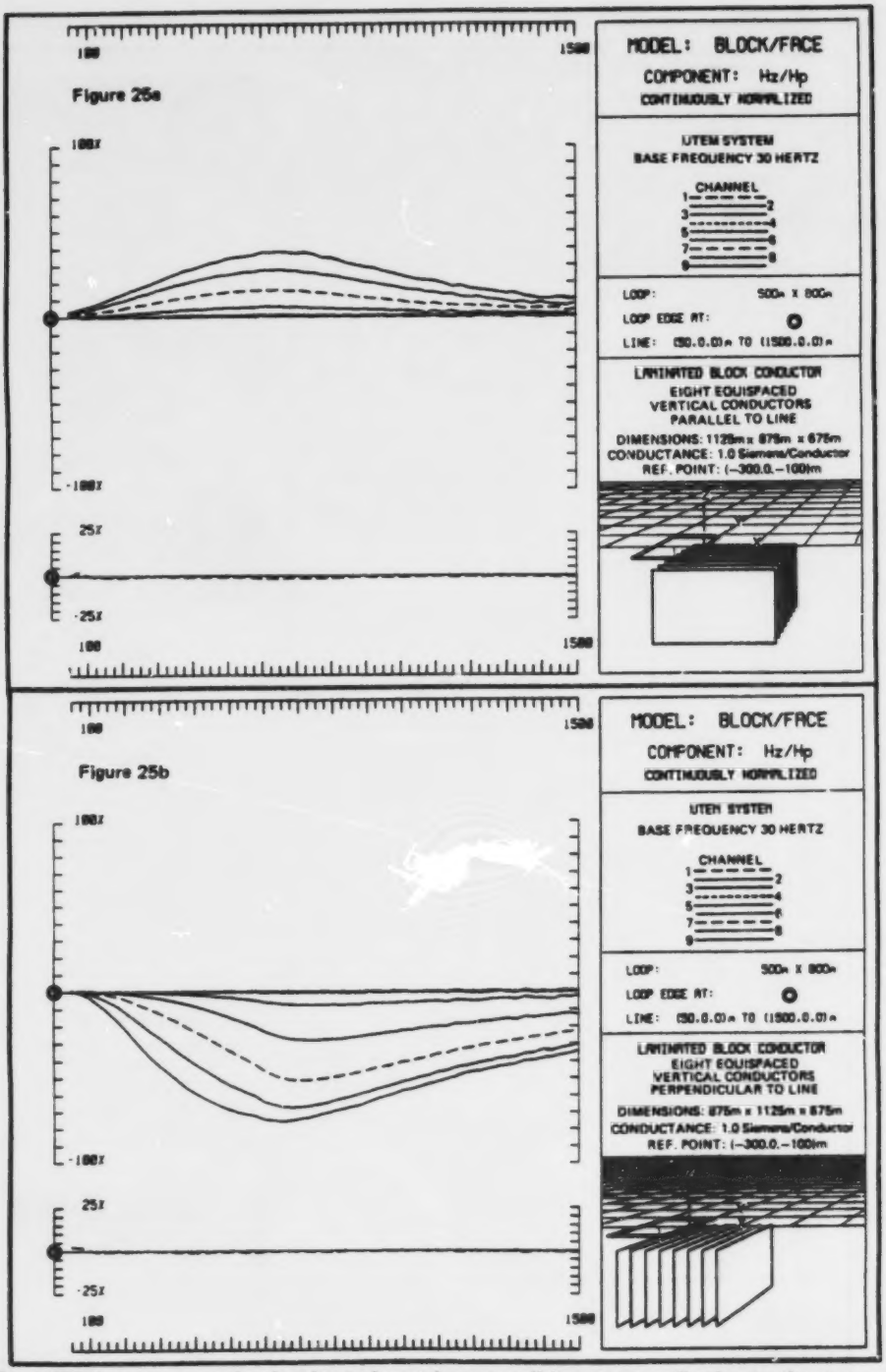

Figure 25a. UTEM response of a laminated conductor striking perpendicular to the transmitter loop edge.
Figure 25b. UTEM response of a laminated conductor striking parallel to the transmitter loop edge.

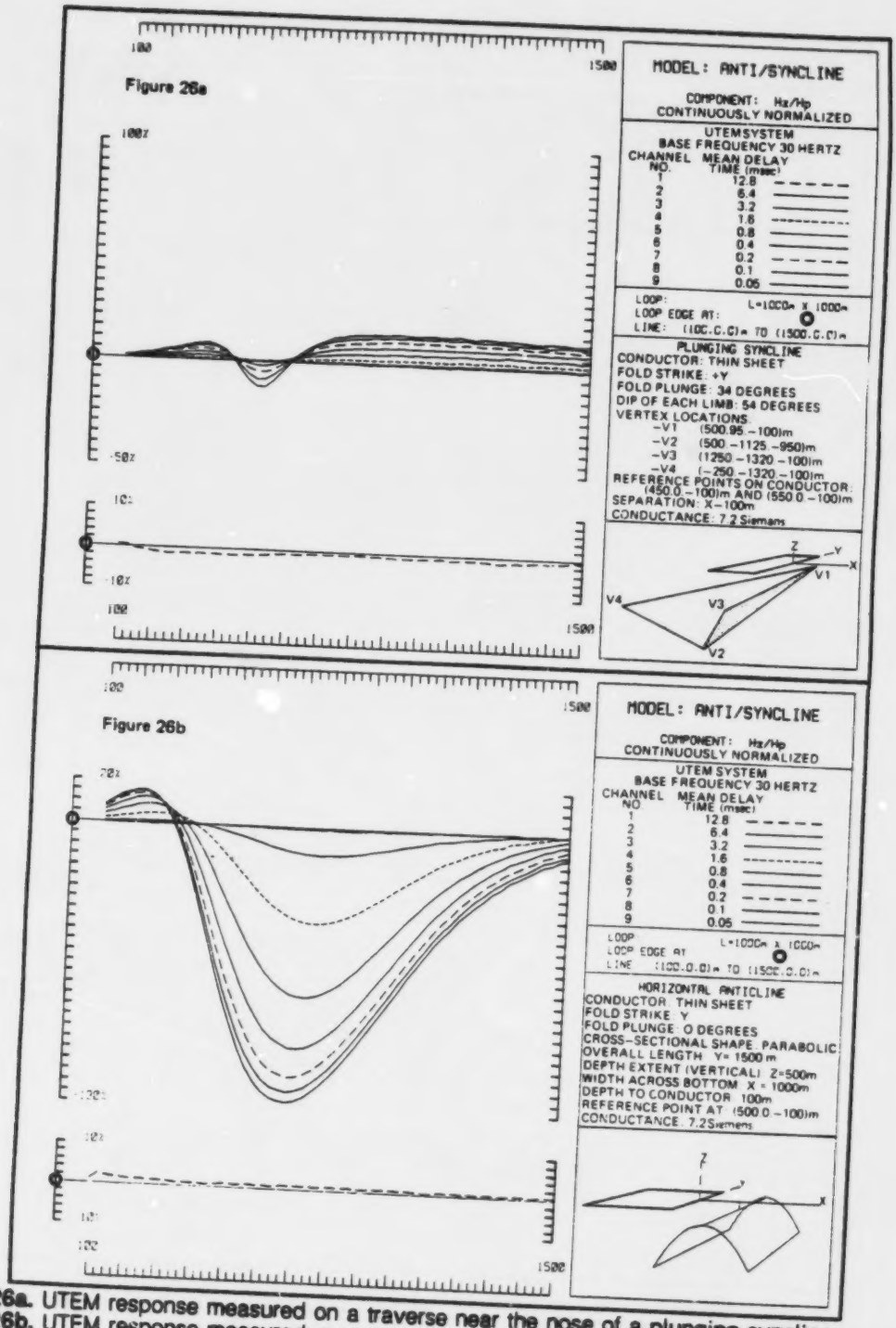

Figure 26a. UTEM response measured on a traverse near the nose of a plunging syncline.
Figure 26b. UTEM response measured on a traverse over a broad anticline.

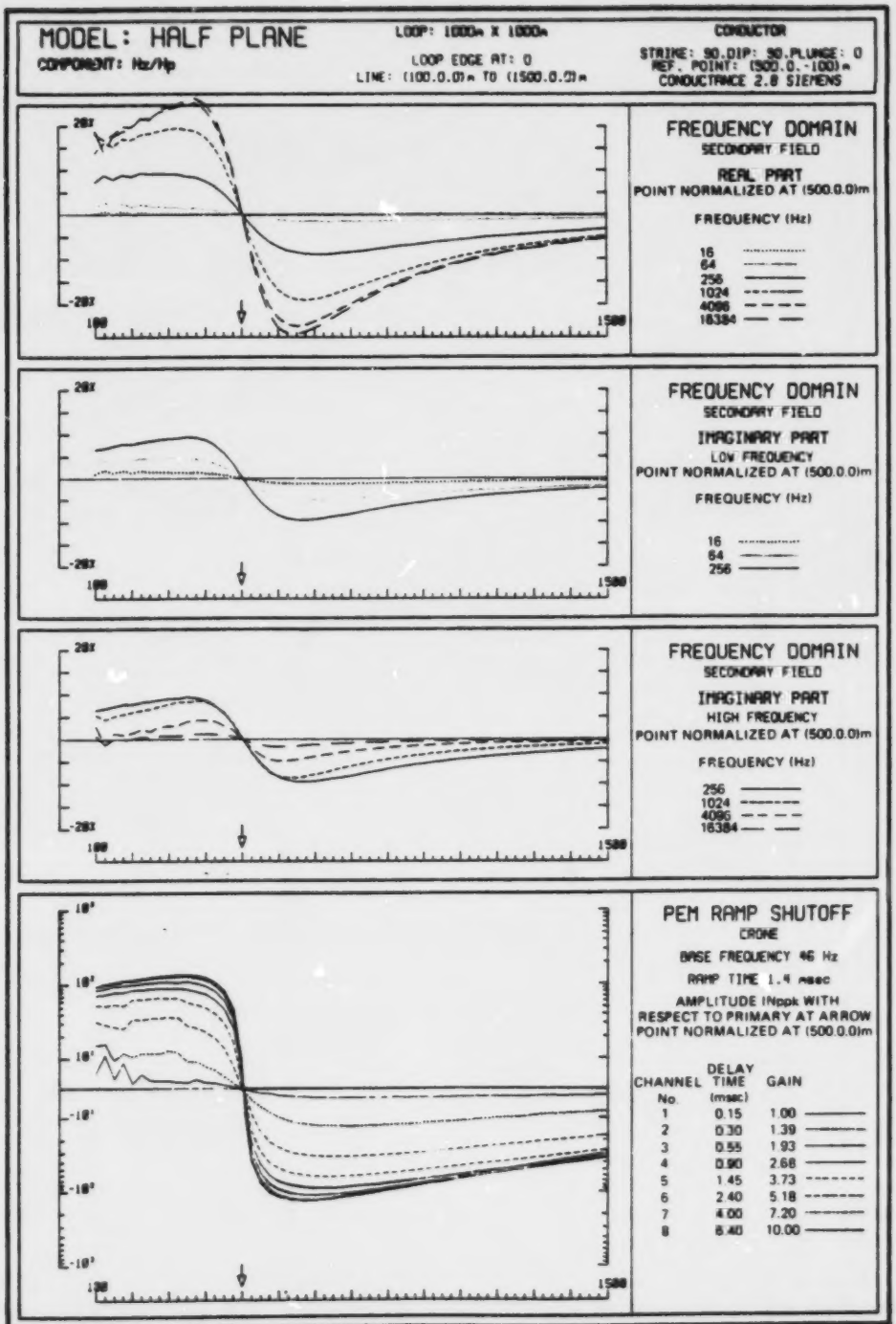

Figure 27. Model responses of Figure 24a transformed into frequency domain (real and imaginary) and into PEM ram shut-off responses.

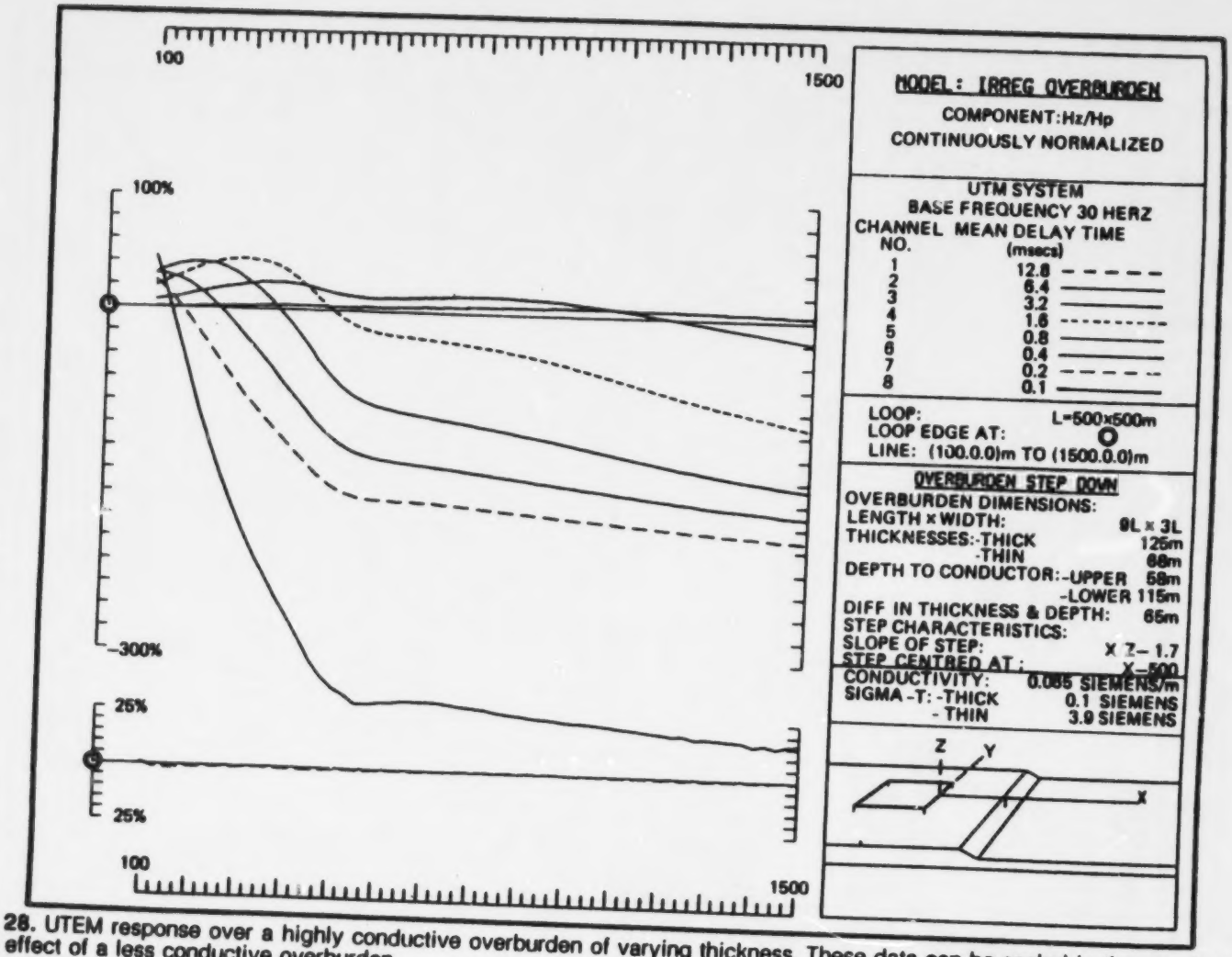

Figure 28. UTEM response over a highly conductive overburden of varying thickness. These data can be scaled in time to obtain the effect of a less conductive overburden.

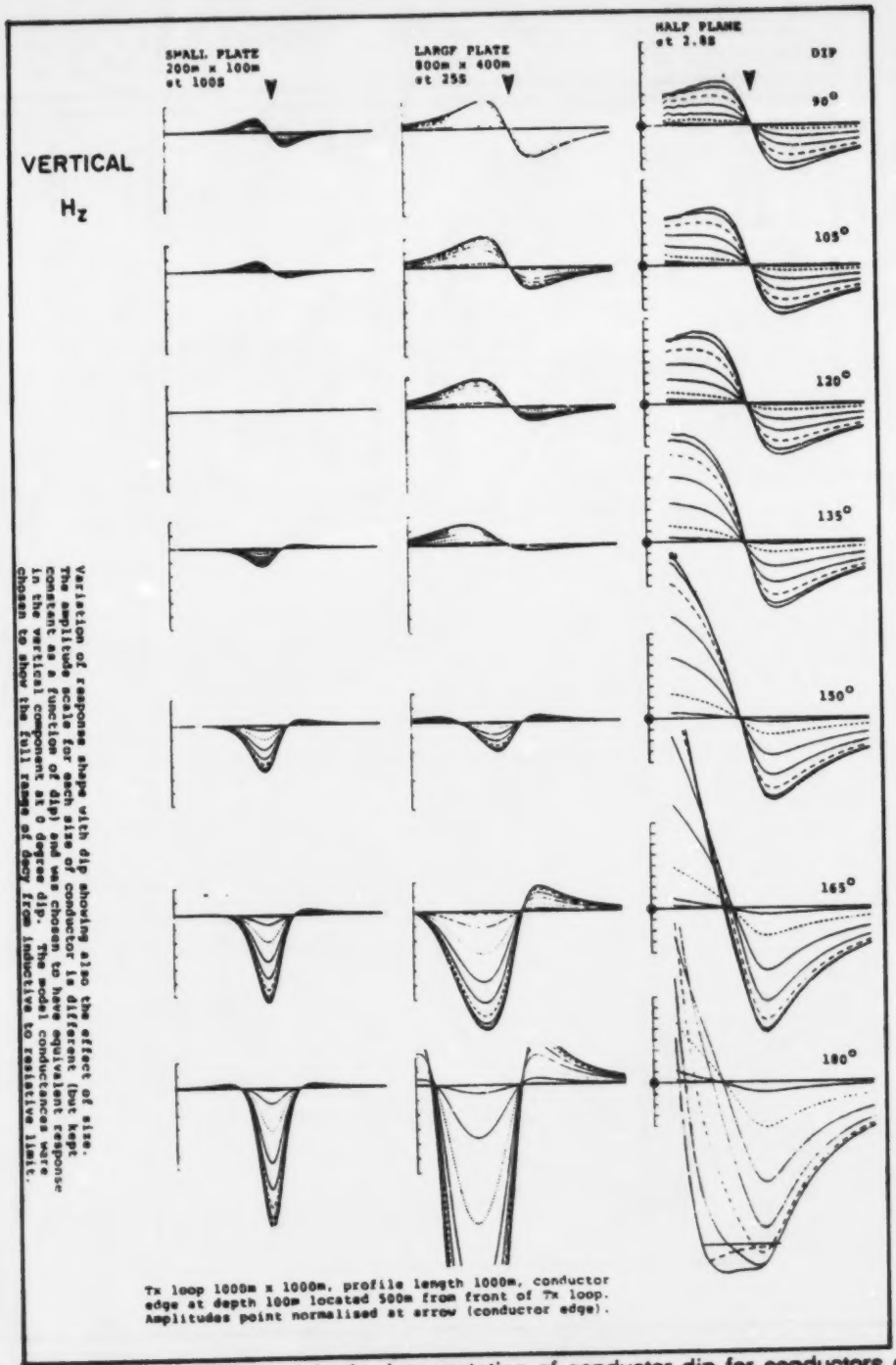
SMALL PLATE
200m x 100m
at 100S
LARGE PLATE
800m x 400m
at 25S
HALF PLANE
at 2.5S
DIP
VERTICAL
H_z
90°
105°
120°
135°
150°
165°
180°
Variation of response shape with dip showing also the effect of size. The amplitude scale for each size of conductor is different (but kept constant as a function of dip) and was chosen to have equivalent response in the vertical component at 0 degree dip. The model conductances were chosen to show the full range of decy from inductive to resistive limit.
Tx loop 1000m x 1000m, profile length 1000m, conductor edge at depth 100m located 500m from front of Tx loop. Amplitudes point normalised at arrow (conductor edge).

Figure 29. Interpretation chart used in the interpretation of conductor dip for conductors of varying sizes.

ACKNOWLEDGMENTS

The development of the borehole system at Lamontagne Geophysics was supported by Cominco Limited, Texasgulf Incorporated, Kidd Creek Mines Limited, St. Joe American Corporation, Sulpetro Minerals Limited, and the Ontario Geological Survey through a Exploration Technology Development Fund (ETDF) grant GR 010 to Lamontagne Geophysics Limited. The careful work of 2 critical reviewers is also gratefully noted.

The early field testing and all software (reduction and interpretation) development involved in these tests were supported by the ETDF program. During the final field trial survey program, the direct field costs were paid for by the Geological Survey of Canada. Alfred V. Dyck, from the Geological Survey of Canada, and Barry Krause of Inco Limited helped us select the boreholes to survey. We thank the geophysical department of Inco Limited for allowing us to use the survey sites and for assistance during the field work.

REFERENCES

Dyck, A.V.
1981: A Method for Quantitative Interpretation of Wide-Band, Drill-Hole EM Surveys in Mineral Exploration; Ph.D. thesis, University of Toronto, available as RAG 23, Geophysics Laboratory, University of Toronto.

Hewlett Packard
1978: Digital Transmission with the HP Fibre Optic System; Application Note 1000, Hewlett Packard, Palo Alto, California.

Lamontagne, Y.
1975: Applications of Wideband, Time-Domain EM Measurements in Mineral Exploration; Ph.D. thesis, University of Toronto, available as RAG 7, Geophysics Laboratory, University of Toronto.

West, G.F., Macnae, J.C., and Lamontagne, Y.
1984: A Time-Domain System Measuring the Step-Response of the Ground; Geophysics, expected publication July 1984.

Grant 011 Development of Computer Software for Geophysical Interpretation

S.W. Reford, N.R. Paterson, and D.J. Misener

Paterson, Grant and Watson Limited, Toronto

ABSTRACT

Computer software has been developed to assist in the interpretation of ground electromagnetometer (EM), airborne spectrometer, and airborne magnetometer data. In addition, a suite of applications and general purpose software has been developed for the IBM Personal Computer. Emphasis has been placed on techniques of direct application to current exploration problems in Ontario. Two programs (SPECMAP and SUSMAP) have been applied to exploration data, and are now in routine use by the mining industry, through Paterson, Grant and Watson Limited. A third program (GEMINV) will soon attain the same status. Work is continuing to further develop these techniques and to test their applicability by means of data sets from a number of well-known areas.

OBJECTIVES

Although numerous programs exist for processing and interpreting geophysical data, many of them have been prepared for research purposes and have limited application to exploration.

With the advent of routine digital recording of multichannel, high resolution, wide-band data sets, and the growing availability of high speed computers (Paterson *et al.* 1982), the need for user-friendly processing and interpretation software is urgent.

The Exploration Technology Development Fund (ETDF) grant was awarded to assist in the development, testing, and application of a variety of software designed to meet the current priorities of exploration organizations in Ontario.

FIELDS OF STUDY

GROUND EM

In 1982, under the same ETDF program, the algorithm AEMINV was developed to perform the inversion of multichannel airborne EM (AEM) data to a halfspace or 2-layered earth model (Paterson *et al.* 1983). Due to the nature of the forward solution, the program could not perform an inversion for the special case when the sensor height approached 0 (i.e. the case for a ground EM survey). After AEMINV proved to give results that were coherent and interpretable, it was decided that a similar program to invert ground EM data should be attempted.

The algorithm GEMINV (formerly SLPI) was developed, in conjunction with R.N. Edwards, University of Toronto. Edwards was also involved in the work on AEMINV.

The software for GEMINV is structured in a similar fashion to that of AEMINV and incorporates the same eigensolution analysis algorithm as well as similar input and output styles. However, there are significant differences between the 2 programs. The forward solution of GEMINV can be adapted to any double-loop configuration. The 'effective radius of the transmitter loop' is specified as an input parameter so that data measured by any system ranging from SLINGRAM (0 radius) to Turam (large radius) can be analyzed. Large, square or rectangular loops may be approximated by a circular loop of 'average' radius if measurements are taken by the receiver sufficiently far from the transmitter loop.

The data are inverted to an n-layer earth model, each layer being of finite thickness except the n^{th} (bottom) layer, which is a halfspace (Figure 1). The improvement of the model from 2 layers for airborne data to n layers for ground data is both valid and feasible. Ground EM data is often measured over a greater number of channels, and the response to local inhomogeneities is more discrete. The multilayer approach allows for greater emphasis to be placed on existing geological and drillhole information. Each finite layer possesses 3 parameters: resistivity, relative permeability, and thickness. The resistivity and relative permeability are specified for the halfspace. Before inversion, initial values for all the parameters of each layer and the halfspace are entered as input by the interpreter. Any number of these parameters may be held fixed or allowed to vary over the course of the inversion. A rule of thumb is that for m free parameters to be calculated accurately, the inversion will require approximately m^2 pieces of measured input data. For example, for amplitude and phase data measured at 2 frequencies (or coil separations), one would allow 2 parameters to vary. To calculate 3 free parameters, one would require in-phase and quadrature values measured at 4, or better still, 5 frequencies. As with AEMINV, GEMINV calculates the eigenvalue and associated eigenvector for each free parameter in order that the interpreter may observe how well-determined each parameter is

and what influence it has on the calculated forward solution. This technique of eigenvector decomposition has been previously described (Paterson *et al.* 1983). Also, the calculated forward solution is compared to the measured data so that one may see the difference for each reading as well as the overall RMS error of the inversion.

GEMINV also differs from AEMINV in the integration method used to calculate the forward solution. Gauss-Laguerre 5-point quadrature integration was utilized by AEMINV. GEMINV uses a method developed by Chave for the numerical integration of related Hankel transforms by quadrature and continued fraction expansion (Chave 1983) which provides a more accurate calculation of the required Bessel functions. This accuracy is necessary because, by its nature, the forward solution for a layered earth model becomes less stable as the sensor height approaches 0. Given the new method of integration, the central processing unit (CPU) time taken on a VAX 11/780 by the GEMINV program for a typical inversion is about 7 times that of its AEMINV counterpart, a necessary sacrifice for the sake of accuracy. The CPU time required by a single inversion varies widely with the number of layers in the model, fitted parameters, and channels of data. The average is on the order of 30 CPU seconds, or $5.00 at current commercial rates, per inversion. Future plans include automation of the program so that a number of inversions may be performed in a single run. This will significantly reduce the cost of processing. The increase in CPU time required by GEMINV may not be significant when one considers that many fewer inversions would be necessary for a typical ground EM survey when compared to an airborne survey.

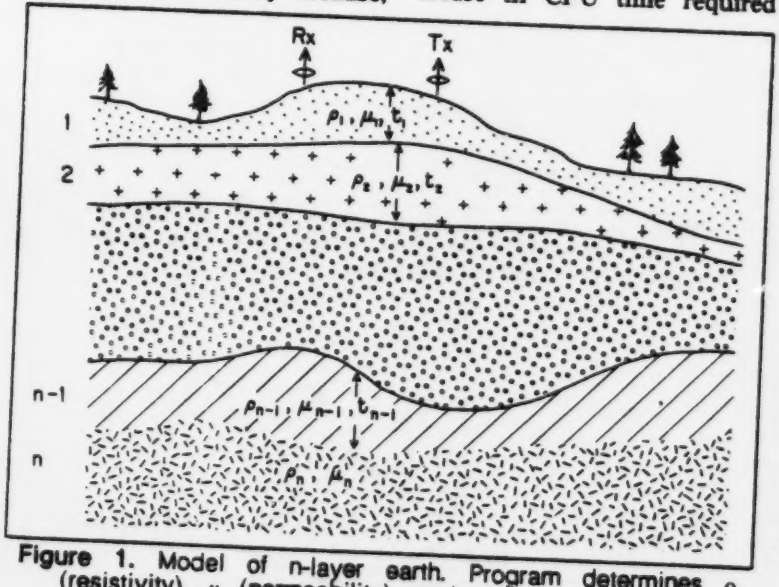

Figure 1. Model of n-layer earth. Program determines ρ (resistivity), μ (permeability), and t (thickness) from, for example, horizontal loop EM data.

Testing of the algorithm was initially conducted on the forward model. Two-and 3-layer models were calculated for various parameters using a standard horizontal loop coil configuration. The results were compared to Eadie's curves (Eadie 1979) and were found to have excellent correlation. Data from certain of Eadie's curves were then inverted. The calculated parameter values were very close to those of the given forward solution.

The Ontario Geological Survey provided real data measured at the Night Hawk Lake test site (Figure 2), from both MaxMin and Turam surveys. Inversion of MaxMin data (at 5 frequencies and 3 coil separations), away from the conductor so as to conform to the layered earth model, resulted in a depth to basement fitted to within 30% of the value obtained through seismic profiling (114 m *vs.* 85 m) (Figure 3).

A good deal of further testing of the GEMINV software is planned for the next year. A variety of model layer configurations will be studied and a number of coil orientations will be tested. Special emphasis will be placed on determining the accuracy and reliability of the method in large transmitter loop situations (e.g. Turam).

It is envisioned that a series of EM soundings will be conducted in the field in an area where the geology is well documented and known to conform to the layered earth

model. It is expected that the data will be acquired by both MaxMin and GEM-5 (or GEM-8) systems. The results will be analyzed using the GEMINV method and will be compared with other geophysical surveys in the area, including, we hope, multichannel airborne EM data.

AIRBORNE SPECTROMETRY

Historically, the interpretation of multichannel gamma-ray spectrometer survey data has required the study of a number of contour maps, which include maps of the intensities of each individual radioelement, and the total count and ratios of the radioelements. Geologically zoning such data can be a tedious and time-consuming task. The more subtle, but perhaps quite important, geological features can easily be missed. A variety of zoning methods have been studied; the use of cluster analysis for example. However, such methods require much hands-on intervention by the geophysicist. To our knowledge, none have been judged to be particularly useful by the exploration industry. A practical and reliable technique of zoning such data, requiring a single map only, would be of benefit to the geophysicist.

The advent of automated colour plotting of geophysical data in recent years has added a new dimension to interpretation. Although a colour plot does not retain all of the information of a contour map, certain aspects are much better defined. The delineation of regional trends in the geology and the correlation of geological units in different locations is facilitated by the use of colour plotting.

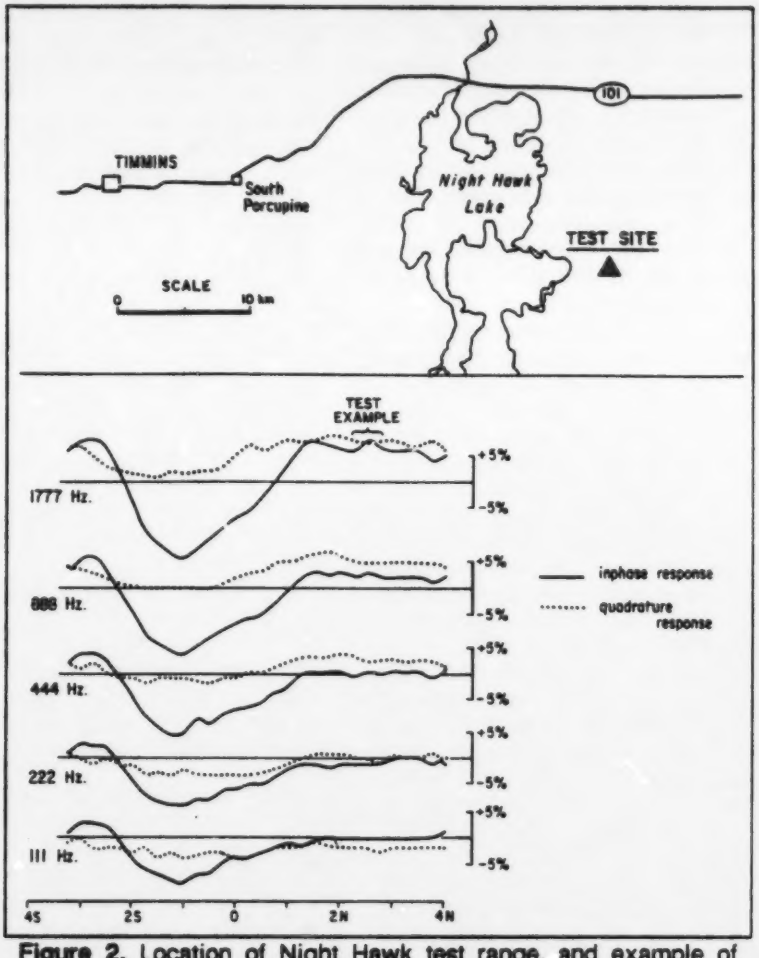

Figure 2. Location of Night Hawk test range, and example of field data from Line 0+00, Night Hawk test range, Ontario, MaxMin III with coil separation of 200 m.

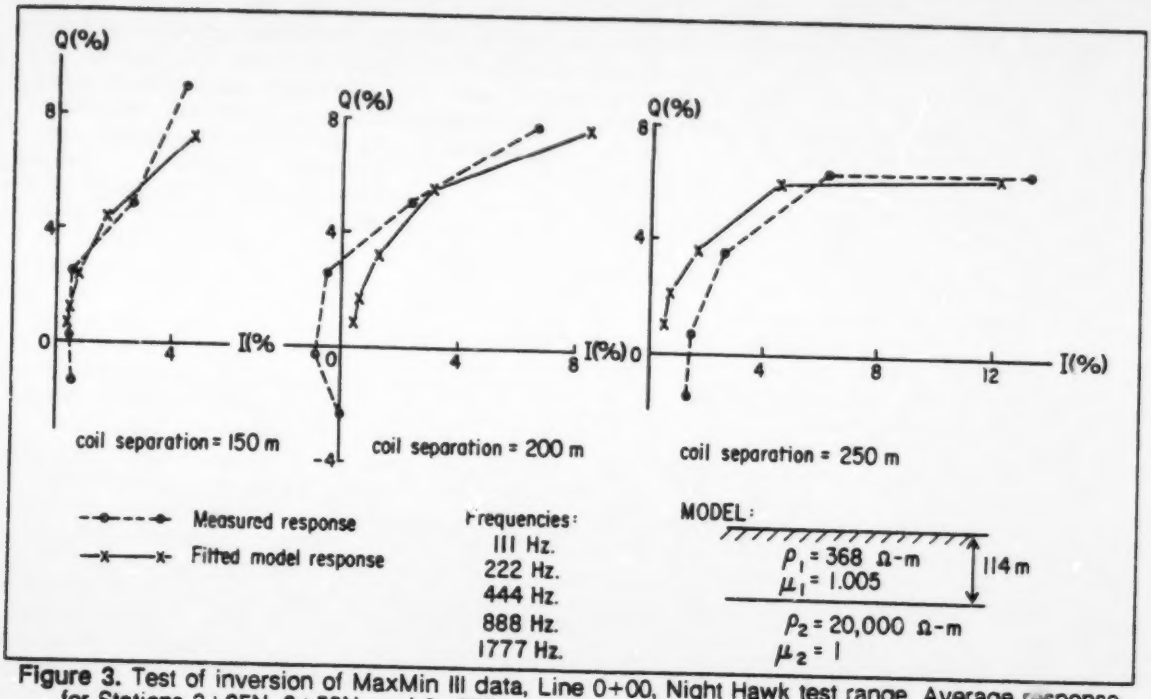

Figure 3. Test of inversion of MaxMin III data, Line 0+00, Night Hawk test range. Average response for Stations 2+25N, 2+50N, and 2+75N.

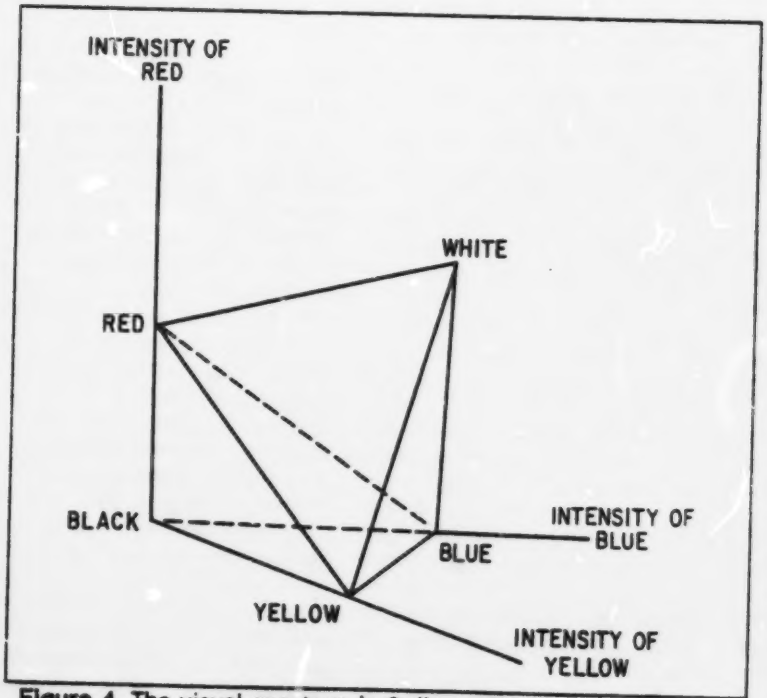

Figure 4. The visual spectrum in 3-dimensional colour space.

The computer program SPECMAP (formerly SPECOLPLT) was developed in cooperation with R.C. Bailey, University of Toronto and Dataplotting Services Incorporated, to plot 3 radioelement gamma-ray spectrometer data on a single colour map, using an Applicon colour plotter. The program is based on the elementary principle of combining the 3 primary colours (red, yellow, and blue). Each of the 3 radioelements (U, Th, K) is assigned a specific primary colour. At a particular data point, the intensity of each of the 3 colours is scaled according to the response of the respective radioelement. The 3 distinct colours are combined in 3-dimensional colour space and plotted at the location of the data point (Figure 4). In this manner, a colour map will show the relative distribution of radioelements at

any one point and their overall intensity.

A geological unit that possesses an anomalously high response in 1 radioelement will appear on the plot as a particular colour. A different unit that is deficient in the same radioelement will be plotted as a different colour. For the situation where 2 units possess the same ratio of radioelements but different overall intensities, the program will produce the same colour, with one unit appearing brighter than the other. By processing and plotting the results of a survey using this program, the interpreter produces a final map which may be zoned according to colour, intensity, and texture.

The Applicon colour plotter uses 3 ink jets, their colours being yellow, magenta, and cyan. These are the 3 primary colours of pigmentation rather than those of the spectrum. The complements of these 3 colours are purple, green, and orange respectively. Figure 5 (see chart, back pocket) shows the range of colour of the Applicon plotter at a medium intensity level, as well as the assignments of the 3 radioelements to the ink colours. The radioelements may be assigned their colours by the 'direct' or 'reverse' methods. For the direct method, the ink colours (yellow, magenta, or cyan) denote a high response for the assigned radioelement whereas the complement colours (purple, green, and orange) signify the lowest response for that radioelement. For example, if a response at a given point were due entirely to uranium, the colour plotted would be cyan. Conversely, orange signifies the presence of thorium and potassium only, no uranium. Combining the 3 radioelements, the highest response areas are plotted as the darkest, the lowest response as the lightest. The assignments for colour and intensity are the opposite for the reverse method; for example a light magenta indicates high values of uranium and thorium with little potassium response.

On the Applicon plotter, each of the 3 ink colours may be plotted at one of 17 intensity levels, ranging from white (no colour) to full colour. Hence, there are 4913 different colour combinations available to the program. The radioelement responses at each data point are plotted in a pixel 0.8 mm square. Consequently, the data must be gridded at a specific interval, depending on the map scale desired.

The satisfactory presentation of spectrometer data in contour form is particularly sensitive to leveling errors. Poor leveling of the data is even more apparent on colour maps because of the conspicuous colour striping. This can occur very easily when more than 1 radiometric sensor is used on a survey and when the spectrometer(s) is (are) not properly calibrated. It was found during testing and production use of SPECMAP that this technique reduces such leveling discrepancies when all 3 radiometric channels 'drift' coherently. Once the data has been leveled satisfactorily, filtering/splining along the flight-lines is necessary to prevent streaking on the map perpendicular to the flight direction. This is especially important when the flight-line separation is much larger than the grid interval.

The survey data input to the program is normalized to a window specified by the user for each of the 3 radioelements. All values lying outside these windows are set to the minimum or maximum. The entire dataset is then normalized (when intensity information is required) to determine the 'brightness factor', so that the resultant map will show a distribution over the entire range of available colours. The user may specify 2 exponential factors that regulate the amount of colour and intensity variation on the map.

Initial testing was conducted on a dataset acquired by the Geological Survey of Canada in the Sharbot Lake area, Ontario. The data were processed and plotted, at 1:50 000 and 1:200 000 scales, a number of times, varying the colour scales and exponential factors, and using both the direct and reverse methods of colour assignment. Maps with both intensity and no-intensity (relative radioelement distribution only) information were produced. One result of this testing was to reduce the colour scale from 17 to 13 intensity levels by omitting the darkest 4 levels, as it is more difficult for the human eye to differentiate between dark colours than light colours.

The final map of the Sharbot Lake dataset was plotted using the reverse method of colour assignment (the highest response equivalent to the lightest colours). The exponential factors used increased the colour variation and reduced the intensity range. The resultant colour plot showed quite good correlation with the mapped geology. It was also apparent that for some rocks grouped as a single unit on the geological map, their radiometric signature varied across the area.

The second test dataset was measured by the Geological Survey of Canada in the Hearne Lake area, Northwest Territories. It was chosen because of the relatively large amount of outcrop in the area. Figures 6, 7, and 8 (back pocket) show the corrected U, Th, and K intensity maps respectively, for the survey area. One can see a large variation in the anomalies from radioelement to radioelement. Conventional methods would require zoning of these 3 maps and most likely ratio maps as well, a cumbersome task.

The colour plotting program was first applied to the data without taking into account the intensity of the radioelement responses. The reverse method of colour assignment was used. In other words, a map that shows only the relative distribution of the 3 radioelements was produced (Figure 9, back pocket). The reader should refer to Figure 5 to correlate the colour with the radioelement distribution. The map does not reflect intensity, except in the areas of the pure colours (yellow, magenta, cyan, and white), where the response of 1 or more of the radioelements is greater than the upper bound of the corresponding normalization window.

The map shown in Figure 10 (back pocket) is the colour plot of the same area that includes the intensity information and is the final product of the program. The exponential factors discussed previously have been applied so as to enhance the colour variation and decrease the intensity variation. The light areas are those of highest radiometric response and the dark areas the lowest response. The bright colours indicate a significant response to 1 or 2 radioelements. Comparing this map to the previous map, one can see that little is lost in the colour but much is gained in the intensity information.

Figures 9 and 10 show not only the distribution and intensity colour plots, but also a simplified version of the Geological Survey of Canada mapped geology on the former and a typical zoned interpretation on the latter. There are both similarities and differences between the mapped geology and the zoning. The dark units marked 'L' on the zoned map are lakes. Some of the other dark units may be the response to water (e.g. swamps) but this could not be definitely determined. Radiometric Unit A, rich in uranium and potassium, shows a good correspondence with geological Unit 11. Unit B, rich in uranium and thorium appears to correlate with Unit 1. Unit C and Unit 2 appear to be the same. The low response of Unit 2 would not have been apparent without the intensity information. Unit D is rich in thorium and potassium; it is mapped as both Units 4 and 9. Much of the rest of Unit 4 shows a medium potassium response and is zoned as Unit E. It does not appear that the boundaries between Units 4a and 4b can be determined by their radiometric signature. Unit F is a small uranium-rich body that is not delineated on the geological map. It could be a volcanic or intrusive feature or a zone of alteration. Unit G is a circular, potassium-rich structure mapped as part of Unit 9. However, the radiometric response suggests that it is its own distinct geological unit.

The SPECMAP technique of geologically zoning radiometric data is a significant improvement over conventional methods. The interpreter can perform his task much quicker, without foregoing accuracy. A single colour map allows for the correlation of similar radiometric units in different parts of a survey area. In the case of overburden attenuation of the radiometric signal, a reduction in intensity (darker) would be seen on the map. However, the colours would remain the same as the relative distribution of the radioelements would not be greatly affected. The correlation between the radiometric zones and the mapped geology suggests that this technique will aid the interpreter both to interpret lithology in unmapped areas and/or to recognize lithofacies that do not show up on reconnaissance mapping. To date, this technique has been applied successfully to 2 large-scale, regional interpretations of radiometric data measured in West Africa.

MAGNETIC INTERPRETATION (SUSCEPTIBILITY MAPPING)

During the 1982 to 1983 fiscal year, the SUSMAP (formerly SDSUSC) technique was introduced (Paterson *et al.* 1983). It is a spatial domain procedure that permits a depth to be assigned to each grid point of an X-Y gridded dataset. The magnetic susceptibility is varied iteratively at each point until the calculated field on the surface of measurement is equal to the measured field. The program had been developed to the point that it had been successfully implemented in production work.

Two application subroutines have been written during this fiscal year as additions to the SUSMAP software. The al-

gorithm of the subroutine GENER generates the total magnetic field, or its derivatives, on any general surface above the source surface. It facilitates the calculation of a constant barometric field from a recorded 'drape' flown aeromagnetic survey, or vice versa. The input values of susceptibility for each prism are those calculated by SUSMAP from the original recorded field.

The second application algorithm is a high frequency filter operator (HIFILT) that will be applied to the original total field data, before susceptibility values are calculated, in order to reduce the high frequency 'noise' from sources shallower than the main magnetic basement that may cause incorrect values of susceptibility over individual grid cells. The 'cut-off' point for the application of the filter is determined by comparing the actual second vertical derivative of the recorded field over a prism to the theoretical value for the second derivative for a prism at the given depth.

PERSONAL COMPUTER SOFTWARE

The company has been applying the IBM Personal Computer to geophysical problems for the past 2 years, particularly for forward modeling and general processing of ground geophysical data. Some of the software has been developed under the ETDF program during the past year. It is written for the general manipulation of geophysical line data. A very simple standard text-file format is used for the data so that any typical text-file editor may be employed. This ensures compatibility between applications and utilities software, such as that for line plotting or filtering. All the software is now written in PASCAL.

Two data reduction programs have been developed. GRAVRED carries out the standard gravity reductions, including calculation of the Bouguer anomaly. It also includes conversion from UTM coordinates to latitude and longitude. TURAMCOR calculates the reduced ratio values and secondary field components for any Turam EM loop configuration. For processing purposes, the program SPLINE will spline profile data to a specified increment using either a cubic or Akima spline.

A good deal of general purpose software has also been developed. PASGRAPH is a powerful, versatile, and device-independent virtual graphics language to support PASCAL graphics on the IBM Personal Computer and compatible systems. More than 25 graphics commands support windows, viewports, automatic scaling, and many device characteristics.

The program GRAPHED plots any number of profiles from a standard line file onto the graphics screen. It allows for the creation of new profiles by the manipulation of existing profiles. PROJECT will project a given profile from its recorded X and Y coordinates onto a specified plane and is used in conjunction with 2-dimensional modeling programs.

Under the ETDF program, a 6-pen colour plotter, the MP1000 manufactured by Watanabe Instruments Corporation, was purchased. Using the plotter's command language and PASGRAPH software, the program PLOTLINE was written on the IBM Personal Computer to plot data of the standard line-data format in profile form. The program is menu-driven and provides the user with a number of options as to scale, size, colours, labels, symbols, number of profiles, etc. PLOTLINE has been adapted to automatically plot the results of magnetic and gravity inversion modeling (the MAGMOD and GRAMOD methods) computed on the mainframe.

Extensive software devlopment is planned on the IBM Personal Computer. It is expected that programs for the inversion of magnetic and gravity data, existing on the mainframe and written in FORTRAN, will be downloaded to the IBM Personal Computer. Software to grid the observed ground line data and to display it on the graphics screen as a colour plot will be written. A suite of 1-dimensional frequency-domain and numerical filters to be applied to line data are being implemented. In addition, existing software will continue to be revised and improved. The company is in the process of making all of the above software available to the exploration community through a marketing program under the tradename GEOSOFT.

FUTURE PLANS

A new ETDF grant has been awarded to the company to further test and evaluate the above and earlier-developed interpretation programs. Some additional development will also be undertaken in the areas of inverse magnetic modeling and joint inversion of multiple datasets.

It is intended that the application (and limitations) of

the newly-developed software will be fully determined and presented to the exploration community in the form of well-documented case histories. Papers on SPECMAP and SUSMAP are planned for the December 1984 meeting of the Society of Exploration Geophysicists in Atlanta, Georgia.

ACKNOWLEDGMENTS

The company is grateful to the Ontario Ministry of Natural Resources for its financial assistance, and for the cooperation of the staff of the Ontario Geological Survey in various aspects of the work, including the provision of test field data.

The authors wish to thank the Geological Survey of Canada for permission to publish examples from studies made in the Hearne Lake area, Northwest Territories. We also acknowledge the important contribution of Dataplotting Services Incorporated in the development of the SPECMAP program.

The following also made valuable contributions to the work described in this paper: R.N. Edwards, R.C. Bailey, P.W. Walker, M. Holroyd, I.N. MacLeod, F.S. Grant, C.V. Reeves, M. Sahib, and R.M. Blaiklock.

SELECTED REFERENCES

Chave, Alan D
1983: Numerical Integration of Related Hankel Transforms by Quadrature and Continued Fraction Expansion; Geophysics, Volume 48, p.1671-1686.

Eadie, Tom
1979: Stratified Earth Interpretation Using Standard Horizontal Loop Electromagnetic Data; Research in Applied Geophysics Number 9, Geophysics Laboratory, Department of Physics, University of Toronto, October 1979.

MacLeod, I.N.
1984: IBM Personal Computer Software; Brochure for GEOSOFT: Software for the Earth Sciences, January 1984.

Newton, A.R., and Slaney, V.R.
1977: Geology of the Hearne Lake Area; map *in* Geological Survey of Canada Paper 77-32.

Paterson, Norman R., Grant, F.S., and Misener, D.J.
1983:Grant 011 Development of Computer Software for Geophysical Interpretation; p.53-61 *in* Exploration Technology Development Program of the Board of Industrial Leadership and Development, Summary of Research 1981-1983, edited by E.G. Pye and R.B. Barlow, Ontario Geological Survey, Miscellaneous Paper 115, 135p.

Reford, Stephen W., Misener, D.J., and Paterson, N.R.
1983, 1984: Development of Computer Software for Geophysical Interpretation; 1984 Progress Reports, Paterson, Grant and Watson Limited, July 1983, October 1983, January 1984.

Reford, Stephen W., and Paterson, N.R.
1984: New Development of Computer Software for Geophysical Interpretation; Computer Applications in Mineral Exploration 1984, January 9-11, 1984, Toronto, Program with Abstracts, p.27-29. Preprint available from authors.

Grant 012 A) Determination of Short-Lived Isotopes by Neutron Activation Analysis and B) Investigation of Commercial Viability of Prompt Gamma Analysis

E.L. Hoffman, A. Pidruczny, S. Landsberger, and W. Hutton

Nuclear Activation Services Limited, McMaster Nuclear Reactor, Hamilton

ABSTRACT

The following report will be subdivided into 2 separate sections, prompt gamma activation analysis (PGAA) and short-lived neutron activation analysis (SLNAA), owing to the very different nature of these projects.

The development of the short-lived neutron activation analysis facility will be described in Section A. This system is currently operating and is providing commercial analyses for certain, selected, trace elements as well as in a multielement mode. A low-cost group of multielement analysis packages have been developed over the past year and data outlining these packages are included.

The prompt gamma facility will be described under Section B. Automation of the prompt gamma facility has now been completed. Upon the arrival of teflon capsules, which we are having manufactured for us, Nuclear Activation Services Limited (NAS) will begin offering low cost, high quality prompt gamma analyses.

A) SHORT-LIVED ACTIVATION ANALYSIS

INTRODUCTION

Neutron activation analysis involves the bombardment of samples by neutrons produced in a nuclear reactor. The neutrons induce nuclear reactions among the elements in the sample, leading in many cases to the formation of radioactive isotopes. As these radioisotopes decay, they emit characteristic radiation which is usually unique to a particul r element. The measurement of the emitted radiation is achieved using high resolution, hyperpure germanium detectors linked to multichannel analyzer-computer systems. These systems can adequately resolve the complex multielement gamma-ray spectra obtained from the activated sample.

The advantage of the technique is that the method can be very accurate, with detection limits for many elements being much lower than those obtained by conventional techniques such as plasma emission, atomic absorption (both flame and flameless), or X-ray fluorescence. Instrumental Neutron Activation Analysis (INAA) is also a multielement technique where quantitative information can be obtained simultaneously on as many as 35 elements, all of this instrumentally with no chemical treatment required, eliminating the problems attendant to chemical treatment. All this can be achieved in a reasonable time frame and at a competitive price relative to other analytical techniques.

As previously described, activation analysis involves the measurement of radiation emanating from an activated sample. One of the factors which governs the delay time after irradiation before counting the sample, is the radioisotopes' half-life. The half-life for different radioisotopes can vary from a fraction of a second to many years. Most of the work done by NAS prior to this Exploration Technology and Development Fund (ETDF) program involved mainly the so-called long-lived isotopes which have half-lives of the order of hours, days, and years. These samples could be batch irradiated and are usually counted 4 to 8 days after irradiation.

The determination of short-lived radioisotopes on the other hand, or those with half-lives of seconds to minutes, involves a different type of procedure. The samples must be irradiated for a brief period, usually a few seconds. The sample which is contained in a 'rabbit' (polyethylene capsule) is then transferred to a high resolution detector for immediate counting. The multielement gamma spectrum obtained is then analyzed.

The technology we have developed by designing, building, and operating our computer-automated delayed neutron counting facility was used extensively in the design of our new transfer system essential for the short-lived radioisotope determinations. With this system, samples are transferred from a sample loader station through a maze of polyethylene tubing to an appropriate sample irradiation facility. After a brief period, usually a few seconds, the sample is transferred to the sample receiving station at the detector where the gamma radiation of the sample will be counted. For certain samples it may be advantageous to wait a few minutes after irradiation to let certain highly active

TABLE 1: MULTIELEMENT CORE PACKAGES WITH DETECTION LIMITS BY INSTRUMENTAL NEUTRON ACTIVATION ANALYSIS.

ELEMENT	DETECTION LIMITS BASIC	EXPLORATION	RESEARCH
As ppm	10	2	1
Au ppb	100	20	5
Ba ppm	1000	150	20
Br ppm	5	1	0.5
Co ppm	5	1	0.1
Cr ppm	10	2	0.5
Cs ppm	2	0.5	0.2
Fe %	0.2	0.05	0.005
Hf ppm	1	1	0.2
Mo ppm	10	5	2
Na ppm	500	100	30
Ni ppm	500	200	50
Rb ppm	100	20	5
Sb ppm	0.2	0.2	0.1
Se ppm	10	3	0.5
Sr ppm	1000	500	100
Ta ppm	2	1	0.5
W ppm	10	3	1
Zn ppm	50	20	5
RARE EARTH ELEMENTS			
Sc ppm	0.5	0.1	0.01
La ppm	1	0.5	0.1
Ce ppm	5	3	1
Nd ppm	20	10	3
Sm ppm	0.5	0.1	0.01
Eu ppm	0.5	0.2	0.05
Tb ppm	-	-	0.1
Dy ppm	0.5	0.5	0.5
Yb ppm	2	1	0.05
Lu ppm	0.2	0.05	0.01
U ppm	5	0.5	0.1
Th ppm	1	0.5	0.2

radioisotopes die away before counting. This can be done with our system by programming in a delay-to-count time. All of the above operations are done under microprocessor control with very little human interaction. The transfer system is linked to a Canberra Series 85 multichannel analyzer which is linked to a PDP 11/44 computer.

PROGRESS REPORT AND ANALYTICAL CAPABILITIES

The past year has seen the very successful conclusion to the development of our short-lived activation project. Over the past year, substantial modifications have been made to our computer system. Our operating system has changed from RSX11/M V3.2 to RSX11/M V4.0. In addition, additional computer disc storage capacity has been added to give us a 340 megabyte capacity. This has been done to increase the speed of analysis and ability to store spectra necessary for providing low cost multielement analyses. Programming modifications were continually being undertaken to optimize and improve the basic data acquisition and analysis systems. The technology we have developed with this project has allowed us to also develop a variety of multielement packages using the data reduction programs.

Table 1 is a list of 3 levels of analyses developed for mineral exploration purposes. The core package consists of as many as 31 elements. In addition to the elements listed, we are currently working at adding an additional 4 elements at no additional cost. To this core package, we have developed a variety of options which can allow for the analysis of up to 50 elements by neutron activa-

tion and an additional 21 elements by a combination of DC plasma or X-ray fluorescence. The activation analysis elements which can be added as options are listed in Table 2.

In addition to the multielement packages listed in Tables 1 and 2, the analytical software has also allowed us to develop a low level biogeochemical prospecting package using vegetation as a sampling medium. This allows the analysis of vegetation without ashing, and one can readily see background levels with a great degree of certainty. This package is listed in Table 3.

TABLE 2: OPTIONAL SHORT-LIVED ELEMENTS WHICH CAN BE ADDED TO THE PACKAGES IN TABLE 1.

ELEMENT	DETECTION LIMIT	ELEMENT	DETECTION LIMIT
Al ppm	10	Mg %	0.05
Ca %	0.2	Mn ppm	0.1
Cl ppm	50	Re ppm	1
F ppm	50	Si %	0.1
Ga ppm	10	Sr ppm	50
Ge ppm	100	Ti ppm	30
I ppm	0.5	V ppm	0.1
In ppm	0.03		

Elements, listed in Table 1, which are also available using the short- lived isotopes include Ba, Br, Hf, Se, Zn, Eu, Dy, U, and Th.

B) PROMPT GAMMA ANALYSIS

INTRODUCTION

Prompt gamma neutron activation analysis is based on the detection of gamma-rays emitted by samples during neutron irradiation. To utilize this technique, a beam of neutrons from the core of the reactor is obtained using a beam port. The sample is encapsulated in a teflon container and is then placed in the beam of neutrons. Interaction of the neutrons with the sample yield prompt gamma-rays which are measured with a hyperpure germanium detector connected to a conventional multichannel analyzer-computer system.

The prompt gamma technique has several advantages. Since the response for all elements is instantaneous, all elemental contributions occur independent of timing. No *a priori* information regarding sample content is needed since it is not necessary to adjust irradiation and counting period parameters. There are also no half-life limitations; the gamma-rays continue to be

TABLE 3: BIOGEOCHEMICAL EXPLORATION PACKAGE USING VEGETATION AS A SAMPLING MEDIUM.

ELEMENT	DETECTION LIMIT	ELEMENT	DETECTION LIMIT
Au ppb	0.1	Mo ppm	0.05
As ppm	0.01	Sb ppm	0.01
Ba ppm	20	Ta ppm	0.2
Br ppm	0.01	U ppm	0.02
Cr ppm	0.3	W ppm	0.01
Co ppm	0.3	Zn ppm	2

Additional elements are available on request.

emitted as long as the sample is being irradiated. All elements interact more or less, so the method is suitable for multielement analysis in geological samples. The method is particularly advantageous in those cases where neutron capture produces no suitable radioisotope for normal activation analysis. Some of the elements which have good potential by this method are Cd, Ni, Si, C, H, Ti, Fe, Cr, B, N, Al, Cu, Gd, and Nd.

DESCRIPTION OF THE PROMPT–GAMMA NEUTRON ACTIVATION ANALYSIS FACILITY

Original development of this facility was initiated in the Physics Department at McMaster University and continued in the McMaster Isotopic and Nuclear Geochemistry Studies (MINGS) research group with the cooperation of McMaster Nuclear Reactor personnel. The feasibility of constructing a dedicated facility which could be used for commercial analytical purposes has been undertaken over the past 3 years. The development as a geochemical research facility has now been extended to commercial applications, through agreement between D.R. Smith, Director, McMaster Nuclear Reactor, D.M. Shaw, of the MINGS research group, and Nuclear Activation Services Limited (NAS), now that the feasibility stage has been completed successfully.

The prompt gamma system involves the extraction of neutrons from a beam port at the 2 MW McMaster Nuclear Reactor. A fairly well thermalized neutron flux of 6×10^7 ns^{-1} cm^{-2} is obtained by filtering out the fast neutrons and gamma-rays by using a combination of silica and sapphire crystals. A more complete description of the beam system is given by Hoffman *et al.* (1983). The sample is placed in front of the neutron beam and the prompt or instantaneous gamma-rays emitted by the sample are detected by an intrinsic germanium detector-MCA-computer network.

Over the past year various modifications have been made to the instrument as described by Hoffman *et al.* (1983). These have included the enlargement of the 'cave' surrounding the neutron beam port to allow easier access for detector inspection and maintenance. Both an interchangeable manual and automatic sample irradiation facility for the prompt gamma have been installed. A lot of time was spent over the past year in obtaining an appropriate irradiation end. A variety of materials were machined and tested. The final choice turned out to be an irradiation end machined from teflon. Although this material is still not ideal, as it contains low levels of boron, it is acceptable. We will, however, continue to try and obtain a lower background material. The transfer system itself was installed and tested successfully over the past year. The design for the teflon capsules for use in the system has been completed. We are awaiting shipment of the capsules from our vial fabrication firm at this time. The computer modifications mentioned previously have allowed us to begin accumulating and analyzing the spectra. On arrival of our teflon vials, NAS will begin offering low cost prompt gamma analyses.

ANALYTICAL PERFORMANCE OF THE SYSTEM

Over the last 3 years, we have determined that the ultimate sensitivity of the prompt gamma system is about 0.1 ppm for boron and gadolinium. With the system automation, these detection lists are degraded and would be about 0.5 ppm. This limit however is still far better than that obtainable with other analytical methods. Detailed values for international standards have been included in Hoffman *et al.* (1983).

A variety of projects involving the MINGS group have been progressing over the past year. These have included a project on the boron content of the earth, boron in feldspars, boron associated with gold deposits, boron in sedimentary rocks, and the oceanic budget of boron. A more complete description of these programs are available in Higgins and Shaw (1983).

CONCLUSIONS

The last year saw the successful conclusion to this program. A wide variety of trace elements have been added to the repertoire of elements NAS has been analyzing by neutron activation analysis. The bulk of these additional elements have been those with short half-lives or those determined by prompt gamma analysis.

A variety of multielement packages have been developed for analyzing geological samples which can include up to 50 elements by INAA and PGAA. In addition, the computer software we have developed have allowed us to improve detection limits quite substantially for a number of elements, and particularly for biogeochemical samples.

It is our opinion that the commercial activation analysis facilities we have developed are unrivalled anywhere in the world.

REFERENCES

Higgins, M.D., and Shaw, D.M.
1983: Boron Abundance and Distribution in the Mantle, and the Bulk Boron Content of the Earth; Geological Association of Canada, Program with Abstracts 8, A32.

Hoffman, E.L., Ernst, P.C., Pidruczny, A., Hutton, W., Higgins, M.D., Truscott, M.G., Shaw, D.M., Bergeron, M., Buffet, G.H., Copley, J.R.D., and Prestwich, W.V.
1983: A) Determination of Short-Lived Isotopes by Neutron Activation Analysis and B) Investigation of Commercial Viability of Prompt Gamma Analysis; p.63-69 *in* Exploration Technology Development Program of the Board of Industrial Leadership and Development, Summary of Research 1981-1983, edited by E.G. Pye and R.B. Barlow, Ontario Geological Survey, Miscellaneous Paper 115, 135p.

Grant 014 The Design of a New Digital Pulse EM Receiver

G.J. Bogden and H.P. Grunenberg

Crone Geophysics Limited, Mississauga

ABSTRACT

The current trend in mineral exploration is towards deeper and more subtle targets. To adequately resolve such deep conductors, not only more data but more noise-free data is necessary. To meet this goal a new Pulse Electromagnetic (EM) receiver has been designed. By taking advantage of new digital technology, the new instrument provides much greater capabilities in terms of anomaly resolution and noise discrimination.

The unit features advanced microprocessor-controlled data sampling and collection. Noise-biased samples are rejected based on threshold detection and automatic gain controls to optimize the signal-to-noise ratio. The unit is compatible with existing Pulse EM systems and may be reprogrammed for virtually any channel configuration.

INTRODUCTION

For nearly a decade the Crone Pulse EM has proven itself a reliable, efficient exploration tool. Recent exploration activity, however, has determined and drilled many of the more obvious mineral targets. For new mines to develop we are forced to look not only deeper but in more complex, highly conductive geological environments.

With the introduction of the Crone 2000 watt Pulse EM transmitter in 1978, the standard Crone Pulse EM system became capable of detecting subsurface conductors at depths in excess of 450 m. The broad, subtle anomalies characteristic of such deep targets however, do not pin-point the conductor's position with sufficient accuracy for drilling. This inaccuracy is further amplified when the target exists in, or near to, a highly conductive environment and is masked or over-printed by the background response.

Coupled with these problems, transient noise from atmospherics often make anomalies very difficult to resolve. Consequently, to aid interpretation, not only more data but more noise-free data is necessary. As the amount of data increases, so does the time required for aquisition and processing. This can become quite costly both in money and man-hours, especially if this vast amount of information is to be recorded and plotted manually.

In an attempt to increase the efficiency of data aquisition and reduce processing costs, the Crone Datalogger was introduced in early 1982. The unit combines the standard Crone Pulse EM receiver with a data logging unit which monitors the input signal and records all 8 time channels simultaneously. The integrated analog-to-digital converter allows a 4 digit reading accuracy. The values are stored in solid-state memory and are output via a serial data port to a field computer for processing.

In spite of the improvements to the receiver with the development of the Datalogger, certain limitations still exist:

1. the statistical reading error is not available
2. the reading accuracy is reduced in electromagnetically noisy environments
3. the memory capacity is limited

Considering these problems and restrictions, significant improvements to the receiver can be made by taking advantage of new digital technology. Such improvements would result in the collection of more data with greater accuracy. This would increase anomaly resolution for deep targets and improve the discrimination of possible targets in areas with transient, coherent, and geological noise.

PRIMARY OBJECTIVES

The primary objective of our research program was to develop a new digital Pulse EM receiver, fully compatible with the existing system which would:

1. improve the quality of field data without increasing the signal energy
2. minimize the effects of transient and coherent noise
3. remain highly flexible so that certain parameters, such as the time base and/or the number of time gates, can be varied upon request
4. transfer data quickly and accurately with little or no operator intervention
5. improve the ease, speed, and quality of subsequent processing of the field data

INSTRUMENTATION

HARDWARE FEATURES

Microprocessor

To satisfy our design criteria the new Pulse EM receiver is controlled by an 8-bit NSC800 microprocessor.

ROM and RAM

Programs for the instrument reside in 8K of read-only memory (ROM) with 16K of random-access memory (RAM) required for execution. Data

storage is allocated to the remaining 40K of RAM.

Input/Output Facilities

The internal input/output (I/O) board supports a full alphanumeric keypad and a 2-line 32-character liquid crystal display (LCD). The LCD 'echoes' all entries from the keypad and can monitor all recorded data. The display is heated to permit operation to -40°C. An integrated 24 character dot matrix printer serves as an auxilliary data check and provides a hardcopy backup of recorded data. An RS-232 serial interface port allows data to be transferred to a field computer directly or via modem for processing.

Math Processing

A 64-bit math board facilitates high-speed arithmetic, used in data sampling and statistical analysis.

Analog-to-Digital Converter

The input signal detected at the receiver coil is amplified then digitized using a 16-bit analog-to-digital (A/D) converter.

Synchronization

A low-power crystal clock oscillator maintains complete synchronization between the transmitter and receiver. Auxilliary radio and cable link facilities have also been included.

All the boards including the central processing unit (CPU) are interconnected by an external 8-bit data bus. Because the devices are of complementary metal-oxide semiconductor (CMOS) construction only a 12 volt DC rechargeable battery supply is required to power the unit. A

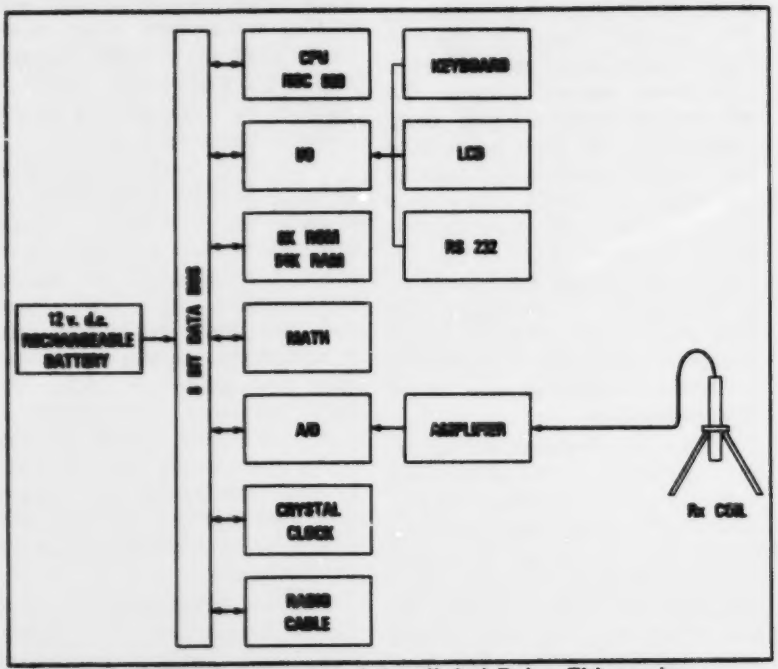

Figure 1. Synoptic diagram of the digital Pulse EM receiver.

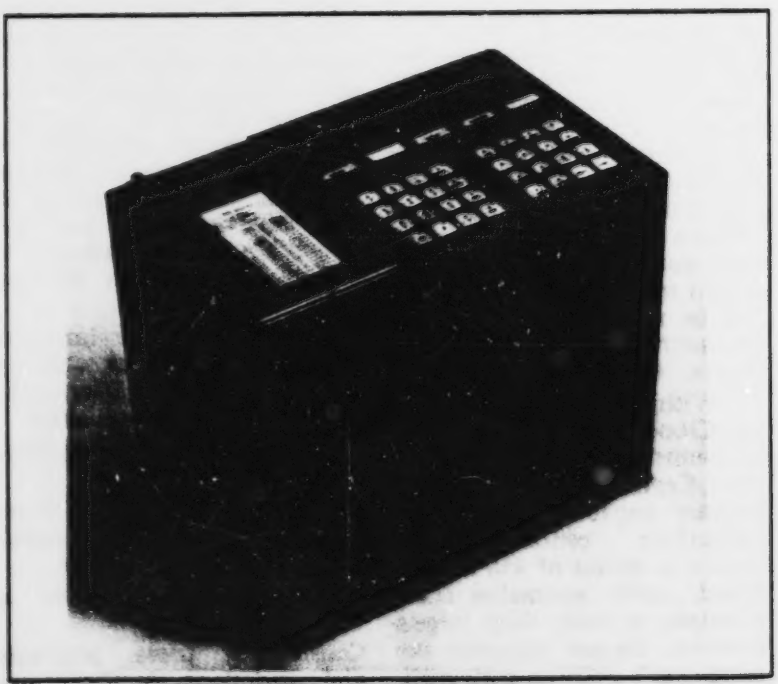

Figure 2. Prototype digital Pulse EM receiver.

TABLE 1: PULSE EM RECEIVER CHARACTERISTICS

	STANDARD PEM	DATALOGGER	DIGITAL PEM
Time gates	8	8	variable (preset for 10 and 20 channels)
Time base (msec)	10, 20	10, 20	variable (preset for 10, 20, 30)
Display accuracy	2 digits	4 digits	5 digits
Synchronization	radio cable link	radio cable link	quartz crystal clock radio cable link
Reading stack count	1000 or more	1000 or more	variable (depends on the reading error)
Noise detection	visual	visual	automatic
Noise filtering	averaging operator	averaging operator	spike rejection automatic
Signal gain	variable	variable	
Data storage medium	N/A	CMOS RAM	CMOS RAM
Data storage capacity	N/A	280 readings	1200 readings and 8 channels
Weight	7 kg	14.5 kg	9 kg

synoptic diagram of the receiver is shown in Figure 1.

SOFTWARE FEATURES

The CPU controls all functions which relate to the synchronous detection of the secondary field and its recording in solid state memory including:

1. Sampling and A/D conversion of receiver voltages:
   The input signal from the receiver coil is digitized in 4.5 μsec slices.
2. Automatic gain controls to compensate for any overflow of the input signal:
   The digitized input signal is amplified based on an exponential gain factor to maximize the signal strength. Should the input signal exceed the preset voltage maximum threshold then the gain is reduced and the signal resampled.
3. Rejection of noise-biased samples based on threshold detection:
   Digitized data remains in temporary memory for 1 complete cycle before being added to the stack. If the preset threshold has been exceeded during the half cycle, then the current and the previous half cycle data is rejected. To prevent any tail of the transient from biasing the stack, rejection continues for 1 complete cycle after the threshold is no longer detected.
4. Statistical reading error:
   The cumulative data stack is checked every 256 samples for reading accuracy using statistical analysis. Should the total value exceed the acceptable limit, then sampling continues for another 256 samples.
5. Binary recording of data:
   The final channel values are stored as binary numbers in CMOS memory. Data input by the operator including the line, station, and component or the hole and depth is recorded in ASCII code.

Other software features include a preset 10- or 20-channel configuration over a 30 msec time base. The unit, however, may be reformatted to any number of channels and gate time positions or can adopt the standard 8-channel Pulse EM format. A prototype instrument is illustrated in Figure 2.

OPERATING FEATURES

The new Pulse EM receiver allows the operator to execute programs in either the Surface or Borehole mode simply by following easy-to-use prompts. The unit will also record N

components of the secondary magnetic field, if desired.

Table 1 summarizes the characteristics for each of the 3 receiver units.

RECEIVER COIL

To further improve data quality, refinements have been made to the receiver coil. The new coil features the same 10 kHz bandwidth sensitivity as the standard coil. The external housing, however, has been reduced considerably both in size and weight. The leveling tripod has also been redesigned to allow for measurements of the horizontal components from 1 coil set-up.

DISCUSSION AND CONCLUSION

At the completion of this research and development project we expect to have a Pulse EM receiver of much improved quality. This will be demonstrated by its ability to improve the resolution of deep target and subtle anomalies in the presence of both geological and atmospheric noise.

Comprehensive testing of a prototype instrument both in the lab and in the field is well under way. From such tests we hope to perfect the software, optimize the hardware, and most importantly, gain experience with the new instrument.

The functions of the new receiver are best illustrated by a comparison with the standard Pulse EM receiver and Datalogger. At the time of writing such studies were incomplete but their results will be included in the final report.

Grant 039 Single Receiver, Frequency Scanning Fixed Source Electromagnetic System

Andrew Rogozinski

Androtex Limited, Mississauga

ABSTRACT

As the search for mineral deposits tends toward greater depths and more complex geological environments, an increased interest in electromagnetic methods using large fixed source transmitter loops is apparent. The present development is a single receiver coil version of the Turam electromagnetic method based on the automatic frequency scanning Elfast system. The new instrumentation results in better measuring flexibility and accuracy in surface measurements and can be operated by 1 person. It also represents a very significant improvement in frequency domain down-hole surveys. The system can also be used for parametric and/or geometric sounding by varying the frequency and/or distance from the transmitting loop.

INTRODUCTION

In its standard version the Turam electromagnetic method consists of a large fixed transmitting source and 2 receiver coils which are moved in tandem at a fixed separation (Figure 1). To assure coherence, measurements of amplitude and phase of the electromagnetic field at each sensor are made in the gradient mode, i.e. in the form of field strength ratios and phase differences.

In the present development the 2 sensing coils are replaced by a single coil (Figure 2). The receiver is provided with a memory, so that each measurement can be directly compared with any previous reading. To maintain coherence in this case the energized electromagnetic field is kept stable in amplitude to 0.1% and phase to an accuracy of 0.1°. This is achieved by means of a stabilized transmitting current and synchronized frequency clocks in the transmitter and receiver.

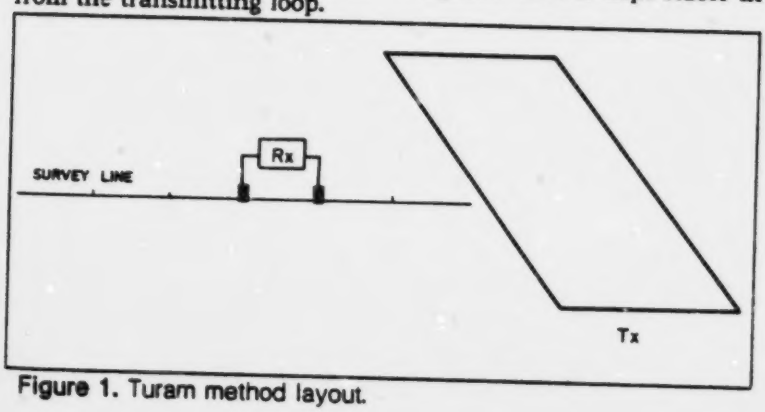

Figure 1. Turam method layout.

In the earlier embodiment of the Turam method by Androtex Limited, the Elfast system, the need for an operator at the transmitter was removed by scanning 5 frequencies automatically. The new single receiver version also has the automatic frequency scanning feature as well as the following additional advantages:

1. The combination of a stable energizing field and programmable automatic frequency scanning, with a single sensor, memory equipped receiver, will permit the survey to be carried out by only 1 operator.
2. The measurements will be more accurate, as 2-channel asymmetry is removed.
3. The measurement of 3 orthogonal components is facilitated, resulting in greater measuring flexibility.
4. In down-hole applications the single receiver overcomes many problems that have until now beset frequency domain drillhole measurements, such as: the inaccuracies resulting from the changing distance between measuring -Vo and reference -Vr coils (Ao,...An); the large values of phase differences and amplitude ratios with increasing depth; the different conditions (temperature) between the receiver (probe) and reference coils; the repeated calibrations at the adaptor

for each frequency. In this configuration. the adaptor is compensating the measured phases and amplitudes corresponding to the operating range of the receiver. The conventional down-hole logging layout is shown in Figure 3. With a single sensor receiver none of the above problems affect the measurements and accurate field strength ratios as well as phase differences can be obtained independent of depth. When lowering the probe, the reading at one station (A) is retained in the receiver's memory and compared with the subsequent reading at the next station (B) (Figure 4).

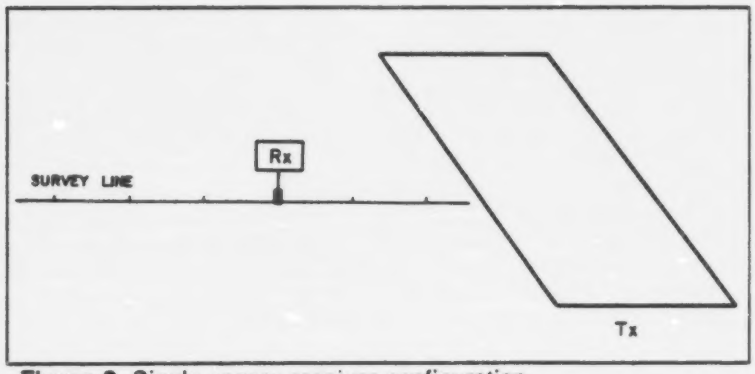

Figure 2. Single sensor receiver configuration.

INSTRUMENTATION

The new development includes the design of:

1. a high power transmitter with stabilized output current and programmable frequency pattern synchronized with the receiver
2. a microprocessor-controlled single sensor receiver provided with solid state memory and an interface for transferring data to the field computer
3. a down-hole logging attachment adapted to a single sensor receiver

TRANSMITTER

The significant features of the new transmitting unit are a current regulator providing a stable energizing electromagnetic field, and circuitry driven from a high stability temperature-compensated crystal-controlled oscillator ensuring synchronization with the receiver.

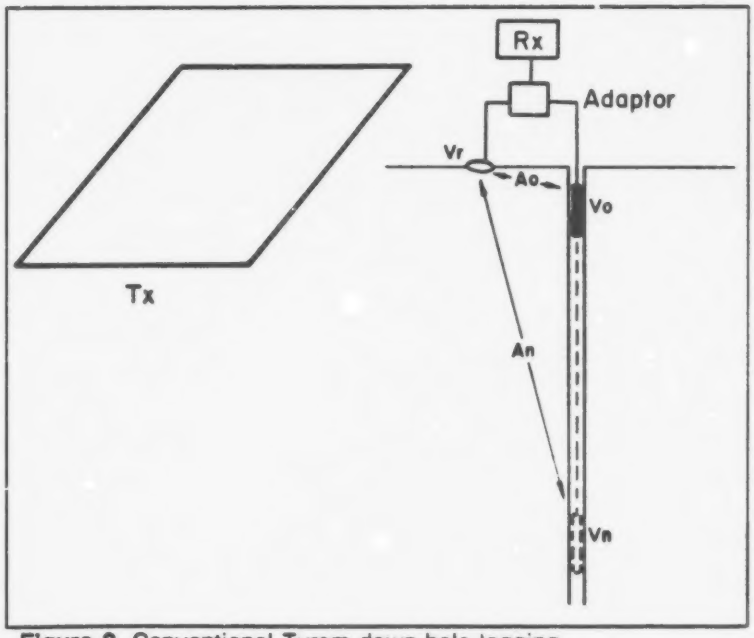

Figure 3. Conventional Turam down-hole logging.

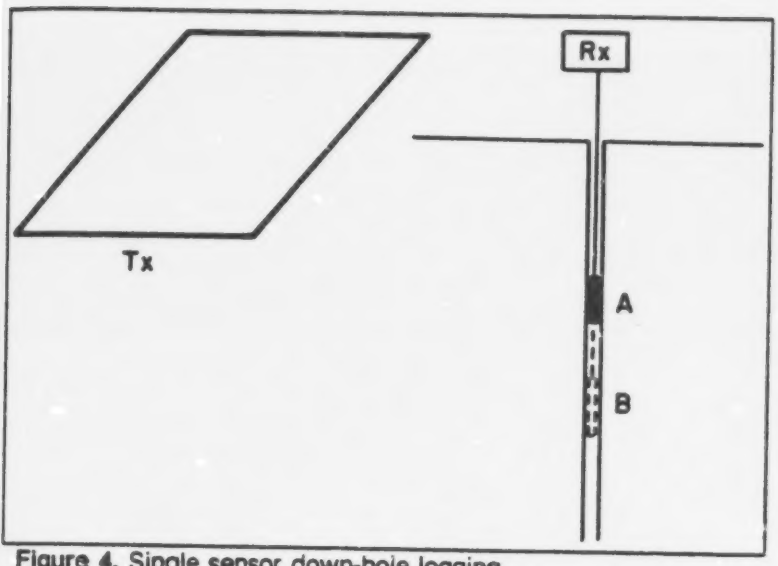

Figure 4. Single sensor down-hole logging.

Transmitter Parameters

Output: Power — 2000 VA

Voltage — 100 to 800 V

Current — 10A maximum stabilized to within ±0.05% for variation of load ±25% and input voltage ±10%

Waveform — square wave

Frequencies — 25, 75, 225, 675, 2025 Hz

Operating Temperature Range: -40° to +70°C, with +75°C limit

Load Limits: 11.0A maximum, 0.5A minimum

Input Voltage Limits: 125V maximum, 100V minimum

Input: Power — 2200 VA

Voltage — 115V nominal

Phase — 3

The transmitter has been described extensively in an

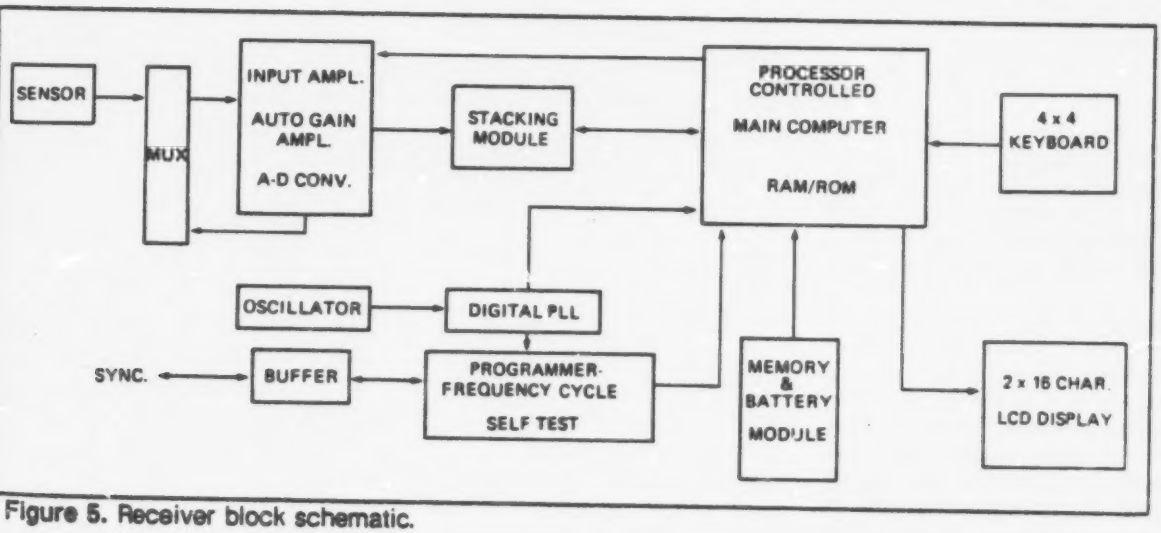

Figure 5. Receiver block schematic.

earlier release (Rogozinski 1983).

RECEIVER

The initial idea of the new receiver incorporates high sensitivity, simplicity of operation, internal data storage, and portability. The receiver design, based on an 8 bit low power microprocessor, consists of:

1. gain controlled input amplifiers with an analog to digital converter
2. processing module
3. microprocessor central processing unit (CPU) system
4. temperature compensated crystal-controlled oscillator and synchronizing circuitry with transmitter frequencies
5. solid state memory module for data storage
6. dual 16 character liquid crystal display (LCD)
7. keyboard
8. battery set

A block schematic is shown in Figure 5.

The microprocessor CPU system controls the overall receiver functions, i.e. sensitivity, signal processing, storage of data in the memory module, keyboard-display communication, and synchronized frequency/cycle time. With the keyboard software routine minimizing data entry, and a dual 16 character display continuously communicating with the operator during the automatic measuring mode, the receiver is extremely simple to operate. Collected data can be transferred via an RS232C port to the field computer for furtner processing and plotting.

Figure 6 presents a prototype of the single sensor receiver.

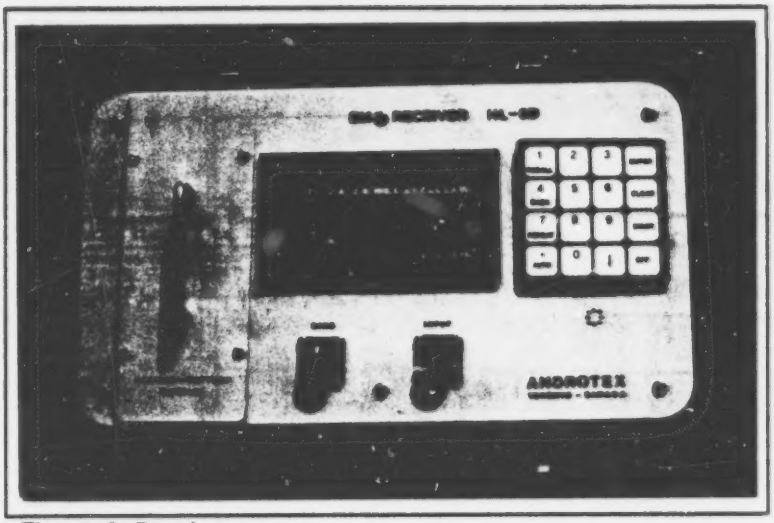

Figure 6. Receiver.

Receiver Parameters

Operating Frequencies: 25, 75, 225, 675, 2025 Hz

Operating Signal Amplitude: 20μV to 2V

Phase Range: +35° to -35°C

Operating Temperature Range: -40° to +60°C

Power Supply: Rechargeable battery 12V/1.5Ah

Dimensions: 36 cm by 20 cm by 20 cm

Weight: 4.3 kg

DOWNHOLE LOGGING ATTACHMENT

The down-hole logging attachment, shown in Figure 7, consists of a measuring probe, cable, and winch. The sensing coil, the electronic transmission circuitry, and the battery operated power supply are all included in the probe assembly.

The signal from the probe is sent to the receiver using a 2 wire shielded cable with kevlar reinforcement.

Down-Hole Logging Attachment Parameters

Probe: Length — 145 cm
Diameter — 3.15 cm
Power supply — batteries 2 x 9V

Cable: Length — 1000 m
Strength — 450 kg

Winch: Portable with tripod

CONCLUSIONS

The objective of the research project is the development of a new version of the Turam fixed source electromagnetic exploration system that combines better cost effectiveness with greater exploration depth, better spatial resolution, and better discrimination. The single sensor version meets these requirements in both surface

Figure 7. Winch and probe.

and down-hole exploration. In surface measurements cost effectiveness, flexibility, and accuracy are improved. In down-hole measurements the single sensor Elfast system constitutes the first effective fixed source frequency domain drill-hole system, permitting measurements of consistent accuracy independent of depth.

REFERENCE

Rogozinski, Andrew
1983: Grant 039 Single Receiver, Frequency Scanning Fixed Source Electromagnetic System; p.131-135 *in* Exploration Technology Development Program of the Board of Industrial Leadership and Development, Summary of Research 1981-1983, edited by E.G. Pye and R.B. Barlow, Ontario Geological Survey, Miscellaneous Paper 115, 135p. Accompanied by 2 charts.

Grant 048 Portable Intelligent Digital Graphic Recorder

Onorio Rocca

RMS Instruments Limited, Mississauga

ABSTRACT

Until recently, chart recorders used for geophysical applications have been primarily of the moving pen type. Considering current trends towards microcomputer-based instruments and to increasing numbers of channels of data, these recorders have several disadvantages; they record only a limited number of channels, they are difficult to interface to digital signals and instruments, they do not have alphanumeric capability, and their operation may not be monitored or controlled by microcomputer-based instruments. The number of data channels is limited by the number of pens used, usually a maximum of 6 or 8 channels for the largest recorders. Signals generated or processed by digital instruments must be converted to an analog signal in order to be recorded since there is normally no provision for digital inputs. Except for some models with limited edge printing capabilities, conventional recorders cannot reproduce alphanumerics; records must be manually annotated in the field with the inherent risk of operator error or omission. Finally, since conventional recorders may not be monitored and controlled by external instrumentation, it is difficult to automate the data recording process.

The proposed recorder can combine graphics and alphanumerics to simplify the documentation of field data, and to improve reliability and accuracy by reducing the possibility of operator error or omission in annotating the record. Interfacing of the recorder to digital signals and instruments will be greatly simplified by the availability of several digital interface options. Control of the recorder by an external instrument will permit an increased level of automation of the data acquisition process, resulting in reduced costs and improved reliability.

INTRODUCTION

In 1980, RMS Instruments Limited undertook a development program, resulting in the manufacture of the Model GR33 Graphic Recorder in 1981. The GR33 is a microcomputer-based recorder utilizing a printhead technology similar to that of the proposed recorder. The proposed project will expand on the knowledge and expertise gained in the development of the GR33, and the GR34 designed in 1983.

The Model GR33 Graphic Recorder incorporates a 12.4 inch (315 mm) thermal printhead with 100 print elements per inch, is capable of recording up to 32 signals, and operates from a 28 volt DC power source. It is packaged in a standard 5.25 inch (133.4 mm) by 17 inch (432 mm) rackmount cabinet, making it ideal for airborne geophysical survey applications. Recorders are currently installed or being installed in helicopters, fixed wing aircraft, and land vehicles to be used for recording geophysical data.

The GR33 is the first recorder of its kind, and its introduction brought several innovations to geophysical data recording. An external instrument such as a data acquisition computer may directly control recorder operating parameters, such as chart speed and signal information, directly in digital format without conversion to analog.

A unique compact operator control panel, consisting of an alphanumeric LED display, several pushbutton keys, and a single rotary control, permits the adjustment of all operating parameters such as chart speed, signal amplitude and position. Plug-in modules permit the recorder to be interfaced to a variety of sensors and instruments.

Paper level is reliably monitored by a solid state sensor and displayed on a unique LED bargraph.

The recorder may operate as a chart recorder, alphanumeric printer, or raster graphic printer, enabling a data acquisition computer to print out; (1) header information as text prior to a survey, (2) record data in a chart format with annotation of survey information, and (3) quality control information or processed data as alphanumerics bargarphs, or X-Y plots on completion of the survey.

PROJECT OBJECTIVES

The objective of the research project described below, is to advance the performance set by the GR33 Graphic Recorder and to further investigate thermal printing and digital electronics techniques, leading to the development and manufacture of a portable, intelligent, digital graphic recorder. This new product will increase the efficiency of real-time and post-time collection and interpretation of data acquired for mineral exploration.

BRIEF DESCRIPTION OF RESEARCH

The recorder will be capable of recording any of the following data formats: multiple channels of analog or digital infor-

mation in a strip chart format with alphanumeric trace annotation and self generated grid patterns; alphanumeric text such as tabulated data or header messages; graphic images such as X-Y plots and bargraphs; alphanumeric messages printed while recording analog information without loss of data in split mode of operation. An external instrument will be capable of monitoring and controlling operation of the recorder via one of several optional digital interfaces. The recorder is expected to increase the efficiency, and thereby reduce the costs of geophysical data acquisition, by improving the accuracy and quality of the displayed data, and by permitting further automation of data acquisition and interpretation. Furthermore, availability of a versatile data recorder with digital interfacing capabilities is expected to encourage the development of other portable intelligent geophysical instruments.

The Digital Graphic Recorder will incorporate a fixed position monolithic thermal printhead with a 10.85 cm (4.27 inch) printspan. The printhead will consist of a single row of approximately 420 individual thermal printing elements spaced 0.25 mm apart. A microprocessor-based control circuit will create graphic images by controlling the energizing signals to the printhead as the thermal sensitive recording paper is advanced across the printing surface. Several digital interface options (RS232 serial, IEEE-488 Instrument Bus, parallel digital) will permit an external digital instrument to easily control and monitor the recorder. The recorder will be capable of operating as an alphanumeric printer, raster graphics printer, or multiple channel strip chart recorder, and either stand alone or under the control of an external instrument.

Operating in the chart recorder mode, the recorder will be capable of recording up to 16 signal traces, with trace identification and internal grid generation. An external instrument may provide alphanumeric messages for printing on the chart to annotate the record. Analog signals, input via an optional analog interface, may be recorded on the chart and may also be output in digital format for further processing by an external instrument. The raster graphics mode permits an external instrument to directly control the printing elements to create graphic images such as X-Y plots, bargraphs, etc., from the processed data. Text such as tabulated data and header messages may be printed using the alphanumeric mode of operation.

RMS Instruments Limited began this project in January 1984 with the evaluation of a number of components. Some of the problems in choosing components for a portable instrument are power consumption, the weight of major components, the total weight, and the size of the completed instrument. With the printhead being a major component, the printing speed, physical size, and reliability of the printhead were important considerations.

At the beginning of this project, the recorder specifications were based on a particular printhead with a resolution of 4 dots per millimetre and a maximum printing speed of 25 mm per second. However, with the advent of high resolution and high speed print heads, we are currently considering a printhead which offers a resolution of 8 dots per millimetre and a theoretical printing speed of approximately 100 mm per second. With this performance, more accurate data recording is possible.

A considerable amount of time was spent in the evaluation of 16-bit microprocessors which eventually led to the selection of the Motorola MC68000. An evaluation has also been carried out on the specifications of different types of light-weight small batteries, suitable for low temperature applications.

We have considered different mechanical concepts regarding the paper transport, package enclosure, overall size, weight, etc. Valuable discussions have been carried out with possible future customers and end-users, collecting ideas and input in regard to their requirements.

Currently, all the necessary test equipment for the support of our development has been purchased. More comprehensive development is planned to begin in July, 1984 using the high resolution printhead. We have determined the external physical size of the recorder to be 5.25 inches (133.35 mm) high, 7.0 inches (177.8 mm) wide, and 14.0 inches (355.6 mm) long. In line with our previous comments, the weight has not been defined, and will be dependent upon the number of optional features installed.

CONCLUSIONS

With the indepth evaluation of end-user requirements and our comprehensive consideration of most up-to-date technological advances, the ground work has been laid and we are well underway toward our goal of

improving data recording on paper. The flexibility and adaptability of the product will prove to be a very important feature.

Grant 050 The Application of Reflectance Radiometry to Semiquantitative Alteration Mineral Determination in Geological Materials

D.R. Gladwell

Barringer Magenta Limited, Rexdale

ABSTRACT

Reflectance radiometric determination of the kaolinite, montmorillonite (smectite), illite, muscovite, chlorite, and biotite contents of rocks and soils was studied. This study included examination of probable causes of error in the radiometric determination. Radiometric mineral determination was achieved by accounting for the empirically observed variance using a FORTRAN computer algorithm. The computer algorithm was tested on 53 rock and soil samples for which X-Ray Diffraction (XRD) mineralogical analyses were available.

INTRODUCTION

A wide range of visual, petrographic, physical, and chemical techniques are now available to aid the exploration geologist to unravel the complex mineralogy of highly altered rocks associated with base metal, precious metal, and uranium deposits. Mineralogical variations within hydrothermal alteration envelopes are frequently important guides to economical ore concentrations, but the determination of subtle alteration mineral changes and particularly semiquantitative measurement of mineral abundances can be slow, costly, and generally only possible through a well equipped laboratory. Studies described in this paper suggest that rapid discrimination and semiquantitative estimation of alteration minerals (e.g. smectite, illite, kaolinite, and chlorite) is feasible in both laboratory and field conditions by analysis of the spectral characteristics of light reflected from geological targets in the near infra red (IR) wavelength range using the Barringer Hand Held Ratioing Radiometer (HHRR).

Analysis of solar reflectance spectra obtained using broad band (half band pass of greater than 50 nm) interference filters has been extensively employed as a remote sensing method for mapping regional geology and identifying large hydrothermal and geothermal patterns (Rowan and Kahle 1982; Sadowski and Abrams 1982). Moreover, the feasibility of routine remote identification of specific alteration minerals has been demonstrated using airborne high resolution spectroradiometers (Goetz *et al.* 1982; Collins and Chang 1982). These workers have, however, stressed the need for *in situ* ground measurements of reflectance to allow accurate calibration of the remote sensing data. The recent development of small, portable reflectance radiometers, such as the instrument described in this work, enables rapid *in situ* confirmation of geological and geobotanical features identified by remote sensing techniques.

Most previous spectral reflectance studies of geological materials have concentrated on generating complete visible to near IR spectra of pulverized, homogeneous, and generally unaltered rock and mineral samples. For example, Hunt and Salisbury (1970, 1971), and Hunt, Salisbury, and Lenhoff (1971, 1973a) determined reflectance spectra from 0.4 to 2.5 microns for most common rock forming silicate, oxide, carbonate, and sulphate minerals. Similarly, more recent research has focused on establishing spectra for different rock types in addition to constituent minerals (Hunt *et al.* 1973b, 1973c, 1974). Hunt and Ashley (1979) recorded the visible to near IR spectra for a suite of hydrothermally altered rocks representing silicic, argillic, phyllic, and propylitic alteration types. Reflectance spectra in the 0.4 to 2.5 micron region may show the following spectral absorption features: a) the intervalence charge transfer transition between iron and oxygen ions; b) absorption due to free (atmospheric) and mineral adsorbed water; c) overtone vibrational transitions of Al-OH groups; d) vibrational transitions of the Mg-OH groups; and e) vibrational transitions of the carbonate groups.

The intensity of these absorption features may be measured using appropriate narrow bandpass interference filters in the Barringer Hand Held Ratioing Radiometer (HHRR). Such measurements, made on drill core and rock samples from 2 hydrothermal gold deposits in northern Ontario successfully located the ore zones (Gladwell *et al.* 1983). However, some petrological knowledge of lithologies encountered was found to be a prerequisite for interpretation of the reflectance data.

In contrast to this situation, it is the aim of the present study to develop a computer algorithm which would be generally applicable to clay mineral analysis of major soil and rock types.

The delineation of clay mineral haloes around hydrothermal ore deposits by remote reflectance techniques has relied chiefly on recognition of the overtone Al-O-H molecular vibrational absorption features in the 2.2 micron region (Goetz *et al.* 1982; Collins and Chang 1982; Gladwell *et al.* 1983). Overlapping spectral absorption features in the region include those due to alunite and gypsum near 2.17 microns, those due to kaolinite, muscovite, and montmorillonite at approximately 2.2 microns, and the illite absorption feature which may be present at approximately 2.22 microns. The overlapping spectral features are very closely spaced, all occurring within 60 nm and 4 out of the 7 features located very close to 2.2 microns. The high density of absorption features in this region precludes its use for confident radiometric clay discrimination (Gladwell 1982).

The Al-O-H fundamental molecular vibrational absorption feature in clay minerals occurs at between 2.7 and 2.8 microns (Van der Marel and Beutelspacher 1976). This wavelength region has not been used for remote sensing as light at these wavelengths suffers intense absorption by atmospheric water. This problem may readily be overcome for radiometric studies, however, by using an active light source and a short target-radiometer viewing distance.

INSTRUMENTATION

HHRR DESIGN

The HHRR is designed to measure reflected light energy from a target in 2 narrow passbands, selectable in the range 400 to 2500 nm. The selectable instrument output (liquid crystal digital display and analog output) provides the power through each passband (channel), and the ratio of the 2 channel outputs (channel 1/channel 2). The instrument has an optical train for each channel which may be focused for optimum instrument performance at 1 m or at greater than 10 m from the target. After passing through a chopper, which modulates the incoming DC reflected energy for both channels, the light is focused onto, and a portion passes through, an operator selectable filter, after which the light is refocused onto a thermoelectrically cooled PbS detector. HHRR design is fully discussed by Daubner *et al.* (1981).

Earlier measurements (Gladwell *et al.* 1983) established that the field of view (FOV) of the HHRR is approximately 28 by 4 cm in size. Since this area is larger than the target size of diamond-drill core an optical device was designed to reduce the field of view to 6 by 1.5 cm. A practical advantage of this simple device is that it can be quickly attached to the HHRR for measurement along drill core.

The spectra of minerals of interest were obtained using a simple scanning spectrometer in which an HHRR was incorporated as the detector. An HHRR was rigidly mounted perpendicular to the exit slit of a Jarrell Ash (Model 82-40) 0.25 m monochromator. A tungsten filament quartz iodide light source was mounted at the inlet slit. The mounting allows adjustment of the light source position in 3 dimensions and permits: focusing of the filament image on the inlet slit using a concave, front aluminium coated mirror with a focal length of 10 cm; and optimum illumination of the diffraction grating and monochromator mirrors. The lamp current is stabilized and the lamp voltage is continuously monitored. An external chopper was mounted close to the monochromator inlet slit and the phase reference signal was fed into the HHRR. The HHRR's internal chopper was disabled during measurement.

The internal mechanism of the monochromator was altered to allow: a scan from 450 nm to 1.0 micron using a 600 blaze grating and 1 order sorting filter at 590 nm (the HHRR acts as the order sorting filter for wavelengths less than 300 mm); and a scan from 1.0 to 2.82 microns using a 300 blaze grating and order sorting filters at 1.0 and 1.6 microns. The PbS detectors in the HHRR are insensitive to wavelengths beyond 2.82 microns without additional thermoelectrical cooling. The monochromator slit width during measurement was 2.57 mm which corresponds to a half-peak bandpass of approximately 25 nm in the 1.0 to 2.82 micron region.

Channel 2 of the HHRR continuously monitors a reference beam, deflected from the exit beam using a front aluminum coated plane mirror. Channel 1 of the HHRR continuously monitors sample reflectance at an angle of 40° from normal.

EXPERIMENTAL RESEARCH

The aims of the experimental portion of the project were:

1. to optimize the spectral measurement methodology and obtain an estimate of the measurement error
2. to investigate the effect of changing ambient humidity on the spectra of the pure minerals
3. to obtain spectra of known interfering minerals
4. to select wavelengths for radiometric measurements, allowing the optimum discrimination between individual minerals, and minimizing interference from other minerals

OPTIMIZATION OF SPECTRAL MEASUREMENTS

The spectral measurement technique was optimized by testing various sample holder configurations since the primary sources of measurement error were observed to be the target-radiometer viewing distance and the placement of the sample directly in the active field of view of the instrument. The error associated with these variables was minimized by constructing rigid cardboard sample holders which moved horizontally along a flat mounting plate.

Optimal instrument response in the 2.7 to 2.8 micron region was obtained by cooling the PbS detectors (described above) to -10°C. Five replicate spectral measurements were obtained on each clay mineral over a period of several days with sample trays refilled before measurements. The results showed that the measurement error (relative standard deviation) varied between 0.5 and 5.0%.

SAMPLE HUMIDITY

In order to investigate the effect of changing humidity on the spectra of the pure minerals, the scanning HHRR described above was placed in a large, sealed perspex glove box and the interior humidity was controlled using appropriate saturated solutions (e.g. a saturated solution of lithium chloride will maintain a constant humidity of 15% in a closed atmosphere, other solutions will maintain different levels).

The interior humidity was homogenized using a circulation fan, the absolute humidity was monitored using a Lyman Alpha detector, and the internal temperature was monitored. The experimental procedure consisted of placing the sample tray with pure mineral samples inside the glove box with the scanning HHRR, the barium sulphate reflectance standard, and the selected solution. The fan was switched on and the closed system was left overnight to equilibrate. Following equilibration, the reflectance of the pure minerals relative to barium sulphate at 1.86, 1.9, 2.1, 2.2, 2.65, 2.71, 2.73, and 2.75 microns was measured. The results obtained are presented in Table 1 and indicate that the observed changes in reflectance are similar in magnitude to the measurement error.

SPECTRA OF INTERFERING MINERALS

Apart from the spectra described above, reflectance measurements were also obtained on samples of biotite, hornblende, augite, alunite, gypsum, talc, pyrophyllite, and an illite/smectite mixed layer clay. The reflectance data are presented in Table 2. Biotite has an absorption feature in the 2.7 micron region and, due to its abundance, was included in the minerals which required determination. Hornblende, augite, talc, and pyrophyllite also show absorption in the 2.7 micron region. However, since they are in general less common than the minerals to be determined, it was decided to allow their selective inclusion in any subsequently developed algorithm by substitution with a mineral not considered to be present. Alunite and gypsum do not show marked absorption in the 2.7 micron region although both show a shoulder at 1.9 microns and an absorption feature at close to 2.2 microns.

The technique for dealing with the presence of either alunite or gypsum is discussed below.

SELECTION OF OPTIMUM WAVELENGTHS

Using a mix of empirical measurements and correlation analysis, the optimum wavelengths for spectral deconvolution were found to be 1.86, 1.9, 2.65, 2.68, 2.71, 2.73, 2.75, and 2.77 microns.

SPECTRAL DECONVOLUTION ALGORITHM

A number of different methods were tested for deconvoluting the component spectra of the minerals described above. These were: solution of simultaneous equations; correlation analysis; stepwise multiple regression; and least squares fit with empirical selection rules. These 4 techniques are described below, together with the problems encountered. The best choice of deconvolution

TABLE 1: REFLECTANCE OF PURE MINERALS RELATIVE TO $BaSO_4$ AT: (A) 18%; (B) 52%; (C) 66% RELATIVE HUMIDITY

WAVELENGTH (microns)	KAOLINITE			SMECTITE			MUSCOVITE			ILLITE			CHLORITE		
	A	B	C	A	B	C	A	B	C	A	B	C	A	B	C
1.86	80	79	79	85	86	88	66	66	68	49	50	51	46	46	47
1.9	80	79	78	69	68	69	67	66	68	46	46	47	48	48	50
2.1	72	72	72	82	83	83	66	66	68	53	53	54	56	55	57
2.2	53	51	51	76	77	78	60	59	61	47	46	47	58	57	59
2.65	42	40	40	57	56	57	61	61	63	39	37	38	58	57	59
2.71	21	18	19	38	36	38	53	52	54	26	24	24	56	55	56
2.73	19	17	17	29	26	28	40	38	40	20	18	19	53	50	51
2.75	23	19	21	26	23	23	29	26	27	20	16	17	41	40	40

TABLE 2: REFLECTANCE RELATIVE TO $BaSO_4$ OF INTERFERING MINERALS

WAVELENGTH (microns)	BIOTITE	HORN-BLENDE	AUGITE	ALUNITE	GYPSUM	TALC	PYROPHY-LLITE	ILLITE/ SMECTITE
2.1	80	75	49	55	67		78	57
2.2	81	75	50	41	57		60	48
2.65	81	75	61	44	36		49	84
2.71	50	49	57	41	31		31	25
2.73	47	43	47	40	30		27	22
2.75	56	50	43	37	29		29	21
2.77	64	63	45	35	29		34	25

algorithm was the use of a least squares fit with empirical selection rules.

SOLUTION OF SIMULTANEOUS EQUATIONS

Gladwell (1982) demonstrates that the functions relating modal percent mineral and HHRR ratio response are linear in the 2.65 to 2.8 micron region. This suggests that the overlapped absorption features of different minerals are a linear combination of the individual feature producing minerals. As a result, the overlapped absorption features may be deconvoluted by the solution of simultaneous equations. The variables in each equation are subject to the restraint of not being less than 0 and not being greater than 1. The former constraint only was imposed by the algorithm.

The algorithm was tested on a suite of 53 rocks and soils on which bulk (weight percent) clay and major phase (quartz, feldspar, etc.) mineralogy was determined by X-Ray Diffraction (XRD). The results of the simultaneous equation algorithm did not agree well with the XRD analyses. Investigation of the causes for this revealed that the results of the algorithm were very sensitive to small changes in the reflectance measurements and that the background spectra of the samples (i.e. with no clay minerals present) were more complex than had been assumed. For these reasons, it became apparent that an algorithm should be devised that accounted for the errors inherent in the measurements.

CORRELATION ANALYSIS

An algorithm incorporating correlation analysis was investigated in order to remove the sensitivity to small changes in reflectance observed with the previous algorithm test. The algorithm consisted of a sequential correlation routine. The sample spectrum was correlated with the spectrum of the pure minerals. The spectrum of the mineral showing the highest correlation was then subtracted in small increments from the sample spectrum until the rate of change of the correlation coefficient increased significantly. The selected mineral was then invalidated and the process repeated until all pure mineral spectra showed a low correlation with the sample spectrum.

The algorithm results on the test sample suite showed that it performed well for some samples and very poorly for others. Examination of the results showed that good results were obtained when the sample initially showed a very high correlation with a calibration mineral. Poor agreement with XRD results was associated with sample spectra which were largely uncorrelated with the pure mineral spectra, either because of a strong background spectrum or due to the number of absorbing mineral species present in the sample.

STEPWISE MULTIPLE REGRESSION

The stepwise multiple regression routine produced slightly better results than the correlation analysis procedure described above, presumably because calibration minerals were considered together during analysis of variance rather than one at a time.

LEAST SQUARES FIT WITH EMPIRICAL SELECTION RULES

The best comparison between reflectance determined and XRD determined clay mineral content for the test suite were obtained using an algorithm which incorporates the least squares best fit criteria and a series of empirical selection rules.

The deconvolution algorithm is relatively simple and consists of 3 steps:

1. For all combinations of pairs of mineral standards, a mixed spectrum is mathematically produced that closely matches the sample (unknown) spectrum.
2. From this spectral set, the best fitting spectra (minimum of 5) are selected, and a weighted average of the amounts of minerals used to form these spectra is calculated as a first estimate of the sample mineral contents.
3. The first estimate is then adjusted using a set of empirically derived selection rules developed to minimize errors due to known spectral interferences. The selection rules are used to decide whether montmorillonite, illite, muscovite, or a mixed layer illite/smectite is present with either kaolinite or biotite and/or chlorite.

RESULTS

XRD and HHRR determined contents are compared in Figures 1 and 2 for muscovite-illite, montmorillonite, mixed layer clays, and kaolinite/biotite respectively for the test suite of 53 samples. The test suite results showed that where a mineral

was present in a quantity greater than 10% (as determined by XRD) the algorithm correctly determined the mineral group (defined as: (1) kaolin/biotite; (2) montmorillonite, muscovite, and illite; (3) chlorite) in 94% of cases. The mean error in estimating mineral quantity was less than 13% absolute. In determining individual minerals, the algorithm correctly classified 67% of the samples with an error of less than 20% absolute in quantification. Of the erroneous classifications, 82% were associated with the classification of muscovite, illite, and montmorillonite. The most common misclassification was in identifying illite as muscovite and a mixture of montmorillonite and illite as montmorillonite.

Although pure samples of kaolinite and biotite are distinguishable in the 2.7 micron region, the test results showed that in natural samples they were not easily distinguished. Therefore, the algorithm outputs the estimated contents of kaolinite/biotite.

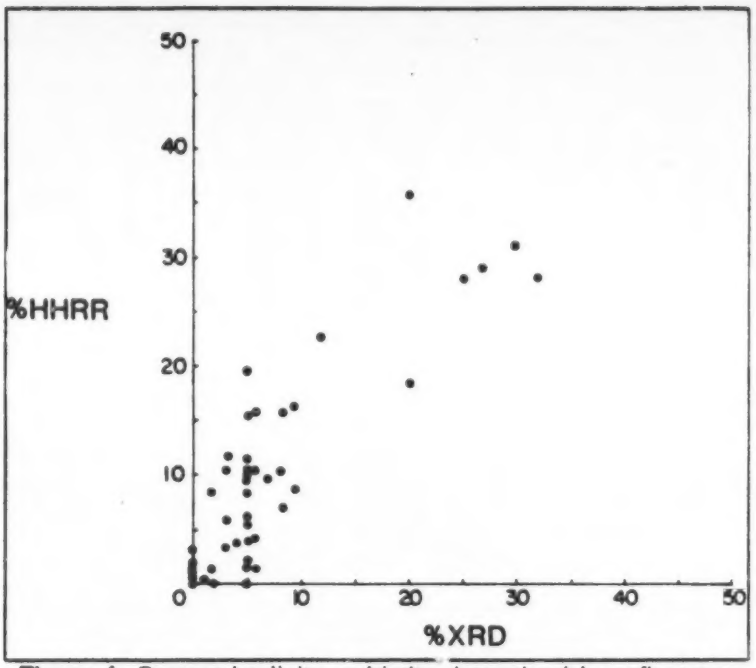

Figure 1. Percent kaolinite or biotite determined by reflectance radiometry (HHRR) and X-Ray Diffraction (XRD).

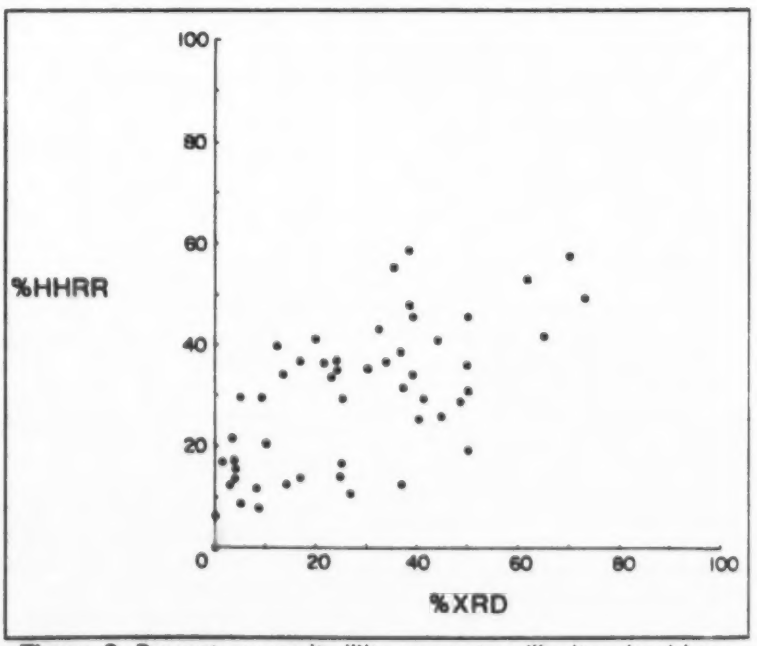

Figure 2. Percent muscovite-illite or montmorillonite-mixed layer clays determined by reflectance radiometry (HHRR) and X-Ray Diffraction (XRD).

ERROR ANALYSIS

Errors may be assigned as follows:

1. The calibration mineral spectra are not similar to those of the minerals actually present in the sample. This is most likely to be a problem with montmorillonite and illite, partly due to the difficulty in obtaining pure, characterized samples.
2. Measurement errors. Experience has shown measurement errors in data collection are less than 4%.
3. XRD analytical errors. XRD is not designed primarily as a quantitative

method and the analytical errors are probably ±10%, particularly where more than 2 minerals are present in the sample. However, XRD misclassification errors are unlikely.

4. The HHRR technique determines modal (by area) mineral content whereas the XRD technique determines bulk (weight %) content. The 2 determinations are not compatible in all cases, particularly where overcoating of minerals occurs.
5. Changes in ambient humidity. Our work has shown that, provided a $BaSO_4$ reflectance target is used, changes in ambient humidity in the range 15 to 66% relative humidity change the reflectance spectra by less than the measurement error.
6. Errors in estimating the background spectrum (the spectrum of the sample with all clays removed) of the sample. This source of error is difficult to quantify and is currently the subject of further research.

SPECTRAL INTERFERENCES

Apart from the minerals mentioned above and the presence of large quantities of organic matter or iron minerals, the only other common spectral interferences are due to the presence of alunite and/or gypsum which have a reflectance shoulder near 1.9 microns. This may be overcome by the use of an additional optical filter with a centre wavelength of 2.0 microns.

The sample reflectances are measured in the 1.9 and 2.7 micron regions, both of which experience atmospheric absorption, therefore we recommend use of a Lowell Omni (tungsten halide) active light source, a viewing distance of approximately 25 cm, and a field of view of approximately 6 by 1.5 cm obtained using the HHRR core-viewing attachment.

CONCLUSIONS

A portable method of semi-quantitative clay mineral determination has been developed using the Barringer Hand Held Ratioing Radiometer and tested on 53 clay mineral-bearing samples under laboratory conditions.

The results of the HHRR algorithm compare well with determinations by conventional (XRD) techniques for samples containing predominantly quartz, feldspar, and some carbonate phases. The best comparison with XRD was obtained using an algorithm which combines a least squares fit and a set of empirical selection rules.

The technique is considered applicable to exploration for precious and base metals and to detecting zones of clay enrichment during drilling for hydrocarbon deposits apart from laboratory clay mineral analysis.

REFERENCES

Collins, W., and Chang, S.H.
1982: Summary of New Airborne Remote Sensing Techniques Developed for Mineral and Oil Exploration and Geologic Mapping; Unpublished Report, Aldridge Laboratory of Applied Geophysics, Columbia University, 65p.

Daubner, L.R., Davies, J.H., and Goetz, A.
1981: A Hand Held Ratioing Radiometer for Remote Radiance Measurements; Proceedings of the 7th Canadian Symposium on Remote Sensing, Winnipeg, p.423-428.

Gladwell, D.R.
1982: Application of Reflectance Spectrometry to Clay Mineral Determination in Geological Materials Using Portable Radiometers; Summary, International Symposium on Remote Sensing, Fort Worth, Texas, 1982, p.196.

Gladwell, D.R., Lett, R.E., and Lawrence, P.
1983: Application of Reflectance Spectrometry to Mineral Exploration Using Portable Radiometers; Paper submitted to Economic Geology.

Goetz, A.F.H., Rowan, L.C., and Kingston, J.
1982: Shuttle Multi-Spectral Infrared Radiometer: Preliminary Results from the Second Flight of Columbia; Presented at the International Geoscience Remote Sensing Symposium, Munich, Germany, June 1-4, 1982, 6p.

Hunt, G.R., and Ashley, R.P.
1979: Spectra of Altered Rocks in the Visible and Near Infrared; Economic Geology, Volume 74, p.1613-1629.

Hunt, G.R., and Salisbury, J.W.
1970: Visible and Near-Infrared Spectra of Minerals and Rocks: I Silicate Materials; Modern Geology, Volume 1, p.283-300.
1971: Visible and Near-Infrared Spectra of Minerals and Rocks: II Carbonates; Modern Geology, Volume 2, p.23-30.

Hunt, G.R., Salisbury, J.W., and Lenhoff, C.J.
1971: Visible and Near-Infrared Spectra of Minerals and Rocks: III Oxides and Hydroxides; Modern Geology, Volume 2, p.195-205.
1973a: Visible and Near-Infrared Spectra of Minerals and Rocks: VI Additional Silicates; Modern Geology, Volume 4, p.217-224.
1973b: Visible and Near-Infrared Spectra of Minerals and Rocks: VII Acidic Igneous Rocks; Modern Geology, Volume 4, p.225-272.
1973c: Visible and Near-Infrared Spectra of Minerals and Rocks: VIII Intermediate Igneous Rocks; Modern Geology, Volume 4, p.273-344.
1974: Visible and Near-Infrared Spectra of Minerals and Rocks: IX Basic and Ultrabasic Igneous Rocks; Modern Geology, Volume 5, p.15-22.

Rowan, L.C., and Kahle, A.B.
1982: Evaluation of 0.46 to 2.36-um Multi-spectral Scanner Images of the East Tintic Mining District, Utah, for Mapping Hydrothermal-

ly Altered Rocks; Economic Geology, Volume 77, p.441-452.

Sadowski, R., and Abrams, M.
1982: Mapping Hydrothermal Alteration Using Aircraft VNIR Scanners at the Rosemont Copper Deposit; Presented at the International Symposium on Remote Sensing of the Environment, Fort Worth, Texas (in press).

Van der Marel, H.W., and Beutelspacher, H.
1976: Atlas of Infrared Spectroscopy of Clay Minerals and their Admixtures: Elsevier, Amsterdam, Oxford, New York, 396p.

Grant 051 Development of Field Portable Apparatus for the Analysis of the Magnetite, Hematite, and Ilmenite Content of Basal Tills

W.A. Morris

Morris Magnetics, Lucan

ABSTRACT

While bulk magnetic susceptibility mapping for drift prospecting is well established, especially in Scandinavia, this technique only accesses in detail a small portion of the information retained by the magnetic minerals of the till. The objective of this project was to design field portable apparatus which can access information on the relative contributions of the individual magnetic species magnetite, hematite, and ilmenite. Resolution of these individual components is achieved through the analysis of the induced remanence characteristics of till samples.

Field portable equipment for the generation of DC magnetic fields, and the measurement of the induced remanence, have been constructed and tested using samples from an uranium prospect in the Northwest Territories. Regional variations of magnetite and hematite over the study area document the ice flow direction of the RAD train, and show the differences that can arise from sand-rich tills as opposed to silt-rich tills. A significant localized enhancement of magnetite, and depletion of hematite, is directly associated with a strong scintillometer anomaly. This marks the signature of a uranium deposit, where the uranium has a magnetite mineral association.

INTRODUCTION

Locating the source of economically important rock fragments found in drift deposits is dependant upon 2 parameters; a) the direction of the source from the observed rock fragment anomaly, and b) the distance between the source and the point of initial observation. Traditionally the methods employed in defining these parameters are geochemical concentration variations, and pebble, or grain fabrics as defined by visual macroscopic or microscopic observations. Drawbacks to these techniques include the time taken to receive chemical analyses from the laboratories.

An alternative rapid, cheap, field portable, and accurate technique for providing the transport direction and distance may be found in the magnetic characteristics of glacial sediments. Especially in Scandinavia, bulk magnetic susceptibility mapping is commonly used in drift prospecting. The measurement of the bulk magnetic susceptibility of a unit volume of sediment provides an approximation of its total magnetite content. Most other common magnetic minerals, with the possible exception of pyrrhotite, have unit bulk susceptibility values much lower than magnetite. Typical exploration targets for this technique may include; the association of magnetite with placer gold, metasomatic magnetite in skarn deposits of copper or lead, and magnetite associated with the hydrous serpentinization of mafic intrusive bodies. A specific example from Northern Finland (Figure 1) shows a direct correlation between the bulk susceptibility and magnesium, chromium, and nickel content of the sediment (Pulkkinen *et al.* 1980).

PROJECT OBJECTIVES

Although it has been shown that bulk susceptibility mapping can yield important information, we know that we are only utilizing a small portion of the total magnetic mineral information that is present in each unit of sediment. First, as well as being dependant upon magnetite content, bulk magnetic susceptibility values are also controlled by the average oxide grain size, and the composition of the magnetite. Since one can assume that the composition of the magnetite does not vary grossly down glacier from a source, the 2 variables are grain size and oxide content. Respectively, variations in these parameters will arise as a result of comminution at the base of the glacier, and dilution of the magnetic mineral content by the uptake of more silicate particles. To permit observation of these effects requires that one examines specific grain size fractions. As the susceptibility of a volume of silt size magnetite is significantly less than an equivalent volume of sand size magnetite, it is possible that all of the observed values are near the detection limit of available equipment. In this instance it would not be possible to statistically differentiate any trends. Second, it is possible that a number of different mineral species are contributing to the total bulk susceptibility. Knowing which minerals are present and in what proportion may be of some importance. For example, in the proximity of a sulphide body it is important to know whether the magnetic mineral is pyrrhotite (ore), or

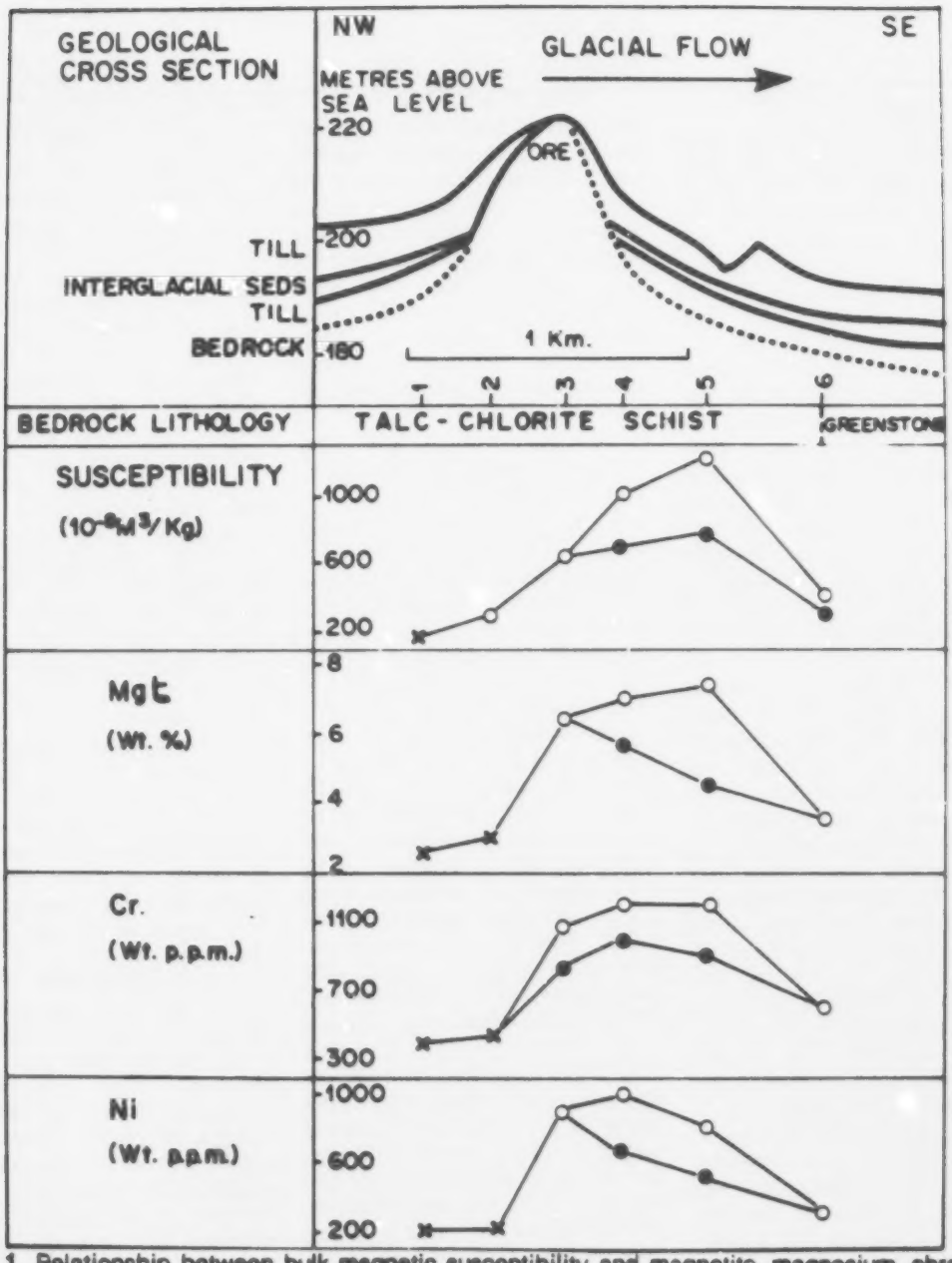

Figure 1. Relationship between bulk magnetic susceptibility and magnetite, magnesium, chromium, and nickel in drift samples from Visasaari area.

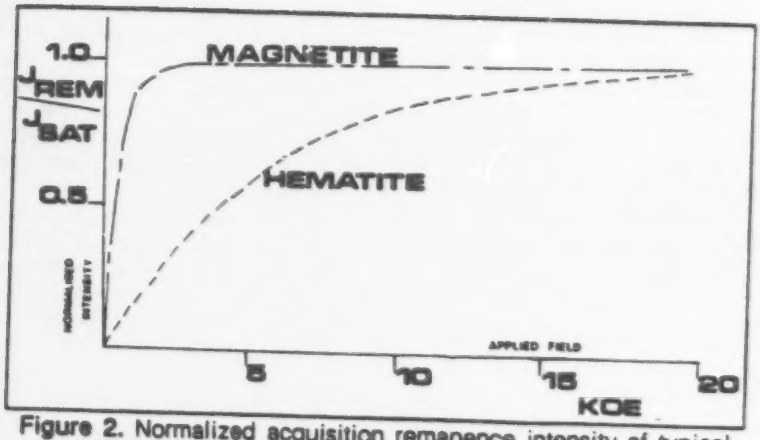

Figure 2. Normalized acquisition remanence intensity of typical silt sized magnetite and hematite samples upon the application of incrementally increasing applied DC magnetic fields (from Dankers 1978).

magnetite (gangue). Third, a special case of this mineral species problem is presented by the mineral (ferro-)ilmenite. Unless of a specific, narrow range of composition, (ferro-)ilmenite is nonmagnetic at common ambient temperatures.

Using the simple bulk susceptibility technique, the contribution of ilmenite to the total magnetic signature is unknown because there is no discrimination between contributing mineral species, and the potential nonmagnetic characteristic of ilmenite at normal temperatures.

From the example shown in Figure 1 it is apparent that bulk magnetic susceptibility surveys can be used as a rapid, accurate, and cheap method for the detection of mineralization anomalies that are known to be associated with significant concentrations of magnetite. It is also apparent that the magnetic portion of any till, soil, or rock sample contains much more information which cannot be accessed by simple bulk susceptibility measurements.

The objective of the research project described below is to develop field portable rock magnetic techniques which overcome the deficiencies of the bulk magnetic susceptibility technique. Specifically, the aim of this project is to develop rapid, accurate, and relatively cheap techniques that can be used to document the variation of magnetite, hematite, and ilmenite in any sample of soil, till, or rock. In addition to providing specific magnetic mineral discrimination, the newly developed techniques should also provide statistically significant data for samples that have hitherto yielded irresolvable data by the susceptibility technique as a result of their overall low magnetic mineral content.

METHODOLOGY

Rather than using the susceptibility properties of the magnetic minerals, the basis of this study is the induced magnetic remanence characteristics of the specimens. This approach has a number of direct benefits. First, by using strong magnetic fields to induce remanence signatures on the specimens, the signal that is to be measured is always enhanced relative to some background noise effects. It is hard to conceive of a situation when this would not give easily detectable signals. Second, the use of a silt size fraction is beneficial to this technique. In contrast to susceptibility, the saturation remanence intensity per unit volume of magnetic mineral is greater for a silt size fraction than it is for a sand size fraction.

To differentiate the relative contributions of magnetite and hematite mineral species, we have used an approach based on the hysteresis characteristics of these 2 minerals. Figure 2 shows typical examples of the field dependent remanence intensity of silt sized magnetite and hematite. There are 2 parameters that differentiate the 2 minerals: a) the field required to magnetically saturate all of the oxide particles present, and b) the per unit volume saturation remanence intensity. Magnetite is characteristically saturated after the application of fields of 2 KOe, and usually has a saturation remanence of the order of 12 emu/g. Hematite in contrast usually requires fields as high as 10 KOe to reach saturation, while its

saturation remanence is only of the order 0.25 emu/g. Some deviations from these average values can arise as a result of variable titanium content in the mineral lattice. These variations will not be of significance within a single study area.

To establish the relative contributions of magnetite and hematite, one can compare the magnitude of remanence intensity increase after the application of incremental specified direct magnetic fields. After correction of the magnetic intensity increment for the individual remanence intensity per unit volume, the exact mass of a specific magnetic mineral becomes readily apparent.

Upon cooling to liquid nitrogen temperatures, both magnetite and hematite exhibit transitions at which the per unit volume magnetic intensity is reduced. In contrast, with decreasing temperature (ferro-)ilmenite shows a gradual increase of per unit volume remanence intensity. Moreover, as shown in Figure 3, the slope and intercept of a plot of temperature versus remanence intensity is a function of the exact molecular composition of the ilmenite. By measuring the saturation remanence of dried till samples after the application of a constant direct field, but at incrementally decreased temperatures, it is then possible to magnetically detect the presence of ilmenite (the lowest detectable concentration appears to be approximately 0.01% per unit weight) and to identify, approximately at least, the molecular composition of the ilmenite.

INSTRUMENTATION

Our objective was to produce a field portable analytical system, so that it is possible to modify the sampling program as field results become available. The analytical system consists of 4 elements:

1. remanence measurement
2. data acquisition and presentation
3. DC field generation
4. low temperature environment

For measuring the magnetic remanence we have used an RFL 101 Fluxgate magnetometer that is connected to a Hewlett Packard DMM. A quasizero magnetic field free area for the measurement of the specimen remanence is created by a nest of high permeability steel boxes. The Hewlett Packard DMM provides connection to an HP-IL interface loop. Data acquisition, storage, and manipulation then is handled by a HP 41CX calculator, which is interfaced with Hewlett Packard printer/plotter and cassette drive peripherals. Two types of DC field generation have been employed. First, a number of Cobalt-Rare Earth permanent magnets have been included in a steel yoke system. Second, magnetic fields were generated in a solenoid by the pulsed discharge of a capacitor bank. The low temperature chamber for the measurement of saturation remanence at liquid nitrogen temperatures is presently under development.

RESULTS

To demonstrate the potential of this method, Figures 4 and 5 present the results obtained from a study of soil samples from a uranium prospect (the RAD area) of Westmin Resources in the Northwest Ter-

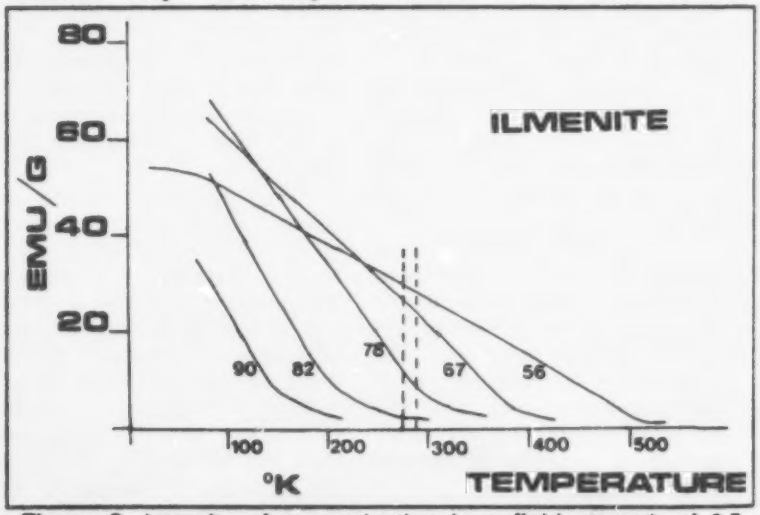

Figure 3. Intensity of magnetization in a field strength of 8.5 KOe versus temperature for ferro-ilmenite specimens. Numbers attached to each curve indicates the $FeTiO_2$ molecular percent of each sample.

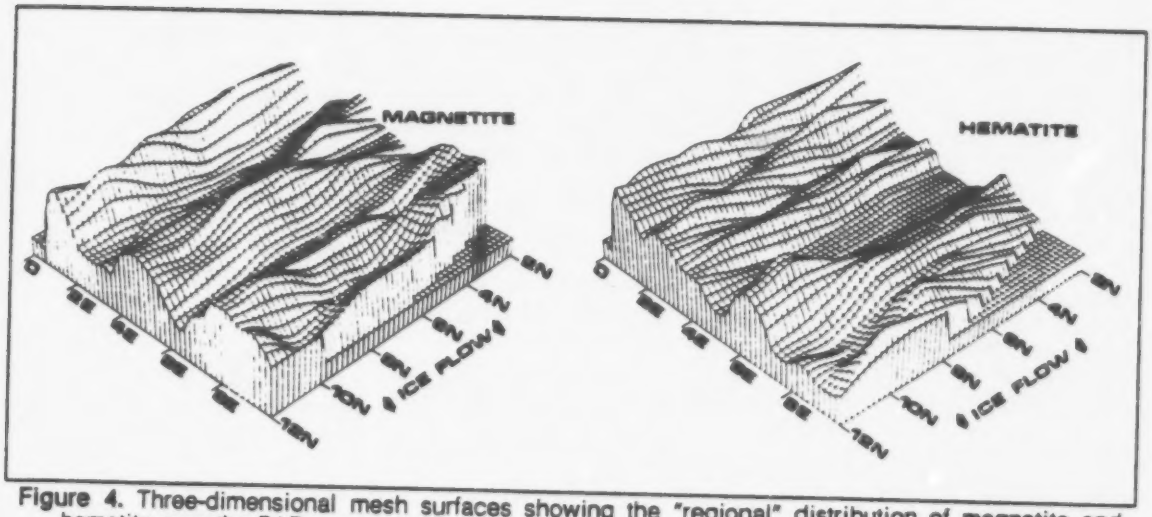

Figure 4. Three-dimensional mesh surfaces showing the "regional" distribution of magnetite and hematite over the RAD area.

ritories. In the RAD area, 2 types of uranium deposits have been detected. In the context of this study we can describe the 2 deposit types as hematite associated and magnetite associated. In particular, the latter type is marked by a localized magnetic anomaly, which is commonly coincident with a scintillometer anomaly. Bedrock outcrop in the RAD area is very poor; a large portion of the area is covered by glacial drift. Mapping of the drift morphology has suggested the presence of 2 ice transport regimes, the RAD train, and the extra-RAD train. The source of much of the drift material is Precambrian sedimentary basin strata which contains only a limited amount of magnetic minerals. Together with the samples having been prescreened, only the silt size fraction remained, the traditional bulk magnetic susceptibility approach did not yield any geologically meaningful information.

This new approach to drift prospecting by magnetic mineral characterization provides information on 2 aspects of the variations of magnetic properties of the soil samples. In simple terms, these 2 aspects may be considered as the 'regional' and the 'residual or local' contributions to magnetic property variations. The 'regional' distribution reflects the effects of distant sources of magnetic minerals, and the large scale flow pattern of the ice sheet as it affects the whole study area. Figure 4 presents the 'regional' magnetite and hematite content variations for the RAD area. As should be expected, both patterns show a very strong alignment of oxide content variations that is subparallel to the main direction of ice flow. These plots outline the RAD train. Both data sets also show, but it is best developed in the hematite plot, a trough between 8N and 12N that is trending at an angle to the main ice flow direction. This trough is subparallel to the trend of the extra-RAD train as defined by geological mapping. Prominent zones of both high hematite and high magnetite content can be recognized between 0 and 2E, and 6E and 10E. Grain size analyses of samples from these areas indicate that these zones were predominantly silt rich soils. The zone between 4E and 6E which is characterized by low hematite content, but enhanced magnetite content is a zone of more sand rich soils.

The 'residual or local' variations of magnetic mineralogy reflect the effects of localized additions, or depletions to the 'regional' magnetic mineral

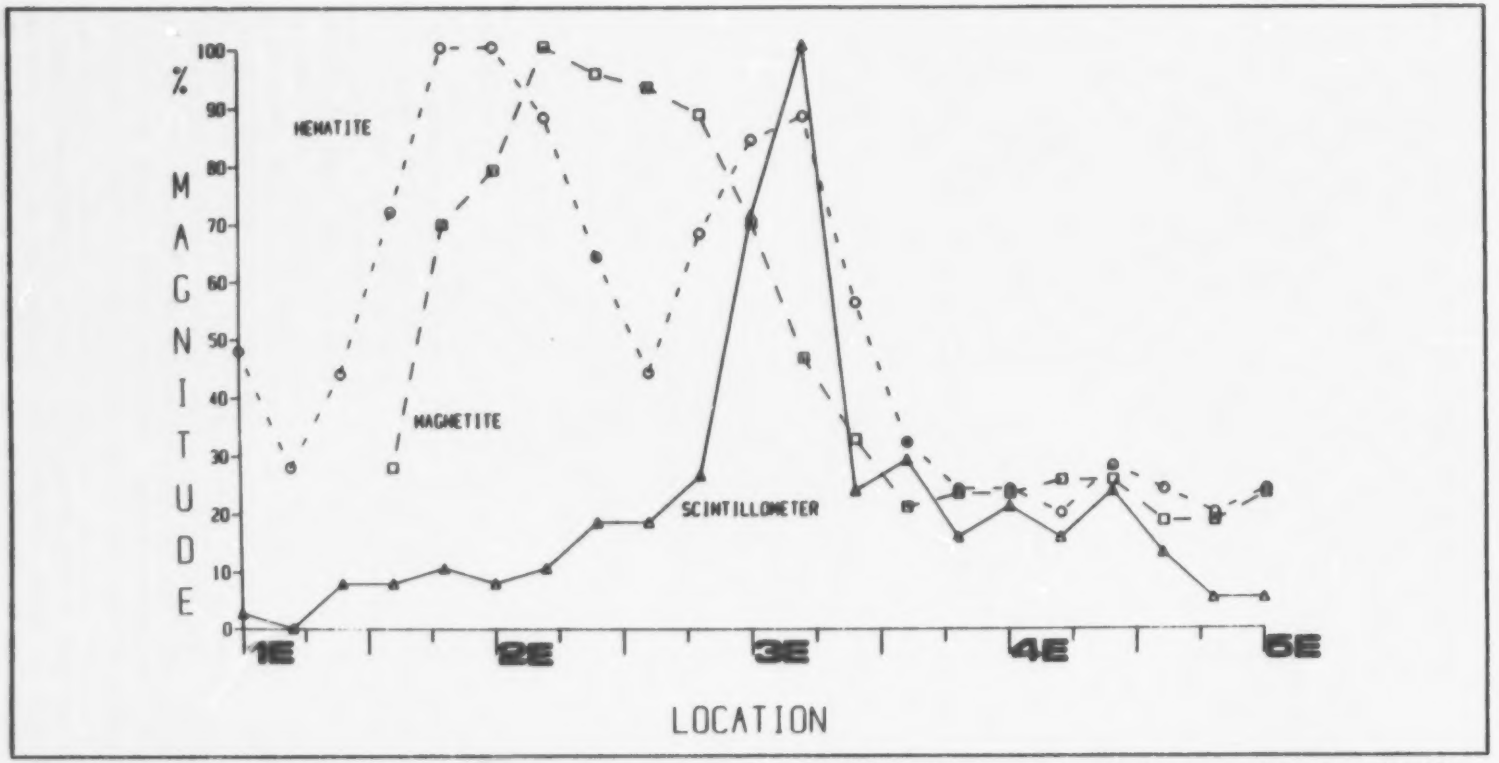

Figure 5. Comparison of the "residual" magnetite and hematite anomalies with a scintillometer survey along line 8N. The "residual" value is the difference between the observed values and the "regional" smooth surface values. The hematite values have been reversed; this zone is hematite depleted not enhanced.

pattern of the soils. The 'residual' variation represents the difference between the 'regional' and the observed raw data. In this instance, the 'regional' was defined by simple visual contouring of the raw data. More sophisticated analytical methods will be available for future commercial studies. Although there were a number of isolated aberrant values these were not considered to be geologically significant. Only on line 8N were there a number of associated aberrant values. Figure 5 compares normalized values of a scintillometer survey against the normalized values of the aberrant 'residual' magnetite and hematite content of the soils. For simplicity the sense of the hematite values has been reversed; that is, this zone is hematite depleted, not enhanced. Scintillometer surveys of lines both north and south of 8N do not show any strong deviations from background. The magnetic mineral content for these adjacent lines also conforms to the regional patterns. On line 8N the scintillometer values reach up to 3 times background levels. On this same line magnetite exhibits a strong enhancement above regional values, while hematite is noticeably depleted over the same area. One may infer from this association that a uranium occurrence is close by, and the mineralogy in this deposit is accompanied by the presence of significant amounts of magnetite. Of course the width of the soil-based mineralogical anomaly is dispersed relative to the scintillometer source related anomaly.

CONCLUSIONS

As shown by the above example, drift prospecting by characterization of the content of different magnetic mineral species provides a field portable method which can provide information on the sense of ice motion, the recognition of zones of lithological variation in the regional soil pattern, and can distinguish the presence of anomalous concentrations of specific oxide types. In this study the correlation of a scintillometer anomaly with enhanced magnetite values suggests the presence of a uranium deposit which has a magnetite-type mineralogical association.

The development of a system for the rapid detection of ilmenite is planned for 1984. Upon completion the system will be tested using both artificial samples, and samples from a known kimberlite occurrence. Further testing of the method will include using samples from the KLIP program where regional mineralogical patterns are well known. This will allow us to completely develop the analytical procedures, perfect our interpretational software, and present a number of examples of this new geophysical technique.

ACKNOWLEDGMENTS

We would like to thank Ernie Nutter and Ron MacMillan of Westmin Resources, and Ed van Hees of Pamour Porcupine for their samples, and their permission to publish this data.

REFERENCES

Dankers, P.H.M.
1978: Magnetic Properties of Dispersed Natural Iron-Oxides of Known Grain Size; Ph.D. Thesis, State University of Utrecht, 142p.

Pulkkinen, E., Puranen, R., and Lehmuspelto, P.
1980: Interpretation of Geochemical Anomalies in Glacial Drift of Finnish Lapland with the Aid of Magnetic Susceptibility Data; Geological Survey of Finland, Report of Investigation, Number 47 p.39.

Grant 052 Production of a 7-Frequency Helicopter Electromagnetic System

P.E. Wessler

Geotech Limited, Markham

ABSTRACT

As a result of an Exploration Technology Development Fund (ETDF) grant that was awarded to Geotech Limited in late December 1983, work has begun on an update of the Geotech EMEX-1 Helicopter Electromagnetic System. This report covers the initial 6 months of work completed since the award of grant GR-052.

This work will advance the state of the art for helicopter electromagnetic (HEM) systems from the current 4-frequency EMEX-1 System to the EMEX-2 System. The EMEX-2 System will operate at 7 independant frequencies and cover a much wider frequency range. This new development, when completed, should culminate the rapid series of technological improvements in HEM Systems which have occurred over the last few years.

As a result of Ontario Geological Survey Grant 018, Geotech developed the first 4 frequency HEM system, the EMEX-1. The techniques that were developed for the EMEX-1 System enabled this further development, allowing expansion to a 7-frequency system incorporating 3 coil geometries. The EMEX-2 system will offer a much wider frequency range than previously available in the EMEX-1 System, ranging from a low of 190 hz to the upper limit of 12 khz. This broad range of frequencies will make the system a superior tool for mapping both structural and formational geology. The ability to detect and resolve poorly conducting zones of mineralization will be a significant improvement over all HEM systems currently available. Improved depth of penetration and resolution should encourage explorationists to refly areas of potential interest.

The EMEX-2 system has been designed for optimum flexibility for the end user. Supportive software is also being developed to allow the 14 channels of EM information to be processed efficiently. The EMEX-2 will provide a major step forward in the state of the art. The Canadian mining community as a whole should benefit from this cost effective exploration tool.

INTRODUCTION

In 1981 Geotech Limited began development of a 'state of the art' helicopter-towed electromagnetic exploration system. This work culminated the following year in the successful field trials of the system. The EMEX-1 4-frequency system is currently being flown in Canada by independant contractors serving the mining community. We expect the 7-frequency EMEX-2 System to be part of the final phase in the evolution of HEM systems. The resulting instrumentation from this project should have widespread applications throughout Ontario and Canada.

The 7 frequencies have been arranged to provide widely spaced frequency transmission on 3 independant coaxially coupled coils, 2 horizontal coplanar coils (whaletail), and 2 vertical coplanar coils (fishtail). All coils are presently maintained at an 8 m coil separation, although other coil separations are possible on special order. The removable transmitter and receiver modules are contained in a 9 m bird (Figure 1). The bird shell is manufactured from a Kevlar composite material. Geotech has produced its own custom designed mandrel for the production of these bird shells in order to maintain a consistent mechanical integrity. The unique construction of the 9 m shell has been tested to demonstrate adequate strength and dimensional stability while at the same time providing weight savings that are critical in helicopter work. Tolerances in the construction can be maintained well enough to allow the interchange of removable structures from one bird to another. This is important from a spareparts or maintenance viewpoint. The additional 3 sets of coils, coupled with the longer bird shell, will result in an overall weight increase of only about 30 kg. Hook load for the EMEX-2 system will be about 210 kg. This is within the load capacity of most small helicopters, such as the Astar 350, and will allow the addition of ancillary sensors to the system without decreasing the fuel load.

Figure 2 shows a pictorial representation of the coil configuration that is utilized in the bird. The following nominal frequencies are incorporated into the standard system:

1. 190 hz horizontal coplanar (whaletail)
2. 870 hz horizontal coplanar (whaletail)
3. 380 hz vertical coaxial
4. 918 hz vertical coaxial
5. 2200 hz vertical coaxial
6. 5000 hz vertical coplanar (fishtail)

Figure 1. Typical airborne Geotech EMEX System. A magnetometer sensor is suspended midway on the tow cable.

7. 12000 hz vertical coplanar (fishtail)

Note that the selection of coil orientation allows for 3 coaxial geometries that can be nominally tuned for any frequency within the range of 190 hz to 12 khz. This also applies to the whaletail and fishtail configurations. As an example of the versatile nature of the design, the whaletail coils could be arranged using 190 hz and 5000 hz operating frequencies. The only restriction on the final selection of the frequencies is that the harmonic relationship between transmitter frequencies must be considered for coils having similar geometries.

Thus 14 channels of geophysical information are provided by the EMEX-2 System, along with optional power line monitors for each frequency. This configuration of frequencies and coil orientations

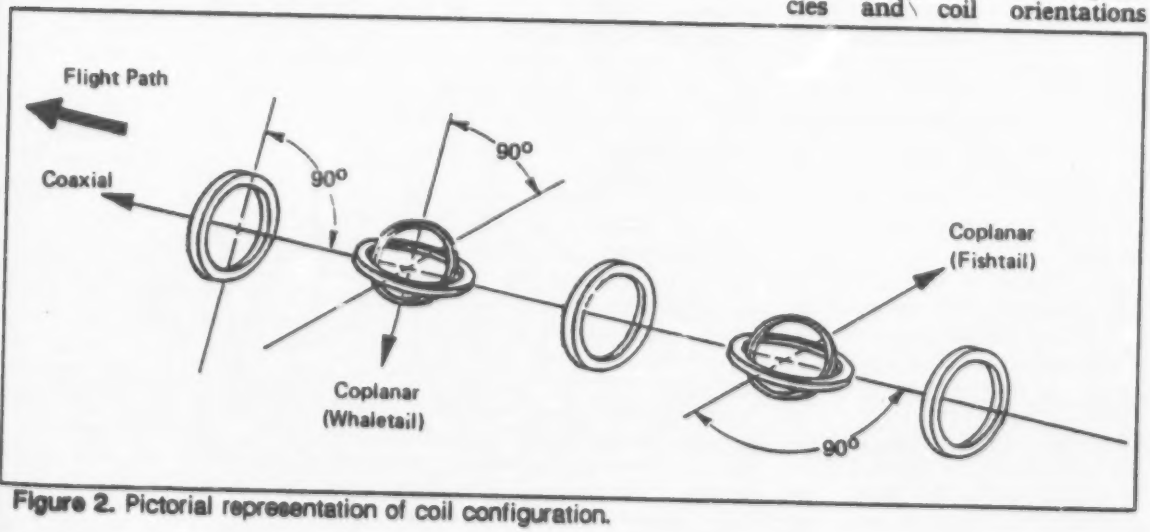

Figure 2. Pictorial representation of coil configuration.

should provide specific information in areas where the geology was previously unknown. Post-flight processing of this large amount of data can accomplish overburden stripping, multilayered earth interpretation, and resistivity mapping, along with dip and strike interpretations.

Figure 3 is a set of graphs depicting response profiles produced by each of the coil orientations, for various conductance-frequency products. Four different conductor geometries are shown. Profile sets A and B show the advantage of having 2 orthogonal coplanar coil sets. In set A, the whaletail and coaxial coils produce only a very small response, while the fishtail coils have maximum coupling with the vertical dike which is parallel to the flight path. In set B, for the same vertical dike but striking 90° to the flight path, there is minimal coupling with the fishtail coils but good responses for the other coil orientations. The advantages of widely spaced frequencies is also apparent in that the response profiles vary remarkably for different conductance-frequency products.

In Figure 4 the effect of coil geometry, coil separation, and flying height is shown for a horizontal sheet. At a flying height of 30 m the absolute value of the response for the whaletail pair is twice that for the coaxial or the fishtail pair. It should be noted here that although the fishtail and coaxial coils produce a similar secondary response from a horizontal sheet, in absolute terms, the number of ppm recorded by the system for the coaxial coils is half that of the fishtail coils. This is because the primary field seen by the coaxial coils is twice that seen by the coplanar coils and it is the ratio of secondary to primary fields that is measured by the EMEX-2 system.

DESIGN OBJECTIVES

There is a prime requirement to minimize the amount of interaction between the complimentary coil pairs. This has been achieved through a unique method developed by Geotech that involves not only the electronic processing modules, but is fundamental in the coil design and construction. These combined techniques allow for the additional use of the fishtail configuration along with the traditional coil orientations. One of the prime design objectives was to produce a system with the absolute minimum amount of interaction between coils that are closely spaced mechanically. This interaction has been a problem with all multi-frequency EM systems.

Geotech has developed a method which largely removes the effective mutual inductance between adjacent coils. This modification, when implemented, means that the coils no longer appear as large anomalies to each other, a refinement which has greatly streamlined the technology. This improvement, coupled with the Geotech electronic crosstalk removal system, allows virtually totall removal of unwanted signals at any frequency from any channel, and it does this without introducing baseline drift such as might occur if traditional filtering was used. This crosstalk compensator module can be seen on the photograph of the EMEX-1 main console (Figure 5). The block diagram of the EMEX-2 module (Figure 6) shows the role of the electronic crosstalk compensator within the system.

Currently the EMEX-2 system requires the use of 2 main electronic consoles in order to handle the 7 transmitted frequencies. The block diagram shows 1 of the 7 modules that are required for the total system. Two crosstalk compensator modules are also required, along with a regulated power supply. Rack space required for the 2 consoles totals 26.7 cm. The potential exists for future mechanical redesign to reduce the size of the system.

In order to reduce baseline drift the internal printed circuit boards (PCB) have been completely redesigned. The signal processor PCB has been upgraded to increase the flexibility and allow 1 board to be used for any of the transmitter frequencies. Testing of the prototype units has shown an apparent improvement in the stability of the electronics to temperature variations. This should result in a significant improvement in baseline drift over the EMEX-1 module. In addition, a modification has been incorporated to reduce the number of harmonics being passed through the system. More sophisticated electronic band-pass filtering has been introduced as well. All these modifications have been designed, built, debugged, and incorporated into the printed circuits. We feel major headway has been made in this area, and on-going changes to further stabilize the baseline will be instituted as the project is completed. These latest modifications will improve the systems overall ability to be used as a geological mapping tool.

In order to accommodate the increase in the number of

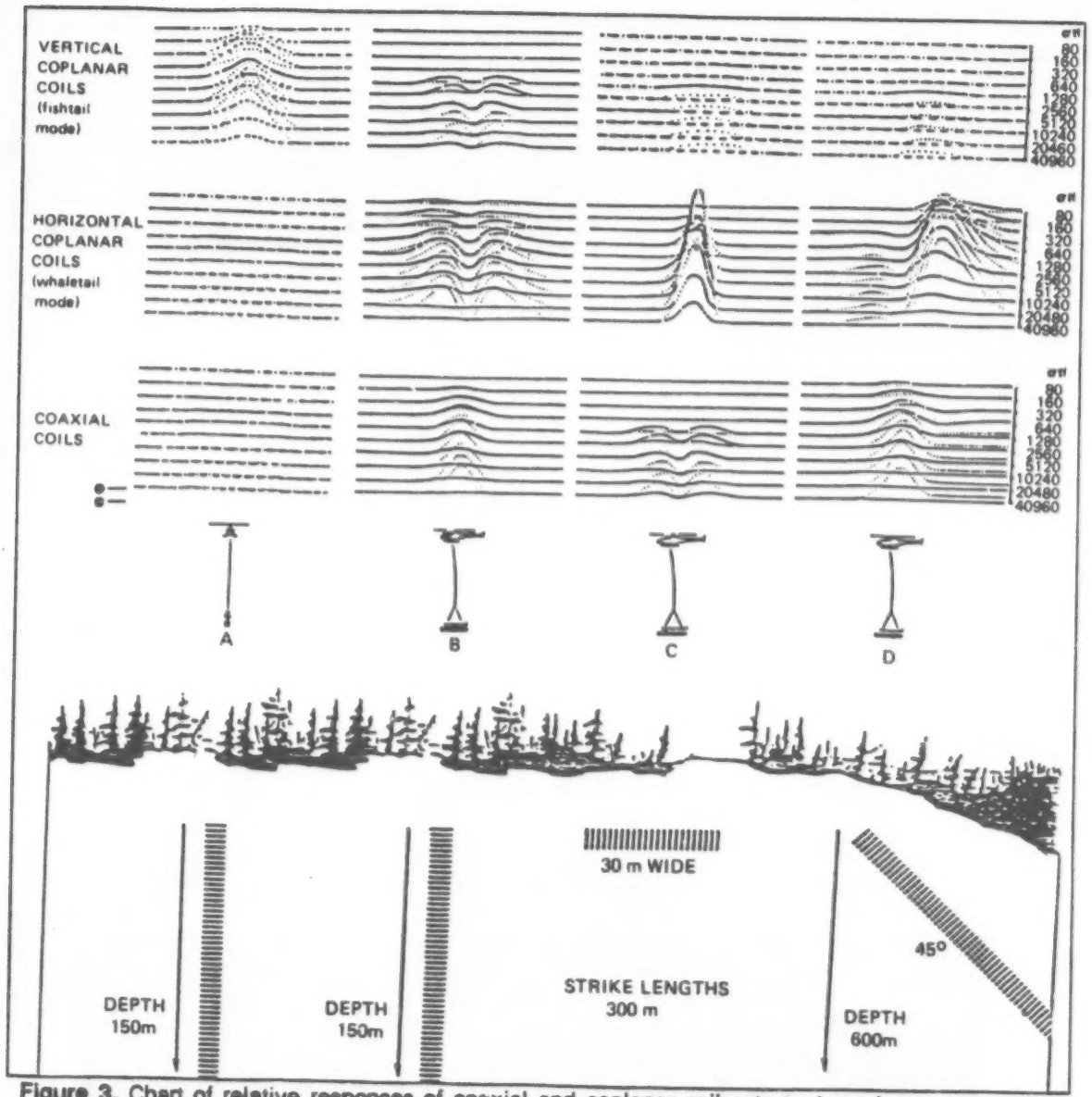

Figure 3. Chart of relative responses of coaxial and coplanar coil sets to 4-conductor geometries. Note the improved interpretation of conductor geometry possible when data is collected in the fishtail, whaletail, and coaxial modes. Response of a conductor with strike parallel to the flight direction is enhanced by the fishtail mode (set A).

preamplifiers in the system, the entire preamplifier assembly has been redesigned mechanically. This required an update of the design of the preamplifier itself. A new preamplifier printed circuit board has been produced. Minor modifications were incorporated to allow flexibility in frequency change-over in the field should it be required. Test jigs were produced to allow individual component testing for such things as inherent noise and temperature stability. The results of the work on the preamplifier remain to be field tested but in-house testing once again shows positive results.

Since client feedback has demonstrated the need for a wider range of transmitted frequencies, Geotech embarked on a program to provide a range of frequencies that should suit most geophysical

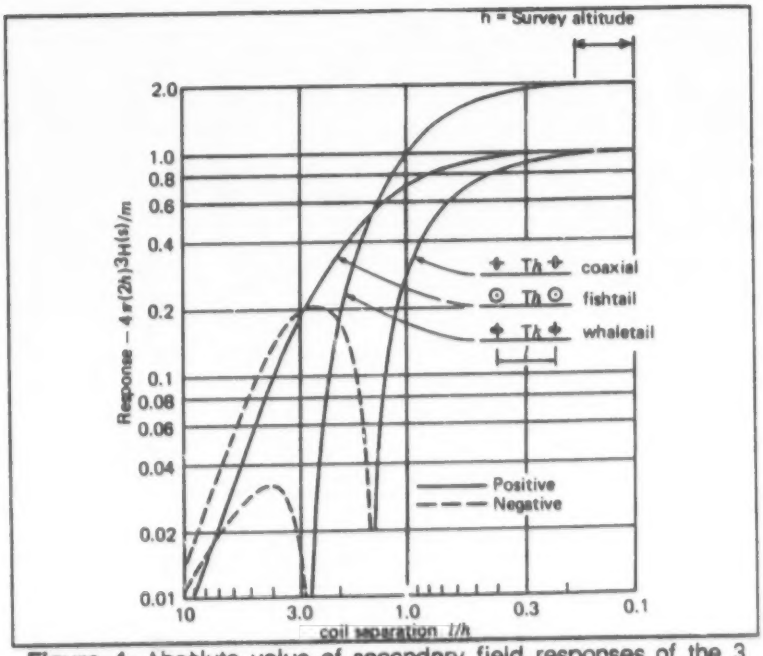

Figure 4. Absolute value of secondary field responses of the 3 coil orientations for a horizontal sheet (after Grant and West 1965).

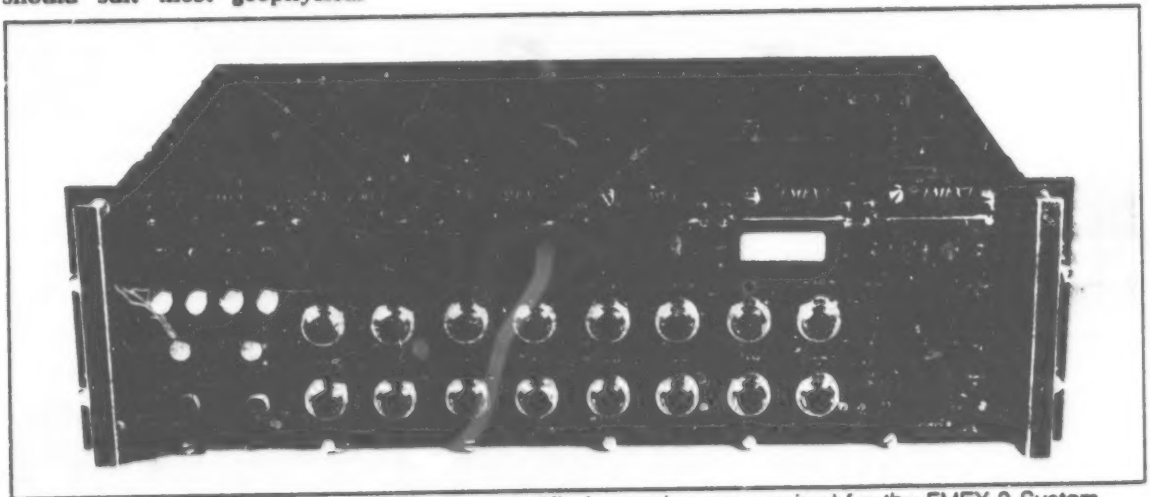

Figure 5. The EMEX-1 main console. Two modified consoles are required for the EMEX-2 System.

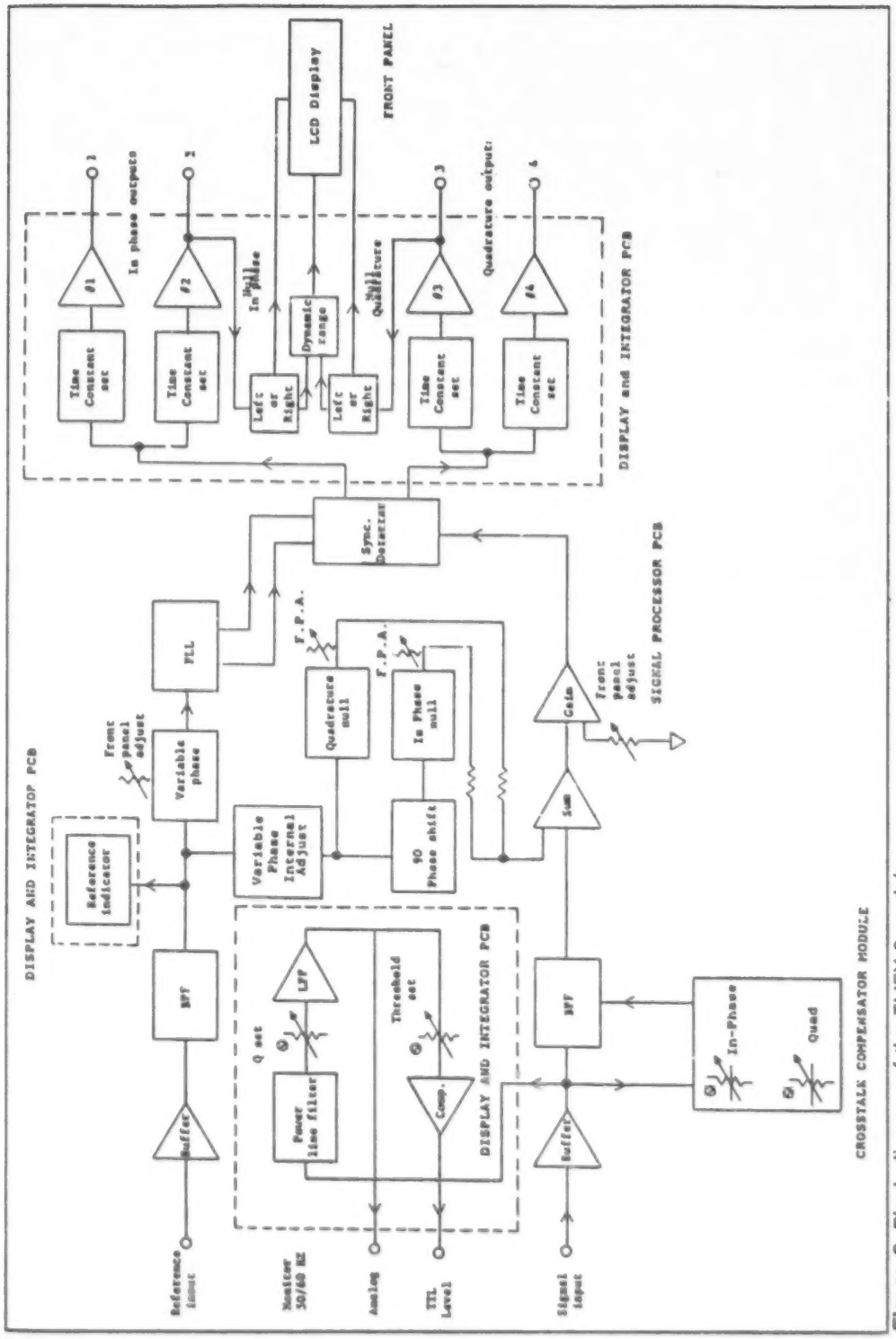

Figure 6. Block diagram of the EMEX-2 module.

applications. The recent emphasis on gold exploration and structure delineation has produced the need for higher frequencies than were previously available. In keeping with this need, Geotech has been successful in producing a transmitter design that allows the efficient transmission of frequencies from below 190 hz to an upper limit of about 12 khz. The possibility also exists to produce a transmitter coil system that can produce the required dipole moment at frequencies well beyond the current 12 khz upper limit. This technique could eventually lead to the development of a new geophysical instrument operating in the VLF range.

In addition to the improvements that have been incorporated in the main console, a significant amount of effort has been incorporated into the bird. Special consideration has been given to the reduction of weight while at the same time maintaining the required integrity of the mechanical structure. Various techniques have been used to reduce the possibility of motion of the transmitter coils relative to both the receiver coils and the bucking coils. Mechanical design for an EM system requires rigid coupling between the receiver and transmitter coils. A 1 ppm change in coil separation will result in a 3 ppm change in signal amplitude. Temperature gradients in excess of 10°C can be encountered from the start to the end of a typical survey flight, thus the temperature coefficients of materials used, becomes important to the airborne performance of the system. Geotech's attention to detail in all aspects of bird design should result in improved performance. Actual airborne testing is required before the benefits of this effort can finally be categorized.

As shown in the block diagram (Figure 6) and the photograph of the EMEX-1 main console (Figure 5), there are 4 external front panel adjustments on each of the EMEX-2 modules. Therefore, a total of 28 front panel controls are available to the field operator. Due to the nature of the electronic design, a minimum amount of operator intervention will be required in actual practice. It would be totally impractical to expect a normal person to make airborne adjustments to all 28 of the external controls. Ground calibration and alignment will be done prior to takeoff with essentially no operator adjustments required when airborne. There is the strong possibility that the system will eventually be manufactured to function under microprocessor control and the required adjustments and alignment would be done by software control in real-time. In this vein we have investigated the requirements for converting this system to a digital design. This conversion will gradually take place, concurrent with the development program and possibly in a future phase of this project.

SOFTWARE DEVELOPMENT

In keeping with the necessity to manage all of the acquired survey data, Geotech has developed a relatively fast automated method for the interpretation of multifrequency airborne EM survey data. The technique is based on a 2-step inversion which uses a good initial guess as the basis for a nonlinear regression algorithm. The relative uniformity to be expected locally in the conductivities of overburden and most basement rock types can be exploited by this interpretation package to generate estimates of subsurface conductivities at various skin depths in the region of interest. These can then be plotted in the form of a resistivity or conductivity pseudosection, which can then be interpreted to yield estimates of overburden thickness and conductivity as well as indicating the presence of other anomalous subsurface features. The wide range of frequencies used in the EMEX-2 system allows for relatively accurate determinations of conductivity variations with depth. It is well known that the maximum depth of penetration depends on the electromagnetic skin depth of the lowest frequency that is used. The skin depth in turn depends on the conductivity of the material that is being penetrated. The upper-most frequency is useful for delineating very shallow and more resistive zones.

Figures 7 to 10 are examples of computer generated data that demonstrate the response of the EMEX-2 system to a variety of geophysical targets. Figure 7 shows the advantage of the fishtail pair when flying along a buried plate. Figure 8 compares the response of the EMEX-1 system to the EMEX-2 system as the bird traverses across a buried plate. Figure 9 compares the response of a buried sphere for the 4-frequency EMEX-1 system to the 7-frequency EMEX-2 system. The traditional Geotech 3-frequency response to a buried plate sphere is provided in Figure 10. The reader may wish to compare Figure 10 to the other computer generated curves. The additional inter-

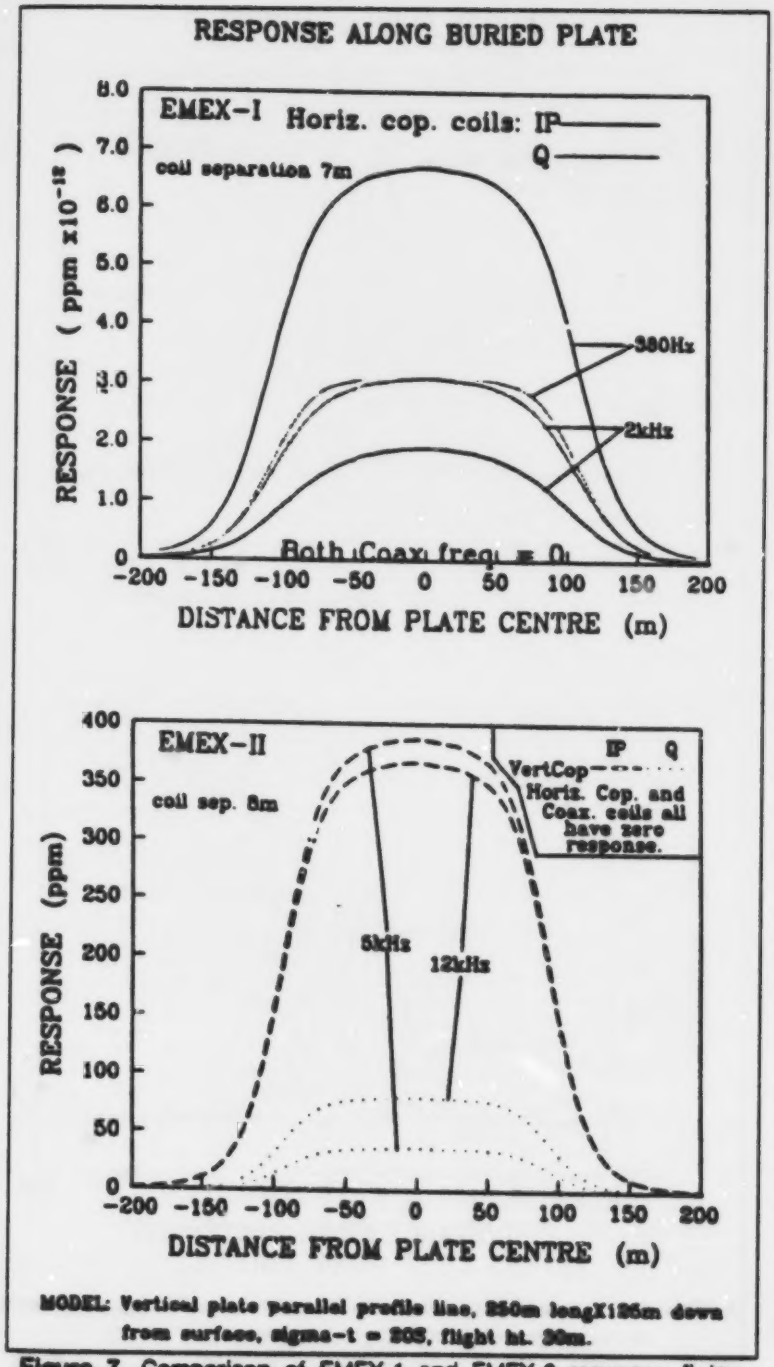

Figure 7. Comparison of EMEX-1 and EMEX-2 response flying along a buried plate.

pretive information provided by the EMEX-2 system can be clearly seen. Both the increased number, range of frequencies, and the addition of the vertical coplanar coil configuration on the EMEX-2 system will allow significant improvements in all types of geological interpretations. Again the advantages of the EMEX-2 system in areas of unknown geology are clearly demonstrated by these computer simulations.

FUTURE PLANS AND CONCLUSIONS

All mechanics associated with the project have been completed and the system is in the the final stages of assembly. We anticipate initial field testing to begin in the immediate future with a flying program to be completed by the end of 1984. The preliminary work that has been done to date is extremely encouraging and we anticipate minimal problems with system debugging since our experience with the EMEX-1 system has produced no unforeseen problems. Geotech intends to continue the development of interpretive software packages that will be required to handle this vast amount of information. With 14 or more channels of EM information it is almost mandatory that computer data compilation be carried out in order to obtain the maximum use of the survey data. This increasing sophistication in the acquisition of airborne geophysical data will provide for maximum utilization of the exploration dollar. Field costs for an EMEX-2 system will be identical to those of any other helicopter EM system.

Through the knowledge and expertise that has been

gained by Geotech personnel while working on this project, Geotech has been able to extend the airborne EM technology to new areas of engineering study. Geotech has recently been awarded a contract to undertake the further development of electromagnetic technology to produce a unique 'Through Ice Bathymetry' system for the Canadian Centre for Inland Waters. This bathymetry system will be used almost exclusively in the Canadian Arctic for measuring the depth of coastal waters beneath the ice, thus providing valuable shipping lane information. Preliminary work done to date shows that the possibility exists to incorporate the Geotech high sensitivity vertical magnetic gradiometer with the EMEX-2 system. This would provide an extremely powerful airborne survey package. In keeping with this eventual goal, the EMEX-2 bird is being designed using non-magnetic materials.

We at Geotech feel that the ETDF funding of this type of project will continue to keep Ontario, and indeed Canada, in the forefront of geophysical instrumentation and services throughout the world.

REFERENCES

Fraser, D.C.
1979: The Multicoil II Airborne Electromagnetic System; Geophysics, Volume 44, p.1367-1394.

Frischknect, F.C.
1967: Fields about an Oscillating Magnetic Dipole over a Two-layer Earth; Colorado School of Mines, Volume 62, Number 1.

Grant, F.S., and West, G.F.
1965: Interpretation Theory in Applied Geophysics; New York, McGraw-Hill Book Company Incorporated, p.456, 501, 502, 326, and 571.

Lodha, G.S., and West, F.G.
1976: Practical Airborne EM Interpretation Using a Sphere Model;

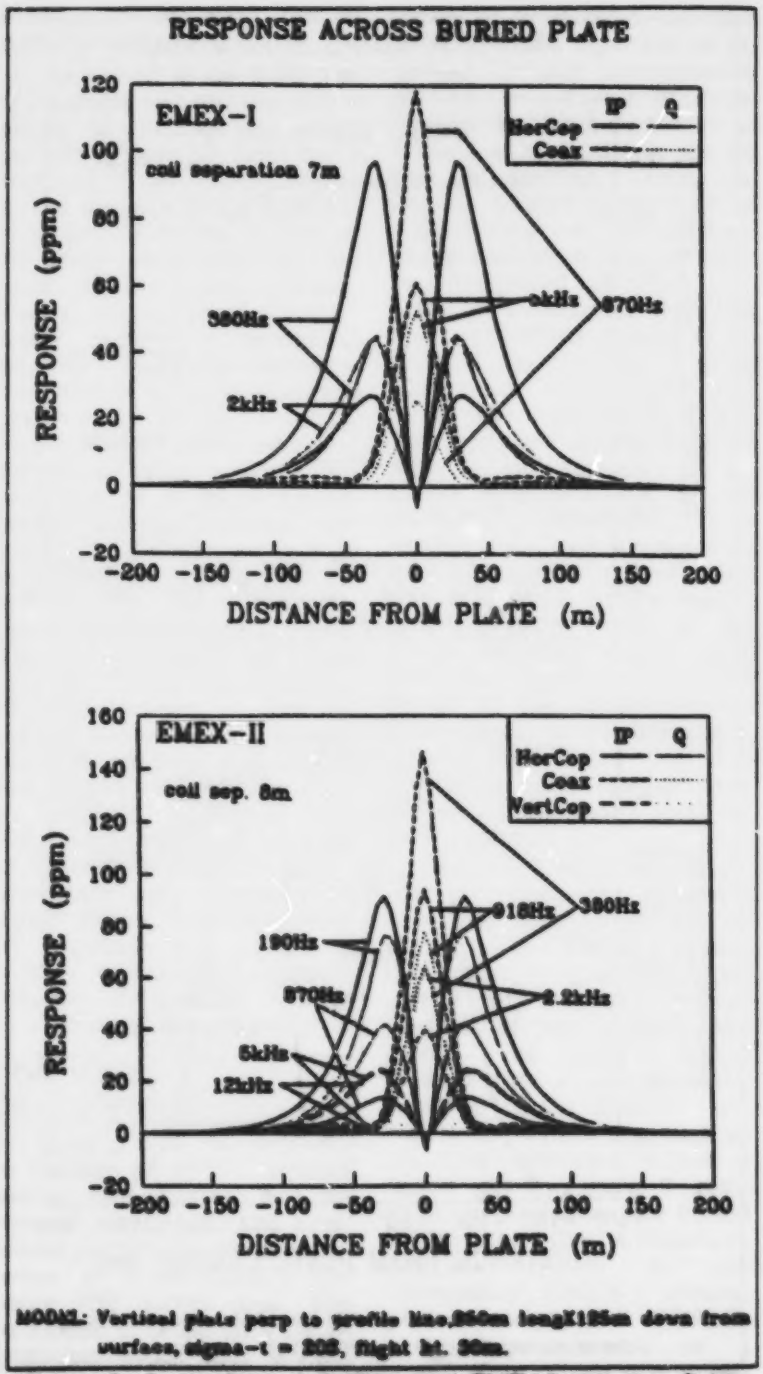

Figure 6. Comparison of EMEX-1 and EMEX-2 response flying across a buried plate.

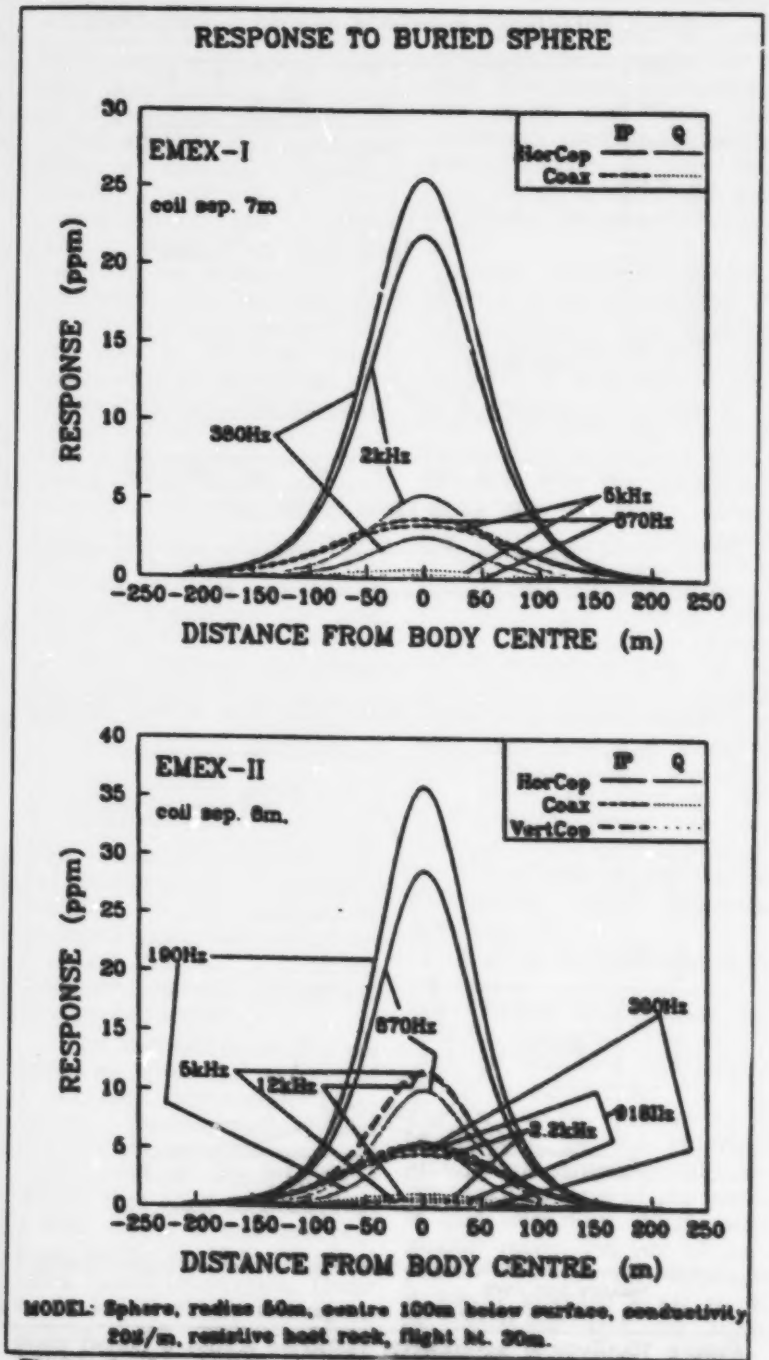

Figure 9. Comparison of EMEX-1 and EMEX-2 response to a buried sphere.

Geophysics. Volume 41, p.1157-1169.

Morrison, E.B.
1983: Grant 018 Development of a Four Frequency Helicopter Electromagnetic System; p.77-82 *in* Exploration Technology Development Program of the Board of Industrial Leadership and Development, Summary of Research 1981-1983, edited by E.G. Pye and R.B. Barlow, Ontario Geological Survey, Miscellaneous Paper 115, 135p. Accompanied by 2 charts.

Paterson, N.R.
1971: Airborne Electromagnetic Methods as Applied to the Search for Sulphide Deposits; Canadian Institute of Mining Bulletin, January, p.29-38.

Pemberton, R.H.
1962: Airborne EM in Review; Geophysics, Volume 27, p.691-713.

Sinha, A.K.
1973: Comparison of Airborne EM Coil Systems Placed Over a Multilayer Conducting Earth; Geophysics, Volume 38, p.894-919.

Sengpiel, K.
1983: Resistivity/Depth Mapping with Airborne Electromagnetic Survey Data; Geophysics, Volume 48, p.181-196.

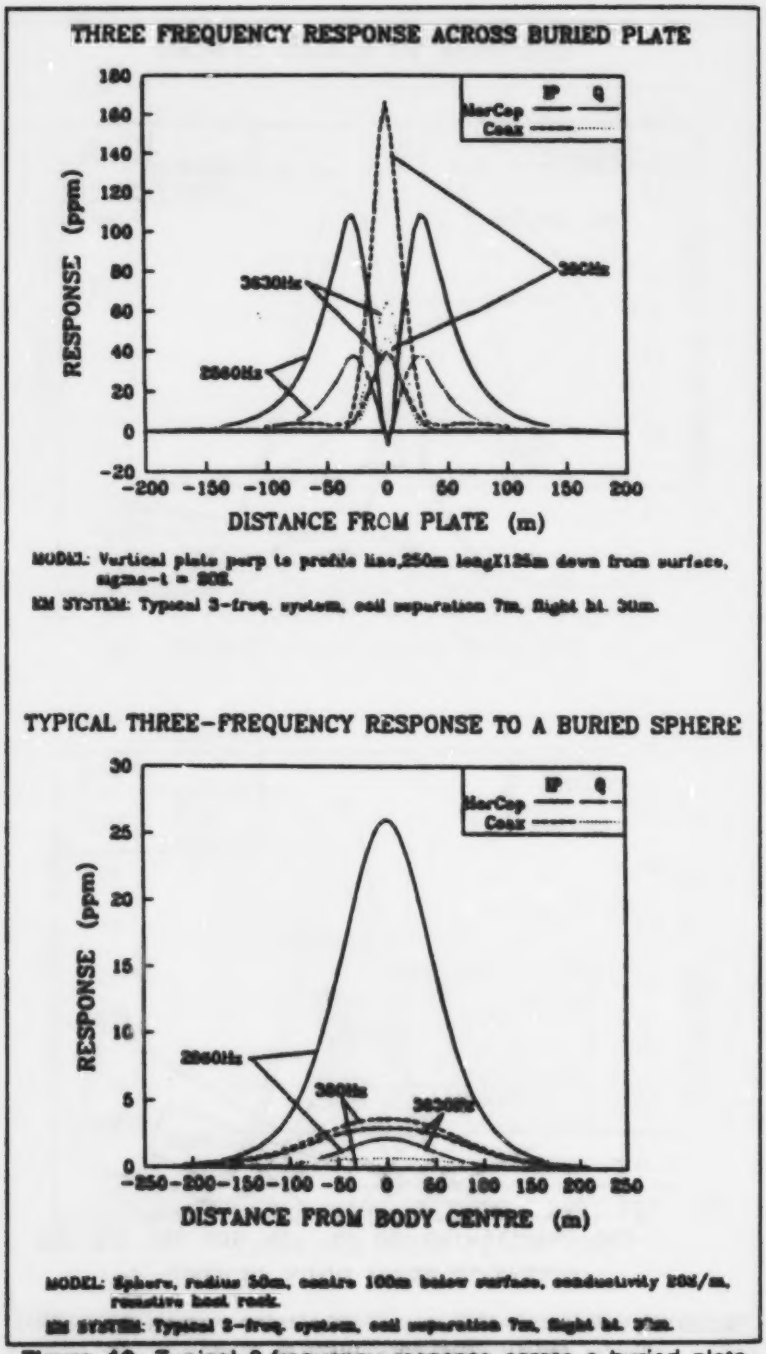
THREE FREQUENCY RESPONSE ACROSS BURIED PLATE
RESPONSE (ppm)
DISTANCE FROM PLATE (m)
MODEL: Vertical plate perp to profile line,250m longX125m down from surface, sigma-t = 20S.
TYPICAL THREE-FREQUENCY RESPONSE TO A BURIED SPHERE
RESPONSE (ppm)
DISTANCE FROM BODY CENTRE (m)
MODEL: Sphere, radius 50m, centre 100m below surface, conductivity 20S/m, resistive host rock.

Figure 10. Typical 3-frequency response across a buried plate compared to a buried sphere.

Grant 053 Improvements to Geochemical Analysis

J.D. Kinrade, W. Kostiak, and J.C. Robbins

Scintrex Limited, Concord

ABSTRACT

Improved techniques have been developed for the analysis of geological materials. The actual analysis was conducted with a compact flameless atomic absorption spectrophotometer, the Scintrex AAZ-2, while flux digestion was used for decomposition of the sample. The flux, designated "Geoflux" is a member of a new class of low temperature fluxes used to decompose geological materials. The principle metals under consideration were gold, copper, lead, zinc, nickel, cobalt, silver, mercury, arsenic, antimony, and tin. A good correlation with reported values was found for the first 7 metals. Of particular interest was the procedure for gold, which did not require the use of acids. Efficient decomposition procedures employing the flux could not be found for antimony, arsenic, mercury, or tin.

INTRODUCTION

This project is concerned with the development of improved methods for the analysis of geological materials using the Scintrex AAZ-2, a compact flameless atomic absorption spectrophotometer.

The methods developed are based on successful aspects of a previous Exploration Technology Development Fund (ETDF) project (Kinrade and Robbins 1983) where it was shown that good recoveries of a wide variety of base and precious metals could be obtained using fusion techniques. These methods involved mixing a sample with an inorganic salt—a flux—which when heated, melted to form a corrosive nonaqueous solution. Such fluxes not only avoid the use of strong acids but are usually considerably faster in operation than the common acid attack. The metals considered in this study were those most commonly used in exploration geochemistry: copper, lead, zinc, nickel, cobalt, silver, gold, antimony, arsenic, and mercury.

The standard extraction procedure for geochemical determinations is the combined HNO_3/HCl attack at a temperature of some 80° to 90°C over a period of at least 3 1/2 hours and preferably 10 to 12 hours. The attack is a partial attack in that the silicate materials are not totally decomposed but rather that metals bonded more or less loosely to the silicate tetrahedra, chains, or sheets are leached from their environment. Foster (1971) presented data on the extraction efficiency of various types of acid as a function of both rock type and elements (zinc, copper, cobalt, and nickel). Only the mixed HF-$HClO_4$-HNO_3 attack was consistently found to give recoveries comparable to the values determined from emission spectroscopy.

A given acid digestion is by no means a universal solvent but requires modification for specific elements. For example, the standard HNO_3-HCl attack is suitable for Cu, Zn, Pb, Co, and Ni, whereas Ag is precipitated by the chloride, and gold is only partially extracted. The form of the metal is also important. Nitric acid attacks many, but not all sulphides. Mercury (II) sulphide is hardly attacked at all, those of antimony and tin form sparingly soluble oxide-hydrates, and lead sulphide is oxidized by more concentrated acid to the sparingly soluble sulphate (Bock 1979, p.196). The list of substances which do not dissolve in hydrochloric acid includes ignited oxides of Al, Be, Cr, Fe, Ti, Zr and Th; the oxides SnO_2, Sb_2O_5, Nb_2O_5 and Ta_2O_5; zirconium phosphate, monazite, xenotime; sulphates of strontium, barium, and lead; alkaline earth fluorides (except of beryllium); spinel; pyrite; sulphides of mercury and some other metals; chromite; ores of niobium and tantalum; and various ores of thorium and uranium (Bock 1979, p.69). Hydrofluoric acid, on its own, works faster than mixtures of it with other acids (Langmyhr 1965). Hydrofluoric acid attacks may result in residues of sparingly soluble fluorides of magnesium, calcium, strontium, barium, uranium (IV), and the rare earths. Quartz and silicates of high aluminum content are attacked only slowly by hydrofluoric acid; zircon and topaz must be attacked at high temperatures (greater than 400°C). The method is not suitable when SnO_2 or pyrite is present (Bock 1979, p.58-60). A need exists for a more versatile solvent.

A number of metals and their compounds that are more or less resistant to attack by acidic or alkaline aqueous solutions can be dissolved by fusion techniques. These techniques take various forms but, in general, the material to be decomposed is mixed with a suitable salt or mixtures of salts which melt at an elevated temperature to form a corrosive, nonaqueous solution. After the reaction has taken place and the melt is cooled it can usually be dissolved in an aqueous solution. The composition of the flux can be chosen so that for a given sample either total digestion as in the

fusion of silicate rocks with lithium metaborate (Van Loon and Parississ 1968) or partial digestion as in the selective extraction of cassiterite (SnO_2) in a silicate gangue by fusion with ammonium iodide (Bond 1970) can be achieved.

There are significant drawbacks to the fluxes that are presently in common use, centring around either the high temperatures called for or the specialized containers required to confine the fusion reaction. Lithium metaborate fusions for instance are typically made at 1000°to 1100°C requiring the use of carbon crucibles. Sodium hydroxide on the other hand has a very low melting point (318°C) but the fusions are normally carried out in a platinum, or platinum/gold crucible.

The fluxes that have been developed at Scintrex are the outcome of work done during the earlier ETDF project on field methods for the preparation of rocks and soils in the determination of tin and tungsten. The strongly oxidizing fluxes fall into 2 main series: an acidic flux (FX series), and a more basic flux (TR series). In general, the basic flux is used for metals and oxides that are normally attacked using strong basic leaches or fusions, for example sodium hydroxide, sodium carbonate. The acid flux is used to replace strong acid attacks. The metals and their compounds successfully tested to date by the acid flux in geochemical applications include gold, silver, titanium, chromium, zirconium, nickel, tin, and iron. The base fusion has been used for molybdenum and tungsten.

TABLE 1: CRUSTAL ABUNDANCES VERSUS AAZ-2 DETECTION LIMITS

ELEMENT	CRUSTAL ABUNDANCE	AAZ-2 DETECTION LIMIT
Antimony	0.5 µg/g	0.002 µg/g
Arsenic	1.7	0.003
Cobalt	18	0.001
Copper	47	0.0004
Gold	0.0042	0.002
Lead	16	0.0008
Mercury	0.083	0.007
Nickel	58	0.003
Silver	0.07	0.0008
Tin	2.5	0.014
Zinc	83	0.00009

ANALYTICAL METHODS DEVELOPMENT

A comparison of the AAZ-2 detection limits for the metals of interest versus their average lithospheric abundance (Rosler 1972) is presented in Table 1. In all cases the instrumental detection limit was lower than the crustal abundance of the element. The AAZ-2 is therefore well suited to this type of analysis.

The majority of the methods development work was carried out on 8 geological standards submitted for comparative analysis by the Geology-Chemistry Group of the Central Research Center, People's Republic of China. These samples, which are described in Table 2, were used since they represented a wide range of rock types with highly variable well documented values for 30 metals.

COPPER

In order that a comparison could be drawn between the efficiency and time required for an acid digestion versus the flux decomposition, the samples were initially acid digested. The procedure was as follows:

1. 10 ml of concentrated nitric acid was added to 0.5 g of material in a pyrex beaker
2. the sample was then digested at 80° to 90°C for 3 hours
3. 1 ml of concentrated hydrochloric acid was added and the sample was digested further until the final liquid volume was approximately 0.5 to 1 ml
4. 50 ml of 0.1N nitric acid was added to the beaker
5. the sample was digested for approximately 1 hour
6. the contents of the beaker were transferred to a 100 ml volumetric flask and diluted to volume with 0.1N nitric acid

TABLE 2: DESCRIPTION OF GEOLOGICAL STANDARDS

SAMPLE NO.	SAMPLE TYPE	SURROUNDING ROCK TYPE
GSD-1	river sediment	Mai-Fu Kwan granite
GSD-2	river sediment	Tai-Mao Mountain biotite granite
GSD-3	river sediment	phyllite, porphyritic granodiorite; porphyry Cu-Mo ore
GSD-4	lake sediment	Triassic limestone
GSD-5	lake sediment	Triassic limestone, diorite; copper in skarn
GSD-6	river sediments	clastic rock, acid volcanic rocks, granite porphyry; porphyry Cu-Mo ore
GSD-7	river sediment	Precambrian schist, marble; lead-zinc deposit
GSD-8	river sediment	acid to intermediate volcanic rocks

TABLE 3: COPPER IN GEOLOGICAL STANDARDS - ACID DIGESTION

SAMPLE	ACID DIGESTION -AAZ ppm	RANGE ppm	REPORTED ACCEPTED VAL ppm
GSD-1	19.7	19.8-23.2	21.7
GSD-2	4.55	4.11-5.60	4.9
GSD-3	212	165-186	177
GSD-4	45.3	34-40	37.2
GSD-5	67.2	128-144	137
GSD-6	364	368-399	383
GSD-7	37.9	35.6-40.0	37.3
GSD-8	2.8	3.5-4.6	4.0

7. the sample was centrifuged and then analyzed for copper

The results are presented in Table 3. In general, the agreement between the reported and experimental values is quite good. If shorter digestion periods were used, however, much poorer recoveries were obtained from the samples.

Having demonstrated that a reasonable recovery could be obtained for copper using an acid digestion, the next step was to test the efficiency of a flux decomposition. The following procedure was employed:

1. 0.5 g of sample was mixed with 3 g of the Scintrex flux, Geoflux, and placed in a glass test tube (e.g. 25 by 200 mm)
2. the tube was heated over a Meker burner (propane flame) until the flux melted, then the heating was continued for a further 4 minutes
3. the tube was allowed to cool, then 25 ml of 2N sulphuric acid (or deionized water) was added
4. the tube was shaken to dissolve the flux, then 10 ml of this solution was withdrawn and placed in a second screw-capped test tube with 10 ml of methyl isobutyl ketone (MIBK) and 200 µl of ammonium pyrrolidinecarbodithioate (APDC; a 6% w/v aqueous solution)
5. this tube was shaken for 2 minutes and the organic phase was analyzed for copper. In order to carry out the analysis on the AAZ-2, 10 µl of the organic phase together with 10 µl of a mercury matrix modifier were placed on the tungsten filament and then the instrumental program for copper was initiated

The results are presented in Table 4, and in Figure 1 as a correlation diagram. Com-

paring the recoveries from the fusion with the reported values indicates that this new technique does show promise.

The solvent extraction step using APDC was used for 2 reasons. First, high salt contents will tend to interfere with the atomic absorption determination; thus, extracting the metal away from the aqueous solution of the flux greatly reduces interference problems. Second, some of the metals of interest occur in very low concentrations in nature so that a preconcentration step would be advantageous.

In principle not all metals would require the extraction step (i.e. if their concentration in the sample were high); however, it would be far simpler if the same sample preparation technique were applied to all metals. In such a case the same solution could be used for the analysis of all of the elements of interest. For this reason APDC was chosen as the chelating agent of choice since experimental work coupled with the reports of previous workers (Stary 1964; Kinrade 1978) indicated that copper, silver, arsenic, antimony, mercury, and lead could be extracted under the same conditions. Carrying out the extraction from solutions more acidic than pH 1.0 minimized the extraction of iron; thus, iron-rich geological matrices could be analyzed without problem. For this reason a 2N sulphuric acid solution was used to dissolve the flux. Simply taking up the flux in deionized water resulted in a solution with a pH around 1.2. Extractions could be carried out at this pH though some iron would extract. This level of iron was not found to interfere with the various analyses.

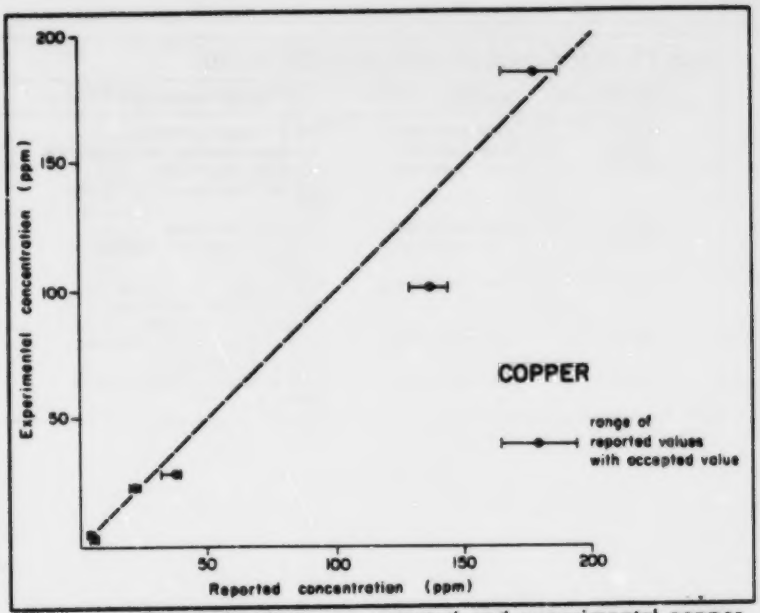

Figure 1. Correlation between reported and experimental copper values.

TABLE 4: COPPER IN GEOLOGICAL STANDARDS - FLUX DIGESTION

SAMPLE	FUSION-AAZ ppm	RANGE ppm	REPORTED ACCEPTED VALUE ppm
GSD-1	25.3,23.5	19.8-23.2	21.7
GSD-2	3.46,3.12	4.11-5.60	4.9
GSD-3	182,190	165-186	177
GSD-4	34.1,22.8	34-40	37.2
GSD-5	89.8,119	128-144	137
GSD-6	449,434	368-399	383
GSD-7	25.1	35.6-40.0	37.3
GSD-8	3.5,7.5	3.5-4.8	4.0

Initially the analytical data obtained from the extracted organic solutions showed very bad scatter. This was believed due to the fact that some of the metals were present as very stable APDC complexes. During the ashing cycle of the instrument these stable complexes would volatilize intact from the filament and covolatilize a number of the other metals with a resulting scatter in the analytical results.

In order to overcome this problem, an attempt was made to convert the metal-organics back into their inorganic form by back extraction into an aqueous solution. The diethyldithiocarbamates (APDC, DDDC, NaDDC, etc.) degrade very quickly in the presence of acids (Stary 1964), especially oxidizing acids. Therefore the MIBK phase was shaken with a variety of nitric acid concentrations (0.1N, 0.4N, 1N, concentrated), with nitric acid in conjunction with hydrogen peroxide, and with nitric acid in conjunction with phenol. All of these backwash solutions succeeded in decomposing the excess diethyldithiocarbamates but failed to break down the metal APDC complexes and render them aqueous soluble.

Another technique which has been used to release metals from chelating agents is based on exchange reactions. In this case an element may be displaced from its chelate compound by any element which forms a more stable chelate. For example, Gottschalk (1963) established a series representing the behaviour of metal ions extracted as diethyldithiocarbamates from solutions at pH 8.5 to 11:

Hg(II) > Ag(I) > Cu(II) > Tl(III) > Bi(III) > Pb(II) > Fe(III) > Co(II) > Cd(II), Tl(I) > Ni(II) > Zn(II) > In(III), Sb(III) > Te(IV), Mn(II)

In principle, then, a given element could be displaced from its chelate compound by any element to the left of it in the series. Note, however, that a change in pH, organic solvent, etc. may result in a change in the sequence of the elements (Zolotov 1970). For example, if the series is re-evaluated at pH 5, Ni(II) is shifted to the left of lead, and will thus displace it from its diethyldithiocarbamate complex (Eckert 1955).

Hg(II), Co(II) > Cu(II) > Ni(II) > Pb(II) > Cd(II) > Fe(II), Fe(III) > Zn(II) > Mn(II)

In the present work, therefore, the MIBK phase was shaken with a 0.1N nitric acid solution containing 1000 µg/ml mercury(II) in order to release all metals less stable than mercury. A problem arose with the purity of the mercury salts, however. Regardless of the analytical quality of the mercury compound used, the concentration of other metal impurities was too high to tolerate. These metal contaminants could not be removed from the aqueous mercury solution.

An alternative to back extracting the organic phase with an aqueous mercury solution was to leave the extracted metals in the organic phase and release them from the chelating agent right on the filament. In this case the mercury was extracted as a bromide into MIBK. This effectively separated the mercury from all traces of contamination. Analytically then, 10 µl of the organic metal APDC phase was placed on the tungsten filament of the atomic absorption spectrophotometer and this was followed by 10 µl of extracted mercury bromide (500 ppm). In principle the mercury should immediately exchange with the various metal chelates (Pb-, Cu-, As-, Sb-APDC, etc.) and form Hg-APDC. This mercury chelate would then readily volatilize from the filament and leave the other metals in their elemental or oxide form, depending on the purge gas used (argon with trace oxygen, or argon-hydrogen). For example, in the case of the lead complex:

(1) $Pb\text{-APDC} + Hg^{2+} \rightarrow Hg\text{-APDC} + Pb^{2+}$

(2a) $Pb^{2+} + 2e \rightarrow Pb^{0}$ (in argon-hydrogen)

(2b) $Pb^{2+} + 1/2\ O_2 + 2e \rightarrow PbO$ (in argon)

In fact, these reactions do appear to take place on the filament since the metals of interest no longer volatilize from the filament when ashing is applied. For example, in the absence of mercury the Cu-APDC complex will volatilize from the filament if any ashing temperature is applied. In the presence of mercury, however, an ashing temperature of about 600°C could be applied to the sample. The bad scatter encountered in the earlier analytical results now disappeared when mercury was used in conjunction with the same solutions.

Having developed a suitable extraction procedure, the question arises as to how much poorer the detection limits for the various metals would be if the extraction were left out. Without the extraction, the salt content of the sample solutions would have to be diluted to some level where its effect would be neg-

ligible. It is this dilution factor coupled with the instrumental detection limit which would determine the overall sensitivity of this procedure. Using 0.5 g of sample, 3 g of flux, dissolving the cooled melt in 5% nitric acid, and finally diluting the solution to the point where the matrix did not interfere with the analysis resulted in a detection limit of 10 ppm for copper in the original geological samples. Therefore if background levels of copper were high, straight dilution and analysis could be carried out. If, however, the background levels were low, the solvent extraction step would be recommended. As little as 40 ppb copper in a geological sample could be detected using fusion followed by solvent extraction.

SILVER

Initially the samples were acid digested. A 1 g sample was mixed with 15 ml of concentrated nitric acid and digested for 8 hours. These solutions were then diluted and analyzed. In general the recoveries were low by at least 20%.

The next step was to test the efficiency of the flux toward silver-bearing samples. These samples were mixed with the flux, fused and extracted by the same procedure as used for copper. A comparison between the reported and experimental values is presented in Figure 2. The agreement between the 2 sets of results is quite acceptable (a correlation coefficient of 0.9991).

Employing the extraction step, as little as 20 ppb silver in the original sample could be detected. If dilution of the sample solution was used instead of extraction, the detection limit for silver in geological samples would be 7 ppm.

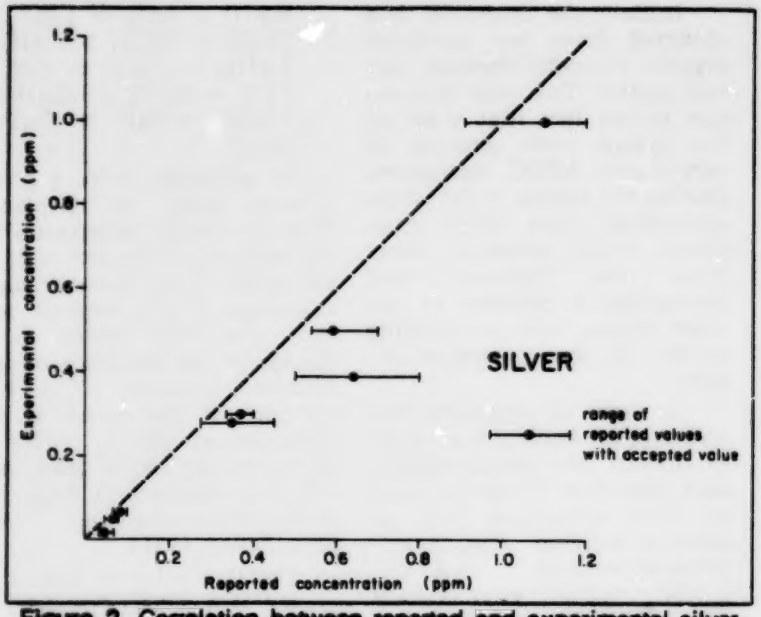

Figure 2. Correlation between reported and experimental silver values.

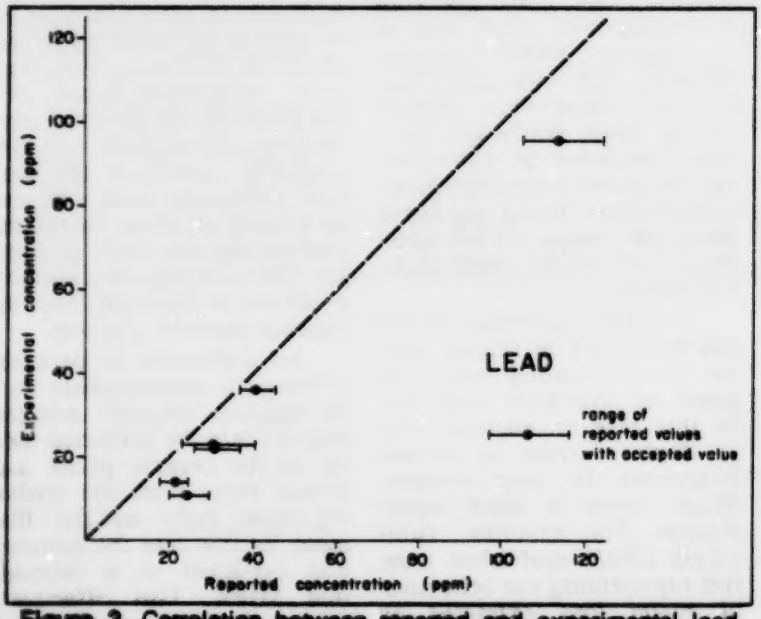

Figure 3. Correlation between reported and experimental lead values.

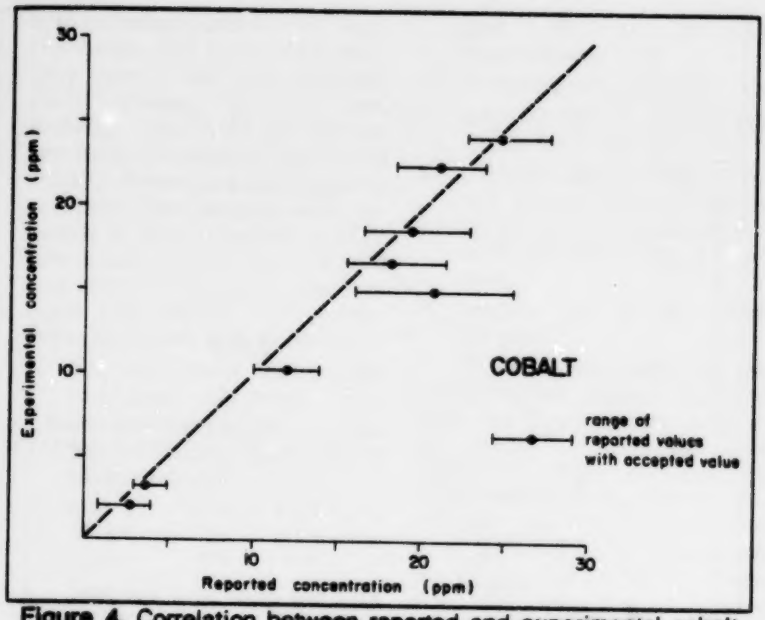

Figure 4. Correlation between reported and experimental cobalt values.

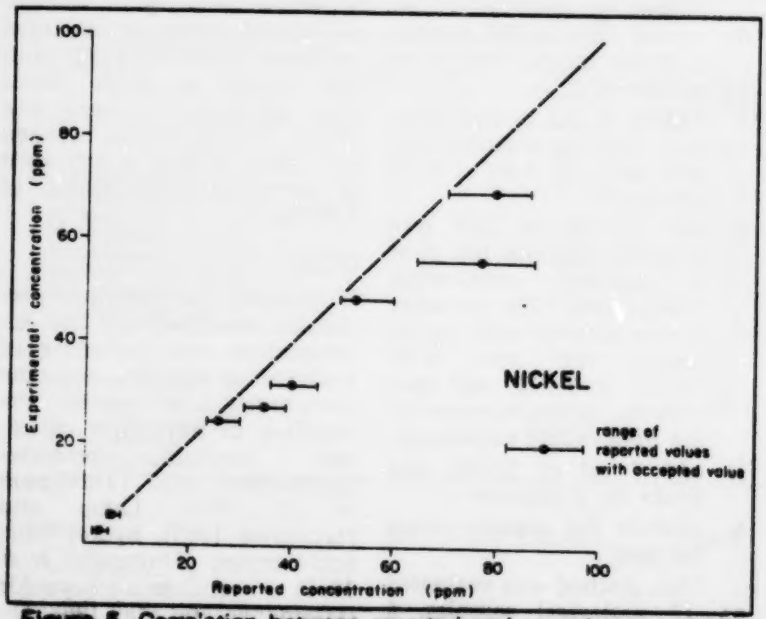

Figure 5. Correlation between reported and experimental nickel values.

LEAD

Figure 3 shows a comparison between the reported lead values and the results generated from the fusion-extraction-atomic absorption. Again the agreement is quite good (a correlation coefficient of 0.9995).

Solvent extraction permits 50 ppb lead to be detected in the geological samples whereas the detection limit would only be 250 ppm if only dilution were used.

COBALT

The cobalt and nickel extractions were carried out from solutions buffered with acetate (0.5% v/v acetic acid) in the pH range of 2.0 to 4.0. A comparison of the fusion-AAZ results and the reported values is presented in Figure 4. A very good agreement (correlation coefficient of 0.9744) exists between the 2 sets of data.

An alternate extraction procedure was also developed for cobalt wherein pH adjustment was not required. Following dissolution of the cooled flux in 2N sulphuric acid, the procedure continued as follows:

1. remove 2 ml of this solution and place it in a second test tube with 8 ml of distilled or deionized water
2. add 1 ml of 20% ascorbic acid and 1 ml of 6 molar ammonium thiocyanate
3. add 2 ml of MIBK and shake for 2 minutes
4. analyze the organic phase for cobalt

This procedure has a detection limit of approximately 50 ppb in the original sample whereas only 25 ppm cobalt could be detected if straight sample dilution was used.

NICKEL

The geological standards were fused and then extracted with APDC between pH 2.0 and 4.0. The resulting experimental values were in good agreement with the reported values (Figure 5; a correlation coefficient of 0.9865). Using solvent extraction, 50 ppb nickel could be detected in the original sample. Simply diluting the sample to the point where the matrix would not interfere with the analysis resulted in a detection limit for nickel of 25 μg/g.

ZINC

The sensitivity for zinc by flameless atomic absorption could be considered as too good. On the primary zinc line (213.9 nm) the working range for zinc is sub-ppb. This sensitivity can be reduced somewhat by changing the purge gas from argon to helium. Even under these conditions, however, background concentrations of zinc in the various reagents cause major interference problems. A solution to this problem was to use a secondary zinc line (307.6 nm) having a working range on the AAZ-2 of 1 to 6 ppm. The use of this line circumvented the problem of background zinc contamination of reagents but was too insensitive to analyze most digested rock samples. Therefore, a simple solvent extraction procedure was again sought.

Originally the zinc was extracted with APDC from acidic solutions of the fused geological samples. Iron, however, severely interfered with this procedure. As a result, an alternate method was developed using thiocyanate as the complexing agent. The procedure was similar to that for cobalt.

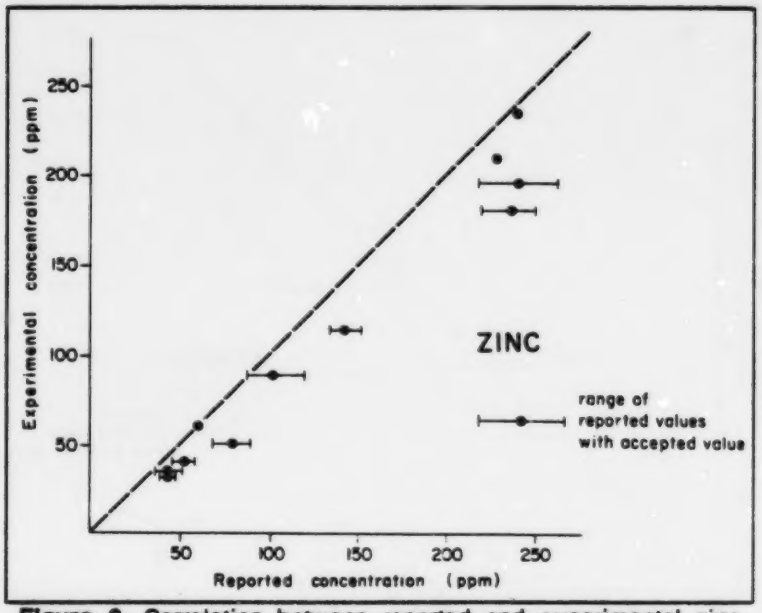

Figure 6. Correlation between reported and experimental zinc values.

Following dissolution of the cooled flux in 2N sulphuric acid, the sample was treated as follows:

1. remove 4 ml of this solution, place in a second test tube and add 4 ml of 0.1N nitric acid
2. add 0.5 ml of 20% w/v ascorbic acid and 100 μl of 6 molar ammonium thiocyanate. (The presence of the ascorbic acid was to reduce the iron from Fe(III) to Fe(II) and thus prevent its interference in the thiocyanate extraction)
3. add 2 ml of MIBK and shake for 2 minutes
4. analyze the organic phase for zinc

This method was evaluated on 12 geological samples, 8 from the Bureau of Geology of the People's Republic of China and 4 phosphate rock samples from the Egyptian Nuclear Materials Corporation. A comparison of results is presented in Figure 6 (the Egyptian samples appear as single points since no range of values was given). The agreement between the 2 sets of data is very good (a correlation coefficient of 0.9838).

GOLD

In general, the literature procedures described for the decomposition and extraction of gold-bearing samples are time consuming and require the handling of hazardous chemicals (sodium bromate-hydrobromic acid (Thompson *et al.* 1968; Lakin and Nakagawa 1965), hydrobromic acid-bromine (Thompson *et al.* 1968), sodium cyanide (Marinenko and May 1968; Olson 1965), aqua regia (Huffman *et al.* 1967), hydrobromic acid (Chow and Beamish 1963), hydrobromic

acid-bromine-phosphoric acid (Holbrook and Rein 1964; etc.). One aspect of the previous ETDF project (Kinrade and Robbins 1983) was the discovery that the present flux could readily decompose gold-bearing samples. The samples were digested in approximately 4 minutes with the flux and the gold was then extracted as the bromide into MIBK. The procedure, in detail, is as follows:

1. dry and crush the sample to at least -100 mesh
2. should the sample contain any sulphides, ignite over a Meker burner
3. mix 6.0 g of flux with 1.0 g of sample in a glass test tube
4. heat the tube until the flux melts and once all gas has evoived the fusion is continued for about 2 minutes
5. allow the tube to cool. Add 30 ml of 5% v/v nitric acid and 10 ml of 3N hydrobromic acid
6. centrifuge the solution
7. add 10 ml of MIBK and shake for 1 minute
8. transfer the MIBK phase to a second tube containing 25 ml of 0.1N hydrobromic acid and shake for 30 seconds
9. analyze the MIBK phase for gold.

Table 5 lists some of the experimental results obtained from the fusion-atomic absorption analysis. Comparing these values to those obtained by other laboratories and/or procedures, one finds reasonably good agreement (a correlation coefficient of 0.9515). Note also that only 1 g of sample was used for the fusions while all other work was conducted with 10 to 25 g of sample.

The fusion procedure was much faster than the procedures reported in the literature but was still unattractive from the view point of handling strong acids. The first move towards further simplifying this procedure was to replace the hydrobromic acid with the salt sodium bromide. With at least 8% w/v sodium bromide, instead of the hydrobromic acid in step 5, the extraction of gold was quantitative; however, the backwash step number 8 was still required to remove the interfering metals. Since the most desirable system would be one involving no acids, the next step was to remove the necessity for nitric acid. From this work evolved the following revised procedure:

1. dry and crush the sample to at least -100 mesh
2. should the sample contain any sulphides, ignite over a Meker burner

TABLE 5: GOLD ANALYSES METHODS COMPARISON

SAMPLE	X-RAY ASSAY F.A. PLASMA	T.S.L. F.A.-A.A.	HOT BROMINE SOLVENT EXTRACTION	BONDAR AND CLEGG F.A.-A.A.	FUSION AAZ-2
	ppm	ppm	ppm		ppm
B122989-Tailings			1.2		0.98
B123033-Tailings			14.7		11.5
23163-Gossan		6.8	10.0		6.3
23119-Gossan		3.4	4.9		4.0
23154-Gossan		6.9	12.6		11.4,12.6
3306-Rock pulp (I.D.?)	5.0	4.4	3.9		5.3
3301-Rock pulp (I.D.?)	2.7	1.7	3.1		1.6
3309-Rock pulp (I.D.?)	2.9	1.7	1.6		2.8
	ppb	ppb	ppb	ppb	ppb
3389-Rock pulp (I.D.?)	140	170	158		201
3385-Rock pulp (I.D.?)	380	350	355		428
RL-1-Massive Sulphide		280-320			342
UM-1-Ultramafic				65/50	79
UM-3-Ultramafic				205	158
					ppm
3305	(5.0)	(4.4)	(3.9)		5.6
Test of homogeneity:					5.3
6 fusions using					6.0
1 g of					5.7
sample each					5.1
					5.9

ABBREVIATIONS
F.A.: Fire Assay
A.A.: Atomic Absorption Spectrometry
T.S.L.: Technical Service Laboratories

3. mix 6.0 g of flux with 1.0 g of sample in a glass test tube
4. heat the tube until the flux melts and once all gas has evolved the fusion is continued for about 2 minutes
5. allow the tube to cool and add 30 ml of an aqueous 10% w/v sodium bromide solution
6. centrifuge the solution
7. add 10 ml of MIBK and shake for 1 minute
8. analyze the MIBK phase for gold

This procedure has the advantage of being fast, and not requiring either acids or a backwash step. A number of gold-bearing samples were analyzed using this procedure and compared to the results obtained when using the methodology advocated by Thompson (1968). Thompson's procedure used 10 g of sample and a hydrobromic acid-bromine digestion. A comparison of the data is given in Table 6. The agreement between the 2 sets of data is very good (a correlation coefficient of 0.9998) and demonstrates the effectiveness of this much simpler methodology.

TABLE 6: COMPARISON OF GOLD ANALYSES

SAMPLE	FUSION -NABR	THOMPSON PROCEDURE
UM3 - Ultramafic	75 ppb	54 ppb
C10731588 - Gossan	570	577
CIP Feed A*	390	430, 400
Mill Feed Comp A*	2700,2800	2650,2700
Leach Feed Comp A*	380,460	400,410
CIP Tail Comp A*	350,390	350

*from Pinson Mines, Nevada

A 1 g sample was used in the fusion procedure in order to keep the experimental setup as simple as possible; 5 g or more of sample proved unmanageable. In general, most gold analyses are performed on samples of 10 g or more, where this larger sample size is recommended in order to avoid the so-called "nugget-effect". This effect might be expected to occur in samples from placer deposits where one could calculate the probability of actually obtaining a representative sample, given the assumption of some particle size (e.g. 1 mg (Clifton *et al.* 1969)). These large particles of gold, however, would occur with less frequency in rocks and soils and therefore sample inhomogeneity should be less of a problem. To date, the validity of this belief appears to be borne out by the fact that this laboratory has encountered no sampling problems when working with 1 g (-200 mesh) rock and soil samples.

ANTIMONY, ARSENIC, AND MERCURY

Antimony, arsenic, and mercury tend to rapidly volatilize when subjected to heat. During analysis on the flameless atomic absorption spectrophotometer, therefore, these elements would readily leave the filament during the ashing cycle unless some form of stabilizer ("matrix modifier") was used. For example, in the absence of a matrix modifier no ashing may be applied during an antimony analysis; the antimony subsequently atomizes at approximately 1300°C. In the presence of 100 ppm nickel, however, antimony atomizes at approximately 2100°C and an ashing temperature of 1000°C can be used to remove any matrix. Likewise, silver, copper, cobalt, manganese, vanadium, and chromium have been used to stabilize antimony and arsenic during analysis and selenium was used to stabilize mercury.

Recognizing that these 3 elements had to be stabilized during their analysis, it was not surprising to find that they would readily leave the sample during fusion unless some form of stabilizer was present. Considerable effort was addressed to the problem of finding such a stabilizer. A variety of salts (Cr_2O_3, CrO_3, $CoSO_4$, $CuSO_4$) in a range of concentrations were added to the flux

before fusion with the sample. These salts all served to partially stabilize antimony and arsenic. The maximum recovery obtained from any given sample was 50%. Additions of selenium to samples containing mercury did not prove effective in suppressing its volatility. Attempts were also made to improve the recovery of these 3 metals by varying the composition and identity of the flux and by changing the identity of the chelating/complexing agent. Again, 50% was the highest recovery obtained.

It would appear from this work that the principle employed was correct, however, none of the metal stabilizers tested could totally prevent volatilization of the antimony, arsenic, or mercury. Therefore, either a stronger stabilizing compound or a lower melting flux is required.

TIN

The primary metals of interest in this study were copper, lead, zinc, nickel, cobalt, silver, gold, arsenic, antimony, and mercury. It was also decided to re-evaluate the decomposition of tin-bearing samples.

The 1981-82 ETDF program considered the use of fluxes for decomposing tin- and tungsten-bearing samples. At this time it was found that poor tin recoveries were obtained from a variety of soil and rock samples. This recovery problem was believed due to the incorporation of a fraction of the tin in minerals such as biotite, hornblende, muscovite, and garnet which are not readily decomposed. In the present work a number of alternate methods were evaluated for extracting tin from geological samples prior to analysis by atomic absorption spectroscopy. Though many of these methods at first appeared promising, no suitable decomposition technique was found. This work is summarized below.

REDUCTION TO METALLIC TIN

Since it is chemically easier to dissolve metallic tin than it is to dissolve tin oxide (the common geological form of tin), attempts were made to reduce the tin present in samples to the metallic form and then dissolve this material in the appropriate solvent.

The first reducing agent used was zinc dust. The sample was mixed with zinc and placed in a 50% v/v solution of hydrochloric acid. In the case of pure tin oxide, all of the material was reduced to metallic tin and this then dissolved in the acid. When a geological sample was used, however, the resulting tin metal appeared to form an alloy of unknown composition with other metals in the sample. This alloy or compound was subsequently found to be acid insoluble.

Similar experiments were conducted using hydrogen as the reducing agent. In this case the sample was roasted in the presence of a flow of 8% hydrogen balance argon. Again, pure tin oxide could be reduced to tin metal however, tin in a geological sample, or when mixed with pure iron oxide, would become reduced to a form which was insoluble in concentrated nitric acid, hydrochloric acid, nitric plus hydrochloric acid, or sulphuric acid.

An attempt was also made to decompose the reduced sample by fusion with potassium pyrosulphate. The results were inconclusive since the high levels of sulphate in the resulting solution interfered with the analysis.

SUBLIMATION WITH AMMONIUM IODIDE

A 0.5 g sample was mixed with 3 g of ammonium iodide in a test tube and heated over a Meker burner. The tin iodide would then sublime and collect along the upper portion of the test tube. This material was then dissolved in 25 ml of 0.5N sulphuric acid. An aliquot of this solution was removed, adjusted to pH 1.7, and extracted with 8-hydroxyquinoline into butyl acetate. The organic phase was then analyzed for tin.

A number of problems were encountered with this procedure. First, tin bound up in silicate lattices was not attacked by this procedure. Second, the efficiency of the extraction appears to be matrix dependent (e.g. large quantities of iron and copper suppress the extraction of tin). Various masking agents were added to the system to prevent matrix interference. These agents, however, did not prove to be effective.

IODIDE EXTRACTION

Tin (II) iodide is known to extract into organic solutions with a high degree of efficiency (Morrison and Freiser 1966). Therefore, an attempt was made to extract the tin iodide generated during an ammonium iodide sublimation. The sublimed material was dissolved in various acid solutions (sulphuric, hydrochloric, nitric) and then extracted into a variety of organic solvents (butyl acetate, methyl isobutyl ketone, xylene). In all cases the

recovery of tin was very poor. There are 2 possible reasons for this. First, it was determined that high levels of some metals (e.g. Cu, Fe) would prevent the extraction of tin. Second, the tin appeared to volatilize as tin iodide from the tungsten filament of the AAZ-2 during the ash cycle. Attempts to suppress this volatilization failed (e.g. using matrix modifiers: nitric acid, mercury bromide, cadmium nitrate).

SUMMARY

The present research program was concerned with the development of improved methods for the analysis of geological materials using the Scintrex AAZ-2, a compact flameless atomic absorption spectrophotometer.

The standard geochemical decomposition procedure is the combined nitric-hydrochloric acid attack at a temperature of some 80° to 90°C for at least 3 hours and preferably 10 to 12 hours. The methods developed in the present work were based on successful aspects of a previous ETDF project where good recoveries of a wide range of base and precious metals were obtained using flux digestion techniques. Such fluxes not only avoid the use of strong acids but are considerably faster in operation. The metals considered in this study were those commonly used in exploration geochemistry: copper, lead, zinc, nickel, cobalt, silver, gold, mercury, arsenic, antimony, and tin.

The analytical procedure involved mixing 0.5 g of sample with 3 g of flux in a glass test tube and fusing for 4 minutes, either individually over a propane flame or in a batch with an electric heater. The tube is allowed to cool and 25 ml of deionized water or 2N sulphuric acid was added.

The analytical working range of the AAZ-2 is in the low ppb to sub-ppb range. Generally, then, when metal levels exceed 25 ppm, the solutions could be analyzed directly after dilution. For lower metal concentrations, when matrix interferences become a problem, an extraction procedure was used. In the case of copper, lead, and silver, an organic APDC solution was added and the tube was shaken for 2 minutes. For nickel and cobalt the pH of the solution must be adjusted to between 2 and 4 before extraction. Zinc is extracted from the aqueous solution using thiocyanate as the complexing agent. Gold is simply extracted as the bromide following dissoluton of the cooled flux in a sodium bromide solution.

These methods were evaluated by analyzing a set of well characterized geological standards. A comparison of the experimental and reported results indicated the fusion-extraction procedure to be highly effective. Though tin, mercury, arsenic, and antimony may be readily analyzed on the Scintrex AAZ-2, attempts to obtain a complete recovery from geological samples proved unsuccessful.

REFERENCES

Bock, R.
1979: A Handbook of Decomposition Methods in Analytical Chemistry; J. Wiley and Sons, New York.

Bond, A.M., O'Donnell, T.A., and Waugh, A.B
1970: Use of Polarographic Methods for the Determination of Tin in Geological Samples; Analytical Chemistry, Volume 42, Number 11, p.1168-1172.

Chow, A., and Beamish, F.E.
1963: Studies of Titrimetric and Spectrophotometric Methods for the Determination of Gold; Talanta, Volume 10, p.883-890.

Clifton, H.E., Hunter, R.E., Swanson, F.J., and Phillips, R.L.
1969: Sample Size and Meaningful Gold Analysis; United States Geological Survey Professional Paper 625-C, 17p.

Eckert, G.
1955: Analyse von Nickellegierungen fur Oxydkathoden; Zeitschrift fur Analytische Chemie, Volume 148, p.14-20.

Foster, J.R.
1971: Geochemical Exploration; Canadian Institute of Mining and Metallurgy, Special Volume Number 11, edited by R.W. Boyle, 554p.

Gottschalk, G.
1963: Grundlagen Photometrischer Analysenverfahren - III Kupferbestimmungen als Carbamidatkomplex in Trichlorathylen; Zeitschrift fur Analytische Chemie, Volume 194, p.321-333.

Holbrook, W.B., and Rein, J.E.
1964: Extraction and Spectrophotometric Determination of Gold; Analytical Chemistry, Volume 36, Number 13, p.2451-2453.

Huffman, C., Jr., Mensik, J.D., and Riley, L.B.
1967: Determination of Gold in Geologic Materials by Solvent Extraction and Atomic-Absorption Spectrometry; United States Geological Survey, Circular Number 544, 6p.

Kinrade, J.D., and Robbins, J.C.
1983: Grant 005 Tin Tungsten Analysis of Geological Samples Under Field Conditions; p.27-37 *in* Exploration Technology Development Program of the Board of Industrial Leadership and Development, Summary of Research 1981-1983, edited by E.G. Pye and R.B. Barlow, Ontario Geological Survey, Miscellaneous Paper 115, 135p. Accompanied by 2 charts.

Kinrade, J.D.
1978: A Solvent Extraction Study of Various Trace Metals in Aqueous Solution; Ph.D. Thesis, University of Toronto.

Lakin, H.W., and Nakagawa, H.M.
1965: A Spectrophotometric Method for the Determination of Traces of Gold in Geologic Materials; United States Geological Survey, Professional Paper 525-C, p.C168-C171.

Langmyhr, F.J., and Sveen, S.
1965: Decomposability in Hydrofluoric Acid of the Main and Some Minor Trace Minerals of Silicate Rocks; Analytica Chimica Acta, Volume 32, p.1-7.

Marinenko, J., and May, I.
1968: Fluorometric Determination of Gold in Rocks with Rhodamine B; Analytical Chemistry, Volume 40, p.1137-1139.

Morrison, G.H., and Freiser, H.
1966: Solvent Extraction in Analytical Chemistry; J. Wiley and Son, New York.

Olson, A.M.
1965: Gold Assay by Atomic Absorption Spectrophotometry, a Preliminary Report; Atomic Absorption Newsletter, Volume 4, p.278.

Rosler, H.J., and Lange, H.
1972: Geochemical Tables; Elsevier Publishing Company, Amsterdam.

Stary, J.
1964: The Solvent Extraction of Metal Chelates; Pergamon Press, Oxford.

Thompson, C.E., Nakagawa, H.M., and Van Sickle, G.H.
1968: Rapid Analysis for Gold in Geologic Materials; United States Geological Survey, Professional Paper 600-B, p.B130-B132.

Van Loon, J.C., and Parissis, C.
1968: Rapid Scheme of Silicate Analysis Based on the Lithium Metaborate Fusion Followed by Atomic Absorption Spectrometry; Analytical Letters, Volume 1, p.519-524.

Zolotov, Yu. A.
1970: Extraction of Chelate Compounds; Ann Arbor-Humphrey Science Publishers, Ann Arbor.

Grant 058 Portable Broadband Multiple Geometry HEM System

R.L.S. Hogg[1], M.S. Granovsky[1], and A.B. Routledge[2]

[1]Aerodat Limited

[2]Right By Design Incorporated

ABSTRACT

Aerodat Limited evaluated several methods for increasing the bandwidth of it's multiple coil geometry rigid boom helicopter-borne electromagnetic system (HEM). The direction that offered the most promise was the adaptation of transient as opposed to frequency domain methods, so a development program was initiated.

The first phase was the development of a suitable transmitter that could produce as wide a bandwidth as possible. The development was completed with the assistance of an Exploration Technology Development Fund (ETDF) grant. The transmitter produces a current waveform with a sustained current level of 200 amperes and a peak of 280 amperes. Pulse length as well as intervening off-times are variable and digitally controlled. The excitation bandwidth achieved ranges from about 2500 Hz to perhaps as low as 15 Hz. The low frequency end is effectively open and the functional lower limit will only be determined when the full system is completed.

INTRODUCTION

The rigid boom helicopter-borne electromagnetic system has been a geophysical exploration method for about 30 years. Many improvements have been made to the system such as higher rigidity, multiple frequency/coil configurations, and electronic refinements. The system has proved to be an effective exploration and mapping tool in many geological environments. Significant improvement may be seen by increasing the bandwidth, in effect broadening the range of frequencies to improve the depth of penetration in conductive areas while maintaining a good response in resistive areas.

Continuing the addition of more coil pairs to achieve more frequencies is a limited approach. Size, weight, inter-coil interference, and adequate moment are major restrictions. Transient or time domain methodology has proven to be an effective alternative approach to achieving a large bandwidth with suitable dipole moment.

The objective of the research program was to incorporate a time domain technique with the current rigid multiple coil geometry HEM system. The development required 3 distinct phases: transmitter design, receiver design, and system integration.

Phase I, the development of an operating transient transmitter, is complete and Phase II, the receiver design, is in progress. This report deals with the aspects of the completed transmitter design.

DESIGN CONSIDERATIONS

The transient electromagnetic system under development utilizes a transmitter current waveform that consists of a pulse of duration T-on followed by a period of T-off, zero current, during which the anomalous response may be measured.

Current will be induced in a ground circuit, due to the change in magnetic flux linking the target. If the geological or ground target is approximated by a simple conducting loop of inductance L and resistance R, then the induced current flow I in the ground may be expressed as:

$$I = I_o e^{-t/\tau}$$

where I_o is the ground current at the start of T-off; t is the time elapsed from the start of T-off; and τ is L/R. the time constant of the target.

It can also be shown that:

$$R_F \propto (1/L) I_o e^{-t/\tau}$$

$$R_V \propto (1/L\tau) I_o e^{-t/\tau}$$

where R_F is the secondary field at the receiver (i.e. step function response) and R_V is the voltage induced in a receiver coil (i.e. impulse response) by the secondary field.

Whether the anomaly is considered to be R_F or R_V, an exponential attenuation with time will be noted. Larger, more conductive targets will have a larger τ and hence decay more slowly.

If the field R_F is measured directly, the initial amplitude I_o is modified by 1/L which is a function of target size. R_V is the derivative of R_F and contains the additional term $1/\tau$ which provides added gain to low τ response.

For either measurement method it is clear that I_o will have a direct bearing on the strength of anomalous signals and its optimization is the key factor in transmitter design. The factors that influence I_o may be expressed as follows:

$$I_o = G \cdot M \cdot F$$

where I_o is the amplitude of the induced current in the target at the start of the measurement period T-off; G is a geometrical factor reflecting the mutual inductance of the transmitter, target, and receiver; M is the dipole moment of the transmitter; and F is the function of current pulse

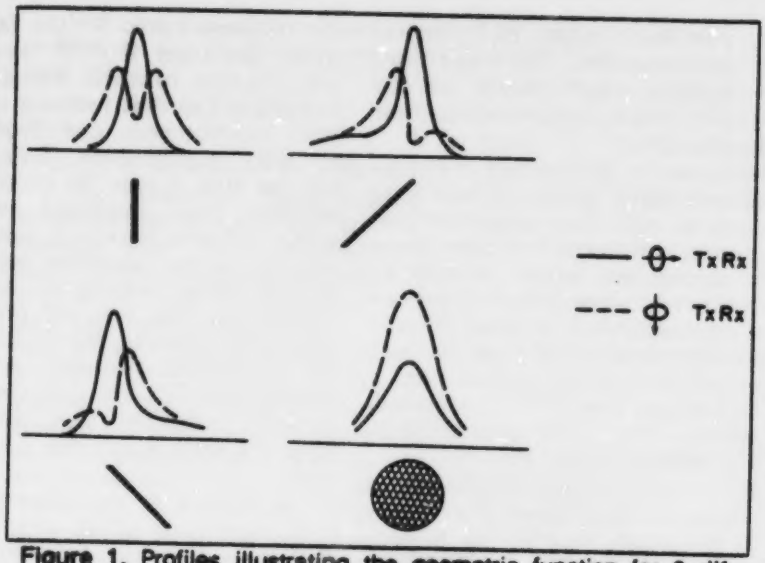

Figure 1. Profiles illustrating the geometric function for 2 different transmitter/receiver alignments for a dipping sheet and sphere targets. The shape is due to changes in inductive coupling of Tx-target, target-Rx. Sign and scale are arbitrary.

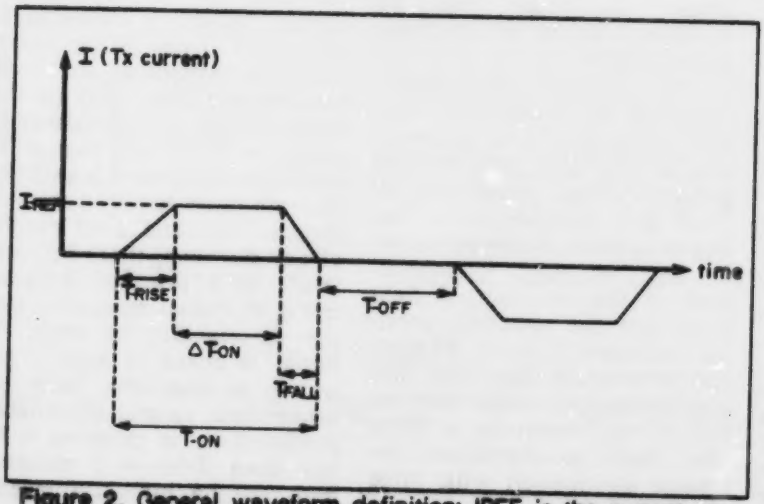

Figure 2. General waveform definition: IREF is the current amplitude reference for normalization, T-on is the full period of nonzero current flow, ΔT-on is the period of constant nonzero current flow.

shape, T-on, T-off, and the τ of the target.

Each of these factors has a bearing on I_s and needs to be considered as part of the system design.

G—GEOMETRICAL FACTOR

For the simple conducting loop, the geometrical factor "G" is independent of the target's conductivity and the difference in behaviour of the function for different transmitter/receiver (Tx/Rx) configurations can illustrate its usefulness for interpreting the targets shape and orientation.

In Figure 1 the G function, or profile shape along a flight line, is shown for both coaxial and coplanar Tx/Rx configurations as planned for the system. A thin sheet conductor can be approximated well by a single conducting loop because current flow is restricted to the plane of the target. In the case of a steeply dipping sheet, a vertical dipole Tx/Rx will be null coupled over the target and a horizontal dipole Tx/Rx will be optimally coupled. A clear, diagnostic signature is apparent; a single simple peak with horizontal dipoles combined with a double peak for the vertical dipoles. The asymmetry of the horizontal Tx/Rx dipole response indicates the direction of dip. In a massive target like a sphere the induced current flow is free to orient on any plane within the body. In this case both the horizontal and vertical dipole pairs will be optimally coupled; however, the vertical pair will be maximum coupled and provide a reponse amplitude ratio (secondary to primary), 4 times greater.

The significance of the geometric factor is that it provides information concerning a

target's shape and orientation. By simultaneously operating 2 Tx/Rx configurations the potential ambiguity of interpretation is greatly reduced and near optimum coupling with any target form is ensured.

M—TRANSMITTER MOMENT

The transmitter moment "M" can be expressed as follows:

$M = nIA$

where n = number of turns; I = current; and A = area

I and A are design constraints; the first is related to the power available and switchable by semiconductor controlled rectifier (SCR) devices, the second relates to the practical size of the antenna. In order to avoid the need for an auxiliary power source the available power is in the order of 150 amperes at 28 volts. A practical antenna area was set at 30 m^2.

For a 4 turn loop, the current level for the pulse is in the order of 200 amperes. It is possible to increase the moment by an increase of n (number of turns). Changing n from 4 to 8 would double the moment; however, the inductance of the Tx antenna would increase by n^2 which would require a 4-times reduction in dI/dt across the coil to stay within the same system hardware constraints. A 2-times increase in moment by a change in n therefore leads to a 4-times reduction of the rate of switch off, a detrimental factor that will be considered in the next section.

F—CURRENT WAVEFORM

The basic objective of the transmitter development was to provide as wide a response band as possible and to provide flexibility where necessary to ensure good response behaviour in a variety of geological environments. The transmitter current waveform "F" is the key factor for attaining these objectives.

A generalized pulse waveform is shown in Figure 2. In this illustration the current rise and fall have been shown as linear ramps although many other functions are possible. Aerodat initially considered a 1/4 sine rise and fall but in the end adopted a 1/4 sine rise and 3/8 sine fall. The final waveform is illustrated in Figure 3.

The relative amplitude of the 3/8 sine turn off function is variable, but in the present configuration it is a 40% increase above the ΔT-on level. The ΔT-on level is nominally 200 amperes. The current level is a function of the power available and performance specification of the SCRs used. These amplitudes can be achieved without an auxiliary power supply.

To evaluate the significance of the transmitter current waveform it is informative to look at I_o, the induced ground current, at the start of T-off as a function of τ. The response has been presented in log/log form with I_o normalized to the transmitted field such that the optimum possible response is unity. The response diagram also takes into consideration the repetitive nature of the waveform, a factor that leads to significant response attenuation with large τ.

Figure 4 shows the 1/4 sine turn on with: a ramp, 1/4 sine, and 3/8 sine turn off. In the case of the 3/8 sine function, the transmitted field during ΔT-on is used as the normalization reference. Also shown for general reference is the response curve for the familiar Barringer INPUT® system 1/2 sine function. For all 4 profiles T-on has been set to 1000 microseconds and T-off to 2500 microseconds. T-Fall for the first 3 was 70 microseconds. The increased response towards lower τ is quite evident for the functions with sharper pulse termination. Although the sine turn off provides the greatest bandwidth, the 3 turnoff functions are closely grouped. The 3/8 sine turnoff yields the most uniform response within the 3 db level.

In Figure 5 the effect of increasing both ΔT-on and T-Fall is evident as a widening of the response band. An increase in ΔT-on alone will produce a minor increase; however, in a practical sense T-off should be at least equal to the τ of the target of interest. In the case of the response sequence shown in Figure 6, T-off = 2.5 T-on. If the bandwidth is defined at the 3 db level we see that τ max (at the upper limit) is approximately equal to T-off and that a T-off/T-on ratio of 2.5 satisfies the minimum requirement. Although T-on and T-off can be of any duration, there will certainly be a practical limit in terms of spatial resolution and the detectability in terms of signal to noise of high τ response at late time. Such an upper limit cannot be reliably predicted but is expected to be less than T-on = 5 milliseconds, the maximum displayed.

To draw a parallel to the Aerodat frequency-domain system we note that the centre of the response band for a simple L-R circuit occurs when $(2\pi fL)/R = 1$.

Defining the achieved bandwidth at the 3 db level we note that:

τ-min = .065 ms, or f = 2450 Hz

τ-max = < 12 ms, or f > 13 Hz

The apparent bandwidth achieved has a maximum frequency less than currently used by the frequency-domain system but the low frequency end may prove to be considerably lower. Current technology in the rigid boom HEM frequency-domain method has limited the spectrum definition to 2 frequencies with coils of similar orientation (coaxial or coplanar). If we assume that to provide adequate response band definition the frequencies should be 1/2 decade apart, then 5 frequencies would be required to produce an equivalent bandwidth.

TRANSMITTER HARDWARE CONFIGURATION

The system block diagram is illustrated in Figure 7. Power is provided by the helicopter power supply and is converted from 28 to 15 volts by the power converter. The controller receives digital instructions from a central monitor as to the desired duration of ΔT-on and T-off. This information is then used by an isolated sense and control interface (Figure 8a) to provide the proper control to the SCR power bridge (Figure 8b) which creates the desired current waveform. The instruction logic also incorporates sensing of the state of the power bridge so that proper system start up is directed automatically and that minimum ΔT-on requirements are met.

RESULTS AND FUTURE PLANS

A transient transmitter was designed and constructed that successfully met the objectives of the system development. Performance has been verified by full power testing. The waveform will provide a relatively uniform response band for conductive targets with a τ ranging from about 70 microseconds to an upper limit in the order of 10 milliseconds. The transmitter itself places no upper limit on τ; it is the practical limitation of signal-to-noise ratio and helicopter speed that will eventually determine the true bandwidth of the system.

The second design phase involving the receiver and bird are currently in progress and full system integration and testing will begin thereafter.

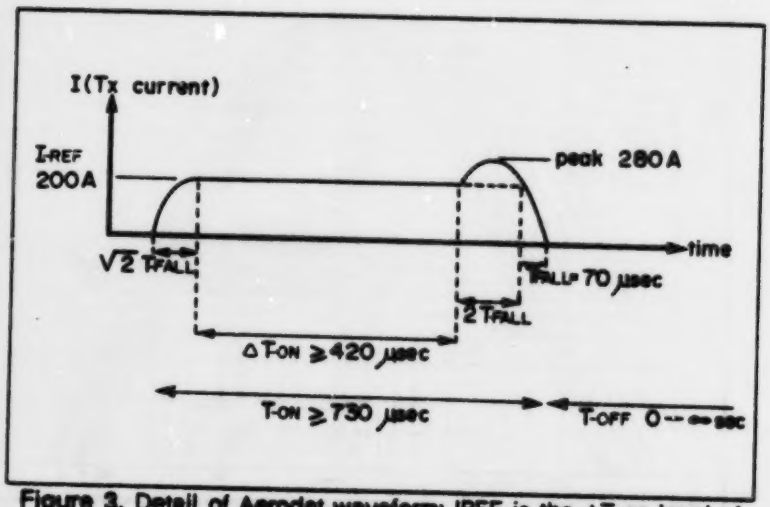

Figure 3. Detail of Aerodat waveform: IREF is the ΔT-on level of 200 amperes. T-Fall for this function is defined as 1/8 of the 3/8 sine turn off.

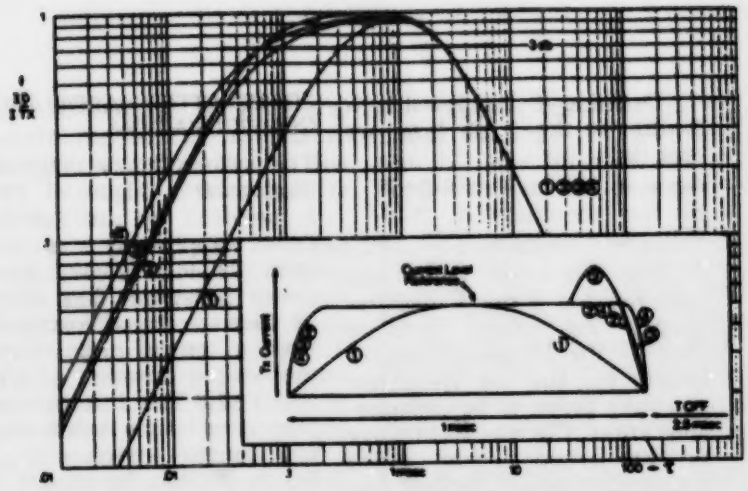

Figure 4. Response diagram for various Tx current waveforms. I_m, the current level in the target circuit at the end of T-on, is normalized to the transmitter current IREF and plotted as a function of τ. The pulse duration, T-on, and off-time, T-off, are 1 and 2.5 milliseconds respectively for all 4 functions.
1. 1/2 sine pulse
2. 1/4 sine rise, ramp fall
3. 1/4 sine rise, 1/4 sine fall
4. 1/4 sine rise, 3/8 sine fall
For 2, 3, and 4 T-Rise and T-Fall are 0.1 and 0.07 milliseconds respectively.

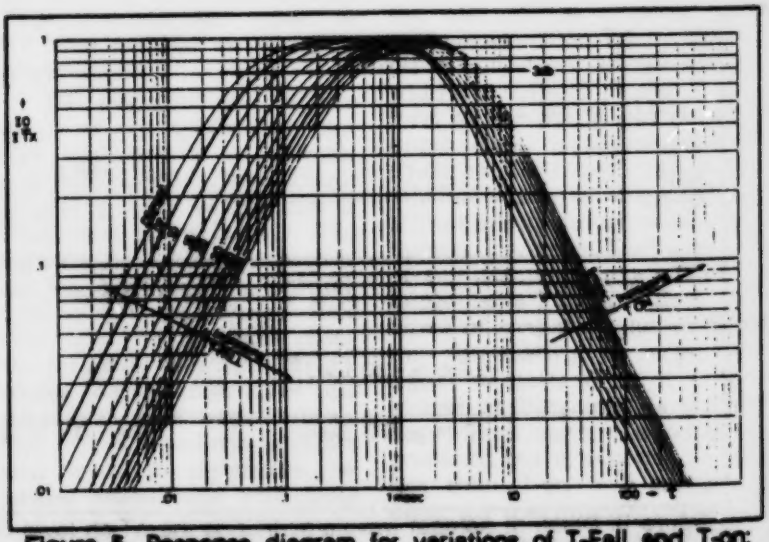

Figure 5. Response diagram for variations of T-Fall and T-on: the response is for the Aerodat 1/4 sine rise and 3/8 sine fall waveform with T-off fixed at 2.5 milliseconds. T-Fall is varied from 0.05 to 0.5 milliseconds by increments of 0.05. T-on is varied from 0.5 to 5 milliseconds by increments of 0.5. The heavier lines illustrate the developed waveform with a T-Fall of 0.07 milliseconds and the 1/2 sine pulse of 1 millisecond duration.

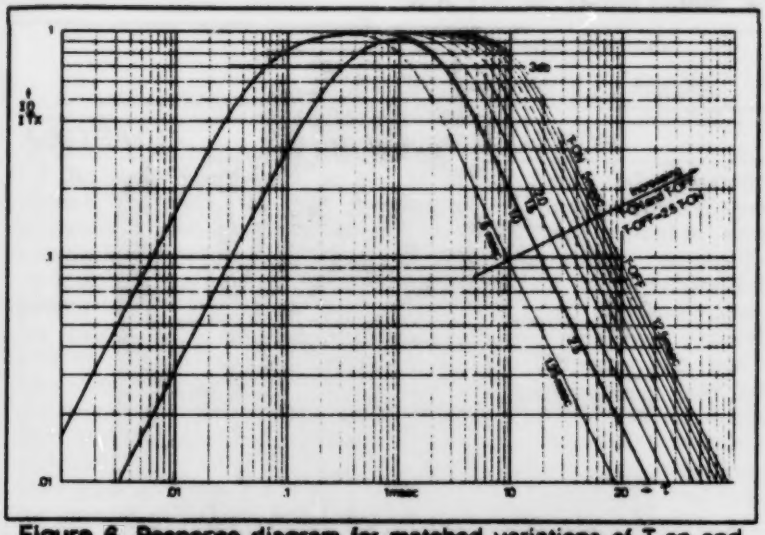

Figure 6. Response diagram for matched variations of T-on and T-off: the response shown is for the Aerodat function with T-Fall equal to 0.07 milliseconds. T-off is maintained as 2.5 T-on, with T-on increased from 0.5 to 5 milliseconds by increments of 0.5. At low τ the upper heavy line is the Aerodat function; the lower line is the 1/2 sine pulse of 1 millisecond duration.

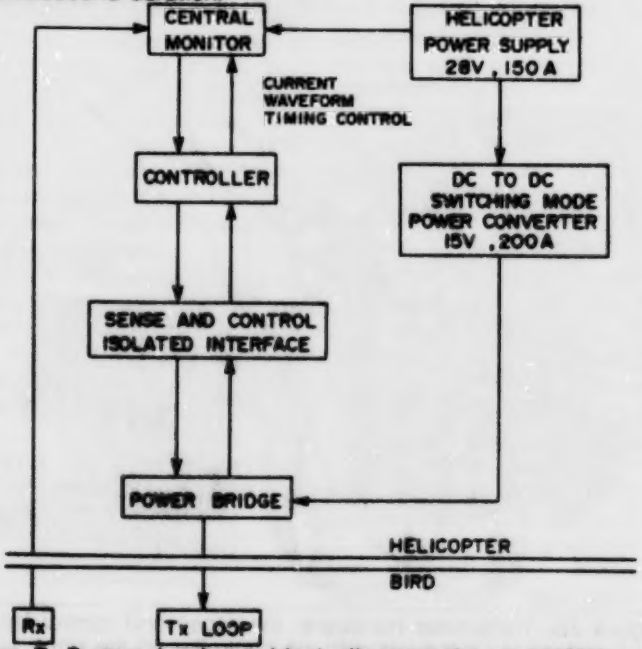

Figure 7. System hardware block diagram: the transmitter, with the exception of the antenna loop, is carried in the helicopter. Design and testing of the elements shown, with the exception of the control monitor and the receiver, is complete.

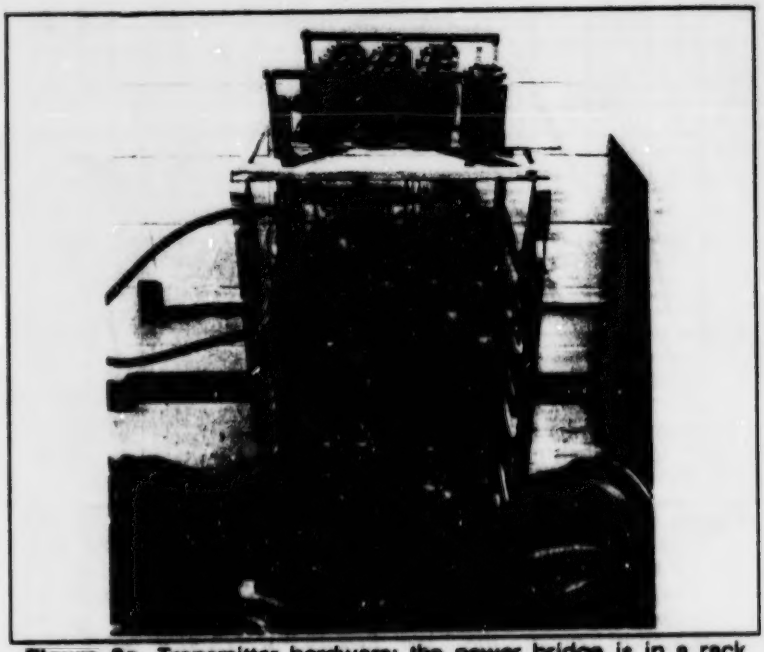

Figure 8a. Transmitter hardware: the power bridge is in a rack mount in the background with part of a dummy load antenna in the foreground.

Figure 8b. Transmitter hardware: the sense and control isolated interface is on the left with the controller on the right.

Grant 059 Development of a Borehole Magnetic Properties Logging System

W.R. Thuma[1], Detlef Blohm[1], and M.T. Hamalainen[2]

[1]IFG Company, Brampton

[2]Geoinstruments Ky, Helsinki, Finland

ABSTRACT

Of the many geophysical techniques available to the explorationist and earth scientist, magnetic properties and their variations perhaps contain proportionally more interpretable information relative to a greater variety of geologically important characteristics than do any other single method. But unlike most other geophysical methods, although they have been well developed for ground and airborne exploration, these magnetic techniques have been difficult to miniaturize and therefore difficult to apply to slim hole logging.

With the advent of stable, high sensitivity ring core magnetometer sensors (Acuna *et al.* 1978; Primdahl 1979), improvements in susceptibility probes, and advances in low power microprocessors, IFG Company, in cooperation with Geoinstruments Ky of Finland, began the development of a radically different portable borehole magnetic properties logging system. The following describes the intended applications of the system, its target specifications and detailed description of major components, progress to date under the Exploration Technology Development Fund (ETDF) program, and future developments.

INTRODUCTION

Magnetic field and magnetic properties measurements on the surface are valuable, and are among those commonly employed for the exploration of a variety of economic mineral resources and for general geological mapping. In addition, these techniques play an important role in science, from age dating and polar wandering to archeological investigations. Basic total field and vertical component surveys are regularly used to establish lithological boundaries, provide a direct or indirect guide to ore occurrences, locate structures such as faults and joint patterns, and to determine depths to basement. Susceptibility measurements, both on the surface and in boreholes, are significant guides to mineralization, including uranium in roll front deposits (Scott *et al.* 1977; George and Scott 1982). These techniques are standard tools in understanding the subsurface geology, and the interpretation of data is quite advanced and well known.

Recognizing that emerging technology in sensor design was making vector measurements more attractive from a functional and cost point of view, IFG began the development of 3-component airborne magnetometer for use in areas of high magnetic gradient and low amplitude horizontal fields. These environments pose a particularly difficult problem for standard proton precession magnetometers.

The airborne instrument employed newly developed ring core sensors which offer high sensitivity, long term stability, and performance superior to the proton precession magnetometer under the above mentioned conditions. These sensors, used by NASA in Magsat and in various interplanetary probes (Adams *et al.* 1976; Acuna *et al.* 1978) have proven to be excellent alternatives to the dimensionally long, temperature sensitive solenoidal sensors previously used in many applications (Primdahl 1979).

In parallel with IFG's development of the new generation of vector magnetometers, Geoinstruments of Finland was developing the hardware necessary to conduct magnetic susceptibility surveys in boreholes as an extension of their expertise in this measurement technique. Their sensor design allowed for the measurement of this important parameter to a level of accuracy and stability which made it an ideal companion to the evolving ring core magnetometers. As a result of these developments, and by adding recent experience in using low power complementary metal-oxide semiconductor (CMOS) microprocessors, IFG initiated the development of the MAGLOG System, a portable state-

of-the-art borehole logging system which would offer the geophysicist an opportunity to extend his knowledge of magnetics into the third dimension.

DESCRIPTION

Although the primary objective of the MAGLOG System is to measure magnetic properties, a decision to integrate other sensors was made early in the development. This offers the operator more interpretable data at practically no extra cost, thereby increasing the value of his logging dollar. The system as it stands today includes the following:

1. total magnetic field (from the vector sum)
2. 3 orthogonal vector amplitudes
3. magnetic bulk susceptibility
4. conductivity
5. differential self (or spontaneous) potential
6. fluid temperature

All measurements are fully compatible and are measured simultaneously at a high sampling rate to permit continuous logging. All data are converted to digital form for recording and for automatic plotting and interpretation.

The resulting data have a wide range of applications in general and economic geology including the identification and characterization of faults and fissures, alteration zones, hydrologic permeability, lithological units and boundaries, age determinations, base metals, uranium, ferrous minerals, and geothermal resources.

The system under development meets several design objectives necessary for commercial acceptance. It is lightweight and compact for portability and use in Canadian "fly camp" operations where transportation is often by foot, canoe, or snowmobile. All components are carefully selected to function over a wide temperature range, high humidity, and frequent exposure to rainfall. Also, the design will withstand the mechanical stress and generally harsh treatment common to field operations. From a functional point of view, the entire system is simple to operate by 1 or 2 technicians, and will require only infrequent calibration and maintenance. All data collected by the system is immediately available for on-site interpretation as well as in a form which can be automatically processed, plotted, and interpreted at a central facility. The system which satisfies these parameters consists of 3 separate units: probe, cable/winch, and console.

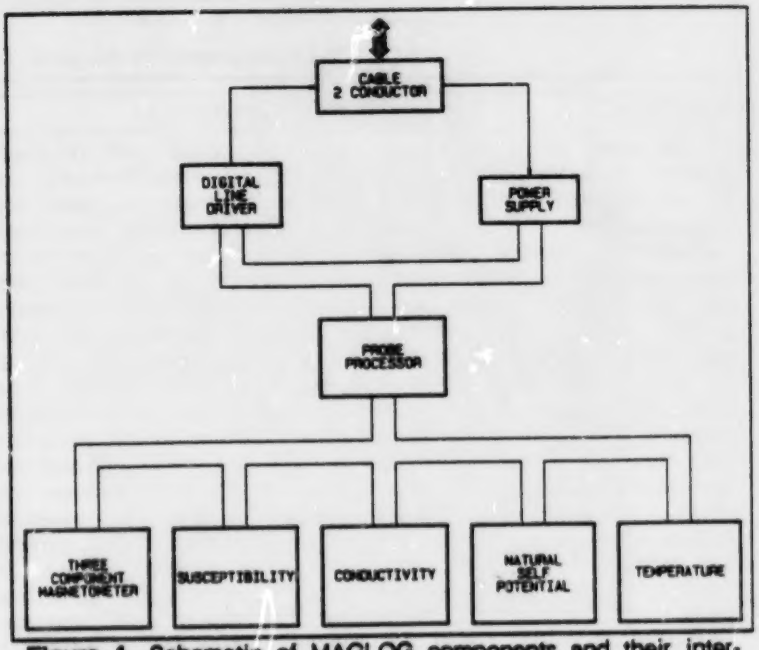

Figure 1. Schematic of MAGLOG components and their interrelationships.

PROBE

Whereas most logging equipment manufacturers place only the sensing elements in the probe and the balance of the electronics at the surface, IFG incorporates everything in the probe. This unique arrangement is in essence a series of complete miniaturized instruments, all of which are under the control of an onboard microprocessor. Power is provided from the surface in unregulated form, and once powered the probe begins sending data to the surface in digital form at a high baud rate. Figure 1 illustrates the various components and their interrelationships.

Physically the prototype probe will be 50 mm in diameter and will consist of 2 sections, each approximately 1 m

long, for convenience in shipping. Beginning at the top, the probe will have a standard 1 inch (2.54 cm) 4 pin Gearhart-Owen header for easy attachment to the cable. Following that will be a stainless steel section containing the power supply regulator, microprocessor, and individual sensor electronics.

The next section is the beginning of the sensor string, the first of which is the triaxial magnetometer sensor. Because of the nature of its measurement, it will largely be constructed of nonmagnetic, nonmetallic materials, including epoxy/kevlar composites which have sufficient mechanical strength to withstand the design pressure of 100 bar, equivalent to 1000 m of water.

The second sensor in line is the susceptibility/conductivity coil. It has been fabricated and tested by Geoinstruments and is based on their production model TH-3 which has proven its performance under Canadian logging conditions (Quentin Bristow, Geological Survey of Canada, personal communication).

The self potential (SP) electrodes are made of lead antimony and are located at either end of the susceptibility transducer. The separation of 70 cm is expected to be adequate to accurately resolve small sources of potential differences likely to originate from features of relatively limited thickness such as open fractures with flowing water.

At the very end of the probe is a cage containing a single thermister for measuring the fluid temperature. This sensor has a small time constant and should react quickly to temperature changes as the probe descends (Bristow 1981).

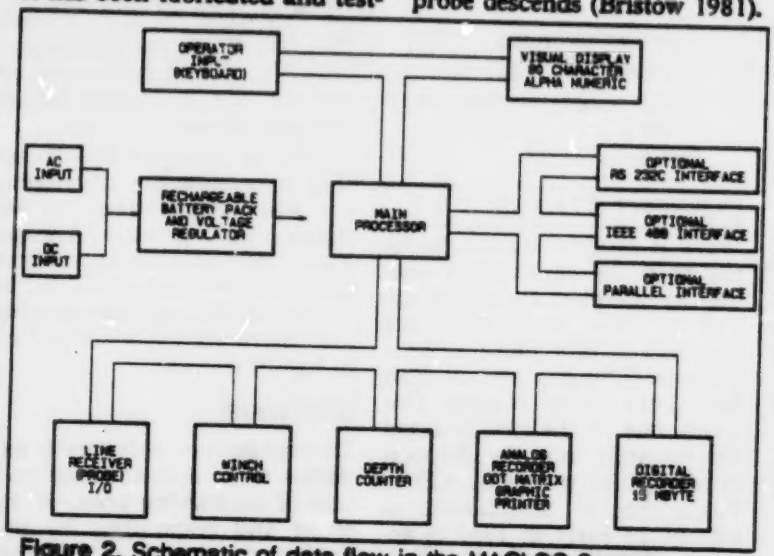

Figure 2. Schematic of data flow in the MAGLOG System.

CABLE/WINCH

For the prototype system, IFG will use the McPhar RD-600 motorized winch with a standard 4 conductor logging cable and a custom designed depth encoder capable of resolving depths to within 1 cm. For future production systems, any of a number of commercially available winches, including backpack versions, and any 2 conductor logging cable may be used.

CONSOLE

Like the probe, this component is unique compared to conventional logging systems. Rather than containing electronics specific to the sensors, the console is a general data acquisition and control unit. As shown in Figure 2, it consists of an operator interface, a microprocessor with a selection of outputs, inputs from the probe and winch, and the recording devices. It is powered either externally by generator-supplied AC or by battery, or from its internal rechargeable battery pack. The entire unit is only 20 by 46 by 41 cm and is easily carried by 1 man.

The interface consists of a 4 by 5 keypad with tactile feedback. Through this the operator enters header information such as date, time, location, drillhole number, and operator code. It also is used to enter control commands such as sampling time, display requests, analog scale factors, and filtering. During a logging run, most of the keys and other panel controls are locked out to prevent accidental change. All information keyed in appears on the 4 line, 20 character/line, low temperature liquid crystal display (LCD) mounted on the panel. This display is used to actively

monitor individual sensor outputs, system status values, and depth during logging runs.

The CMOS microprocessor acts to control, manipulate, and format incoming data and to send it on to the recorders. It has the capacity to perform real time processing including multipoint running averages, reconstructed SP from differential measurements, and temperature gradients.

All information is recorded on a high capacity 4 track cartridge tape in raw form for later processing and archiving. A verification routine insures that no errors are recorded. The dot matrix analog recorder monitors the incoming data and provides a hard copy for on-site interpretation.

PRELIMINARY SPECIFICATIONS

Measured Parameters, Resolution, and Ranges:

- Total field magnetics, 0.5 nT from 0 to 100 000 nT
- Vector components, 0.25 nT from 0 to ±100 000 nT
- Magnetic susceptibility, 5×10^{-5} SI from 0 to ±200 000×10^{-5} SI
- Electromagnetic conductivity, 0.1 mho/m from 0.1 to 1000 mho/m
- Differential self potential, 0.01 mV/m from 0.01 to 10.0 mV/m
- Fluid temperature, 0.01°C from 0 to 100°C

Measurement Format:

- Continuous with operator controlled time averaging

Depth Capacity:

- 1000 m

Probe Output:

- Serial BCD at 9600 baud or greater

Power:

- Console, 10 to 30 V DC, 110/220 V AC, or internal rechargeable batteries
- Probe, unregulated DC from surface

Cable:

- Standard 2 or 4 conductor cable with 1 inch 4 pin Gearhart Owen header assembly

Data Recording:

- Digital, Kennedy 6455 Cartridge with 15 Megabyte capacity
- Analog, Microplot 44 Dot Matrix Graphic Printer

Time Control:

- 0.25 to 60 seconds

Weights/Dimensions:

- Probe, 8 kg, 50 mm diameter by 2 m long
- Console, 11 kg, 20 by 46 by 41 cm

Software:

- Reconstructed SP from differential
- Running averages
- Temperature gradient
- Total magnetic field from vectors
- Self tests

CURRENT STATUS

Work is progressing satisfactorily with the objective of testing the complete system in the Fall of 1984. Field trials are expected to take place at Bells Corners (Ottawa) and at East Bow Lake (near Massey, Ontario), one of the sites selected for research into the disposal of radioactive wastes by AECL. Production is anticipated to commence early in 1985 to accommodate the following summer field season.

FUTURE DEVELOPMENTS

HARDWARE

Because the console is designed to accept any digital input, and the probe electronics and microprocessor have additional capacity, it is reasonable to expect that other devices can be added to the probe which will extend the capabilities of the system accordingly. At present it is possible to include gamma ray scintillometry, normal resistivity, and hole calipers without compromising the performance of the system and maintaining the simultaneous measurement of all parameters. It may also be highly desireable to investigate the possibility of encorporating the capability to measure pH and oxidation potentials (Dyck 1975). The difficult problem of sensor orientation using nongyroscopic methods will be under consideration as an extension to this project. This will relate the vectors to a known reference frame and allow for the interpretation of magnetic poles.

As a peripheral device, IFG is considering developing a tape duplication device which will provide backup copies of field tapes. These copies could then be mailed to a central facility for plotting and interpretation without fear of loss in transit.

SOFTWARE

Development of software is expected to be a continuing process of identifying areas of interest and responding by upgrading the operating, processing, and interpretational programs. In addition to the automatic interpretation package being developed for the MAGLOG System by Morris Magnetics Limited, IFG will likely proceed with an expand-

ed range of addressable data filters available through the keypad, providing a program to merge a surface base station magnetometer with the downhole data to correct for diurnal drift, and one to reduce the thermal drift of the system.

CONCLUSIONS

The project to develop a commercially viable portable magnetic properties borehole logging system is progressing toward an expected completion date of early 1985. Comprehensive testing will have been concluded by that time and production will likely commence prior to the 1985 summer field season. At this time, most target specifications appear to be achievable.

The level of interest in the MAGLOG System has been relatively high and is expected to increase as the recession abates and exploration activity accelerates. Marketing and sales will be initiated upon the successful testing of the system in the field.

ACKNOWLEDGMENTS

The authors would like to thank William Morris of Morris Magnetics, Quentin Bristow and Patrick Killeen of the Geological Survey of Canada, and Pierre Lapoint of Energy, Mines and Resources Canada for their advice and support of this project. IFG is especially grateful for the cooperation and financial assistance made available for this development through the ETDF Program and the Ontario Geological Survey.

REFERENCES

Acuna, M.H., Scearce, J.B., Seek, J.B., and Scheifele, J.
1978: The Magsat Vector Magnetometer—A Precision Fluxgate Magnetometer for the Measurement of the Geomagnetic Field; NASA Technical Memorandum 79656, p.1-31.

Adams, D.F., Hartman, U.G., Lazarow, L., Maloy, J.O., and Mohler, G.W.
1976: Vector Magnetometer Design Study (by Time Zero Laboratories of Ball Corporation); Internal NASA Document CR-144825, p.1-171.

Bristow, Quentin
1981: Temperature Gradient Measurements in Boreholes using Low Noise High Resolution Digital Techniques; Paper presented at the Second Biennial Conference of the Australian Society of Exploration Geophysicists, August 1981.

Dyck, A.V. (editor)
1975: Borehole Geophysics Applied to Metallic Mineral Prospection: A Review; Geological Survey of Canada, Paper 75-31.

George, D.C., and Scott, J.H.
1982: Review of Magnetic Susceptibility Logging and its Application to Uranium Exploration: NEA/IAEA Symposium on Uranium Exploration Methods, p.837-856.

Primdahl, F.
1979: The Fluxgate Magnetometer; Journal of the Physics of the Earth: Scientific Instrumentation, Volume 12, p.241-253.

Scott, J.H., Barth, J.J., and Summers, G.C.
1977: A Magnetic Susceptibility Well Logging System for Mineral Exploration; United States Geological Survey, Open File Report 77, p.1-17.

Grant 061 The Development of a Geochemical Analytical Method for Simultaneous Determination of Gold, Antimony, Arsenic, Tellurium, and Mercury

R. Jackson and R.E. Lett

Barringer Magenta Limited, Rexdale

ABSTRACT

This report describes the research activities carried out under 2 grants, GR016 and GR061 from the Exploration Technology Development Fund.

Research directed towards development of a lower cost analytical method based on laser ablation and atmospheric helium induced plasma emission spectroscopy for simultaneous determination of Au, As, Sb, Te, and Hg in geochemical sample media is described in this report. Technical problems related to incomplete sample atomization were experienced during the program and proved difficult to eliminate. Consequently, efforts related to engineering design and instrumental development were discontinued and conceptual studies were directed towards the application of Inductively Coupled Plasma/Mass Spectroscopy (ICP/MS) to LASERTRACE™.

INTRODUCTION

The main objective of the proposed research was the development of a low cost geochemical analytical method for simultaneous determination of Au, As, Sb, Te, and Hg based on a modified laser vapourization technique combined with atmospheric helium induced microwave plasma emission spectroscopy. This research was based on instrumentation previously developed by Barringer Magenta Limited and efforts were directed towards improving the laser vapourization system to enable routine estimation of sample mass and modification of an atmospheric pressure helium microwave plasma MPD 6-channel direct reading spectrometer to enable sensitive, simultaneous measurement of Au, As, Sb, Te, and Hg.

The proposed system, when developed, would have considerable economical benefit in view of the continued high level of gold exploration activity in northern Ontario and would be particularly suitable for analysis of submicroscopic forms of gold in clay minerals and water suspended material. In addition, the technique would be compatible with Barringer's existing airborne geochemical exploration techniques, AIRTRACE™ and SURTRACE™, for gold exploration.

BACKGROUND

ANALYSIS OF VOLATILE ELEMENTS USING HELIUM MICROWAVE PLASMA EMISSION SPECTROSCOPY

Inductively coupled argon plasma (ICAP) torches have been used extensively in recent years as a source for optical emission spectroscopic analysis (Greenfield *et al.* 1975; Scott *et al.* 1974). The plasma (a partially ionized gas formed electromagnetically by radio frequency induction coupling of argon) causes excitation and emission zones which can be resolved spectrally, producing a relatively clean background spectrum consisting essentially of argon lines. This low background, combined with a high signal-to-noise ratio of analyte emission, produces detection levels typically in the ppm range. Due to the geometry of the ICAP plasma source, when an analyte is carried directly through a narrow channel in the centre of the plasma discharge, it experiences a high excitation temperature (9000°K) and long residence time (2 ms). Although the high temperature of the radiation zone ensures the complete breakdown of chemical compounds it also causes certain elements, particularly As, Se, and Sb, to be readily ionized. Due to the degree of ionization of these elements in the plasma, analytical sensitivity is markedly suppressed.

One method of avoiding the ionization problem in the case of As, Se, and Sb, is to generate the element-hydride and introduce this into the plasma. This approach is commonly employed in both ICAP and atomic absorption spectroscopy analysis for As, Se, and Sb. Direct introduction of solutions and solids into the plasma for analysis of these elements is still not feasible. However, the problem of poor sensitivity due to ionization during direct analysis of As, Se, and Sb can theoretically be avoided by using an atmospheric helium microwave plasma as the source for optical emission. Basically, the microwave (plasma) emission detector (MED) system consists of a nonconductive discharge tube placed in a resonance cavity which serves to focus the energy from the microwave power supply onto the plasma. The MED operates at less than 100 watts, using either argon at atmospheric

pressure or helium at reduced pressure as a working gas. The energy required to maintain the plasma in the discharge tube is provided by a microwave power supply via a resonance cavity which maximizes the energy field at some point within its volume. Different cavity designs have been developed which enable the helium plasma to be maintained at atmospheric pressure (Beenakker 1976).

The high excitation capability and the greatly improved stability of atmospheric pressure helium microwave plasmas formed using the Beenakker cavity have proved ideal for providing an excitation source for metallic elements such as As, Sb, Se, Te, and Hg (Quimby *et al.* 1979).

ICP ANALYSIS USING LASER VAPORIZATION

Briefly, the LASERTRACE analytical system described in detail by Abercrombie *et al.* (1978) comprises an ARL-QE-137 spectrometer, a radio frequency argon plasma torch, and a high energy CO_2 TEA laser ablation unit. Analysis involves volatilization of particulate sample material mounted on an adhesive tape by the laser. The resultant aerosol is swept by an argon carrier gas directly into the plasma and emission of the sample analyzed for 25 major, minor, and trace elements by the AQ-137 spectrometer.

LASERTRACE has many unique aspects which make it possible to analyze microgram quantities of material. The laser transfers a large amount of energy in a very short time span (microseconds). Therefore, the sample is volatilized quickly in a short pulse. Hence the signal-to-noise ratio is enhanced greatly and the required detection limits for the analysis of 25 elements can be achieved. LASERTRACE operates by complete automation in which the tape is advanced, the sample is volatilized and carried into the plasma. The system is programmed to analyze a sample every 8 seconds. In practice, an operator can analyze up to 1500 samples per day for the following elements: C, Al, Ca, Cu, Cr, Co, Fe, Pb, Mg, Mn, Mo, Ni, Ag, Be, Sr, Ba, Zn, Cd, Na, Si, P, B, Ti, V, and K. Since the LASERTRACE system is linked to an SEL computer the raw multielement data is readily available for further statistical reduction and processing.

Currently, element concentrations are measured using a mathematical algorithm to estimate the relative amount of oxygen in the sample. The algorithm is based on assumptions that major elements are present as oxides (which allows for an estimate of oxygen in the sample) and that the sum of the oxides represents a large fraction of the sample (which allows for indirect estimation of element concentrations other than oxygen). Because the accuracy of the laser ablation method is limited by the absence of analytical results for oxygen and sulphur, previous research focused on the development of other methods for directly estimating sample mass. One system, based on a quartz microbalance linked to a 2-stage electrostatic precipitator, proved to be capable of detecting changes of particle content in carrier gas flowing from the laser ablation chamber. Results of preliminary research on the application of this system for direct mass measurement indicated that further extensive studies would be necessary to establish the effect of different particle size, shape, and charge polarity on response. Since this approach was beyond the scope of the existing financial resources available, other procedures were considered.

EXPERIMENTAL

INSTRUMENTATION DEVELOPMENT

A key part of the originally proposed research involved the redesign of the entrance optics and secondary slits of a 6-channel direct reading spectrometer to provide wavelengths capable of detecting Au, Sb, Hg, Se, As, and Zr. At the start of the current project, however, the opportunity arose to purchase a 32-channel ARL ICAP spectrometer, and the necessary modifications to detect gold and pathfinder elements were made to this instrument. Components of the modified system are illustrated in Figure 1. Specific modifications to the existing spectrometer include the following:

1. The selection of optimal spectral lines for the detection of elements by helium microwave plasma was made. A conventional film emission spectrograph was attached to the helium microwave plasma torch in order to establish wavelengths most sensitive for the detection of Se, Sb, As, Au, Ag, Te, Cr, and Al. Adjustments were necessary to make the film ultraviolet light sensitive in order to detect the complete range of elements. The relative intensity of emission for Cr and Al, obtained using helium microwave, was compared to that obtained by conventional argon plasma and was found to be similar. Based on this comparison, the wavelengths for the weakly

ionizable elements (e.g. Ca, Mg, Sr, Cr) given in the literature for argon plasma emission spectroscopy were employed in the helium microwave plasma spectroscopy. A compilation of wavelengths derived from literature, and by examination of the film spectrograph results for the helium microwave plasma, are given in Table 1. These wavelengths were selected as optimal lines in the modification of the 32-channel ARL spectrometer.

2. Construction and mounting of an optical alignment system for the microwave cavity on the ARL spectrometer was carried out.

3. Development of a suitable interface to transfer signal data from the ARL multielement direct reading spectrometer to the SEL 32-bit minicomputer system was carried out. This also entailed ex-

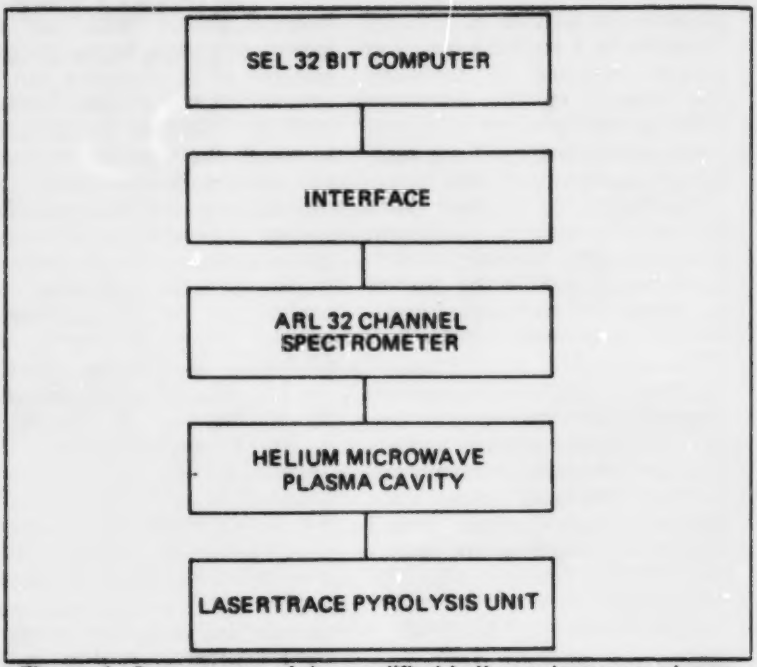

Figure 1. Components of the modified helium microwave plasma 32-channel ARL spectrometer system.

TABLE 1: WAVELENGTHS ESTABLISHED FOR HELIUM MICROWAVE EMISSION SPECTROSCOPY FROM LITERATURE SOURCES AND FILM EMISSION SPECTROGRAPHIC MEASUREMENTS.

ELEMENT	WAVELENGTH	ELEMENT	WAVELENGTH	ELEMENT	WAVELENGTH
C	1930.9	Mn	2576.1	Co	3453.5
Se	1960.8	Mg	2795.5	Cr	3579
Zn	2055.0	Pb	2833.3	Ni	3619
I	2062	Si	2881.6	Fe	3719.9
P	2136.2	V	3102.8	Mo	3864.1
As	2288	Be	3130.4	Ca	3934
Sb	2312	Cu	3247.5	Al	3961
Te	2385	Ag	3280.7	K	4047.2
Au	2428.0	Na	3302.3	Sr	4077.7
B	2497.7	Ti	3349.4	Ba	4554.0
Hg	2537	Zr	3438.2		

TABLE 2: COMPARISON OF DETECTION LEVELS FOR Hg, C, AND P OBTAINED BY INTRODUCING ELEMENT VAPOUR INTO 2 TORCHES WITH HELIUM MICROWAVE PLASMA.

Triethyl phosphate was employed in the measurement of C and P detection levels. Introduction of vapours into the plasma was made over a 10 s period.

TORCH	Hg	C	P
Quartz tube, 1 mm ID	0.6 pg/s	10 pg/s	15 pg/s
Helical torch	3.0 pg/s	100 pg/s	200 pg/s

tensive software development to enable data transfer.

In addition to the development of a suitable spectrometer system for detecting both readily ionizable and weakly ionizable elements, preliminary experiments also indicated that major redesign of the LASERTRACE sample vapourization box and the microwave cavity were also required. Modifications to these units of the system involved the following:

1. redesign of the LASERTRACE sample box to allow maximum transfer of the sample to the plasma and to minimize material hang-up
2. construction of a 2.5 cm microwave cavity and helical torch to provide sample introduction following volatilization

Experiments were carried out using the modified ARL spectrometer attached to the microwave cavity fitted with a 1 mm ID torch. Although acceptable sensitivity for readily ionizable elements (e.g. As, Hg, Sb) was obtained with this system, severe hang-up of material in the torch could be observed during individual laser firings. Moreover, a substantial amount of material passing through the cavity from the laser box was not excited. This detrimental effect appeared to reflect both the high sample flow rate and the short residence time of material in the plasma. To overcome this problem, a helical torch was constructed based on the design of Bollo-Kamara and Codding (1981). The advantage of this torch is that the tangential gas flow produced by the helical design prevents the plasma from touching the internal walls of the torch body.

Tests were also made to establish the ability of the plasma to break down the particles from the laser ablation using a helium plasma. The laser beam was directed at right angles to the exit stream of the torch. With the laser off, there was obvious scatter from many small particles as the ablated material passed out of the torch. With the plasma lit, however, there was no obvious scatter of the laser beam and so the particles were effectively vapourized in the plasma.

RESULTS

Although the problem of sample hang-up was completely avoided using the helical torch design, severe matrix effects were observed on laser volatilization and helium microwave plasma analysis for refractory elements and elements which require a high temperature for atomization. An experiment was carried out whereby Hg, C, and P in vapour form were introduced in a continuous stream into both plasma torches and the detection level of each element determined. Results shown in Table 2 indicate a 4-fold decrease in sensitivity for Hg determined using the helical torch but a 10-fold decrease in sensitivity for C and P. The detection limits obtained using the 1 mm ID torch are comparable to values reported in the literature and to results obtained previously by BML using another spectrometer. The 5- to 10-fold decrease in sensitivity with the helical torch is to be expected due to the higher gas flow rates through the torch. Even with the decreased sensitivity using the helical torch, good signals should be obtained for several more refractory elements (Si, Ca, Pb) based upon detection limits reported for these elements in the literature. However, no

adequate signals were observed for these elements for a number of soil and rock standards. This poor sensitivity of the refractory elements in the helium microwave plasma compared to the argon plasma is considered to reflect the inability of the helium microwave plasma to atomize small particles of weakly ionizable elements and thus induce emission. Consequently, the proposed use of Zr as a normalizing factor and the application of the currently developed LASERTRACE algorithm, which uses the analysis of major elements to normalize for variations in sample mass entering the plasma, is not possible.

DUAL ICP/HELIUM MICROWAVE ANALYSIS

To overcome the problems of poor sensitivity for weakly ionizable elements in the helium plasma and at the same time enable determination of readily ionizable elements, a new system was developed. This system would allow (1) splitting of the LASERTRACE sample for introduction into both argon and helium plasma sources, (2) normalization of the proportion of the sample split to each plasma by monitoring carbon on each system, and (3) integrating and merging of all signals from a 32-channel ARL spectrometer and a 6-channel direct reading spectrometer in the electronics console of the ARL system.

This approach would allow for the LASERTRACE determination of the volatile GOLDPRINT elements in addition to 25 major, minor, and trace elements conventionally determined in LASERTRACE MK I. This new system shown in Figure 2 in schematic form would also enable evaluation of the normalization technique using Zr as an internal standard outlined in the original proposal.

INSTRUMENTATION

Preliminary instrumentation development for the dual ICP/Helium microwave LASERTRACE system involved 5 stages.

1. Spectrometer Design

Scale drawings of the MPD 850 6-channel direct reading spectrometer were prepared and, based on these specifications, a diffraction grating was selected to cover those elements excited by helium microwave plasma (As, Sb, Te, and Hg).

2. Helium Microwave Cavity Mount Fabrication

In order to connect the helium microwave plasma cavity to the MPD 850 spectrometer, the design and manufacture of a suitable mount was necessary. A mount was therefore designed to enable the necessary connection and also to include a X-Y stage for optical alignment. Following design, the mount was manufactured and fitted to the system.

3. Installation of the New Diffraction Grating

The new diffraction grating was installed in the MPD 850 spectrometer to allow improved reduction.

4. Software Development

Basic units of the dual (ARL and MPD 850) spectrometer LASERTRACE system required the merging of signals generated by both ARL and MPD spectrometers, and consequently the computer software required modification to enable signals from both sour-

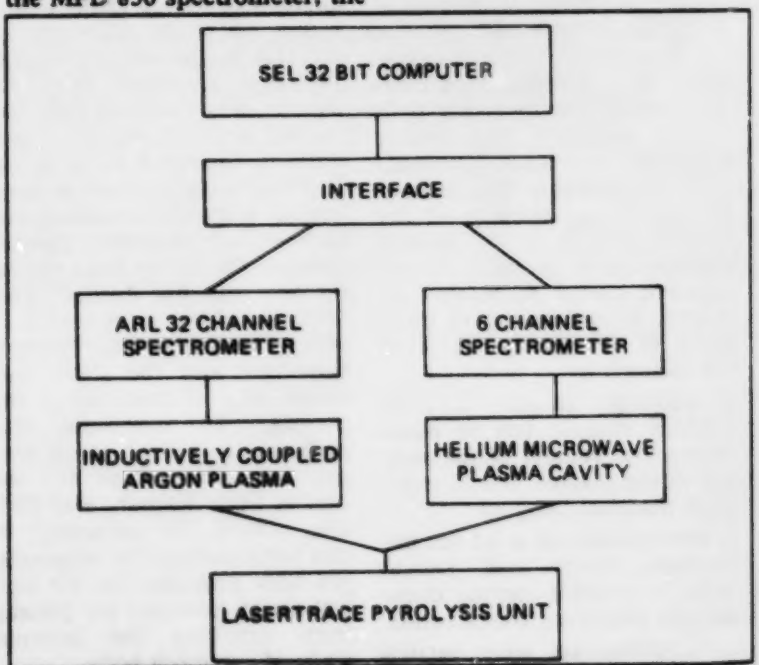

Figure 2. Components of the dual spectrometer system.

ces to be interfaced with the HP 9830 microcomputer.

5. Circuitry Design

Circuitry had to be designed to allow photomultiplier signals from the MPD 850 spectrometer to be integrated with the ARL spectrometer. This design was implemented to simplify the transfer of data through the HP 85 computer to the SEL 32-bit minicomputer.

RESULTS

During fabrication of the dual plasma systems, a series of tests aimed at establishing the efficiency of the helium microwave plasma revealed a serious limitation to the concept of utilizing laser ablation-helium microwave vapourization for the determination of volatile elements. Observations aimed at establishing the efficiency of decomposition and atomization of sample material entering the plasma from the LASERTRACE unit suggested that atomization was incomplete and thus subsequent measurements of element concentration would be unreliable. Therefore, it was realized that considerable effort would be required in improving atomization of sample material in the helium microwave before reliable analysis would be possible.

DISCUSSION

Rather than to continue further effort on the dual plasma system in resolving atomization problems by increasing energy of the helium plasma source, a decision has been made to review an alternative multielement analytical system which would eliminate the problems of incomplete solid sample atomization and offer improved sensitivity for a wider range of elements.

This alternative method is based upon sample introduction by laser ablation (LASERTRACE), atomizaton by inductively coupled plasma (ICP), and multielement detection by mass spectroscopy. One of the characteristics of inductively coupled argon plasma (ICP) sources operating at roughly 7000°C is that dissolved solids, when introduced into the plasma torch, are atomized and most elements comprising the solids are highly ionized. Consequently, an ICP is an excellent source of ions for atomic mass spectroscopy. The concept of sampling ions from a high temperature plasma operating at atmospheric pressure was first demonstrated using a capillary arc (DC) plasma. Interelement and matrix effects limited early investigations, and consequently an ICP was substituted for the DC plasma. Studies demonstrated significant improvement of results with the ICP-quadruple mass spectrometer system, suggesting an excellent possibility for application to LASERTRACE analysis.

Components of a typical ICP/MS system are shown in Figure 3. Samples are introduced to the ICP by conventional solution nebulization. A portion of the ionized gas is extracted from the tail flame of the ICP into the mass spectrometer through a small hole (typically 0.5 mm) drilled in a water-cooled Cu, Ni, or Ni-alloy cone. The vacuum system operates in 3 stages. Extracted gas forms a molecular beam in Stage 1 (Figure 3) (operating at 1 torr pressure) and the centre of the beam passes through a skimmer aperture into Stage 2 (operating at 10^{-3} torr pressure). The ions are focused through a differential aperture into Stage 3 (operating at 10^{-6} torr pressure) containing the quadruple mass filter and detector. The quadruple mass filter scan is synchronized with the sweep of a multichannel scaling data system so that the signal from ions of a particular mass to charge ratio (m:z) is recorded in a particular channel or group of channels.

The ICP/MS analytical system has several advantages in comparison to other multielement analytical instruments. One major advantage of the ICP/MS analytical system is that element isotopic abundances can be determined. Hence a wide range of elements can be determined (most elements in the periodic table) and it may be possible to determine oxygen content in samples using laser ablation. This determination would, undoubtedly, aid in providing more accurate analysis since the computer algorithms for the determination of element concentration would no longer require assumptions as to the oxide content in each sample analysis.

A second advantage of ICP/MS analysis is that instrumental detection levels are significantly lower than those obtained using conventional ICP emission spectroscopy (ICPAES) or flame atomic absorption spectrophotometry (FAAS). This is of major importance because many of the trace elements in LASERTRACE analysis are currently below the detection limit (i.e. Au, Hg, Te, Se, Pb, As). A comparison of instrument detection levels obtained with ICP/MS, ICPAES, and FAAS is given in Table 3 and emphasizes the improved sensitiv-

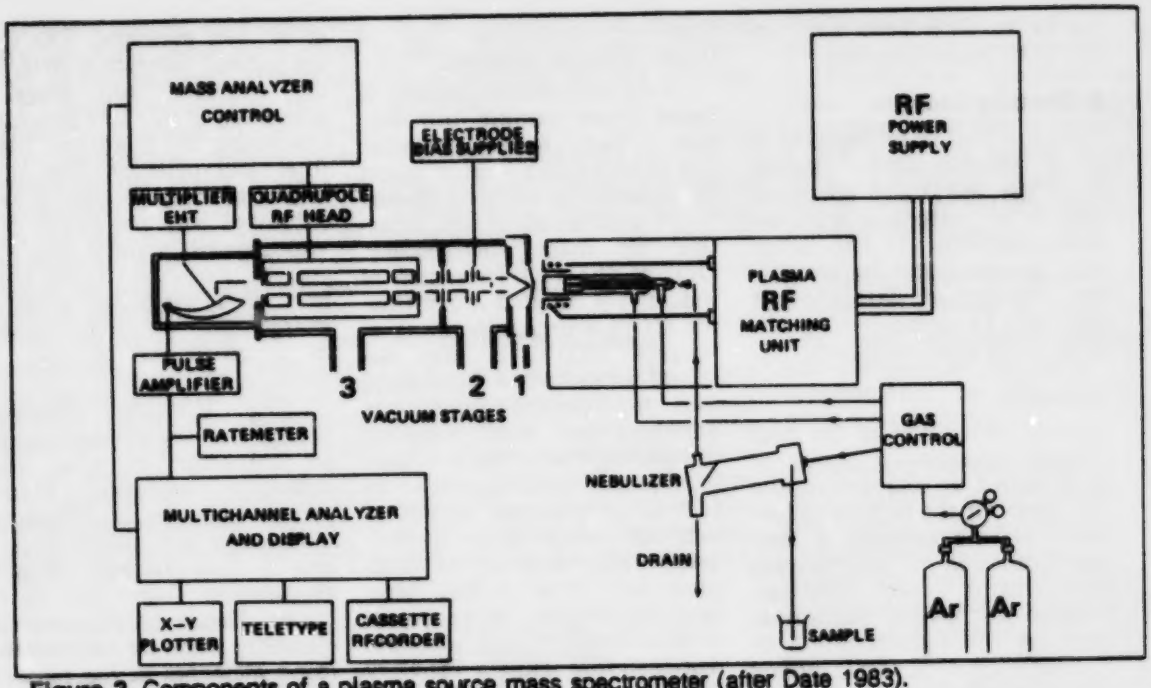

Figure 3. Components of a plasma source mass spectrometer (after Date 1983).

ity of ICP/MS. The 2 commercial ICP/MS systems currently available are manufactured by VG Isotopes Limited and Sciex Limited. Both instruments have the same basic design as shown in Figure 3, but differ in the aperture design, pumping system design, and rate of pulse counting employed to detect individual ions (Douglas 1983; Date 1983; Date and Grey 1983).

Currently, sample introduction in both systems is by conventional solution nebulization. In practice, however, any techniques may be used for sample introduction into the ICP plasma source. Methods which have been employed include ultrasonic and pneumatic nebulization, hydride generation, electrothermal vapourization, and flow injection. Consideration has also been given to the direct introduction of solid samples by la-

TABLE 3: COMPARISON OF DETECTION LIMITS.

For Inductively Coupled Plasma Mass Spectroscopy (ICPSMS), Inductively Coupled Plasma Atomic Emission Spectroscopy (ICPAES), and Flame Atomic Absorption Spectrophotometry (FAAS); 2 blanks ng/ml.

ELEMENT	ICPSMS	ICPAES	FAAS
Lithium	3	1.9	2
Boron	1	3.2	1000
Magnesium	0.5	0.1	0.2
Aluminium	0.6	15	20
Titanium	0.3	2.5	30
Vanadium	0.4	3.3	20
Chromium	0.2	4.1	3
Manganese	0.8	0.9	3
Cobalt	0.5	4	5
Zinc	3	1.2	0.6
Germanium	1	1	50
Arsenic	7	35	100
Selenium	15	30	100
Rubidium	0.3	–	2
Silver	0.2	4.7	2
Cadmium	0.5	1.7	1
Indium	0.1	42	30
Tellurium	0.5	27	70
Caesium	0.1	–	15
Barium	0.3	0.9	20
Lanthanum	0.2	6.7	1600
Cerium	0.2	32	–
Tungsten	0.5	20	300
Gold	0.2	11	10
Mercury	0.4	17	200
Lead	0.3	28	20
Bismuth	0.2	23	40
Thorium	0.2	45	–
Uranium	0.4	170	7000

ser ablation (Date 1983), however, currently no research has been devoted to this area. Conceptually adapting ICP/MS to LASERTRACE would provide greater sensitivity, less matrix interferences, and provide a method for normalization for sample mass (i.e. determination of element concentration in ppm).

CONCLUSIONS AND FUTURE PLANS

Research aimed at developing an analytical technique based on laser ablation-atmospheric helium emission spectroscopy for simultaneous determination of Au, As, Sb, Te, and Hg has determined that although increased sensitivity for Hg can be achieved with a helical design plasma torch, refractory elements such as Si, Ca, and Pb show dramatically decreased sensitivity compared to that obtained with argon plasma analysis. The poor sensitivity can be attributed to the inability of the helium microwave plasma to atomize small particles of weakly ionizable elements and thus induce emission. For this reason, the proposed method of measuring the sample mass vapourized by the laser using Zr as a normalizing factor would not be feasible. Consequently, the proposed research aimed at overcoming both the limitations of the helium microwave plasma and problems of measuring sample mass would involve development of a dual ICAP/Helium microwave system. Another system under conceptual review would involve a combination of the laser pyrolysis system with ICP/mass spectrometry. However, the design and manufacture of such a system is clearly beyond the scope of the proposed program since estimated capital expenditures would be in excess of $250 000 and a further $100 000 would be required to implement the technique.

ACKNOWLEDGMENTS

The authors would like to thank A. Murray for critically reviewing the manuscript and Alan Date (British Geological Survey) for valuable information with respect to ICP/MS systems.

REFERENCES

Abercrombie, F.N., Barringer, A.R., Bradshaw, P.M.D., Cruz, R.V., and Murray, A.D.
1978: Multi-element Geochemical Analysis using a Radio Frequency Argon Plasma with Conventional Acid Digestion and Laser Vapourization; Paper presented at Geoanalysis '78, A symposium on the analysis of geological materials sponsored by the Geological Survey of Canada and CANMET.

Beenakker, C.I.M.
1976: Developments in Helium Microwave Plasma Analysis; Spectrochimica Acta, Volume 31B, p.483.

Bollo-Kamara, A., and Codding, E.G.
1981: Consideration in the Design of a Microwave Induced Plasma Utilizing the TM010 Cavity for Optical Emission Spectroscopy; Spectrochimica Acta, Volume 36B, Number 10, p.973-982.

Date, A.R.
1983: An Introduction to Inductively Coupled Plazma Source Mass Spectrometry; Trends in Analytical Chemistry, October 1983, Volume 2, Number 10, p.225-230.

Date, A.R., and Gray, A.L.
1983: Development Progress in Plasma Source Mass Spectrometry; The Analyst, February 1983, Volume 108, p.159-165.

Douglas, D.
1983: ICP/MS: Technologies Marry to Produce Better Analysis; Canadian Research, April 1983, p.55-60.

Greenfield, S., McGrechin, H. McD., and Smith, P.D.
1975: Plasma Emission Sources in Analytical Spectroscopy; Talanta Review, Volume 22, p.1-15.

Quimby, B.D., Delaney, M.F., Uden, P.D., and Barnes, R.M.
1979: Determination of Trihalomethanes in Drinking Water by Gas Chromatography with Microwave Plasma Emission Detector; Analytical Chemistry, Volume 51, p.875.

Scott, R.H., Fassel, B.A., Kniseley, R.H., and Nixon, D.E.
1974: Inductively Coupled Plasma-Optical Emission Analytical Spectrometry: A Compact Facility for Trace Analysis of Solutions; Analytical Chemistry, Volume 46, p.75.

Grant 065 Development and Adaptation of Geochemical Techniques to Gold Exploration in Glacial Drift

C.F. Gleeson[1], V.N. Rampton[2], R.D. Thomas[2], and S. Paradis[2]

[1]C.F. Gleeson and Associates Limited, Iroquois

[2]Terrain Analysis and Mapping Services Limited, Carp

ABSTRACT

A shallow overburden sampling program was completed in eastern Ontario to determine the most effective sample media and sampling pattern to utilize in outlining areas of gold mineralization at a regional scale, and pinpointing the location of the gold mineralization at a detailed scale. The sampled area was characterized by a sequence of Late Precambrian supracrustal rocks intruded by granitic and gabbroic complexes and sheared and faulted along a number of major structures, and by extensive but relatively thin loose ablation till, interrupted by some major glaciofluvial systems. Known gold occurrences are present in quartz- and quartz-carbonate-filled fractures in sheared dolomites and intercalated volcanic and volcaniclastic rocks.

The sampling program determined that all sampled materials (humus, "B" soils, and the -5 mesh, -250 mesh, and the heavy mineral fraction of the parent material, generally till) were successful to different degrees in outlining areas of known or potential gold mineralization at the regional scale and pinpointing gold mineralization at the detailed scale. Humus was determined to be the most cost effective medium to sample in detailed sampling programs, and the -250 mesh fraction of the till appeared to be the most cost effective medium to sample in regional sampling programs. However, the heavy mineral fraction of the till gave the best anomaly contrast and definition of areas of higher mineral potential, and allowed for additional useful geological and mineralogical data to be obtained from microscopic examination of the heavy minerals.

INTRODUCTION

GENERAL

In order to establish the most effective shallow overburden sampling techniques for regional exploration, an area of some 180 km^2 was systematically sampled at 1 km centres. In order to establish the most effective techniques at more detailed scales of exploration, sampling at 100 m centres was carried out in the vicinity of 2 known gold occurrences. At each sample site humus, "B" soil, and till samples were taken. The first 2 sample media along with a -5 mesh (-4 mm), a -250 mesh (-0.063 mm), and a heavy mineral fraction from the till were then analyzed for gold. Complete heavy mineral identifications and pebble counts were carried out on each sample, and the surficial and bedrock geology of the area was mapped (selected rock samples were analyzed for gold), to determine the nature of the gold dispersion in the Quaternary deposits and to explain the results obtained from analyzing the various media.

LOCATION AND ACCESS

The area studied is located some 82 km southwest of Ottawa and makes up the northeastern quarter of NTS Sheet 31 F/2 (Figure 1). The research area takes in parts of Lavant and Darling Townships, Lanark County, as well as small portions of Blithfield and Bagot Townships, Renfrew County.

The region is about 50 km northwest of Perth on Highway 511 toward Calabogie. Inside the project area access generally is good from a series of gravel roads that service small communities such as Clyde Forks and Gordon Rapids (Joes Lake).

PRESENT INVESTIGATION

The field work for this project involved 3 phases: sampling of surficial materials, mapping of surficial geology, and mapping of the bedrock geology. The regional program was designed to systematically sample the surficial material at 1 km centres. In the vicinity of 2 gold occurrences more detailed sampling at 100 m centres was completed. From previous experience the regional sampling pattern was thought to be adequate to identify the main zones of gold mineralization. The detailed grids were designed to determine the most effective media and fraction to sample in delineating areas of gold mineralization, as well as to determine the optimum sampling pattern to identify specific sources of regional gold anomalies. At all sites decomposed humus and "B" soil samples were taken. Also hand pits were dug (0.5 to 1.0 m deep) to obtain samples of the parent material, generally till if available at the sampling site. In places where till was not present within a reason-

able depth or distance from the desired location then glaciofluvial material was sampled and so noted. For the regional program 154 sites from some 180 km² were sampled, and on the detailed grids 79 sites were sampled.

The surficial mapping program was designed to outline the distribution of the surficial deposits, to determine the ice flow or transport directions of the materials, and to determine the interrelationships of the surficial deposits. This information is required to properly interpret the geochemical data and to design follow-up programs. The bedrock geology mapping program was designed to verify and add to the geological picture as shown on maps by Peach (1958), Pauk (1983), and Carter (1981). Special emphasis was placed on features such as structure and alteration patterns that might be related to gold mineralization. Where possible, rock samples for gold analyses were obtained near each site sampled on the regional program. In addition, all mineral occurrences that could be found were sampled and analyzed for gold. The geochemical data from the rock samples was believed necessary to facilitate interpretation of geochemical gold results from the surficial materials.

Office studies included the preparation of bedrock and surficial geology maps and contoured geochemistry maps. Fifty pebbles obtained at each sample site were identified and counted. A 2 g representative sample of heavy minerals from each site was examined under a binocular microscope and a mineralogical analysis completed on each sample. All data was computerized, and gold in all sample media, pebble

Figure 1. Location of the research area.

TABLE 1: LITHOLOGIC UNITS FOR THE CLYDE FORKS AREA

Precambrian
Late Intrusive Rocks
7 Diabase
6 Granite and pegmatite

Intrusive Contact

Intrusive Rocks
5 Lavant Gabbro Complex
4 Addington Gneiss Complex

Intrusive Contact

Hermon Group
3 Carbonate metasedimentary rocks
2 Clastic metasedimentary rocks and associated carbonate rocks
1 Mafic to intermediate metavolcanic rocks (1310±15my) with metatuffs and carbonate phases

counts, and mineralogy were computer plotted. Basic statistical parameters were calculated for both the regional and detailed data. This data will all be presented in the final report with appendices (Gleeson *et al.* in preparation).

GEOLOGY

BEDROCK GEOLOGY

The area lies in the eastern portion of the Hastings Basin, which forms part of the Central Metasedimentary Belt, a subdivision of the Grenville Province defined by Wynne-Edwards (1972). The Hastings Basin contains the thickest succession of supracrustal rock in the Grenville Province. The base of its stratigraphic section is characterized by a sequence of mafic volcanic rocks containing intercalated metatuffs and carbonate sediments. The top of the section comprises an alternating sequence of carbonate and clastic sedimentary rocks.

The stratigraphic position of the local supracrustal succession within the Grenville Supergroup is poorly defined. Most workers (Sangster 1970; Nikols 1972; Carter 1981; Pauk 1983) tend to make them correlative with the Hermon Group as defined by Lumbers (1967) in the Madoc-Bancroft area. Some of the clastic metasedimentary rocks in the western part of the area may correlate with the Flinton Group (Pauk 1983), which rests unconformably on the Hermon Group (Moore and Thompson 1972).

In the project area the basal volcanic rocks consist of a mafic to intermediate sequence with minor interbedded marble. The volcanic rocks are overlain by carbonate metasedimentary rocks, which contain beds of clastic metasedimentary rocks. The clastic rocks have been interpreted as volcanic detritus eroded from adjacent volcanic highlands. According to Lumbers (1982) the carbonate facies was deposited both during and after volcanism, so that this facies is intercalated with most of the volcanic and volcaniclastic rocks. The supracrustal assemblages have been intruded by a variety of felsic to mafic syntectonic and late tectonic intrusive rock sequences. The general succession of the rocks is given in Table 1.

Tectonism has affected all supracrustal rocks in the region; generally they have been folded around axes that trend northeast and north-northeast. One major fault zone, the Robertson Lake Shear Zone, can be traced from the project area southerly and southwesterly for some 90 km to where it is covered by Paleozoic rocks. The Robertson Lake Shear Zone is one of a series of similar northeasterly trending structures and lineaments marking this part of the Grenville Province. The northern sector of the region is cut by a series of late east-trending faults associated with the Ottawa-Bonnechere Graben.

LITHOLOGIES

Metavolcanic Rocks and Associated Carbonate Rocks

The metavolcanic rocks and associated carbonate rocks form the basal unit of the supracrustal succession in the area. The metavolcanic rocks tend to be transitional into the overlying carbonate sequence. They are common along the Robertson Lake Shear Zone. Small areas also occur in the western and northern portions of the region. Jackson (1980) suggests that the metavolcanic units may be more extensive in the north central part of the research area than is shown in Figure 2.

The metavolcanic sequence comprises 4 basic lithologies: mafic to intermediate flows, felsic tuffs, mafic tuffs, and carbonates. The mafic to intermediate flows are the most common units, tuffs are relatively sparse, and intercalated carbonate sedimentary rocks and/or carbonatized volcanic rocks are common. Carbonate rocks tend to be fine grained, being composed of ferroan dolomite and calcite.

Within the Robertson Lake Shear Zone, all metavolcanic rocks are highly altered and mineralized. The alteration is generally moderate to high chloritization and carbonatization and slight to moderate sericitization, the latter alteration being most characteristic of acid tuffs. Silicification and quartz veins are locally very extensive, particularly in the vicinity of gold occurrences. Finely banded and disseminated magnetite, and in places ilmenite, are common in close association with chlorite. Variable proportions of pyrite are common throughout the volcanic assemblages. Chalcopyrite and specular hematite also occur at a few locations. Outside of the Robertson Lake Shear Zone, the metavolcanic rocks are moderately to highly chloritized, but other forms of alteration are slight or absent.

The carbonate rocks associated with the metavolcanic rocks are an important host for gold mineralization. The gold is associated with tetrahedrite, pyrite, and chalcopyrite in dolomite and

dolomite-quartz layers and lenses (Carter 1981).

Clastic Metasedimentary Rocks

A thick sequence of clastic metasedimentary rocks underlie most of the western side of the map area. They also wrap around the northern end of the Addington Gneiss and Lavant Gabbro Complex across the northern part of the area. Small bodies of clastic metasedimentary rocks occur along the western side and in the southern part of the Robertson Lake Shear Zone and as roof pendants and xenoliths within the gabbro complex. Generally the metasedimentary rocks are well banded to schistose, fine to coarse grained, medium to dark grey biotite-hornblende-quartz-plagioclase±muscovite schists and gneisses.

Two iron deposits are located within the metasedimentary sequence; the Caldwell pyrite deposit and the Radenhurst-Caldwell magnetite deposits (Wilson 1920; Carter *et al.* 1980).

Carbonate Metasedimentary Rocks

Carbonate rocks are the youngest sedimentary rocks recognized in the area, probably being equivalent to the Dungannon Formation of the Mayo Group (Lumbers 1967). They occur throughout the area, but especially in the northern and southern sectors, with smaller concentrations near the eastern and western boundaries, and locally as screens in the gabbro complex.

Three types of carbonate metasedimentary rocks are present: dolomitic marbles, calcitic marbles, and calcareous (dolomitic) metaclastic rocks

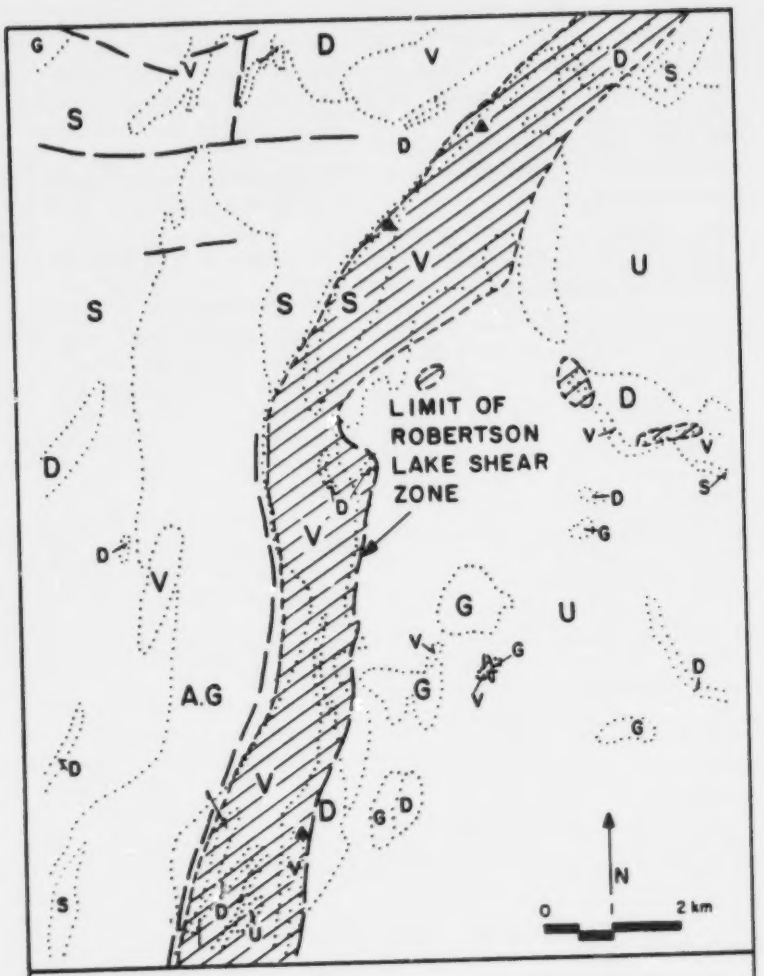

Figure 2. Bedrock geology of the research area.

and tuffs (Carter 1981). The dolomitic marbles frequently include veinlets of quartz, 1 to 2 cm in width. According to Carter (1981), the calcitic marbles contain no veins or lenses of quartz.

Alteration of the marbles frequently involves silicification in the form of quartz lenses and stringers. All gradations may be found from dolomite with quartz lenses, to dolomite-quartz veins, to quartz veins (Carter 1981). Chlorite may form as blebs in the marble, and sericite is found in places where the carbonate is highly sheared. Pyrite is a common accessory mineral, especially in the vicinity of the gold and copper occurrences.

Addington Complex

The Addington Complex (Pauk 1983), also referred to as the Addington Granite (Carter 1981) or Lavant Gneiss (Smith 1958), forms a north-trending body lying to the west of and partly incorporated into the Robertson Lake Shear Zone. The Addington Complex has been mapped by Pauk (1983) and Wolff (1982) for a distance of 100 km southwest to Tweed. Throughout its length it lies in the same stratigraphic-tectonic position. It is interesting to note that Jackson (1980) indicates a northerly trending mylonite zone cutting the northwestern section of the Complex through Tower Lake and coalescing at its northern extremity with the Robertson Lake Shear Zone. At this point the trend of the shear zone changes to a northeasterly direction.

The Addington Complex is made up of pink to greyish pink, weathering white to pink to medium red leucocratic, fine grained, equigranular granite, and quartz monzonite. It has a weak foliation and banding caused by variable concentrations and alignment biotite. Where sheared, the granite gneiss is aphanitic, with a well developed coarse to fine cleavage or foliation. Where it is close to, or within, the shear zone it is gneissic and may contain carbonate, chlorite, and sericite as alteration products along shear planes.

Gabbro–Diorite (Lavant Gabbro Complex)

Gabbro-diorite (Lavant Gabbro Complex of Pauk (1983)) (Lavant Intrusive Complex of Carter *et al.* (1981)) underlies the eastern half of the map area and satellite bodies intrude the metavolcanic rocks in the northern part of the area. It is part of a conformable intrusion that measures 40 km by 10 km and extends south from the research area for some 25 km. The western (and northern) boundaries are in contact with metavolcanic, carbonate, and metasedimentary rocks; the western edge of the complex is cut by the Robertson Lake Shear Zone. Screens and xenoliths of metavolcanic, carbonate, and metasedimentary rocks lie within the complex. The gabbro has been intruded by late stage granite, aplite, and pegmatite. The Lavant Gabbro Complex is composed of gabbro, diorite, and granodiorite. The relationships between the rock-types are uncertain, although Pauk (1983) suggests that several intrusive stages are responsible for the heterogeneity of the complex.

Where the gabbro-diorite lies within the Robertson Lake Shear Zone as well as at a few other locations where shearing has occurred, the gabbro has been carbonatized and chloritized. Highly chloritized gabbro is difficult to distinguish from chloritized metavolcanic rocks; possibly some of the rocks shown in Figure 2 as metavolcanic rocks are mylonitized gabbro. Sericitization is rare and occurs in minor amounts along shear planes in the most intensely sheared parts of the rock.

Magnetite mineralization is common within the gabbroic phase of the complex (Carter *et al.* 1980; Peach 1958). Generally it consists of fine euhedral to subhedral grains disseminated throughout the rock, or concentrated along fracture planes. In some places, appreciable concentrations of magnetite with intergrowths of ilmenite occur.

Granite

Late stage granitic rocks include intrusive bodies of granite to granodiorite, pegmatite, and aplite. The granite intrusive rocks are mainly in close association with the diorite and gabbroic rocks of the Lavant Gabbro Complex. Within the research area the granitic rocks are exposed over areas of 0.1 to 1.5 km in diameter and are medium to coarse grained, pink, weathering light pink to white, granite and granodiorite.

Pegmatites injected into metasedimentary rocks are most abundant in the western and northwestern sector of the area. They are composed of very coarse quartz-K-feldspar-tourmaline-muscovite. In places dikes and stringers of aplite intrude the metavolcanic rocks, metasedimentary rocks, and the gabbro complex.

MINERAL OCCURRENCES

The known gold-copper and copper-gold occurrences in the area are for the most part hosted in fine grained, dark grey dolomitic marble intercalated with carbonatized mafic volcanic rocks. The gold and copper mineralization is associated with quartz zones in the marble. The quartz appears as pods, lenses, fracture fillings, veinlets, and stringers. The ore minerals consist of tetrahedrite, chalcopyrite, pyrite, and native gold. They occur as blebs, disseminations, stringers, and fracture fillings. The gold-copper zones are associated with bleaching of the dolomite, silicification, and minor sericitization. Gold is present in its native state and in tetrahedrite and pyrite. Jonasson (Geochemist, Geological Survey of Canada, personal communication, 1983) who has analyzed mineral separates from the Joes Lake occurrence, found 100 000 ppb Au in tetrahedrite and 5300 ppb Au in pyrite. During this research project visible gold has been found in heavy mineral concentrates from the gossan over the Joes Lake showing and in heavy mineral concentrates from tills in the vicinity of the other known gold occurrences.

Magnetite iron occurrences are hosted in the metasedimentary, metavolcanic, and gabbroic rocks. The Radenhurst and Caldwell deposits in the western sector of the area, examples of metasediment-hosted deposits, consist of *en echelon* lenses of magnetite with minor pyrite, pyrrhotite, and trace of chalcopyrite in hornblende gneiss, amphibolite, and quartzofeldspathic gneiss. Samples from these occurrences contain 10 to 35 ppb Au. The Yuill deposit in the northeastern sector of the area, an example of a metavolcanic-hosted deposit, consists of a massive magnetite lens with minor pyrite in mafic volcanic rocks in contact with calcitic marble (Carter *et al.* 1980). Gold content of this occurrence varies from 1 to 12 ppb. Intrusion-hosted magnetic occurrences are relatively common in gabbroic rocks. The Lavant iron deposit in the southeastern part of the area (Carter *et al.* 1980) is typical of this type of mineralization. It consists of fine grained magnetite with lesser amounts of ilmenite, pyrrhotite, and traces of chalcopyrite disseminated in gabbro. This zone contains 1 to 5 ppb Au.

One sulphide iron deposit occurs within the project boundaries; the Caldwell (Blithfield) deposit located in the northwestern portion of the area. It consists of conformable massive pyrite lenses hosted in metasedimentary rocks (hornblende-biotite schists). The pyrite is associated with quartz and/or quartz and calcite. A sample of the massive pyrite from this deposit contains 34 ppb Au.

Apart from the high gold values found associated with known gold occurrences, anomalous gold values ranging from 29 to 1913 ppb have been found in various samples of altered volcanic and dolomitic rocks from the Robertson Lake Shear Zone.

SURFICIAL GEOLOGY

Regional striae patterns indicate that during the Late Wisconsinan the Madawaska Highland was glaciated by ice moving in a southerly direction (Gadd 1980). This is supported by the majority of striations observed in the map area (Figure 3). Ice flow during part of the Late Wisconsinan may have been minimal locally if the main components of regional ice flow were channeled down the St. Lawrence Lowlands to the east and across the Madawaska Highland to the west. Gadd (1980) believes that ice flow across the Madawaska Highland was less dynamic than flow in adjacent lowlands because of topographic control. During the waning stages of the Late Wisconsinan glaciation, glacial and subglacial tunnels developed in the ice, channels were formed in the subglacial bedrock, and eskers, kames, and kame deltas were formed. Further ice wastage resulted in partial uncovering of the area and development of a glacial lake in the Clyde River valley as evidenced by deltas in the valley. This lake must have been short lived because no significant amount of glaciolacustrine sediment was noted in the valley. The valley also must have been ice infested during its formation, as the deltas show structures and morphology characteristic of the melting out of buried ice-blocks.

In the Ottawa Valley, glacial ice flow in a general southeasterly direction may have persisted for a short period after deglaciation of the Madawaska Highland (Gadd 1980). South-southeast trending striations in the northern part of the research area support this hypothesis. During this interval, ice-contact stratified deposits likely formed in a marginal zone parallel to the scarp marking the northern edge of the Madawaska Highland (Barnett and Clarke 1977); meltwater flowed in a

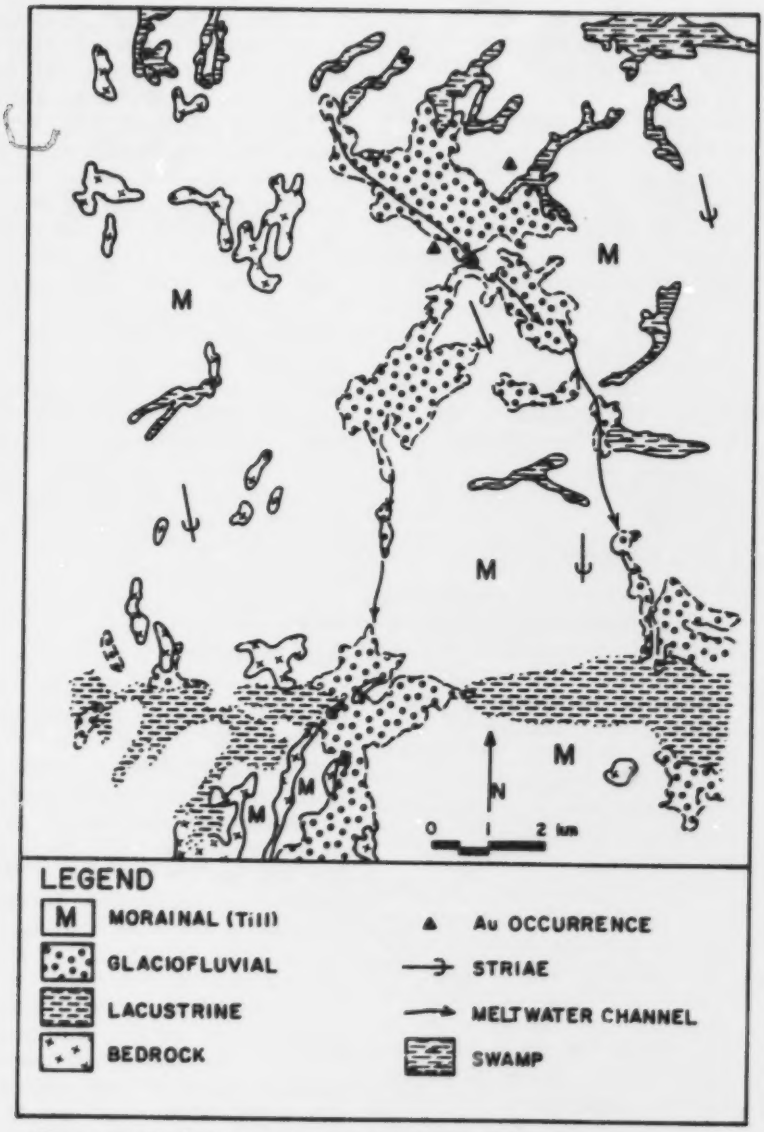

Figure 3. Surficial geology of the bedrock area.

general east-southeast direction.

The Champlain Sea did not directly affect the study area as its maximum elevation was only 175 m in adjacent areas (Fransham and Gadd 1977; Barnett and Clarke 1980); the study area all lies above this elevation.

Ablation till covers most of the area. It is generally characterized by a light yellowish brown (10YR6/4) colour and is loose to compact. It varies in textural composition from sandy (sM) with sand constituting 50 to 80% of the till and coarser clasts forming a significant portion (commonly 10 to 20%) of the remainder, to stoney (aM) with pebble-sized and larger clasts commonly constituting 15 to 35% and sand forming 40 to 70% of the till. The stoney tills may contain a significant portion of rock fragments dislodged by frost action from the underlying bedrock at a few localities, especially where the till is relatively thin. In addition, some of the ablation till on hill slopes may have incorporated rock fragments from the slopes where both the rock fragments and till have moved downhill under the influence of mass wastage processes.

The ubiquitous distribution of the ablation till throughout the area has made it the prime sampling target for the exploration program, which involved shallow sampling of unconsolidated materials. Ablation till is generally believed to be much further travelled than lodgement till, especially basal lodgement till, and thus a more difficult medium to utilize in the search for mineral deposits. However, in this study, it is apparently clear that gold from known occur-

rences has been incorporated into the glacier, and a recognizable amount of it has been deposited with the ablation till anywhere from about 3 km down-glacier (e.g. from the Little Green Lake gold occurrence, Figures 4 to 8) to a few 10s of metres (e.g. at the Darling gold occurrence, Figures 9 and 10). Generally the dispersion trains of all media paralleled the glacial flow directions determined from glacial striae.

Glaciofluvial deposits in the form of ice-contact stratified drift and outwash occurs mainly in a belt in the central part of the area and along the southern edge of the area (Figure 3). Glaciofluvial deposits include those sediments deposited by meltwater both in contact with glacial ice and in a proglacial environment. They range from crudely stratified silty gravels with isolated boulders to stratified well sorted sand and gravel.

Care must be taken in interpreting geochemical gold anomalies found in glaciofluvial deposits because the down-glacier distance between gold anomalies in glaciofluvial deposits and their source may be much greater than the down-glacier distance between gold anomalies in till and their source. In addition, direction of transport by water depositing the glaciofluvial materials may also differ from the flow direction of glacier ice. For example, in the north central part of the map area meltwater flow, according to the trend of esker segments and cross-bedding in these areas, appears to have been in southeasterly and south-southeasterly directions respectively (Figure 3). Thus, anomalous gold values found in glaciofluvial deposits southeast of the 2 gold occurrences in the central part of the area could be interpreted as reflecting local bedrock sources of gold or as gold transported from the area surrounding the 2 occurrences.

Brown forest soils have developed on calcareous tills, whereas Podzols have developed on glaciofluvial deposits and noncalcarious tills. "B" horizons generally extend to a depth of 0.2 to 0.4 m. However, even the "C" horizons in parent materials show evidence of oxidation due to groundwater percolation.

RESULTS OF REGIONAL SURVEY

DATA PRESENTATION

Gold data for each sample media was hand plotted and contoured on the maps at a scale of 1:25 000. One set of hand contoured geochemical maps included the data for all sample sites and another set excluded the results from localities underlain by glaciofluvial deposits (Gleeson *et al.* in preparation).

Computer-plotted maps showing the gold analyses and moving average contours have been completed at a 1:25 000 scale. Also maps showing the percentage of heavy minerals and pebble counts at each site have been computer plotted on 1:50 000 scale maps.

A computer file was assembled incorporating all information collected on gold, heavy minerals, and pebbles from the research area. In addition, standard statistical parameters for gold in the various sample media and fractions have been calculated for all data, for only the regional data, and for the detailed areas.

STATISTICS

A statistical summary for gold in the various sample fractions and media from the 154 regional sites are shown in Table 2. Full compilations along with histograms will be presented in the final report (Gleeson *et al.* in preparation). Because of the log normal nature of the data, the geometric mean will be used in this report. The means for gold in the mineral soil samples are: 5 ppb, 3 ppb, 2 ppb, and 2 ppb for the heavy mineral, -250 mesh, -5 mesh, and "B" soil fractions respectively; for humus it is 4 ppb. The humus is definitely enriched in gold relative to the mineral soils. Depletion of gold in the "B" soils relative to the tills is also apparent.

RESULTS

Gold in Humus

Gold in humus (Figure 4) shows an increase to generally greater than 10 ppb over the gold-bearing alteration zones underlain by the volcaniclastic rocks through the centre part of the area. The trend more or less follows the attitude of the underlying geological formations along the Robertson Lake Shear Zone (Figure 2). A second southeasterly trend is present east of the Green Lake Grid. The trend continues weakly southeastward over gabbroic rocks to the edge of the map area. An easterly trending increase in gold also occurs east of Joes Lake. All maps show poor response for gold in humus south of Joes Lake toward the Joes Lake gold occurrence. Obviously a sampling density for humus at 1 km centres is not sufficient to define the known gold mineralization in this area.

Significant increases in gold occur (up to 119 ppb) at

TABLE 2: STATISTICAL SUMMARY FOR GOLD (ppb) IN REGIONAL SAMPLES

HORIZON	ARITHMETIC MEAN	STANDARD DEVIATION	GEOMETRIC MEAN	LOGARITHMIC DEVIATION	RANGE MINIMUM	RANGE MAXIMUM
Humus	7.4	14.9	4.2	2.6	<1	119
"B" soil	5.7	21.7	1.5	3.6	<1	223
-5 mesh(till)	8.4	41.9	2.2	3.5	<1	506
-250 mesh(till)	11.5	39.8	3.4	4.0	<1	480
Heavy Minerals (till)	91.3	425.9	5.3	7.8	<1	4358

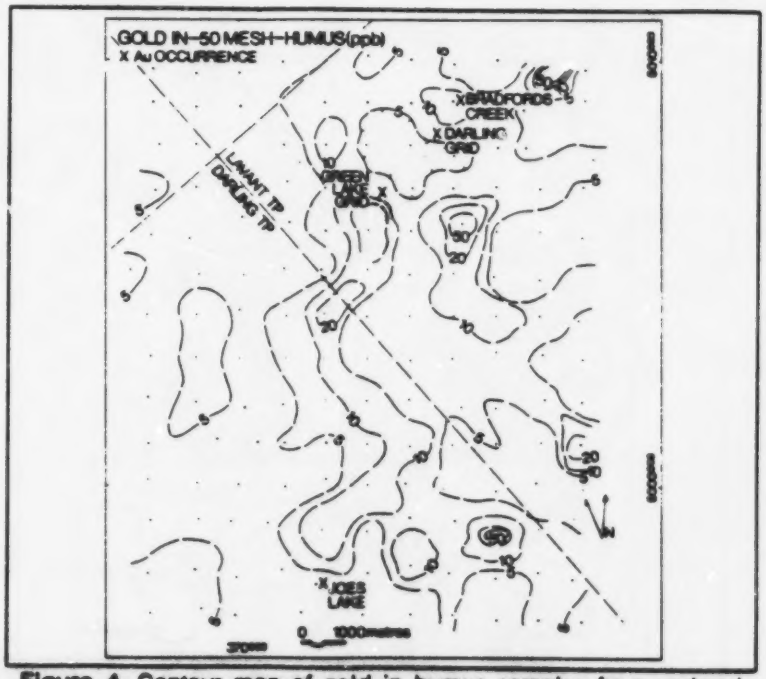

Figure 4. Contour map of gold in humus samples from regional grid.

various places within the above trends where no gold occurrences are known (e.g. in the northeastern and southeastern corners of the map area). These locales are target areas for more detailed work. Also a weak northerly trending anomaly enclosing values of 6 to 9 ppb Au is evident on the hand contoured maps over metasedimentary rocks in the western part of the area. Similar anomalies are present in the southwestern corner of the map area and along the western edge of the map area where anomalous gold values have been found in magnetite-rich rocks.

Gold in "B" Horizon

The gold trends for the "B" soils (Figure 5) are somewhat stronger than for the humus samples, although a similarity to the general trends exists. Greater than 3 ppb Au values

in the "B" soils trend northerly along the Robertson Lake Shear Zone from south of Joes Lake through to near Bradfords Creek. East of Highway 511 anomalies become somewhat disjointed and lack continuity on these maps. The reason for this may be the presence of glaciofluvial materials at several sites east of the highway.

Two areas of above normal values for "B" soils occur over a mix of altered gabbroic-carbonate-volcanic rocks in the east central part of the map area. Isolated highs occur southwest of the Darling/Lavant Township boundaries and west of the Green Lake grid that are underlain by granite gneiss. Carbonate-chlorite-sericite alteration has been mapped at the westerly location.

Gold values in the "B" soils in close proximity to known gold occurrences near Joes Lake and Little Green Lake range from 27 to 31 ppb. No sources of gold are presently known near the most northerly anomaly where a value of 223 ppb Au occurs and at a location 2 km south of it where a value of 134 ppb Au occurs.

Lower gold values generally found in "B" soils may be a function of the composition of this horizon. It was found in places that the "B" horizon soil was developed in loess-like or lacustrine material, probably with a different composition than the underlying till. Better anomaly definition is generally attained where the soil has developed on till.

Gold in Till (−5 Mesh, "Total Till")

A general increase in gold occurs in the total till over the

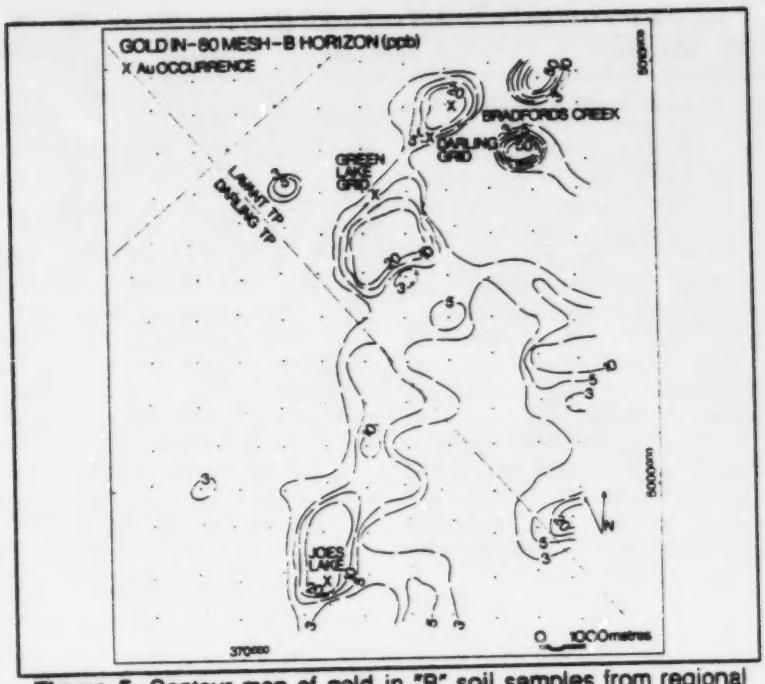

Figure 5. Contour map of gold in "B" soil samples from regional grid.

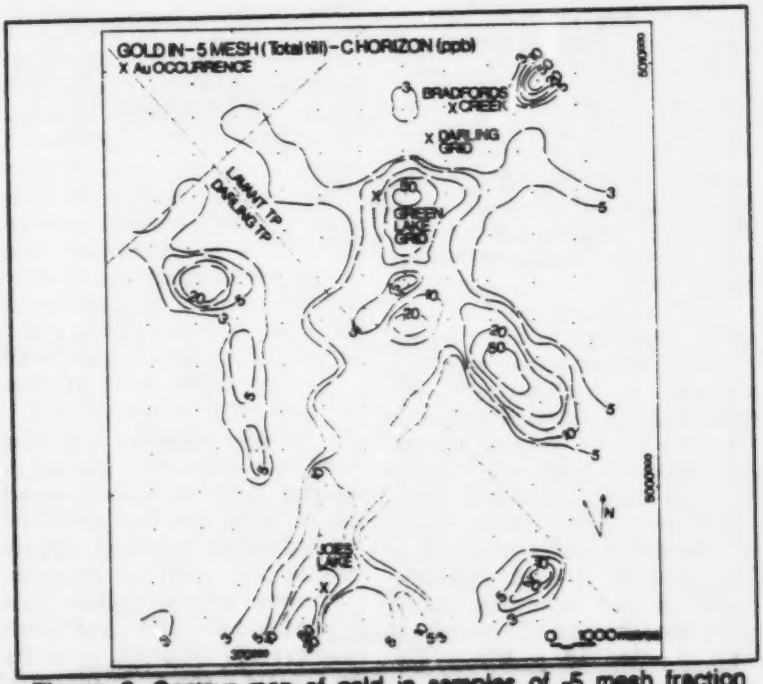

Figure 6. Contour map of gold in samples of -5 mesh fraction (total till) of parent material from regional grid.

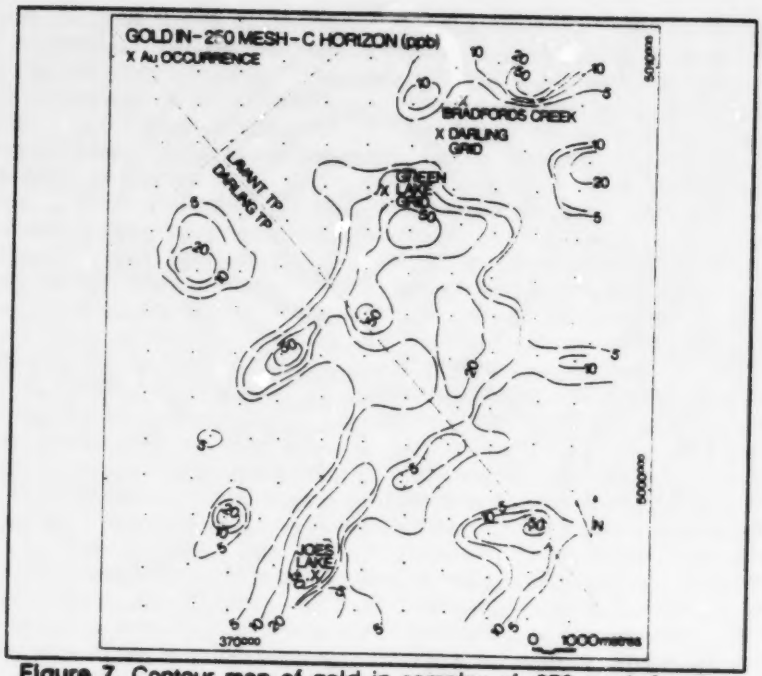

Figure 7. Contour map of gold in samples of -250 mesh fraction of parent material from regional grid.

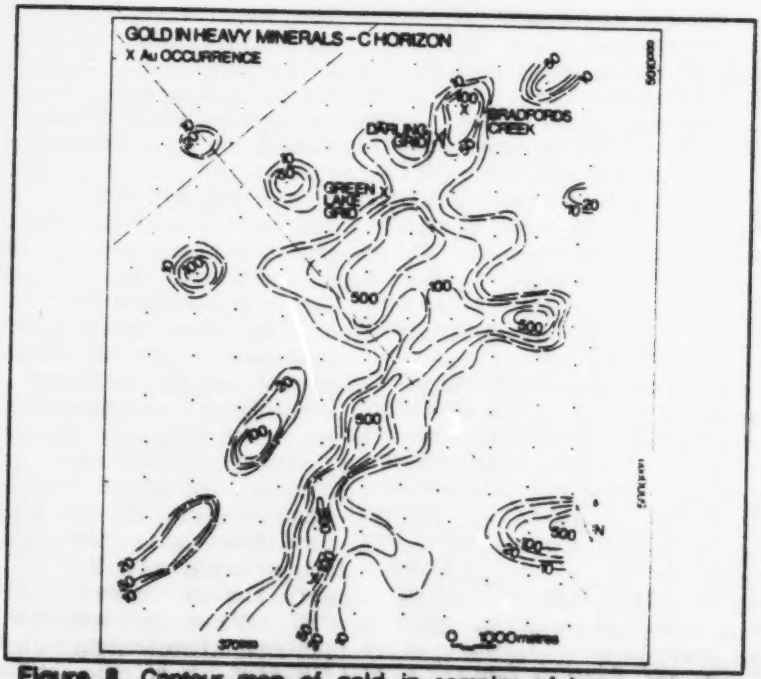

Figure 8. Contour map of gold in samples of heavy mineral separate of parent material from regional grid.

Robertson Lake Shear Zone (Figure 6) as with the humus and "B" soil samples. The trend starts at the southern edge of the project area and continues to the south of the Darling grid where it comes to an abrupt end. The presence of glaciofluvial materials in this area may account in part for this interruption. The anomaly picks up again in the northeastern corner where a value of 506 ppb Au occurs in the till. A southeast trend to the high gold values east of the Green Lake grid continues to the edge of the project area. An altered mix of gabbro-carbonate-volcanic rocks underlie this area. Another increase in gold values is apparent in the southeastern corner of the area where gabbro is present. A group of above normal gold values occurs over metasedimentary rocks in the western part of the map area for a distance of some 6 km.

Individual sites contain from 27 to 71 ppb Au near and down-ice from known gold occurrences at Joes Lake and Little Green Lake. However, the presence of many other anomalous values in areas of favorable geology would indicate more widespread gold mineralization in this area than previously delineated.

Gold in Till (−250 Mesh)

Gold in the fine fraction of the till is shown on Figure 7. The anomaly patterns in the -250 mesh fraction over the Robertson Lake Shear Zone are not markedly different from the -5 mesh anomaly patterns. However, the values in the -250 mesh fraction are higher and the anomaly contrast is more marked. A gap in the anomalous trend occurs north of the Green Lake grid. This gap is thought to be due in part to

the presence of glaciofluvial deposits in this area. In the northeastern corner of the map area, a value of 460 ppb Au occurs over metasedimentary rocks. Other increases in gold values occur along the eastern margin of the area directly east of the Darling grid where gabbro-volcanic rocks are present and 3 km southeast of the Green Lake grid (>20 ppb Au) where altered gabbro-volcanic-carbonate units are present. The trend in high values in the later feature is south of east from the Robertson Lake Shear Zone. The lobate character of the anomaly suggests a possible cross-structure for the control of the gold mineralization. In the west central sector of the area, and to the northwest of the Joes Lake showing, anomalies occur over clastic metasedimentary rocks. Also in the southwesterly trend along the Robertson Lake Shear Zone from the Green Lake grid, till (-250 mesh) over altered granite gneiss contains up to 98 ppb Au.

Gold values near and down-ice from known gold occurrences at Little Green Lake and Joes Lake range from 14 to 117 ppb Au. Many other sites with similar or higher values occur where no gold is known to occur. These sample sites are viable targets for future exploration.

Gold in Till (Heavy Minerals)

The distribution of gold in the heavy mineral fraction and for heavy minerals from all "C" horizon samples is shown on Figure 8. The dominant north-northeast trend over the Robertson Lake Shear Zone is very definitive. The trend has sharp boundaries defined by the 10 ppb contour. North of the Green Lake grid, there is more continuity to the main anomalous gold trend in the heavy mineral fraction than with the other till fractions. South of the Green Lake grid it becomes lobate to the east where the highest gold value (4358 ppb) for this suite of samples occurs. Altered gabbroic-volcanic-carbonate rocks underlie this site. This bulging of the anomalous pattern is evident on all maps (Figures 4 to 8). It suggests the presence of an auriferous cross-structure striking south of east in this area.

An increase in gold (up to 1374 ppb) occurs in the southeastern sector of the area, an area where other media show high values. The source and nature of the gold in this area is not known and will require additional studies to evaluate. Other anomalous areas of gold values outside the main gold belt include a northeasterly trending anomaly in the southwestern corner of the area. This is interesting geologically because it occurs near the Fernleigh-Clyde Fault Zone (Smith 1958) or unconformity (Moore and Thompson 1972). Gold has been found in quartz veins (Boerth prospect) on this structure some 16 km to the southwest. During this study a quartz vein containing 34 ppb Au was found along the trend of this anomaly. The underlying metasedimentary rocks show signs of alteration (chlorite, carbonate, sericite) and it should be noted that the trend continues northeast into altered gneissic granite (Addington Gneiss) along the projection of Smith's Fernleigh-Clyde Fault Zone.

Several single site gold in heavy mineral anomalies occur in the northwestern part of the area. All areas are underlain by clastic metasedimentary rocks where no gold occurrences are known. However, at one site, chalcopyrite occurs disseminated in the underlying formations and high background values for gold are present in the rocks. A pyrite deposit (Blythfield deposit) near one anomalous site contained above normal gold (31 ppb). Obviously the pyritiferous metasedimentary rocks are slightly auriferous and are probably the source of the gold in the tills of this area.

Individual gold values in proximity to the known gold showings in the Robertson Lake Shear Zone vary from 124 to 868 ppb Au. The number and extent of the anomalous gold zones found through the central part of the area would suggest the presence of a gold belt far more extensive than previously envisioned.

DISCUSSION

The lowest background value for gold from the various materials sampled is 1.5 ppb for the "B" horizon soils. This value contrasts sharply with the humus material which averages 4.2 ppb Au. The tills are more auriferous (-5 mesh with 2.2 ppb, -250 mesh with 3.4 ppb, and heavy minerals with 5.3 ppb) than the "B" soils. One reason for the low values at many locations in the "B" soils may be that the "B" soils appear to be developed in loess-like or lacustrine materials, which have quite different compositions (including gold content) and origins than the underlying till. "B" soils developed directly on auriferous tills are generally not depleted in gold. The low values of gold in "B" soils is generally not a problem when dealing with labile elements because they are transported hydromorphically from bedrock or underlying

tills and enriched in the higher exchange capacity medium of the "B" soil. However, gold bypasses the "B" soil horizon because it is mainly taken up by the root systems of the overstory vegetation and returned to the surface when the leaves fall to form the humus. This phenomena has been reported on by Gleeson and Boyle (1979) for the Duparquet area.

The regional anomalous patterns for gold from the various sample media and sample fractions are in a general way similar, although gold appears more dispersed in humus samples than in the other fractions. Most humus samples from the eastern and central part of the area contain 5 ppb or more gold. However, in detail significant differences occur between the anomaly patterns of the different sample media. For instance gold in humus does not reflect the presence of the gold mineralization defined by all other sample media south of Joes Lake at this scale of sampling. Specific bedrock sources of gold, where known gold showings occur or which are suggested by high gold values in other sampled media, are defined by relatively low gold values in humus (slightly greater than 10 ppb) in the eastern and central part of the area.

Known areas of gold mineralization are defined with the "B" soils, but anomalies in the central part of the gold belt between Joes Lake and the Lavant-Darling Township line and to the southeast of the Green Lake grid are relatively weak. Also, anomalies delineated by other sample media in the western part of the area are not defined by anomalous gold values in the "B" soils.

In the till samples the heavy mineral fraction gives the best anomaly definition and anomaly contrast for gold. The -250 mesh fraction also gives relatively good anomaly contrast, but anomaly limits are not as sharp. This might be an expected feature for glacially dispersed fine-grained gold. In some places the disperal distance for gold in the silt-clay fraction appears considerably longer than for the heavy mineral fraction. For example, near the southeastern corner of the map area the -250 mesh gold anomaly can be traced some 2 km down-ice, whereas the heavy mineral anomaly shows little down-ice dispersion. Similarly the southeastern edge of the -250 mesh anomaly associated with the Robertson Lake Shear Zone northeast of Joes Lake is smeared about 1 km farther down-ice than the heavy mineral anomaly.

The areas of known gold mineralization at the Darling showing is only well defined by the heavy minerals, but the gold mineralization at Joes Lake and Little Green Lake is defined by all till fractions. The heavy mineral fractions give the best anomaly definition for the areas between the 3 above showings. However, the multifraction gold in till anomalies throughout the Robertson Lake Shear Zone indicates that both fine- and coarse-grained gold is present in the host rocks.

The distribution patterns based on pebble counts from till samples (Gleeson *et al.* in preparation) would indicate limited down-ice movement of material. For instance, the Addington Gneiss pebbles have not been transported more than 1 km from their source area. Contacts of the major lithologies in the area can generally be defined by the pattern of pebble frequencies.

Dispersal distances for the heavy minerals are short and similar to the pebbles (i.e. in the order of 1 km) based on the distribution patterns of magnetite and other heavy minerals, such as the red garnets associated with the Lavant Gabbro Complex and chalcopyrite in the northeastern part of the area (Gleeson *et al.* in preparation). Tetrahedrite and gold have also been identified in the heavy concentrate a very short distance from the Joes Lake showing.

RESULTS OF DETAILED GRID SURVEYS

GENERAL

Detailed sampling at about 100 m centres was carried out in the vicinity of 2 known gold occurrences in Darling Township (Figure 4). Both occurrences are hosted by fine-grained dolomitic marble intercalated with mafic volcanic rocks trending northeast. Fractures in the marble are filled with quartz-carbonate stringers containing blebs and disseminated grains of tetrahedrite, chalcopyite, pyrite, and occasionally native gold. In places fine-grained sericite fills fractures in the dolomite. Both grids are underlain primarily by a blanket of relatively thin sandy till.

Thirty-six sites were sampled on the Darling grid and 43 sites on the Little Green Lake grid. Field and laboratory procedures were the same as those used in the regional study.

DATA PRESENTATION AND STATISTICS

Geochemical information on gold in all fractions for the 2

detailed areas were plotted and contoured on 1:5000 scale maps (Gleeson *et al.* in preparation). Geochemical data and all pebble and mineralogical data have been computer plotted (1:5000 scale) and these maps along with the relevant statistical parameters can be found in appendices in Gleeson *et al.* (in preparation).

By way of summary and for comparative purposes, the geometric means for gold in all sample fractions and media from regional and detailed samples are shown in Table 3. The means for gold are substantially higher for samples from the detailed areas than from the regional survey. The averages for gold in the -5 mesh and -250 mesh till fractions are about the same for both detailed areas. Gold is slightly higher in the heavy mineral fraction from the Little Green Lake grid than the Darling grid. Gold in the humus and "B" soils from the Darling grid is higher on the average than gold in the humus and "B" soils from the Little Green Lake grid.

TABLE 3: AVERAGE GOLD CONTENT OF SURFICIAL MATERIALS FOR REGIONAL AND DETAILED AREAS

SAMPLE TYPE	GEOMETRIC MEANS FOR GOLD (ppb) REGIONAL	DARLING	LITTLE GREEN LAKE
Humus	4.2	15.3	8.8
"B" soils	1.5	8.2	6.4
-5 mesh(till)	2.2	13.0	13.0
-250 mesh(till)	3.4	20.5	22.3
Heavy Minerals(till)	5.3	81.7	105.6

DARLING GRID RESULTS

General

Gold in all sample types and fractions effectively define the site of known gold mineralization (Figures 9 and 10). Maximum gold values over the zone for each sample type are as follows: humus, 1795 ppb; "B" soil, 540 ppb; -5 mesh till, 373 ppb; -250 mesh till, 676 ppb; and heavy minerals in till, 5360 ppb. Values drop off very quickly down-ice; even in the heavy mineral samples gold drops to 14 ppb 150 m down-ice from the gold occurrence. All maps show second and third anomalous zones about 360 m and 570 m respectively

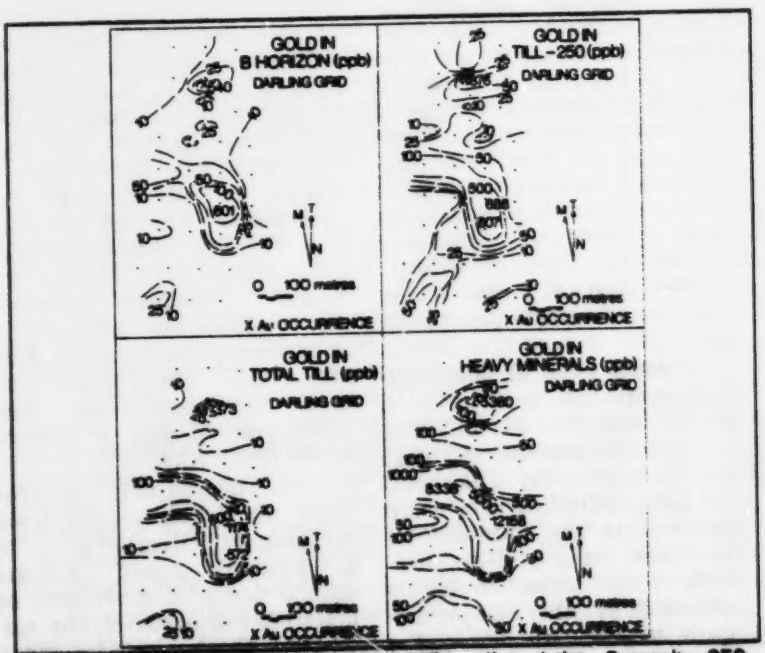

Figure 9. Contour maps of gold in "B" soil and the -5 mesh, -250 mesh, and heavy mineral fraction of till from the Darling grid.

south of the known gold showing. Gold values over the former are very high: humus, 30 to 516 ppb; "B" soils, 20 to 601 ppb; -5 mesh till, 18 to 1174 ppb; -250 mesh till, 72 to 807 ppb; and heavy minerals in till, 617 to 12 158 ppb. Tetrahedrite float has been identified (Campbell 1969) along the northern side of the anomaly. The third anomalous zone occurs at the southern limit of the sampled grid and encloses the following gold values: humus, 38 ppb; "B" soil, 31 ppb; -5 mesh till, 39 ppb; -250 mesh till, 92 ppb; and heavy minerals in till, 52 to 366 ppb.

All these gold values are very high and in marked contrast to the regional results from this area. The only regionally sampled media that provided positive results near the Darling grid were the heavy minerals. The Darling grid is located between one regional site to the east, which is in glaciofluvial material, and one to the west, which is outside of the gold belt. This might explain the lack of anomalous results for other sample media from nearby sites. However, anomalous trends to the south in other sample media could be projected over the Darling grid. Hence in following up regional gold anomalies in any sample media attention should be given to the extent and trend of the interpreted anomalies as well as to the gold values at specific sample sites.

Discussion

The detailed geochemical study over, and in the vicinity of, the Darling gold occurrence shows that at 100 m centres all sample media and fractions effectively define the known gold mineralization and outline 2 significantly anomalous gold zones to the south. The heavy mineral fraction gives the best anomaly definition and contrast.

From a study of the pebbles and the mineralogy of the heavy mineral concentrates, minimal down-ice transport of materials is indicated, probably not more than 50 m (Gleeson *et al.* in preparation). The rather rapid down-ice decrease in gold values, over a distance of 100 to 150 m, to near regional background values in all till fractions from the known gold showing and a central anomalous belt also suggests that down-ice transport of materials is confined to short distances. Glacial smearing seems most prevalent in the -250 mesh fraction (Figure 9).

The best heavy mineral indicators for gold at the Darling showing are pyrite, hematite, and sericite (Gleeson *et al.* in preparation). Barite may also be an indicator as it can be found in appreciable quantities near the known gold occurrence and over the gold anomaly at the southern end of the grid. Dolomitic float containing tetrahedrite is associated with the central anomaly and a grain of angular native gold was identified in a sample from the central anomalous belt. The central anomaly would appear to be underlain by dolomite and carbonatized mafic volcanic rocks intruded by gabbro.

LITTLE GREEN LAKE GRID RESULTS

General

The Little Green Lake gold occurrence is not marked by large or intense geochemical gold anomalies in the surficial materials, although it sits on the northern flank of gold anomalies in all sample media (Figures 10 and 11). Hence such a small gold occurrence is not pinpointed at 100 m centres. However Robertson and Gleeson (1980) found large values (up to 2440 ppb Au and 225 ppb Au in humus and "B" soils respectively) immediately over the trenched showing at a more detailed scale of sampling (Gleeson *et al.* in preparation). The humus anomaly from this study, albeit weak, is lobated to the northeast and coincides with the trend of the rocks here. This trend is also evident in the gold results from the till.

Much stronger and more extensive anomalies in all sampled materials trend west-northwest across the central portion of the grid. The anomalous zone is some 100 m wide, 500 m long, and is open to the west and east. The range of gold values enclosed by this anomalous zone are as follows: humus, 10 to 518 ppb; "B" soil, 14 to 113 ppb; -5 mesh (till), 17 to 174 ppb; -250 mesh (till), 35 to 231 ppb; and heavy minerals (till), 52 to 3448 ppb. At the southeastern end of the grid the gold anomalies have a northeasterly trend. Gold values to be found here range as follows: humus, 17 to 35 ppb; "B" soils, 22 to 40 ppb; -5 mesh (till), 32 to 63 ppb; -250 mesh (till), 38 to 80 ppb; and heavy minerals (till), 80 to 1071 ppb. In general, "B" soil anomalies are weaker than those of the humus and till.

The results would suggest that gold in this area is controlled by northwesterly and northeasterly structures. This is compatible with the gold trends found in the regional study. The magnitude and extent of the gold anomalies further suggest that gold mineral-

ization is more extensive in the Little Green Lake area than previously known. The results also indicate that gold mineralization is confined not only to the dolomite but also is found in the underlying mafic volcanic, and possibly gabbroic rocks (Gleeson *et al.* in preparation). All sample fractions and media are effective in defining areas of above normal gold at 100 m centres, although to determine the exact directions of gold lineaments will require more detailed sampling.

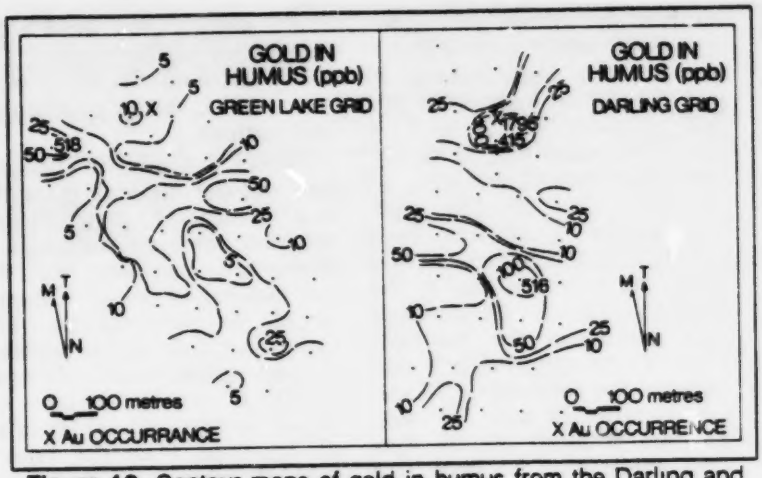

Figure 10. Contour maps of gold in humus from the Darling and Green Lake grids.

Discussion

Geochemical results for gold from the Little Green Lake grid show a low intensity humus (6 ppb) anomaly and somewhat higher gold values in the "B" soil (43 ppb), -5 mesh till (26 ppb), -250 mesh till (101 ppb), and heavy mineral till (770 ppb) fractions 60 m down-ice from the known gold occurrence. At the next site some 100 m down-ice from the above, the following gold values were obtained: humus, 33 ppb; "B" soil, 2 ppb; -5 mesh till, 2 ppb; -250 mesh till, 2 ppb; and heavy minerals in till, 18 ppb. Hence it would seem that the glaciogenetic gold anomaly terminates 100 m or less down-ice from this small gold occurrence.

Pebble lithologies are of little help in defining or understanding controls for gold mineralization on the grid, but heavy minerals such as pyrite, goethite-limonite, and hematite closely relate to gold mineralization (Gleeson *et al.* in preparation). Major alteration patterns can be defined by the abundances of chlorite and sericite in the heavy mineral fraction of the till. Presence of visible gold in some of the heavy concentrates adds credi-

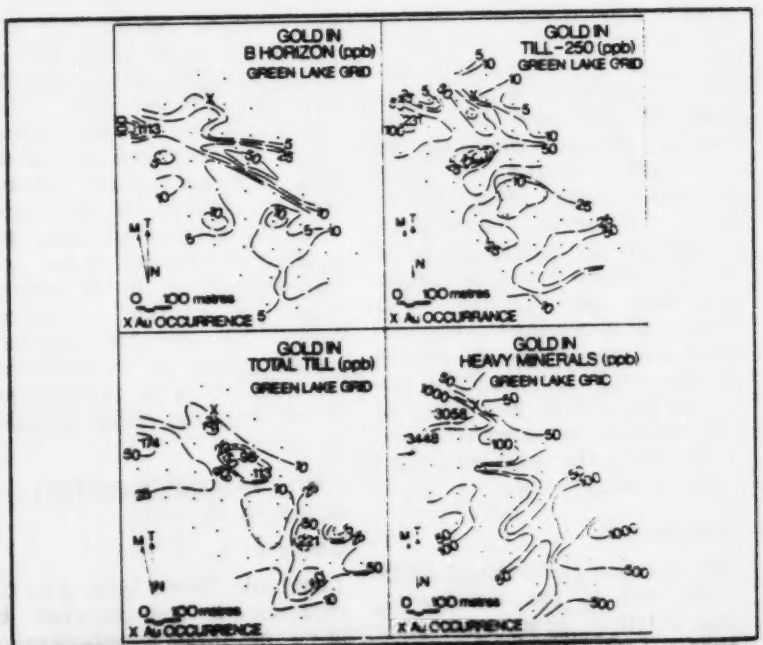

Figure 11. Contour maps of gold in "B" soil and the -5 mesh, -250 mesh, and heavy mineral fraction of till from the Green Lake grid.

bility to the heavy mineral till anomalies.

EFFECTIVENESS OF SHALLOW SAMPLING

GENERAL

Shallow sampling and analysis of surficial materials, consisted of sampling the humus, "B" soil, and 3 fractions of the parent material from test pits dug to a depth of between 0.5 and 1.0 m (the preferred parent material being till). The sampling and analysis was successful in: outlining on a regional scale the extent of major alteration and shear zones (most notably the Robertson Lake Shear Zone) that are in part known to host, and in part suspected of hosting, significant gold mineralization; delineating on a regional scale areas where highly anomalous gold values in the sampled media indicate the possibility of new gold occurrences; locating known gold occurrences and defining the trend of gold-enriched lineations on a detailed scale; and defining styles of gold mineralization and determining minerals and rock types associated with the gold. The program was successful in spite of the fact that the sampled parent material was generally oxidized ablation till, rather than lodgement till, which is the media sampled in most till sampling programs. This, of course, suggests that bedrock fragments were sheared up close to the glacier terminus and transported a short distance down-ice to where the fragments finally were deposited as a part of the ablation till. The screening of sample sites and materials in the field so as to focus on morainal deposits, be they ablation or lodgement till, and to generally avoid the sampling of other deposits (e.g. glaciofluvial, colluvial, lacustrine deposits) except where absolutely necessary, may also have contributed to the success of the program. Sampling of glaciofluvial deposits can compliment till sampling, but anomalies in glaciofluvial deposits require additional knowledge of the glaciofluvial flow patterns and present more difficulty in interpretation. This was determined by comparing the contour maps based on values from heavy minerals and -5 mesh fractions of till samples only with the contour maps where values from both the till and glaciofluvial samples are included. Changes in anomalies and anomalous patterns noted on the contour maps by inclusion of values from glaciofluvial samples suggested 2 possible interpretations: (1) the changes are caused solely by glaciofluvial transport; or (2) the changes are due to glaciofluvial erosion of gold-enriched rocks undetected by the till samples only (Gleeson *et al.* in preparation).

The basic objectives were met, not only by analysis of the absolute gold values or the gross value of the deviation from background shown by the analyzed samples at sites, but also by analysis of the relative deviation from the background shown by each sample media. For example, values of 200 ppb for a heavy mineral sample may have no more significance than 20 ppb for other sample media because the arithmetic and geometric means and the standard and logarithmic deviations of the heavy mineral population are much greater than such values for the other sample types (Table 1). This is to be expected due to the high factor of concentration involved with heavy mineral concentrates. In this program this factor varied from approximately 50 to 1000. The threshold for meaningful anomalous results is clearly much lower for most sample media than for heavy minerals (Figures 9 to 11).

Patterns obtained from contouring the gold results for each media are also meaningful. For example, in this study even though the orientations of the Robertson Lake Shear Zone and of major east-west faults were known, the patterns shown by the contours suggest that the Robertson Lake Shear Zone extends to the northern edge of the project area, that an east-west lineament crosses the central part of the area, and that both structures could host gold mineralization. The patterns generated by some of the lower value contours are also important. For example, on Figure 4 (gold in humus) a north-trending anomaly is shown by the 5 ppb contour. Even though this value is less than 1 logarithmic deviation above the geometric mean, it may outline a zone of gold mineralization. The low values could be the result of thick overburden, choice of sample sites, or some other less obvious reason.

Sampling heavy minerals has the advantage that the heavy minerals can be examined under a microscope and further mineralogical and geological data obtained. For example, in this study it was determined from examination of the heavy minerals that a depletion of amphibole or increases in chlorite, pyrite, sericite, and magnetic aggregates were indicators of gold mineralization and that 2 possible styles of gold mineraliza-

tion were probable, one related to pyrite-rich horizons in metavolcanic rocks and one related to altered dolomites (Gleeson *et al.* in preparation). Also, the presence of gold and tetrahedrite in the heavy mineral separates gave some insight into the actual nature of the gold mineralization.

The effectiveness of the different sample media and sampling intervals vary according to whether the objective is regional sampling to locate possible areas of gold mineralization and potential targets for more detailed examination or whether the objective is detailed sampling to pinpoint the location of gold mineralization. The effectiveness of sampling the different media toward these objectives within the study area during this project are discussed in the following sections.

REGIONAL SURVEYS

Results from all sampled media at 1 km centres were effective in outlining the main areas of alteration and shearing where gold mineralization is known. However, anomaly definition and contrast for the different sample types and media, and effectiveness of the different media in locating known gold occurrences varied.

The contoured results from the humus samples (Figure 4) indicate that humus is effective in defining general areas of above normal values such as the east central part of the map area in addition to outlining the general trends of gold bearing structures. However, the results did not detect all of the known gold showings, most notable the 2 showings near Joes Lake. Gold in humus is not considered the best media to utilize in regional surveys as evidence suggests that it generally reflects gold in bedrock, rather than gold in transported materials. This is a distinct advantage in detailed surveys, but not in low density regional surveys. In low density regional surveys fluvial and glacial materials may be more effective in indicating auriferous areas due to the smearing action of streams or glaciers.

Contoured results from the "B" soils (Figure 5) delineate the Robertson Lake Shear Zone. However, the anomalous patterns southeast of the Green Lake grid, which is evident on contoured maps of other sample media, result in disjointed patterns. Also, gold anomalies in the western part of the area, which are indicated in all till fractions, are absent in the "B" soils. Obviously gold does not show the same enrichment in the "B" soils as would more labile elements. "B" soils also are in some places developed in thin layers of lacustrine or loess-like materials that differ compositionally from the underlying till or glaciofluvial materials. In any case, the absence of anomalies in the "B" soils over areas of anomalous results by other media suggests that it is not the most effective media to sample for regional exploration.

For the different till fractions, the heavy mineral contour maps (Figure 8) give the best anomaly definition and contrast over the suspected mineralized belts. The heavy mineral maps also have patterns that would lead to more detailed exploration in the vicinity of all known gold occurrences (Gleeson *et al.* in preparation). On the other hand, the -5 mesh till fraction and the -250 mesh till fraction, especially the latter, seem to show more glacier smearing than the heavy mineral till fraction. This is a phenomena that has some advantage in mineral exploration through drift prospecting when searching for relatively small targets. The regional -5 mesh and -250 mesh contour maps also did not have patterns that indicate gold exploration targets in proximity to gold occurrences at Bradfords Creek on the Darling grid (Figures 6 and 7). It is difficult to evaluate whether this is simply due to the sampling interval not being adequate or to the fact that relevant sites, which lie to the south of these 2 gold occurrences, are underlain by glaciofluvial deposits containing material which for the most part is far travelled and probably relatively barren in gold. Also, some of the gold giving the anomalous values on Figures 6 and 7 south of the Green Lake grid may in part be transported gold from the area of the Darling grid and Bradfords Creek. However, if the sampling interval had been decreased to 0.5 km intervals, the Darling occurrence would have become an exploration target. This is based on the assumption that results from 2 of the sample sites from the Darling detailed grid would have been included in a 0.5 km grid.

The -5 mesh and -250 mesh fractions have the advantage of being much cheaper to collect, process, and analyze than the heavy mineral concentrates (Gleeson *et al.* in preparation). However, anomaly contrasts in -250 mesh and -5 mesh fractions will not equal those shown by the heavy mineral fraction, although similar anomaly defini-

tion could probably be achieved by the -250 mesh and -5 mesh fractions with increased sampling density. In the case of the -250 mesh fraction, the sampling density could be doubled and still not approach the cost of a heavy mineral survey (Table 6). However, one could miss indications of coarse gold mineralization by analyzing only the fine fraction. Also, useful mineralogical data would be missed by not processing the heavy minerals fraction of the till. The -5 mesh fraction might seem to be an ideal compromise in that it should contain both coarse and fine gold. However, of all 3 media, the -5 mesh fraction would be most severely affected by the nugget effect. It also shows less anomaly contrast than the -250 mesh fraction and is slightly more expensive to prepare for analysis than the -250 mesh fraction.

DETAILED SURVEYS

At the Darling occurrence, all sampled media effectively defined the known gold mineralization and indicated a second zone of gold mineralization some 300 m to the south of the known gold occurrence.

On the Little Green Lake property, the known gold occurrence is adjacent to a weak gold in humus anomaly and is a few tens of metres to the north of strong anomalies in gold values from other sample media. Previous sampling on a 100 by 50 feet (30.5 by 15 m) grid had shown that strong anomalies in gold values from humus and "B" soils occur immediately over the showing (Gleeson *et al.* in preparation). This suggests that a smaller sampling interval is required to locate gold mineralization similar in nature to the Little Green Lake occurrence. The gold in humus values on the Green Lake grid defines a number of anomalous zones, mainly an east-west linear feature in the central part of the grid and a northeast-trending feature at the southeastern end of the grid. These patterns were reflected in a general, but inexact, manner by contoured gold values from the other sample media. Differences in the contour patterns for the gold in heavy mineral and -5 mesh till fractions from the contour patterns for the gold in other media at the eastern end of the grid suggest that another factor, perhaps transportation of coarse gold, is affecting the gold values obtained in the heavy mineral and -5 mesh till fractions in this area. Comparison of the effectiveness of the different media in accurately defining mineralized zones on the Green Lake grid is difficult because of the uncertainty concerning the actual location of bedrock containing above normal contents of gold.

The study suggests that on detailed grids where the sampling intervals are 100 m or less the most cost effective medium to sample is humus. Humus is as effective as any medium in defining areas of gold mineralization and it is the cheapest medium to collect and analyze (Gleeson *et al.* in preparation). These conclusions can only be applied to areas similar to the project area.

SUMMARY AND CONCLUSIONS

The area covered by this investigation is underlain by supracrustal volcanic, volcaniclastic, calcareous, and clastic sedimentary rocks of probable late Precambrian age. The sequence has been intruded by granitic and gabbroic complexes. Bounding the western edge of the gabbro complex is a major fault zone that trends north and northeast through the area and is underlain mainly by volcanic, volcaniclastic, and carbonate rocks. Along this shear zone (Robertson Lake Shear Zone) extensive areas of chloritization, carbonatization, sericitization, silicification, and pyritization are present. Most known gold occurrences in the region are found within this structure. They are associated with quartz and quartz-carbonate filled fractures and veins in fine-grained grey dolomites intercalated with mafic volcanic and volcaniclastic rocks. The ore bearing minerals include tetrahedrite, chalcopyrite, and pyrite.

The surficial cover in the area is extensive but relatively thin. The deposits consist mainly of sandy to stoney ablation tills with lesser amounts of glaciofluvial, lacustrine, and organic deposits, mainly in the valleys. The dominant direction of ice advance was from the north, but glacial meltwater followed both southerly and southeasterly flow directions.

Regional sampling of all surficial materials (humus, "B" soils, and tills) was carried out at 1 km centres over some 180 km^2. In addition, 2 areas in the vicinity of known gold occurrences were sampled in detail at 100 m centres. All collected surficial materials (humus, "B" soil, -5 mesh fraction, -250 mesh, and heavy minerals fractions of the parent materials; the parent material was generally ablation till) were analyzed for gold, as the objective was to test the

effectiveness of the various sampled materials in defining gold exploration targets.

The regional surveys were effective in outlining the extent of the gold belt and in establishing promising targets for further exploration. Although all sample types are more or less effective on the regional scale of sampling, some are more effective than others. Gold in the heavy mineral fraction of the till gave the best anomaly definition and contrast. Gold in the -5 and -250 mesh till fractions also seemed relatively effective in providing exploration targets. Caution must be exercised when using the "B" soil horizon for gold geochemistry as this horizon frequently appears to be formed on a loess-like, lacustrine, or slope-wash material, which at best will mean different (generally lower) gold values than in the underlying parent material and at worst be ineffective in detecting underlying gold mineralization. The -250 mesh fraction is the most cost effective of the 3 till fractions to use in geochemical till sampling for gold. Sampling and analysis of the -250 mesh till fraction at 0.5 km intervals would probably result in anomaly definition equal to or better than that obtained through sampling and analysis of the heavy mineral fraction at 1 km intervals, and could be completed at less cost. However, coarse-grained gold mineralization could be missed by analyzing for gold only in the fine fraction of the till. Another advantage to using heavy mineral concentrates in regional till studies is that additional useful geological and mineralogical data can be obtained from microscopic examination of the heavy mineral separates. For instance, in this study heavy mineral separates indicated that a depletion of amphibole and increases in chlorite, pyrite, sericite, and magnetic aggregates were indicators of the presence of gold mineralization. Occasionally such minerals as tetrahedrite and gold can be seen in the heavy mineral separates. This helps to confirm the heavy mineral geochemical gold anomalies and to define the form in which gold may be present in the bedrock. The heavy mineral mineralogy is also useful in studying glacial dispersal patterns and thus assisting in interpretation of geochemical gold results. For instance, in this research program dispersal distances in the order of 1 km were determined by using such indicator minerals as magnetite from magnetite iron formation, red garnets from more felsic phases of the gabbro complex, and chalcopyrite from clastic metasedimentary rocks.

For the detailed surveys all sample types are relatively effective in reflecting known gold mineralization. In this area, use of the humus media for detailed surveys is extremely cost effective as well as technically effective.

A better understanding of the geology and mineralization and a more complete evaluation of the geochemical data within the area was obtained by mapping the bedrock geology and Quaternary deposits. For example: (1) multiple possibilities to the origin of certain geochemical anomalies were determined by delineating the extent of glaciofluvial materials and their direction of origin; (2) shearing and alteration along linear elements were mapped that coincided with linear geochemical anomalies and confirmed that gold mineralization was concentrated along these features; and (3) dispersal patterns were determined by analyzing and comparing the trend of contoured geochemical anomalies, distribution of pebbles and heavy minerals, location of different bedrock lithologies, and direction of independently determined glacial flow patterns.

Indications are that gold mineralization in the area is more widespread than previously thought. In the northern half of the area geochemical gold lineaments suggest that a complex of structural features controls the emplacement of gold in the rocks of this area. To the south, the Robertson Lake Shear Zone follows a southerly direction where it continues to be a major control for gold mineralization.

Shallow till sampling programs are not only cost effective but technically effective. They would appear to be applicable to many areas of the Canadian Shield that are covered with extensive but relatively thin glacial deposits.

ACKNOWLEDGMENTS

This project was funded by an Exploration Technology Development Fund Grant through the Ontario Geological Survey and by Lac Minerals Limited of Toronto. We wish to gratefully acknowledge the support given by these 2 organizations.

REFERENCES

Barnett, P.J., and Clark, W.S.
1980: Quaternary Geology of the Renfrew Area, Renfrew County; Ontario Geological Survey, Preliminary Map P.2365, Geological Series, scale 1:50 000.

Campbell, E.E.
1969: Report on Geology, Tetrahedrite Project, Darling Township, Ontario; Ontario Geological Survey, Assessment Files Research Office, Technical File 63-A-530.

Carter, T.R.
1981: Copper-Antimony-Gold-Silver Deposits of the Lavant-Darling Area, Southeastern Ontario: Geology, Genesis, and Metallogenetic Significance; Unpublished M.Sc. Thesis, University of Toronto.

Carter, T.R., Colvine, A.C., and Meyn, H.D.
1980: Geology of Base Metal, Precious Metal, Iron and Molybdenum Deposits in the Pembroke-Renfrew Area; Ontario Geological Survey, Mineral Deposits Circular 20, 186p. Accompanied by Preliminary Map P.2211, scale 1:126 000 or 1 inch to 2 miles.

Fransham, P.B., and Gadd, N.R.
1977: Geological and Geomorphological Controls of Landslides in Ottawa Valley, Ontario; Canadian Journal of Earth Science, Volume 14, p.531-539.

Gadd, N.R.
1980: Late-Glacial Regional Ice-flow Patterns in Eastern Ontario; Canadian Journal of Earth Science, Volume 11, p.1439-1453.

Gleeson, C.F., and Boyle, R.W.
1979: Consider Geochemistry When Seeking Gold; The Northern Miner, March 8, 1979, p.4.

Gleeson, C.F., Thomas, R.D., Paradis, S.P., and Rampton, V.N.
In Prep: Development and Adaptation of Geochemical Techniques to Gold Exploration in Glacial Drift; Ontario Geological Survey, Open File Report.

Jackson, V.A.
1980: Geologic Setting of Mylonitic Rocks in the White Mountain Area, Grenville Province, Southeastern Ontario; B.Sc. Thesis, Carleton University, Ottawa.

Lumbers, S.B.
1967: Geology and Mineral Deposits of the Bancroft-Madoc Area: Guidebook, Geology of Parts of Eastern Ontario and Western Quebec; Geological Association of Canada, 1967 Annual Meeting, Kingston, p.13-29.
1982: Summary of Metallogeny, Renfrew County Area; Ontario Geological Survey, Report 212, 58p. Accompanied by Maps 2459 to 2462, scale 1:100 000.

Moore, J.M., and Thompson, P.H.
1975: The Flinton Group, Grenville Province, Eastern Ontario, Canada; 24th International Geological Congress, Section 1, Precambrian Geology, Montreal, p.221-229.

Nikols, C.A.
1972: Geology of the Clyde Forks Mercury-Antimony-Copper Deposits, Lanark County, Ontario; M.Sc. Thesis, Queen's University, Kingston.

Pauk, L.
1983: Precambrian Geology of the Lavant Area, Frontenac and Lanark Counties; Ontario Geological Survey, Map P.2610, Geological Series - Preliminary Map, scale 1:15 840 or 1 inch to 1/4 mile.

Peach, P.A.
1958: The Geology of Darling Township and Part of Lavant Township; Ontario Department of Mines, Annual Report for 1956, Volume 65, Part 7, p.47-60. Accompanied by Map 1956-4, scale 1:63 360 or 1 inch to 1 mile.

Robertson, D.M., and Gleeson, C.F.
1980: Geochemical Orientation Survey — Green Lake Gold Property, Darling Township, Lanark Ontario; Assessment report submitted on behalf of Dungarvon Resources Limited.

Sangster, A.L.
1970: Metallogeny of Base Metal, Gold and Iron Deposits of the Grenville Province of Southeastern Ontario; Unpublished Ph.D. Thesis, Queen's University, Kingston.

Smith, B.L.
1958: Geology of the Clarendon-Dalhousie Area; Ontario Department of Mines, Annual Report for 1956, Volume 65, Part 7. Accompanied by Map 1956-4, scale 1:63 360 or 1 inch to 1 mile.

Wilson, M.E.
1920: Mineral Deposits in the Ottawa Valley; Geological Survey of Canada, Summary Report 1919, Part E, p.30E-35E.

Wolff, J.M.
1982: Geology of the Kaladar Area, Lennox and Addington and Frontenac Counties; Ontario Geological Survey, Report 215. Accompanied by Map 2432, scale 1:31 680 or 1 inch to 1/2 mile.

Wynne-Edwards, H.R.
1972: The Grenville Province; p.264-333 *in* Variations in Tectonic Styles in Canada, edited by R.A. Price and J.W. Douglas, Geological Association of Canada, Special Paper Number 11.

Grant 066 Luminescent Mineral Analyzer/Data Acquisition System

T.B. Nagel

Scintrex Limited, Concord

ABSTRACT

The phenomenon of mineral photoluminescence is known to any geologist who has used a "black light" or ultraviolet (UV) lamp. Such tests of luminescence lack specificity, are not quantitative, and cannot be made in daylight.

Utilizing a new technology, Scintrex Limited introduced the LG-2 Luminescent Mineral Analyzer (LMA) in 1982. The LG-2 is similar in principle to the geologist's black light, but a sensitive fluorescence detector replaces the human eye. A photomultiplier, coupled with signal processors, analyzes the luminescence to indicate mineral type. This lightweight handheld instrument is ideal for finding luminescent boulders or outcrops and identifying their mineralization. One of its main advantages over previous techniques is that measurements are taken in daylight.

Under the present program, with assistance provided by the Ontario Exploration Technology Development Fund (ETDF), Scintrex developed a portable, automated, microprocessor-based Borehole Logger Luminescent Mineral Analyzer. The system, called LG-3, has resulted from the integration of 2 advanced technologies, namely: a) the LG-2 Luminescent Mineral Analyzer, and b) the IGS-2 Integrated Portable Geophysical System, a field proven, microprocessor-based, low power, lightweight data acquisition and processing system.

The LG-3 borehole LMA system has been initially tailored to the determination of a specific mineral, scheelite. Later on it will be amenable to other fluorescent ore or pathfinder minerals. The initial application targeted is as a tool for grade control (drillholes under 30 m, for blasting, etc.). The critical role of the LG-3 is the initial identification and quantification of scheelite from the fluorescent returns and the storage of corrected data. The sampling and integration are under microprocessor control, which also corrects for varying hole geometries. In addition, the LG-3 borehole LMA system is capable of outputting corrected data via an RS-232C port, in a variety of forms (e.g. as tabular listings, as plots on a digital printer, or as traces on an analog recorder).

INTRODUCTION

Scintrex Limited has developed the LUMINEX method, a new exploration technique, the result of years of discoveries and development in the field of photoluminescence, which permits the direct detection and quantification of certain ore and pathfinder minerals using handheld or aerial survey instrumentation. High levels of specificity and sensitivity have been demonstrated in field tests of this new technique.

The LUMINEX method (an acronym for LUminescent MINeral EXploration) is based on time-resolved mineral luminescence created by an ultraviolet light source. It has the ability to resolve a group of key minerals which include scheelite, powellite, hydrozincite, a variety of uranyl minerals, and certain alteration minerals. Most of these are indeed difficult for a geologist to distinguish by visual examination either in outcrop or drill core. These are often characteristic of economic deposits of tungsten, zinc, molybdenum, gold, uranium, tin, and other metals. Of particular interest is the potential application of LUMINEX in mineral exploration for the detection of scheelite as a pathfinder to gold mineralization.

The relationship between scheelite and gold has long been recognized (Eardley-Wilmont 1942; Boyle 1979). The geochemical behaviour of these elements in hydrothermal systems has recently been discussed (Foster 1977). Gold mineralization is accompanied by scheelite in many of the major gold camps. In Ontario the Hollinger Mine at Timmins is the prime example having produced 56 000 tons of scheelite from 1942 to 1943. A compilation of gold production statistics (Bertini 1983), scheelite data (Little 1959), and the National Mineral Index, reveals that of the 156 past and present gold producers in the Superior province, 52 have reported scheelite (Seigel, Johnson, and Hennessy 1984).

This association of scheelite with gold is being used as an exploration tool in Australia, where residual scheelite in laterites is sought as an indicator of gold in the underlying rock.

LUMINEX PRINCIPLES

The luminescence of minerals has been known and used qualitatively in mineral exploration for many years. However, there are over 500 minerals which are known to be at least occasionally luminescent. In addition, any prospector who has used a mercury lamp at night will know that much organic matter luminesces, for example lichens and even scorpions. Just as the eye finds difficulty in resolving the luminescence of minerals from that

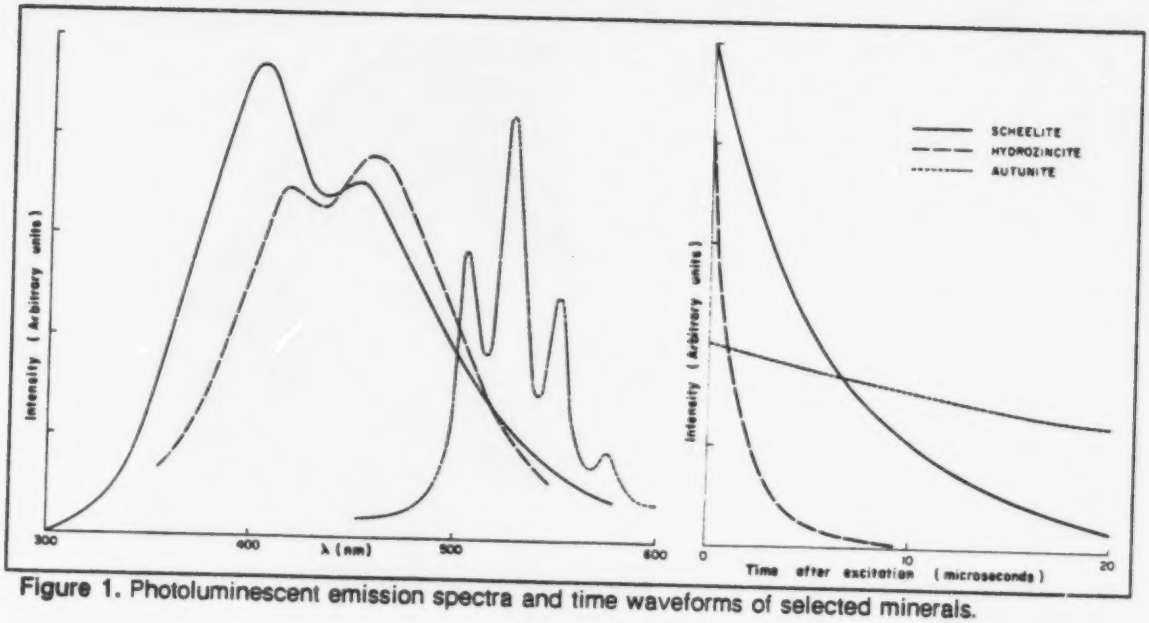

Figure 1. Photoluminescent emission spectra and time waveforms of selected minerals.

of organic materials, it also has its limitations at sorting out minerals from one another by their luminescent colours.

The luminescence of minerals can be characterized by: their excitation spectrum (the change of fluorescent intensity at a given emission wavelength as the excitation wavelength is varied); their emission spectrum (the spectral variation of intensity of the emission for a given excitation wavelength); and the lifetime of fluorescence (the time fluorescence takes to decay after the source of excitation is interrupted).

As an example of the difficulty found in sorting out minerals, Figure 1 shows the photoluminescent emission spectra of scheelite, hydrozincite, and autunite. It is clear that there is a considerable similarity in spectrum between scheelite and hydrozincite and a great deal of overlap. On the other hand, the autunite emission spectrum is clearly separated from the other two. The right hand side of Figure 1 shows the time waveform of decay of the photoluminescence of the same 3 minerals. It is apparent that the lifetimes of photoluminescence of scheelite and hydrozincite are radically different and that these 2 minerals may therefore be readily resolved through their lifetime differences even if not through their emission spectral characteristics (Seigel and Robbins 1982, 1983).

The excitation spectrum is rarely used, because of practical difficulties. On the other hand, the emission spectrum can be approximated by using filters to isolate parts of the spectrum for comparison. In the LUMINEX instruments 2 spectral channels are used, blue (400 to 450 nm) and green (500 to 550 nm), with the data being ratioed (green/blue, β).

The decay time, which for the minerals of current interest is in the region of 0.5 to 50 microseconds (10^{-6} seconds), can be estimated by observing the decaying luminescence at different times after the excitation is cut off. Again, in the LUMINEX equipment 2 time channels are used, fast and slow; by their comparison an estimate of the decay time represented by the ratio α (slow/fast) can be made.

The 2 ratios are used in a field diagram ("Mineral Index Diagram", Figure 2) in which the β value forms the abscissa, and the α value the ordinate. The identity of a mineral is obtained from its position within the diagram.

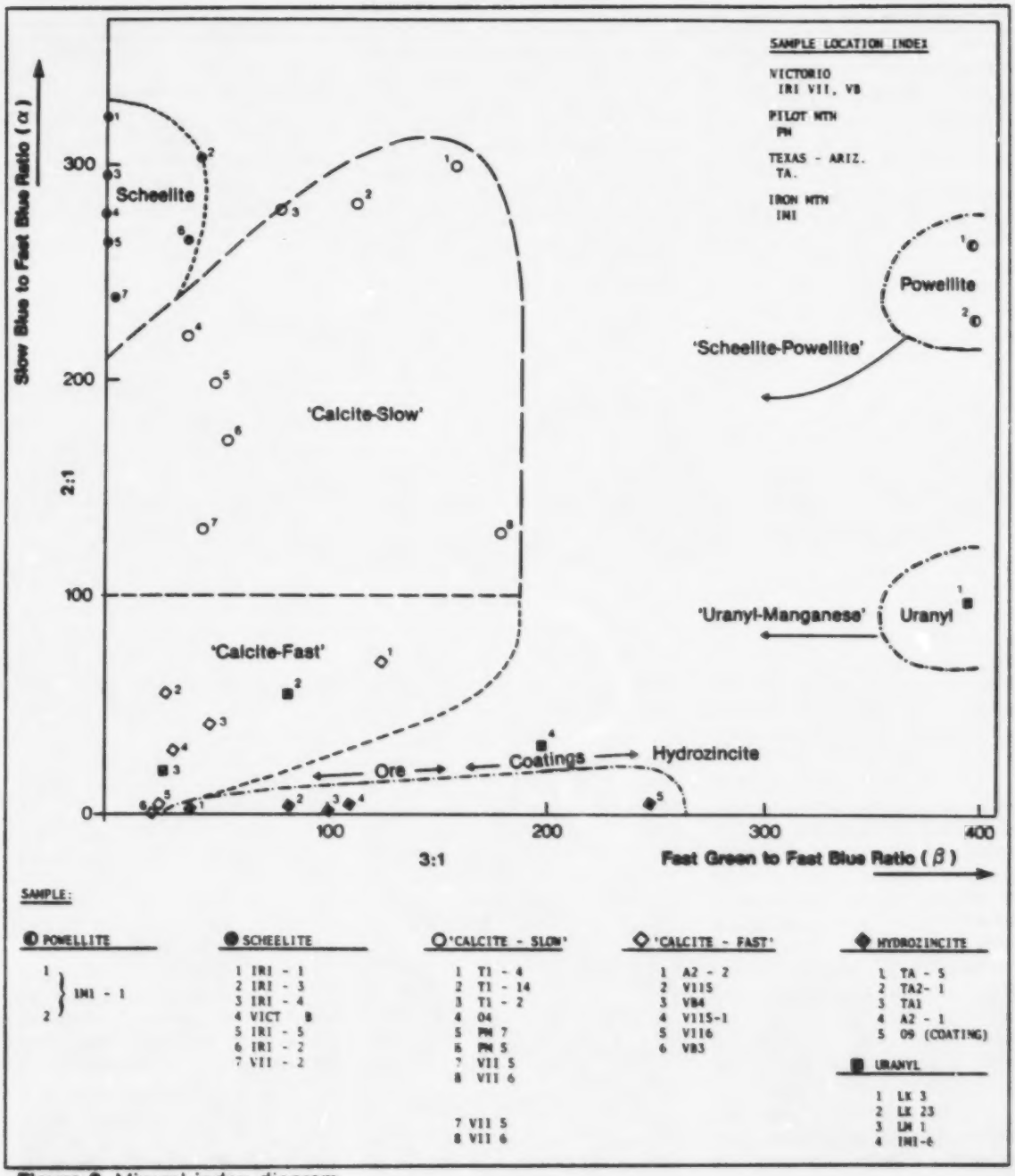

Figure 2. Mineral index diagram.

Figure 3. LG-2 handheld luminescent-mineral analyzer.

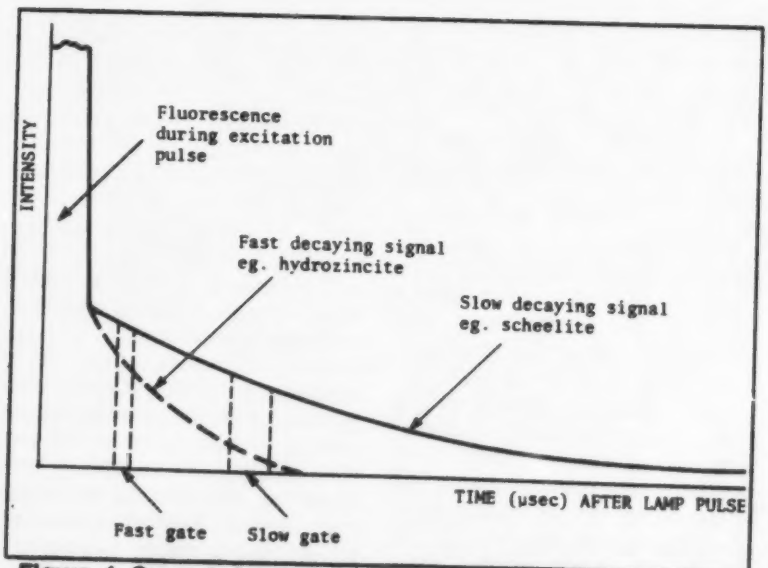

Figure 4. General shape of induced fluorescence transient pulse.

METHOD OF MEASUREMENT

In order to understand the operation of the LG-3 Borehole LMA, first a detailed analysis of the LG-2 LMA is required. The portable handheld LG-2 LMA, on which much of the LG-3 borehole instrument design is based, collects data and is used in much the same way by geologists and prospectors as they would use a gamma-ray scintillometer in uranium exploration. When the operator presses the handheld sensor against a rock, the digital readouts indicate the presence and amount of any responsive photoluminescent mineral. Figure 3 shows the LG-2 in operation.

The LG-2 is based on a modulated mercury lamp. In order to properly identify minerals, it has the capability of acquiring 2 spectral channels and 2 time channels for each spectral channel. For this purpose, the LG-2 incorporates blue and green filters and measures fast and slow responses, permitting 4 parameters (blue-fast, blue-slow, green-fast, and green-slow) to be measured. Of these 4 readings, 2 may be made simultaneously and are displayed on the handheld sensor's 2 digital displays. From the 4 readings, mineral identification can be made. For quantitative determinations of the percentage of responsive mineral by area over the 6 cm^2 field of view, calibration curves are used.

In order to understand the details of the interpretation process, the procedure of acquiring data has to be examined first. The electrical outputs from the photomultiplier are transient pulses initiated by the return of the fluorescence from the rock face. The general shape of the pulse is

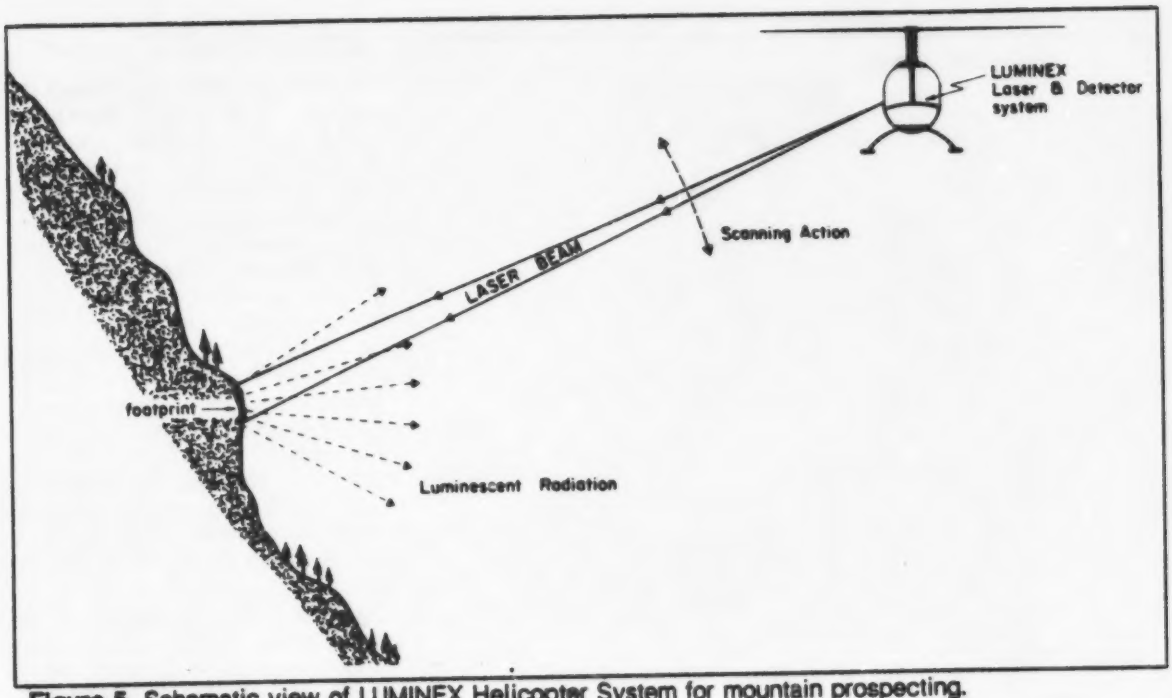

Figure 5. Schematic view of LUMINEX Helicopter System for mountain prospecting.

shown in Figure 4 and consists of a slowly decaying exponential waveform. The decay time and magnitude of this waveform are determined by the mineral type and the amount of its exposure, as illuminated by the mercury lamp. Two components of the slow decay, fast and slow, are measured for the purpose of signal processing. For every measurement cycle the following 4 quantities are displayed: blue-fast, blue-slow, followed by green-fast, green-slow.

Mineral identification is based on the 2 ratios that represent (a) the lifetime of fluorescence, and (b) the colour of fluorescence. These are calculated from the ratios of blue-slow to blue-fast, and green-fast to blue-fast. These 2 ratios can be combined in an X-Y diagram to form the "Mineral Index Diagram" shown on Figure 2. The position of the minerals and an indication of the spread within the field of different samples of a nominally similar mineral type is also shown in Figure 2.

The major identifier is the variation in fluorescence lifetimes. Emission from scheelite, powellite, and the uranyl minerals is generally slow; that from fluorite, hydrozincite, and some caliche coatings is much faster and can be readily distinguished. The colour ratio is used to spread out and resolve different minerals with similar lifetimes, although some overlap between mineral fields still exists as shown in Figure 2.

The airborne LUMINEX system operates on the same principle as the surface prospecting instrument. Figure 5 shows a schematic view of an aerial LUMINEX system mounted in a helicopter for mountain prospecting. For this purpose a high power ultraviolet laser of the excimer type is mounted in the helicopter and fires from the side of the helicopter on the mountain slopes being traversed, approximately 30 to 60 m away. Each target or "footprint" excited is only about 400 cm^2 in area. The laser fires at approximately 30 pulses per second which normally creates a footprint at about 1 m intervals along the track of the helicopter. A telescope which is optically coaxial with the laser beam detects luminescence arising from each footprint, analyzes it, and records it in 4 channels of temporal and spectral data. The limiting sensitivity of the system is approximately 0.2 to 0.5% by exposed area for most of the minerals of interest, under average sunlight conditions.

PROJECT OBJECTIVES

The target for this 1-year ETDF assisted research and development project was the production of the prototype hardware and software for a microprocessor-based borehole Luminescent Mineral Analyzer/Data Acquisition System.

The following goals were set for the LG-3 borehole LMA prototype system:

- initial design tailored to the determination of scheelite grades (future versions will accommodate other fluorescent ore or pathfinder minerals)
- initial instrument dedicated to production drilling, short holes, less than 30 m in depth (future versions to accommodate deep holes, exceeding 300 m)
- range of measurements: ±10% accuracy at 3% scheelite by weight; threshold sensitivity about 0.1% scheelite
- single colour filter (blue, optimal for scheelite)
- probe outside diameter: 35 mm; intended to work in holes from 48 mm to 152 mm diameter

System partitioning was designed in such a way as to ensure compatibility of electronic assembly with both a present downhole logger probe and eventual future surface heads. In line with this goal, the system was configured so as to bring the full luminescent decay signal in real time up to the above ground electronics console for processing. This approach minimized the electronics packaged in the downhole probe itself (where packaging constraints result in higher production costs). Therefore, the bulk of the signal processing and control circuitry was designed to be contained in the above ground package.

Another prime objective was to take maximum advantage of the versatile hardware and extensive software of the IGS-2 Data Acquisition System. The heart of this system is the NSC800 CMOS microprocessor, memory (EPROM and RAM), and peripheral electronics which permit a geophysical operator to perform a number of functions:

- control a variety of sensors via a LCD display and a multifunction keyboard
- Record data in solid-state memory at the push of a button
- play back, calculate, list and/or plot data on a digital printer at the end of the survey

Alone, the IGS-2 console is an electronic notebook into which geophysical, geological, or other data can be entered via a keyboard. Specially designed IGS-2 sensor options can be added, which permits the IGS-2 to become a magnetometer, a VLF receiver, etc. (Figure 6).

Scintrex developed the IGS-2 as a universal building block with a unique "geophysical buss" which is the core of a variety of geophysical instruments. Thus, the LG-3 borehole LMA is an IGS-2 with a module inserted in its card cage, and LMA application-specific software in its programmable read only memory (EPROM). All of the geophysical instruments which have the IGS-2 as their core electronics share this common characteristic: their EPROM memory contains all of the general purpose data acquisition and processing software routines required to make the IGS-2 an operational instrument. In addition, they also contain application-specific software which customizes the instrument to the specific application. The IGS-2 interfaces to the user via a 14 push-button keyboard which comprises only numbers and easily understood commands. A 32 character LCD display spells out messages unambiguously, in plain language, which makes the IGS-2 an instrument very easy to master.

DEVELOPMENT OF THE LG-3

The following tasks were required in order to convert the LG-2 LMA from a surface prospecting instrument into a borehole LMA and integrate it into the IGS-2 system:

1. Redesign the LG-2 control modules (2 printed circuit boards), presently housed in the belt mounted unit. The present medium scale integration control logic was converted to microprocessor control and interfaced to the IGS-2 CPU module via its "Geophysical Buss".
2. All components of the LG-2 now housed in the belt mounted unit (control modules, battery pack, power supplies, etc.) were integrated into the IGS-2 console. IGS-2 power supplies were expanded to accommodate the LG-2 electronic's requirements.
3. The LG-2 handheld sensor and electronics were redesigned into a borehole probe. This step required mechanical, optical, electronics, and packaging design. This was possibly the most difficult and time-consuming part of this project.

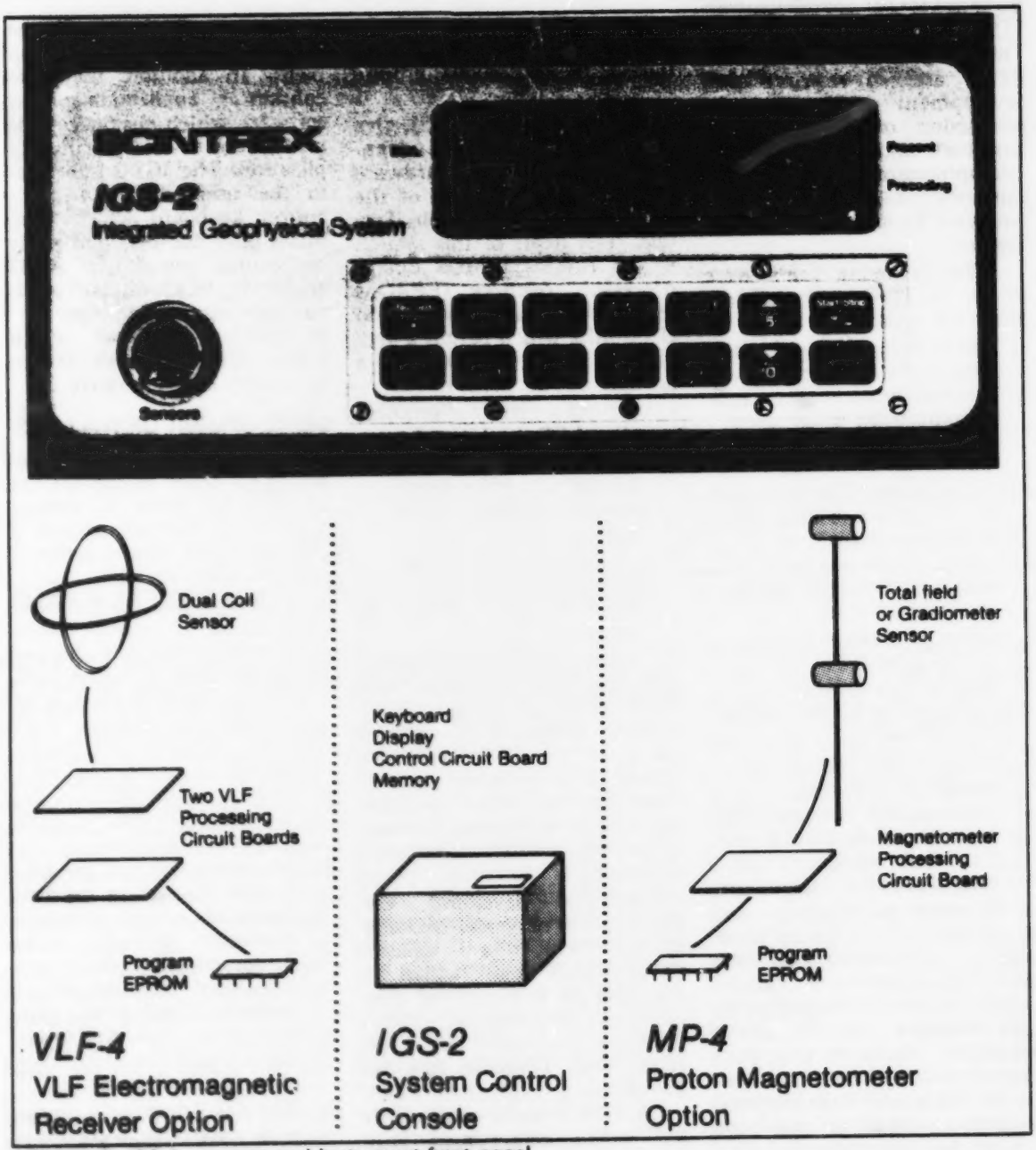

Figure 6. IGS-2 concept and instrument front panel.

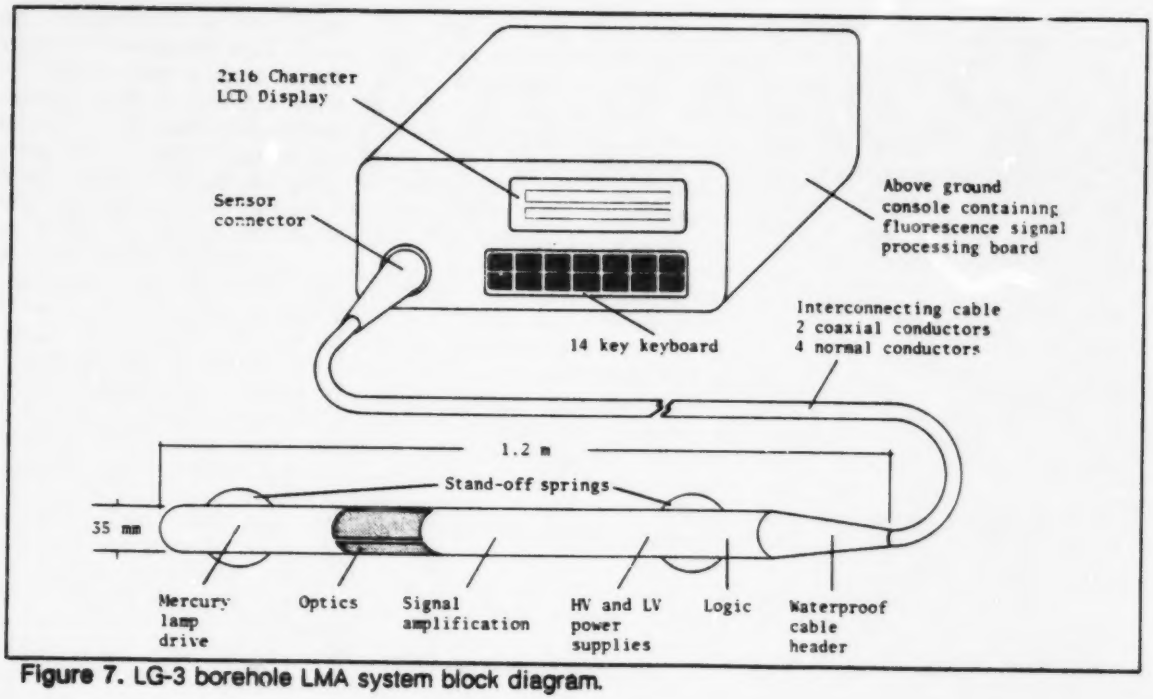

Figure 7. LG-3 borehole LMA system block diagram.

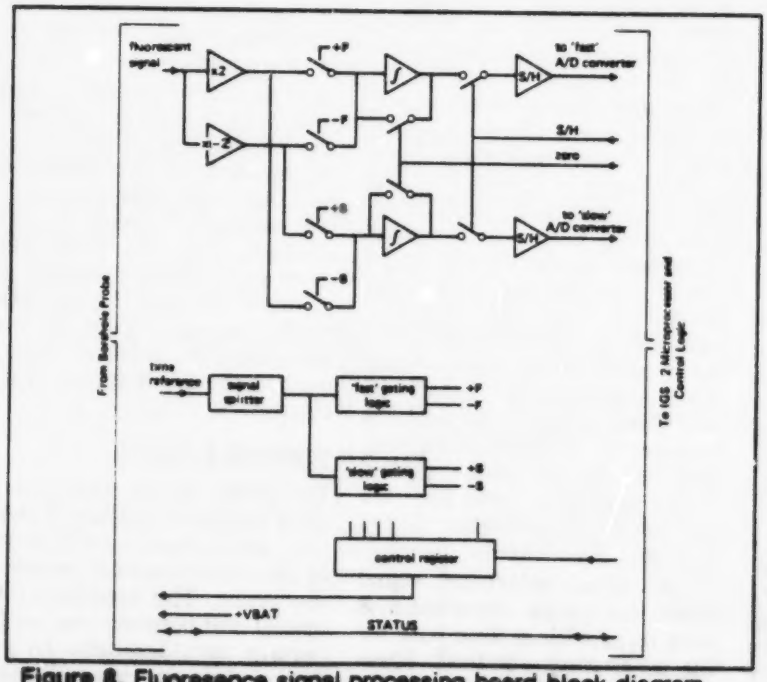

Figure 8. Fluoresence signal processing board block diagram.

4. Software development;
   a) automation of the measurement cycle under IGS-2 control
   b) control of the measurement cycle duration
   c) data formatting for storage in solid-state memory
   d) data display, as well as user messages for interactive operation of keyboard and display

LG–3 HARDWARE OVERVIEW

The LG-3 borehole LMA consists of 2 main components: the above ground control console, and the borehole probe and its interconnecting cable. Figure 7 is a pictorial describing these components.

CONSOLE

The LG-3 console provides the operator interface, the control, data storage and output func-

tions, and the fluorescence signal processing circuitry.

The operator interface, via the keyboard and the LCD display, shares the unique feature of all IGS-2 based instruments: all data and messages to the user are spelled out unambiguously in 2 lines of 16 characters each. Every keystroke generates an "echo" from the display providing immediate user feedback. Menu type displays prompt the operator for suitable inputs, allowing scrolling to the desired menu items. The keyboard is the dual function type, allowing either numerical entry with decimal point, or direct access to a particular menu item.

A 5 slot backplane in the console contains the control microprocessor/peripheral electronics board, 1 or 2 file and program memory boards, and the fluorescence signal processing board. Ample memory expansion capacity is provided: a single memory board configuration allows up to 64 Kbytes of file memory, while a 2 memory board system can accommodate 192 Kbytes. The standard LG-3 is supplied with 16 Kbytes of file memory.

The hardware development effort, as related to the aboveground control console, concentrated on the fluorescence signal processing electronics. A detailed description of this subsystem follows.

The multitude of signals expected from a target under test require circuitry to discriminate between "very fast", "fast", "slow", and "very slow" fluorescence returns. One possible error of a "very slow" return is a DC offset signal caused by small light leaks into the detection area. "Very fast" fluorescences have time constants of fractions of a microsecond, thus mostly fall out due to the delay and window width employed. The term "fast" is used for delays of about 1 to 2 microseconds. To capture these, the first measuring window is placed 1 microsecond after the excitation source is turned off. For the "slow" return the delay and window width are set to 7 microseconds, in order to give maximum response to delays in this time range.

All of the analog signal processing contained in the console is implemented in the fluorescence signal processing board. The block diagram of this subsystem is shown in Figure 8.

Some of the design constraints were caused by the limited number of pins available for interconnections. The downhole probe cable has bidirectional multiplexing of some signals, due to a desire to keep it as simple as possible, as well as to satisfy the pin-out of the standard IGS-2 sensor connector. The compact size of the instrument limits the number of possible backplane interconnections. Therefore, all IGS-2 sensor electronics communicate with the microprocessor control board via a 2-line serial input/output (I/O). A 33 bit serial-in, parallel-out control shift register is used in the fluorescence signal processing board to download commands such as change of detector sensitivity and control of probe power. This approach permits the control of 33 different events with just 2 I/O lines.

A time reference signal from the probe electronics is used to provide a time base for the measuring windows. Identical coaxial cables are employed, both for the time reference and the fluorescence signal. This approach assures equal propagation delays for both signals, thereby making the system less dependent on the actual length of the probe cable. A signal splitter circuit separates the combined time reference signal, carried by one of the coaxial cables, into the fast and slow control signals. These in turn actuate 4 switches which connect the integrators' input to the normal or inverted fluorescence signal. One integrator each is used for the fast and slow channel. Once a second, each integrator output is sampled by the sample and hold (S/H) circuits. The S/H outputs are converted by the analog to digital converters (located on the microprocessor and control board) into digital data. Following the sampling of the integrators' output by the S/H circuitry, the integrators are briefly reset by the "zero" command which gets them ready for the next measurement.

The fluorescence signal processing board is resident in one of the sensor option electronics slots of the IGS-2 console. As is the case with any of the multiple sensor options available for this instrument, there is no need to modify the standard console in any way, either mechanically or electronically, in order to accommodate the LG-3 sensor option electronics.

BOREHOLE PROBE

The probe design utilizes a coaxial approach. Figure 9 shows the mechanical arrangement of the electro-optical section of the probe. The spacing of the optical components was an important consideration. In general, a close spacing will maximize the fluorescent radiation intercepted by the photomul-

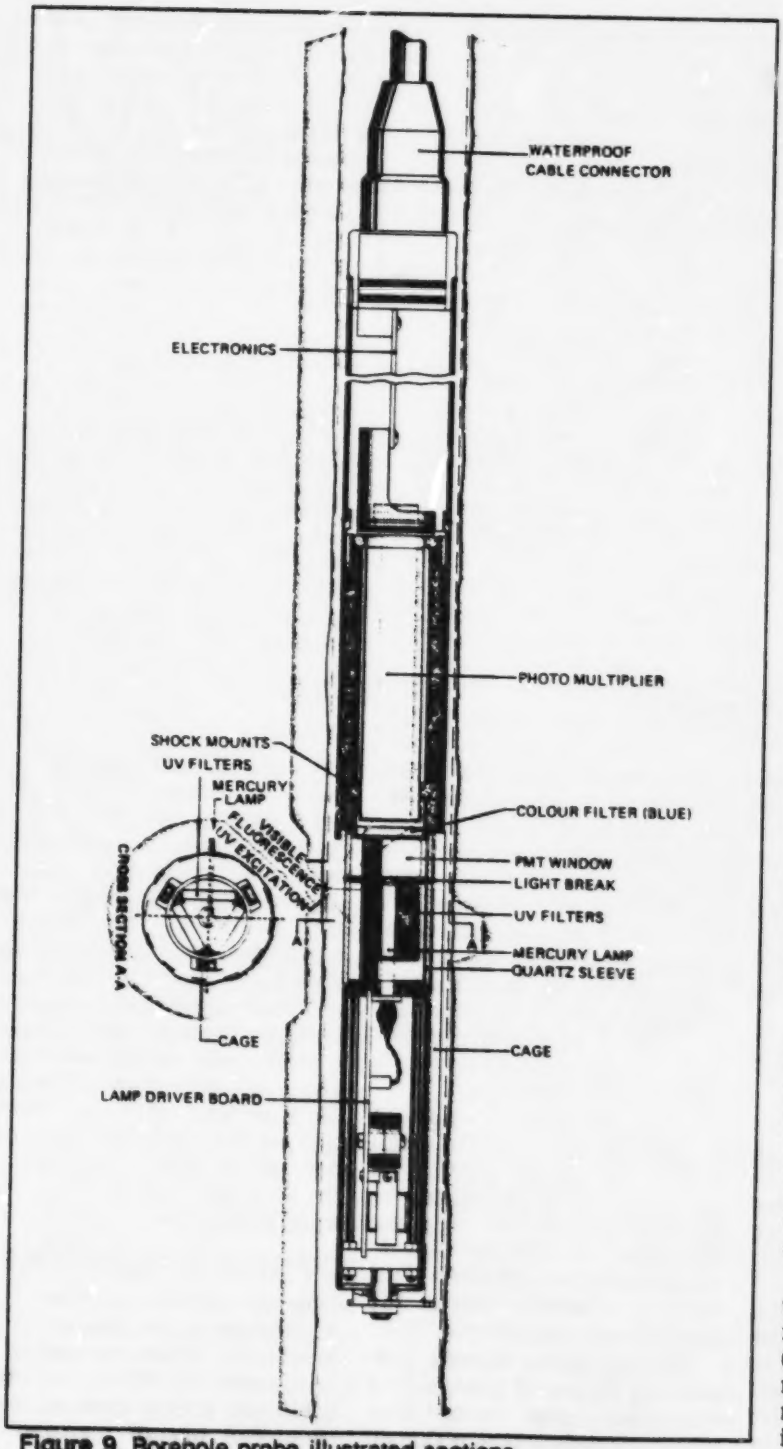

Figure 9. Borehole probe illustrated sections.

tiplier tube (PMT). The need to place a screen between the source and the detector introduces some masking of light emitted by the lamp, but more critically, it significantly masks the central portion of the photocathode. The final geometry was arrived at upon testing a number of different possibilities. To this effect, a computer simulation program was written to evaluate all of the various interacting elements' sizes and positioning. The fixed parameters were the PMT diameter and lamp length. The spacing between the photocathode and screen(s), the radius of the screen(s), and the diameter of the borehole were the variables tested.

One of the problems that had to be solved was how to keep direct light from the lamp from striking the photosensitive area of the PMT, thus severely overloading the system. At the same time care had to be taken to maximize the transparent window area while keeping the structure of the probe strong enough to withstand the pressure in a 30 m hole, in some cases filled with water.

The initial plan called for a cylindrical excitation filter. This was replaced by 3 flat filters arranged in triangular formation around the lamp. The reason for this approach is that ultraviolet filter glass appears to be unavailable in any other form than in flat stock of varying thicknesses.

Two emission filters are used in series. The first section is a blue transmitting glass (Schott BG25), the peak transmission of which corresponds reasonably well with the peak in emission spectrum of scheelite. This filter has appre-

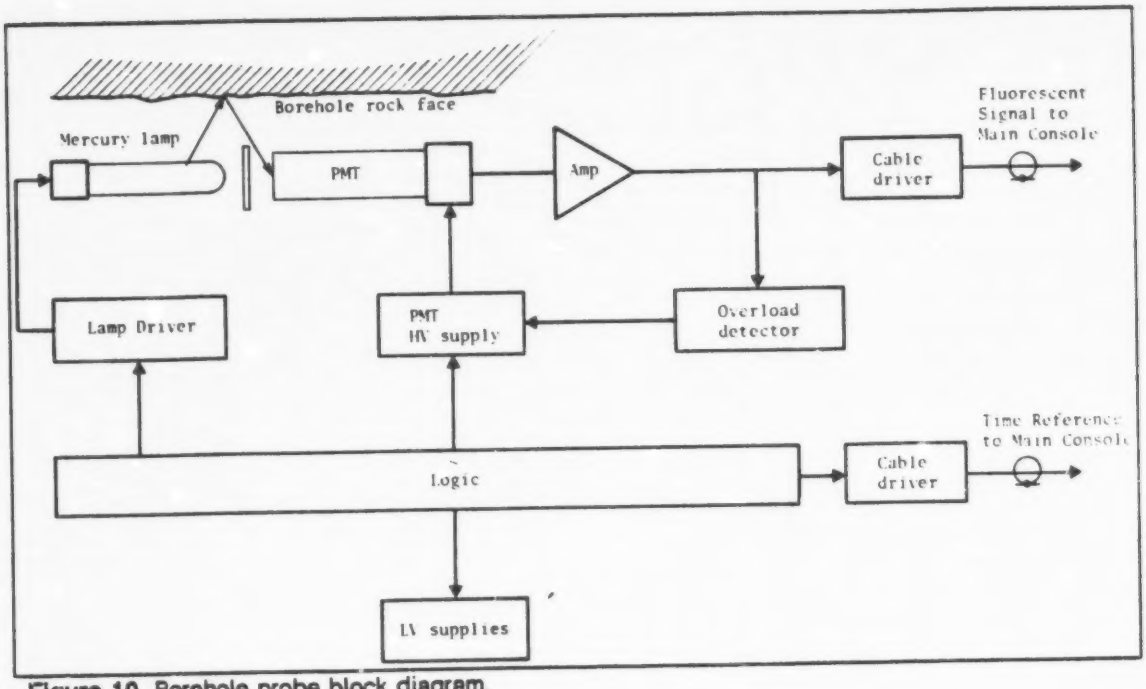

Figure 10. Borehole probe block diagram.

ciable transmission in the middle ultraviolet and permits significant amounts of 365 nm lamp emission to reach the photocathode. It is therefore necessary to augment the blue filter with a sharp cutoff filter (Schott GG400) which attenuates very strongly below about 400 nm. This second filter is strongly fluorescent and it is important that it is behind and not in front of the blue filter.

The dimensions of the probe are such that it can be used in a wide range of hole diameters, the smallest being 48 mm. For larger diameter holes provision was made for stand-off springs (3 at 120°) which will properly position the probe in the centre of the hole for holes up to 152 mm in diameter. The probe itself measures 35 mm in diameter and approximately 1.2 m in length.

Figure 10 shows the block diagram of the borehole probe. The logic controls the various elements such as the mercury lamp drive and the high voltage (HV) supply. Bipolar HV pulses of 2 microsecond duration each are applied to the lamp every 20 microseconds during the "fast" drive period. The "slow" excitation consists of a 40 microsecond burst of bipolar drive pulses.

The operating voltage of the PMT is approximately 600 V DC. All power supplies in the probe are synchronized by the logic in order to keep the inevitable interference outside of the sampling windows. This noise is primarily due to the long ground conductors.

The amplifier (AMP) indicated in Figure 10 is actually a current-to-voltage converter which transforms the small PMT current pulses into voltage pulses. The DC output of the AMP is monitored by the overload detector. Excessive light entering the PMT results in an increased amplifier DC output which in turn triggers the overload protection which acts by turning the PMT HV supply off, thus protecting the PMT.

The amplified signal is buffered by the cable driver which sends the signal to the above ground console. Particular care was taken in the design of the cable driver in order not to alter the shape of the detected signal pulse due to reflections in the cable.

CONSOLE TO PROBE CABLE

The current version of the LG-3 borehole LMA uses a 30 m long cable which consists of 2 conductors of RG-122 coaxial cable and 4 individual conductors. The overall diameter is approximately 11 mm. The cable has equally spaced markers

which are used to signal to the operator the length of cable being withdrawn in a given time period. In other words, the markings on the cable are used in conjunction with timing signals produced by the console, thus, they provide a "pacer" to the operator in order to ensure constant probe travel speed while it is being withdrawn.

LG–3 SOFTWARE OVERVIEW

As indicated earlier, the LG-3 is an IGS-2 Data Acquisition System with a borehole LMA sensor option. The software controlling the LG-3 can be divided into 2 categories: application-specific (borehole LMA option), and IGS-2 general purpose data acquisition and processing software. The following sections describe both of these.

LG–3 SOFTWARE FUNCTIONS

The application-specific software for the borehole LMA, which runs under control of the IGS-2 operating system, was entirely developed under this project. The major tasks have already been listed under Project Objectives. The functions of the application-specific software, from the operator's perspective, are described below:

1. The sequencing program ensures that proper time is allowed for the PMT to warm-up when the instrument is turned ON for the first time, or when left OFF for a while. It directs the logic to delay any further operation for 2 minutes, while it displays a message to the user indicating that the instrument is in the warm-up mode.
2. When the instrument is in the set-up mode, the user can use the keyboard to enter or change any parameter, such as sensitivity, line (borehole number), date, "pacer rate", etc.
3. The program that controls measurement cycle duration accepts user-entered "pacer rates" in the range of 0 to 99 seconds. Each measurement cycle requires the operator to pull the probe a predetermined length (as marked on the cable). The objective is to pull at a constant rate, so that the probe can sample luminescence of the rock face over equal distance intervals. The console warns the operator that a measurement cycle is complete, by either flashing a light, or by sounding a buzzer/horn (depending on the option installed).
4. The filing program stores data or parameters in the format suitable for borehole operation. The present version of this instrument has the following format:

   a) DATA 0: slow decaying luminescence (range 0-999)

   b) DATA 1: sensitivity (high or low)

   c) DATA 2: depth (range 0-9999)

   Provision was made to accomodate possible future requirements:

   d) DATA 3: fast decaying luminescence (range 0-999)

   e) DATA 4: filter colour (blue or green)
5. The formatting programs provide data listings or profile plots of the luminescent data stored in the file memory. Figures 11 and 12 show examples of these outputs.

IGS SOFTWARE FUNCTIONS

The software functions of the IGS-2 which are pertinent to the operation of the borehole LMA are:

- a built in operating system which controls all instrument operations
- interfaces to the user via keyboard input processor programs and LCD display output processor programs
- for general purpose applications, a program which records header information, observed values, station number, line number, and time for each observation. When some of these are not required by a given option, the application-specific software provides the required customization. For example, in the case of the borehole LMA sensor option, the station number is equivalent to the depth of the borehole probe, the line number is equivalent to a borehole number (borehole ID), and time is not recorded automatically at each measurement. In the latter case, the operator has the option to manually select and record time (see below)
- in addition to automatically recorded measurement values, a program which allows manual entry of ancillary data. Such data is entered under the "information" header, and can consist of up to 8 blocks and up to 5 digits signed decimal numbers. Time (hours, minutes, and seconds) can also be recorded as ancillary data.
- a program which allows data recall. By keystroke

SCINTREX V1.3 *** LUMINESCENT MINERAL ANALYZER *** Ser No: 817096.
Correction factor: 1. Sensitivity(S): H=High L=Low Operator: 1.
Line: 0. Grid: 0. Job: 5. Date: 84/05/20

S	Station	Data	Change	Information
L	0.	0		09:04:06 B: 50. C: 40. D: 40. E: 50. F: 30. G: 40. H: 50.
L	10.	5	5	
L	20.	10	5	
L	30.	15	5	
L	40.	22	7	
L	50.	27	5	
L	60.	34	7	09:04:25 B: 50. C: 40. D: 30. E: 20. F: 20. G: 5. H: 0.
L	70.	40	6	
L	80.	47	7	
L	90.	54	7	
L	100.	63	9	
L	110.	73	10	
L	120.	76	3	09:05:37 B: 50. C: 50. D: 50. E: 40. F: 60. H: 0.
L	130.	86	10	
L	140.	95	9	
L	150.	101	6	
L	160.	102	1	
L	170.	100	-2	
L	180.	97	-3	09:06:39 B: 80. C: 40. D: 50. E: 50. F: 0. G: 0. H: 50.
L	190.	92	-5	
L	200.	83	-9	
L	210.	74	-9	
L	220.	66	-8	
L	230.	57	-9	
L	240.	57	0	
L	250.	54	-3	
L	260.	48	-6	
L	270.	44	-4	
L	280.	46	2	
L	290.	49	3	

Figure 11. Example of LG-3 data listing.

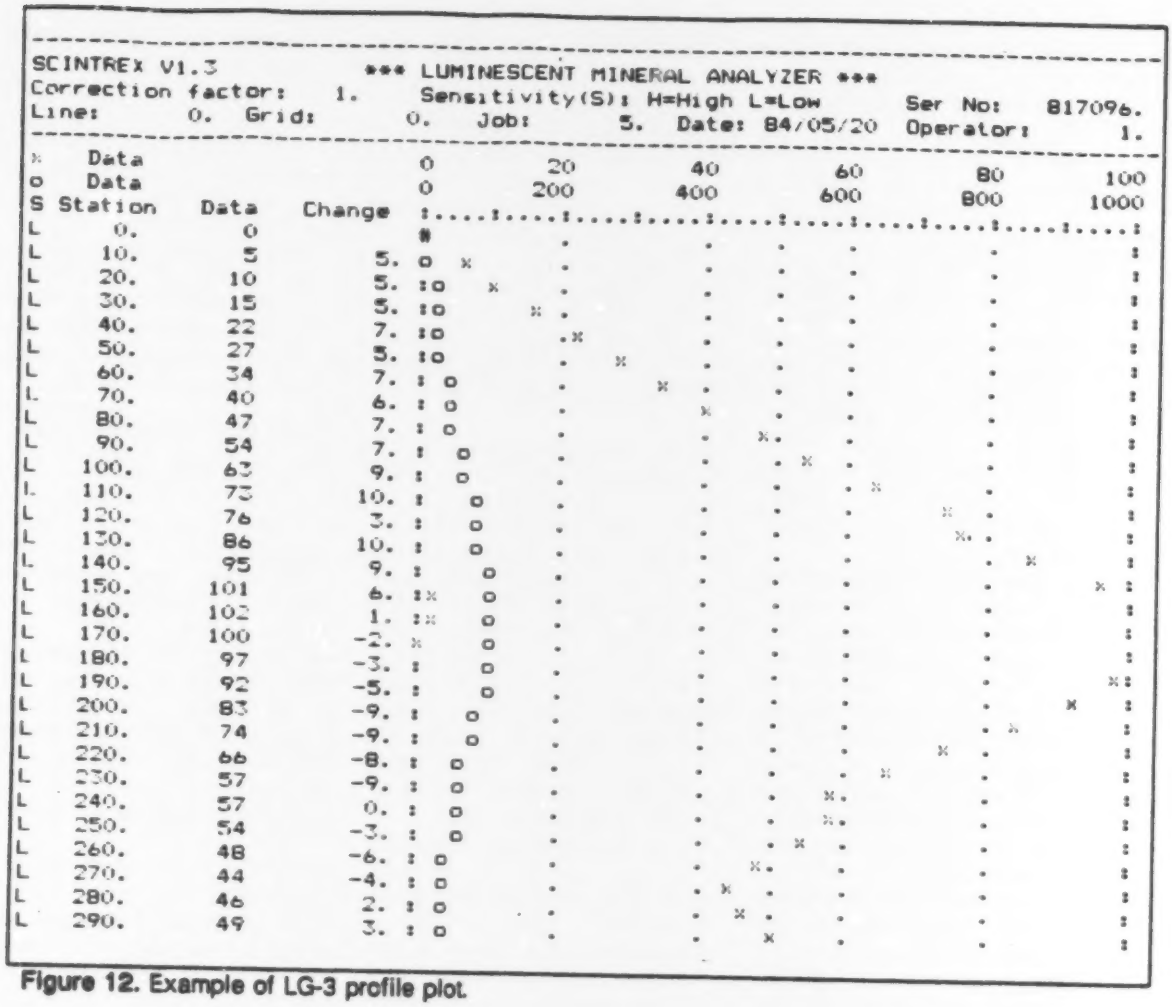

```
SCINTREX V1.3          *** LUMINESCENT MINERAL ANALYZER ***
Correction factor:  1.     Sensitivity(S): H=High L=Low      Ser No:   817096.
Line:       0.  Grid:      0.   Job:       5.  Date: 84/05/20 Operator:      1.
```

	Data			0	20	40	60	80	100
o	Data			0	200	400	600	800	1000
S	Station	Data	Change	:....:....:....:....:....:....:....:....:....:....:					
L	0.	0		#					
L	10.	5	5.	o x					
L	20.	10	5.	:o x					
L	30.	15	5.	:o x					
L	40.	22	7.	:o .x					
L	50.	27	5.	:o x					
L	60.	34	7.	: o x					
L	70.	40	6.	: o x					
L	80.	47	7.	: o x					
L	90.	54	7.	: o x					
L	100.	63	9.	: o x					
L	110.	73	10.	: o x					
L	120.	76	3.	: o x					
L	130.	86	10.	: o x					
L	140.	95	9.	: o x					
L	150.	101	6.	:x o x					
L	160.	102	1.	:x o x					
L	170.	100	-2.	x o x					
L	180.	97	-3.	: o x					
L	190.	92	-5.	: o x					
L	200.	83	-9.	: o x					
L	210.	74	-9.	: o x					
L	220.	66	-8.	: o x					
L	230.	57	-9.	: o x					
L	240.	57	0.	: o x					
L	250.	54	-3.	: o x					
L	260.	48	-6.	: o x					
L	270.	44	-4.	: o x					
L	280.	46	2.	: o x					
L	290.	49	3.	: o x					

Figure 12. Example of LG-3 profile plot.

entry, any recorded value can be called up on the display. For example, over an anomaly it might be useful to compare values recorded on an adjacent line (borehole number). To do this, the operator enters the adjacent line (borehole number) and station (depth), and depresses a memory key. Instantly, the recalled value appears on the lower line of the display. Once one value is recalled, he can move up or down the line recalling data, station by station, with a single keystroke per station

- a program which allows revision of data. To change information already in the memory, the Edit Mode can be used to change line (borehole number), station (depth), or header data
- upon completion of a measurement, the display program which displays to the user the present and previous data. The newly acquired data value is shown in the upper line of the display, while the value for the previous station (depth) is shown in the bottom line. This allows the operator to compare values, an important consideration in maintaining data quality
- a program which accepts operator entered header information, which is entered at the beginning of the survey. These are as follows: (1) instrument serial number, (2) grid number, (3) job number, (4) date, and (5) operator code. This program will also repeat header information, at the beginning of the data list or profile for each line, when data are output. This ensures that all data are properly and unambiguously labelled
- the display of the percentage of free memory at any time, after 2 keystrokes. The file memory control program ensures fail-safe operation. The memory can only be erased by a series of keystrokes which would be virtually impossible to duplicate accidentally
- the output programs which provide flexible data dumps to many peripheral devices, using the RS-232C port. The program accepts various user-selected baud rates and "carriage return delays". The output programs service digital printers (to print data as listings or as profile plots), magnetic recording media (to archive safely the acquired data), computers (for further processing), etc.
- the formatting programs which provide in-field printing of data listings or profile plots. When pseudo-analog profiles are output onto a printer, any 2 parameters can be selected for simultaneous plot printing. One of five full scales can be either zero centred or have their zero at the left-hand side of the space allotted to the profile. In the profile displays, the actual station numbers (depth) and data values are also printed numerically
- the display programs which have also provision for alarm messages to ensure data quality. Improper measurement conditions are reported to the user by displaying a warning on the LCD display
- display programs which also allow the instrument to "speak" a number of languages, provided they use latin characters. The standard instrument is provided with the capability of displaying messages in either English or French, at the choice of the operator. If another language is required, this can be programmed easily, in conjunction with English.

STATUS AT THE END OF FISCAL YEAR 1983–1984

Prototype borehole probe, cable, and fluorescence signal processing board were completed, assembled, and individually tested. Development of borehole LMA control software was completed. The system elements were assembled in an IGS-2 card cage and brought into operation. System integration of software and hardware was completed successfully, producing a function testbed.

Redesign of some of the detailing in the probe to improve mechanical strength and integrity was under way and a new probe is being constructed.

FUTURE PLANS

One of the key tasks remaining is the fabrication of mechanical parts suitable for a field-worthy prototytpe of the borehole probe. These parts will hold the optical system and the electronics housed in the probe. Circuit boards are also to be made and tested. When the prototype of the completed instrument is operational, bench tests and later on, field tests, are to be carried out in cooperation with Canada Tungsten Mine Limited and the Geological Survey

of Canada (Pat Kileen). It is anticipated that these field tests will take place in the summer of 1984. On the basis of feedback from the users, some changes may be made to the present design in order to arrive at a "production" prototype. The manufacture and sale of production LG-3's will ensue thereafter, based on market demand.

REFERENCES

Bertoni, C.H.
1983: Gold Production in the Superior Province of the Canadian Shield; Canadian Institute of Mining and Metallurgy, Bulletin 76, Number 857, p.62-64.

Boyle, R.
1979: The Geochemistry of Gold and its Deposits; Geological Survey of Canada, Bulletin 280, p.155-157, 195-196.

Eardley-Wilmot, V.L.
1942: Tungsten: Canadian and World Situation; Canadian Institute of Mining and Metallurgy, Transactions, Volume 45, p.437-454.

Foster, R.P.
1977: Solubility of Scheelite in Hydrothermal Chloride Solutions; Chemical Geology, Volume 20, p.27-43.

Little, H.W.
1959: Tungsten Deposits of Canada; Geological Survey of Canada, Economic Geology Series Number 17, p.250.

Seigel, H.O., and Robbins, J.C.
1982: Luminex: New Scintrex Development — Valuable Tool in Search for Minerals; The Northern Miner, Volume 68, Number 38, p.C4-C5.

1983: Exploring with Luminex; Mining Engineering, Volume 35, Number 7, p.729-732.

Seigel, H.O., Johnson, I., and Hennessy, J.
1984: Different Methodology: Geophysical Aids to Gold Exploration; The Northern Miner, Volume 69, Number 52, p.B17-B18.

Grant 068 Isotope Ratios and Trace Elements in Gold and Base Metal Occurrences in Ontario: An Application of Plasma/Mass Spectrometry

E.J. Brooker

X-Ray Assay Laboratories Limited, Don Mills

ABSTRACT

The appiication of stable isotope data to geochemistry and the significance of lead isotope data to o're genesis is considered. A suite of 10 lead bearing samples from various well known deposits was analyzed for lead isotope concentrations. National Bureau of Standards (NBS) standard 981 was used for reference purposes. These data were applied to a trilinear plot after Cannon *et al.* (1961, 1971). Instrumentation used in this project was the recently developed ELAN 250 plasma/mass spectrometer (SCIEX Laboratories, Thornhill, Ontario.) Data obtained with this instrument are compared with values obtained by a conventional mass spectrometer. Precision and standard deviation of the measurements on solutions prepared from 20 mg samples is given. Performance appears adequate for most geochemical and ore genesis applications.

INTRODUCTION

The application of stable isotope data to mineral exploration is not new. Cannon *et al.* (1961), and Doe and Stacey (1974) have long advocated lead isotope ratios as a means of identifying potential massive sulphide deposits. More recently a number of authors have applied stable isotopes to geochemistry. Most notable among these are J. Franklin at the Geological Survey of Canada and B.L. Gulson at the Commonwealth Scientific and Industrial Research Organization, Australia. One of the factors which has inhibited the growth of this technology has been the high cost of stable isotope analysis. Recently a new instrument has been developed which may revolutionize analytical chemistry. Although the impact of this instrumentation on elemental analysis is yet to be established, the impact on stable isotope analysis is assured. This new instrumentation, the plasma/mass spectrometer (P/MS), is the result of the marriage of an inductively coupled plasma torch with a high resolution quadrupole mass spectrometer. The majority of the development work on this instrument has been done in Ontario at SCIEX Laboratories in Thornhill.

Although the precision of the P/MS is not of as high a quality as that obtained with conventional mass spectrometers, it does provide suitable precision for most geological applications of lead isotopes and is more than adequate for screening the large number of samples required to assess the suitability of this method.

The objectives of this research are to apply the newly developed plasma/mass spectrometer to the determination of lead isotope ratios around gold and base metal deposits in Ontario and to evaluate these data with respect to typing deposits in such a way as to enhance the search for new deposits.

GEOLOGICAL SIGNIFICANCE OF LEAD ISOTOPES

To assist those unfamiliar with this subject, lead isotope variations will be reviewed briefly. Lead has 4 isotopes (^{204}Pb, ^{206}Pb, ^{207}Pb, and ^{208}Pb). At the time of the formation of the earth it is assumed that there existed a fixed ratio of these 4 isotopes. This primeval lead isotope ratio is usually considered to be similar to that found in the troilite phase of meteorites (Franklin *et al.* 1983). A present day lead isotope ratio has evolved from an initial lead isotope ratio plus additions of radiogenic lead from the radioactive decay of ^{238}U to ^{206}Pb, ^{235}U to ^{207}Pb, and ^{232}Th to ^{208}Pb. These 3 isotopes referred to as radiogenic lead accumulate at different rates due to the different half-life of each parent and the relative abundance of each parent. The absolute abundance of ^{204}Pb has apparently remained constant since it has no known radioactive parent.

Each sample will have a set of lead isotope ratios related to: the original uranium, thorium, and lead abundance; to the time that has passed since the orebody was first formed; and to any remobilization and metamorphism which may have occurred. For a more detailed discussion *see* Doe (1971). Lead isotope ratio data are generally interpreted by viewing the interrelationship of various isotopic ratios and particular lead evolution model curves.

Lead evolution models are principally based on data from conformable volcanogenic massive sulphide deposits which are assumed to have evolved by a "single stage" process. Such models assume that the

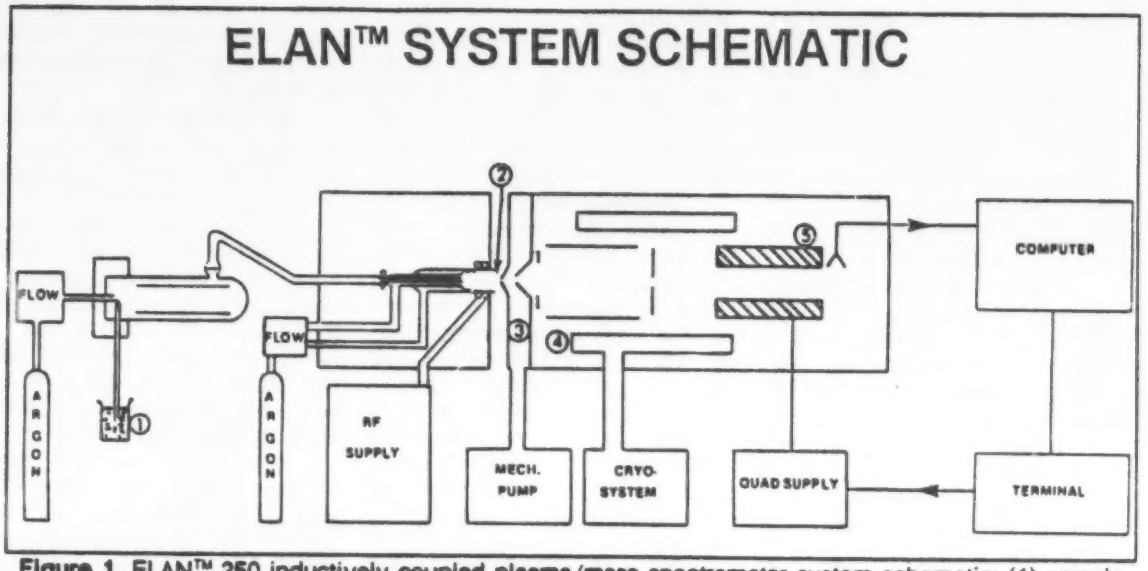

Figure 1. ELAN™ 250 inductively coupled plasma/mass spectrometer system schematic: (1) sample solution, (2) inductively coupled plasma, (3) differentially pumped interface, (4) helium cryopump, (5) quadrupole rods.

relative proportions of uranium, thorium, and primeval lead are unchanged, except through the generation of radiogenic lead by radioactive decay between the starting time and the time of separation of the sample from its source. Although lead data in many deposits plot on or near single stage growth curves, lead data from some deposits plot far off such curves. Such samples are termed anomalous and interpretation of their histories requires multistage models.

Cannon *et al.* (1961, 1971) suggested an interesting way to compare lead isotope ratios by presenting the data in terms of $^{206}Pb + {}^{207}Pb + {}^{208}Pb = 100$, on trilinear coordinate graphs. This approach differs from others in that ^{204}Pb is not used as a reference value to which the other lead isotopes are compared. A prime advantage of this approach is the elimination of the uncertainty associated with the measurement of the rather small quantity of ^{204}Pb typically found in any assemblage. Figure 3 is an example of a trilinear plot. As with previous models a growth curve for "single stage" leads can be plotted using trilinear coordinates. Cannon *et al.* (1961, 1971) divided the whole lead field into 4 sectors by joining the 0 isochron of the growth curve to pure thorium-lead and to pure uranium-lead being formed today. As previously noted, a majority of data plot on or near the growth curve defining a narrow crescent sector. The other 3 sectors are associated with anomalous data and have been defined as, (1) U-lead, (2) Th-lead, (3) J-lead (Joplin, Missouri type).

INSTRUMENTATION

A prototype model of the newly developed ELAN 250 inductively coupled plasma/mass spectrometer (SCIEX, Thornhill) was used throughout this study. A schematic of the instrument is shown in Figure 1. A more detailed instrument description can be found elsewhere (Douglas *et al.* 1983; Douglas and Quan 1983). This instrument combines an inductively coupled argon plasma (ICP) as an ion source, with a quadrupole mass spectrometer. A sample solution is nebulized into the ICP and the metal ions are extracted from the plasma gas into the mass spectrometer. The interfacing arrangement between the plasma and the mass spectrometer is similar to that reported by Gray and Date (1983) but differs in some important details which provide some operational benefits. For example, the

sampling orifice lifetime is many months (c.f. 30 hours reported by Gray and Date (1983)), doubly charged ions, which are a potential source of spectral interference, are present at much lower levels, and no ions characteristic of the orifice material (Ni) appear in the mass spectrum.

This configuration immediately provides the analyst with the capability of determining isotopic concentrations with the same ease with which he has become accustomed to carrying out elemental analyses. In fact, any elemental analyses done on this instrument are in essence isotopic analyses. Low detection limits (0.1 to 1 ng/ml) and a wide dynamic range (5 to 6 orders of magnitude) are possible, as might be expected of any instrument using an ion counter for spectral measurement. Date and Gray (1983a) have also reported the use of an ICP/mass spectrometer system for the determination of lead isotope ratios. A precision of about ±0.5% was found, but the plasma sampling arrangement used was reported to have severe limitations. An improved sampling arrangement was later reported by these authors (Date and Gray 1983b) and a recent review of ICP/mass spectrometry has appeared (Date 1983).

EXPERIMENTAL PROCEDURES

About 20 mg of sample was weighed into a beaker. Ten millilitres of reagent grade hydrochloric acid was added, and the sample was refluxed for half an hour. Five millilitres of nitric acid were added, and the sample was heated to complete dissolution. The sample was cooled and diluted to 100 ml with distilled water. An aliquot of solution (20 ml) was diluted by a factor of 5 for measurement of the lead isotopes. The undiluted solution was used to determine the trace element spectra on 2 samples.

The lead isotope data were produced by repeated peak hopping between ^{204}Pb, ^{206}Pb, ^{207}Pb, and ^{208}Pb using a dwell time of 2 seconds per isotope and a total measurement time of 10 minutes per sample. A total of 300 isotope measurements were obtained on each sample. After collecting the data on a computer storage disc, each set of measurements was divided into 7 blocks of 40 measurements each. Within each block the average count rate of each isotope was calculated and the isotope ratios determined. The individual ratios of each block were then averaged and the standard deviation calculated. The uncertainties of Table 1 are one standard deviation (not the standard deviation of the mean). Approximately 1 to 2 mg of lead were required per sample.

Trace element spectra were obtained by scanning the mass spectrometer between masses 42 and 80 atomic mass units (AMU). The tie per scan and number of points per scan are variable. The data are available in log or linear format. In this paper all spectra are presented using linear format.

RESULTS AND DISCUSSION

A typical lead isotope spectra (Geological Survey of Canada -galena TQ65-14) produced by the ELAN 250 plasma/mass spectrometer is shown in Figure 2. The lead isotopes are well resolved. Tailing to another of lower mass is less than 1 part in 10^5 requiring negligible correction for the precision and accuracy reported here.

Accumulated lead isotope data on the entire suite of samples are tabulated in Table 1. National Bureau of Standards (NBS) lead isotopic standard 981 was used as a reference. A comparison between the ELAN 250 results and NBS 981 certified values shows agreement with certified values to be within ±2% in the worst case and is typically ±1% without correction.

Agreement between data produced with the ELAN 250 and data supplied by the Geological Survey of Canada (GSC) varies from moderate ($^{206}Pb/^{204}Pb$, $^{207}Pb/^{204}Pb$, $^{208}Pb/^{204}Pb$) to good ($^{207}Pb/^{206}Pb$, $^{208}Pb/^{206}Pb$). The Geological Survey of Canada results were obtained in the early 1960s using thermal ionization mass spectrometry. The advantage in using ^{204}Pb as a benchmark is offset by the uncertainty associated with measuring the small ^{204}Pb peak.

No isotope values were available for the Royal Ontario Museum samples. Values appearing in the literature for deposits from which these samples were taken are given where available. In summary it can be concluded that lead isotope ratios of moderate accuracy and precision are attainable by plasma/mass spectrometry and that sample throughput rates are vastly improved. It should also be noted that these results were obtained on the prototype model of the ELAN 250.

The uncertainties of Table 1 derive mainly from ICP flicker noise and ICP fluctuations caused by the nebuliser. Sufficient counts were collect-

TABLE 1: LEAD ISOTOPE RATIOS ON LEAD SAMPLES BY PLASMA/MASS SPECTROMETRY

SAMPLE NUMBER	SAMPLE LOCATION		206/204	207/204	208/204	207/206	208/206
NRS 981	National Bureau of Standards, U.S.A.	a)	16.98±0.60	15.81±0.38	36.63±0.86	0.9311±0.013	2.157±0.032
		b)	16.94	15.49	36.73	0.9146	2.168
			(0.2%)	(2.0%)	(-0.25%)	(1.8%)	(-0.5%)
SP-1392*	George L., Canada	a)	16.90±0.56	15.79±0.78	35.43±1.65	0.9343±0.014	2.096±0.031
		c)	16.51	15.53	36.06	0.9409	2.184
TQ65-14*	Echo Bay, Canada	a)	20.19±0.36	15.62±0.37	37.01±1.09	0.7737±0.012	1.830±0.027
		c)	20.35	15.85	39.74	0.7791	1.940
SP-706*	Brunswick #6, Canada	a)	19.05±0.88	16.32±0.57	39.95±1.54	0.8567±0.013	2.097±0.032
		c)	18.28	15.66	38.22	0.8593	2.091
RFA84-417*	Kerr Addison, Canada	a)	14.64±0.75	15.95±0.72	36.20±1.85	1.089±0.016	2.473±0.037
		c)	13.69	14.69	33.53	1.073	2.449
TQ70-150*	Detroit Algoma, Canada	a)	25.36±0.71	17.30±0.51	38.33±1.68	0.6822±0.010	1.511±0.015
		c)	25.82	17.32	40.31	0.6710	1.561
M22498**	Sadon, N. Caucasus U.S.S.R.	a)	18.63±0.26	15.74±0.31	38.34±0.77	0.8450±0.011	2.058±0.030
M27901**	Nigadoo R. Mines Bathurst, N.B.,Can.	a)	18.34±0.27	15.59±0.31	37.85±0.76	0.8501±0.009	2.064±0.031
		d)	18.20	15.65	38.11	0.8600	2.094
M14679**	Worthington Mine, Sudbury, Can.	a)	26.37±0.37	16.89±0.35	51.63±1.03	0.6405 ±0.008	1.958±0.029
M14093**	Secondary S. Mine Broken Hill, Aust.	a)	16.19±0.23	15.56±0.28	35.99±0.68	0.9610±0.013	2.223±0.033
		e)	16.98	15.37	35.56	0.9616	2.225
M32209**	Pine Point Mine, N.W.T , Canada	a)	16.67±0.28	16.31±0.31	40.50±0.80	0.8645 ±0.015	2.146±0.032

* Samples courtesy of Geological Survey of Canada, Ottawa, Ontario, Canada.
** Samples courtesy of Royal Ontario Museum, Toronto, Ontario, Canada.
a) Values obtained with the ELAN 250 (ICP/MS).
b) NBS certified values.
c) Values supplied by Geological Survey of Canada.
d) B.R. Doe and J.S. Stacey (1974).
e) B.L. Gulson and K.J. Mizon (1979).
Value between brackets is percent difference.

ed to give a relative standard deviation of 0.2 to 0.3%, substantially less than those of Table 1. Since this initial work the stability of the plasma has been improved somewhat. The sensitivity has also been improved (by about 10 times). This suggests better precision will be possible in the future.

The problem of obtaining accurate ^{204}Pb results prompted Cannon *et al.* (1961, 1971) to use only the ^{206}Pb, ^{207}Pb, and ^{208}Pb isotopes. As discussed earlier, these isotopes were normalized to 100% and plotted on trilinear plots (Figure 3). Plotting 1200 analyses of lead materials documented in the literature enabled Cannon *et al.* (1971) to draw the following conclusions:

> The discovery of typical U-lead in galena from a mineral prospect implies a very high probability that this particular galena is associated with uranium mineralization. Other...types include the...J-lead that is typical of the major lead districts of the Mississippi Valley...ordinary (normal) lead of about zero model age may convey little information about the mineral occurrence—except that the deposit almost certainly is of Phanerozoic age. Another variety of ordinary lead, with model age about 1,600 m.y., is a favourable omen in the search for major sulphide deposits—lead, zinc, copper or nickel—in Precambrian rocks...On the other hand a galena containing ordinary lead with a model age about 2,850 m.y. should interest the gold hunter—because such leads are found almost exclusively in gold mines in very old Precambrian rocks.

The Geological Survey of Canada and Royal Ontario Museum samples in Table 1 have also been plotted using trilinear coordinates (Figure 3). The single stage growth curve used in this trilinear plot is adapted from Doe and Stacey (1974). The samples plot much as would be expected, based on the conclusions of Cannon *et al.* (1971). The Kerr Addison galena is from a gold deposit and plots on the growth curve

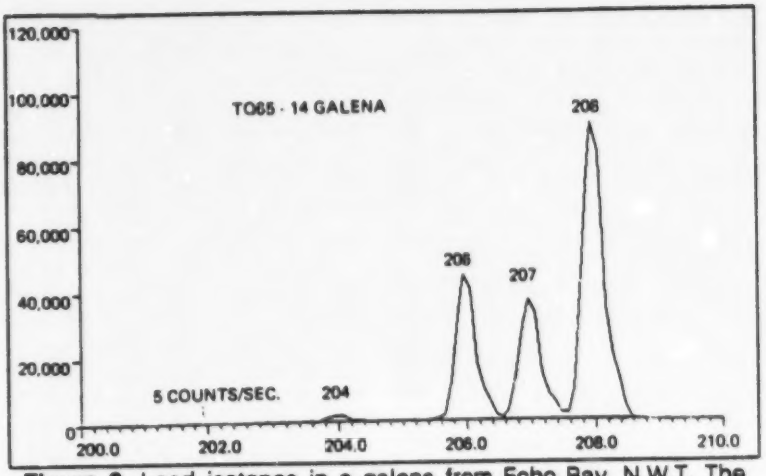

Figure 2. Lead isotopes in a galena from Echo Bay, N.W.T. The plasma/mass spectrometer was scanned from mass 200 to 210.

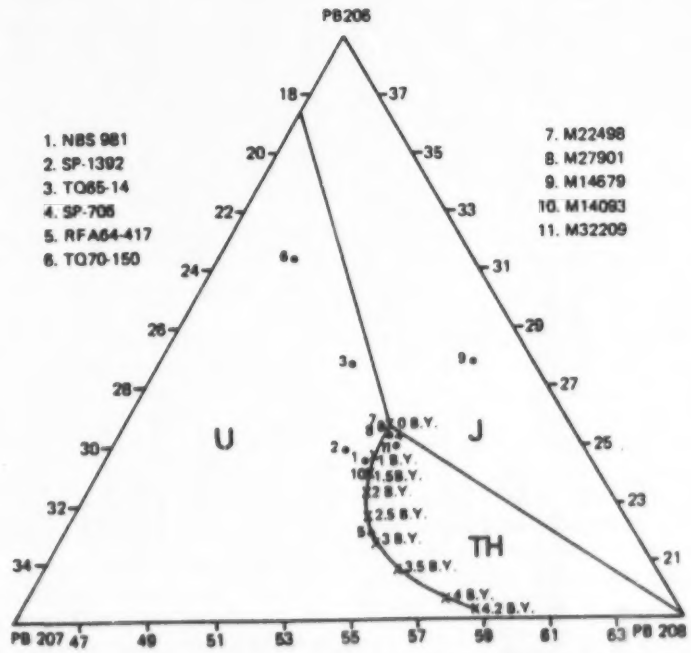

Figure 3. A trilinear plot of lead samples in Table 1 (after Cannon *et al.* 1961). The growth curve is adapted from Doe and Stacey 1974.

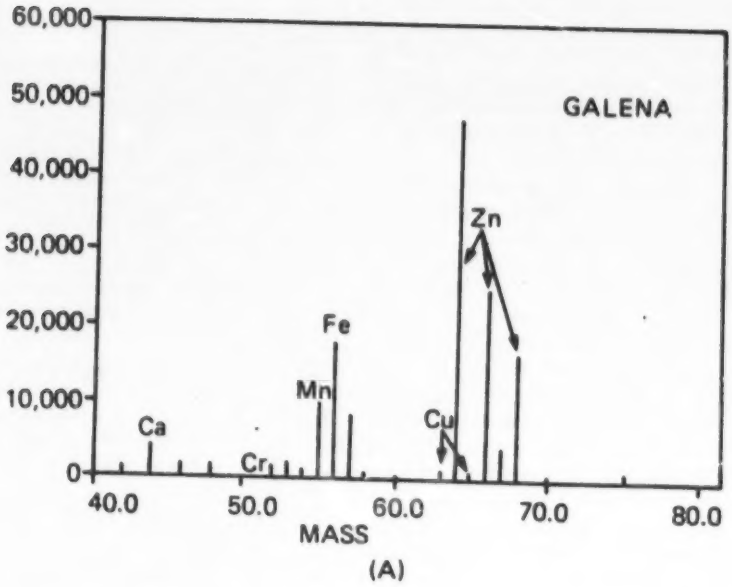

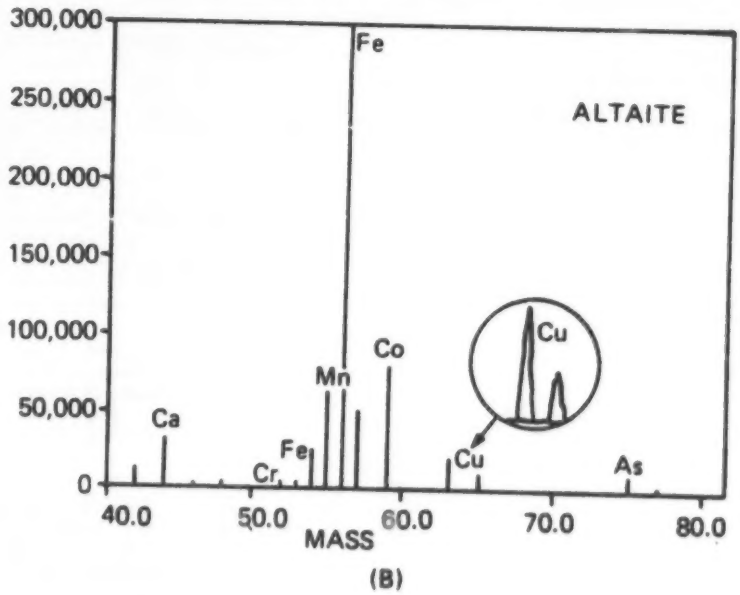

Figure 4a. Trace element scan of a galena (Echo Bay, N.W.T.) on the plasma/mass spectrometer from mass 42 to 80. Results are blank subtracted.

Figure 4b. Trace element scan of an altaite (Mattagami, Quebec) on the plasma/mass spectrometer from mass 42 to 80. Results are blank subtracted.

at approximately 2.8 b.y. The Broken Hill galena plots on the curve at approximately 1.5 b.y. The Bathurst, New Brunswick, galenas plot near 0 b.y. as would be expected, and the Echo Bay and Detroit-Algoma vein galenas plot in the U-lead area of the diagram suggesting a uranium-rich source rock for these samples. Interpretation of the other samples is more difficult and will not be attempted here. Thus, plotting of our isotope data using trilinear coordinates supports the findings of Cannon *et al.* (1971) that useful genetic information can be obtained with trilinear plots.

Heavy metal isotopes are not known to fractionate as do stable light isotopes and they hold their isotopic signature throughout most physicochemical processes. Thus, the lead isotope signature can be recognized in the ore body itself or in the lead dispersed in surrounding rocks, soil, plants, or water (CSIRO 1981). Lead isotopes associated with economical massive sulphide deposits tend to have lead isotope ratios that are uniform, and plot on or near growth curves. Those associated with barren or subeconomical mineralization tend to be nonuniform, and plot off growth curves (Gulson and Mizon 1979). A consequence of this is that few lead isotope ratios are needed to evaluate economical and noneconomical stratiform massive sulphide mineralization. As more lead isotopic data become available the ability to predict promising and unpromising isotope ratios for an area will improve. Statistical treatment at the moment is hampered by over-representation of economical deposits.

Trace element data are available simultaneously with

isotopic data on the plasma/mass spectrometer. The trace element contents of a galena from Echo Bay, Northwest Territories, and an altaite from Mattagami, Quebec, over the mass range of 40 to 80 AMU are shown in Figure 4. The galena (Figure 4a) shows the trace elements Ca, Cr, Mn, Fe, Cu, and Zn, with Zn being predominant. The altaite (Figure 4b) shows the trace elements Ca, Cr, Fe, Mn, Co, Cu, and As, with Fe and Co being predominant.

The availability of both isotopic and trace element data enhances the concept of fingerprinting mineral deposits and improves the chances of finding new economical mineralization. For example, Franklin *et al.* (1983) found that intrusive-related and conformable gold deposits can be effectively discriminated in the Canadian Shield, because the former have younger, commonly anomalous, model ages and high $^{238}U/^{204}Pb$ values, relative to the latter.

The discussion here has centred on the analysis of mineral separates but the technique could, in principle, be extended to the analysis of lead in rocks provided that the lead was present in a sufficiently high concentration (>10 ppm per given current instrument sensitivity). Such data may show up subtle local differences between economical and noneconomical mineralization which may not be significant on a regional scale. They may also highlight unusual geological processes that have taken place and signify different mineralization and possibly new economical mineral assemblages.

Another area of geochemistry in which P/MS will have an immediate impact is the analysis of rare earth elements. The mass spectra of a sample containing rare earth elements has at least 1 interference-free isotope line for each element in the rare earth group. One of the major problems in rare earth analysis has been spectral interferences from other rare earths or from the matrix. The introduction of a method without spectral interferences will result in a reliable analytical package for the entire rare earth group.

ACKNOWLEDGMENTS

We thank J.M. Franklin and R. Thorpe of the Geological Survey of Canada, and J.A. Mondarino of the Royal Ontario Museum for supplying the galena samples used in this study.

REFERENCES

Cannon, R.S., Jr., Pierce, A.P., and Antweiler, J.C.
1971: Suggested Uses of Lead Isotopes in Exploration; p.457-463 *in* Geochemical Exploration, edited by R.W. Boyle and J.I. McGerrigle, Canadian Institute of Mining and Metallurgy, Special Volume 11.

Cannon, R.S., Jr., Pierce, A.P., Antweiler, J.C., and Buck, K.J.
1961: The Data of Lead Isotope Geology Related to Problems of Ore Genesis; Economic Geology, Volume 56, p.1-38.

CSIRO
1981: Lead Isotope Signatures for Mineral Exploration; Australian Mining, August, p.25-31.

Date, A.R.
1983: An Introduction to Inductively Coupled Plasma Source Mass Spectrometry; Trends in Analytical Chemistry, Volume 2, p.225-230.

Date, A.R., and Gray, A.L.
1983a: Progress in Plasma Source Mass Spectrometry; Spectrochemica Acta, Volume 38B, Numbers 1/2, p.29-37.
1983b: Isotope Ratio Measurements on Solution Samples Using a Plasma Ion Source; International Journal of Mass Spectrometry and Ion Physics, Volume 48, p.357-360.

Doe, B.R.
1971: Lead Isotopes: Springer Verlag, New York, 137p.

Doe, B.R., and Stacey, J.
1974: The Application of Lead Isotopes to the Problem of Ore Genesis and Ore Prospect Evaluation: A Review; Economic Geology, Volume 69, p.757-776.

Douglas, D.J., and Quan, E.S.K.
1983: Paper 402; 1983 Pittsburgh Conference, Atlantic City, N.J., U.S.A.

Douglas, D.J., Quan, E.S.K., and Smith, R.G.
1983: Elemental Analysis with an Atmospheric Pressure Plasma (MIP, ICP)/Quadrupole Mass Spectrometer System; Spectrochimica Acta, Volume 38B, Numbers 1/2, p.39-48.

Franklin, J.M., Roscoe, S.M., Loveridge, W.D., and Sangster, D.F.
1983: Lead Isotope Studies in Superior and Southern Provinces; Geological Survey of Canada, Bulletin 351, p.60.

Gray, A.L., and Date, A.R.
1983: Inductively Coupled Plasma Mass Spectrometry Using Continuum Flow Ion Extraction; Analyst, Volume 108, p.1033-1050.

Gulson, B.L., and Mizon, K.J.
1979: Lead Isotopes as a Tool for Gossan Assessment in Base Metal Exploration; Journal of Geochemical Explorations, Volume 11, p.299-320.

Grant 072 Microprocessor-based Digital Receiver Console for the DIGHEM$^{III/IV}$ Helicopter Airborne Electromagnetic System

S.J. Kilty

Dighem Limited, Toronto

ABSTRACT

On December 1, 1983, Dighem Limited began the development of a digital receiver console. The basic premise behind the receiver was that high speed sampling, filtering, and stacking of incoming electromagnetic data would significantly improve the overall resolution of the DIGHEM$^{III/IV}$ system. The high speed sampling and filtering should result in a significant increase in the signal-to-noise ratios. In addition, a system using microprocessor-based logic should reduce the amount of manual intervention required during survey operations.

INTRODUCTION

All helicopter-borne electromagnetic (HEM) systems comprise 2 major subsystems, namely the towed sensor and the on-board signal analyzers. The analyzers transform the raw received signal into in-phase and quadrature responses of the secondary field with respect to the primary field.

In 1982, Dighem Limited developed the DIGHEM^{III} multifrequency HEM system with financial assistance from the Exploration Technology Development Fund (ETDF). This project (as described by Kilty (1983)) was predominantly centred around the redesign of the electromagnetic sensor. In December of 1983, Dighem Limited was awarded a seed grant which provided financial aid for the development of a digital receiver console that will replace the present analog signal analyzers. The requirement for a digital receiver design has become necessary because of new applications for HEM systems that require a high degree of accuracy in terms of system calibration and high quality recorded data.

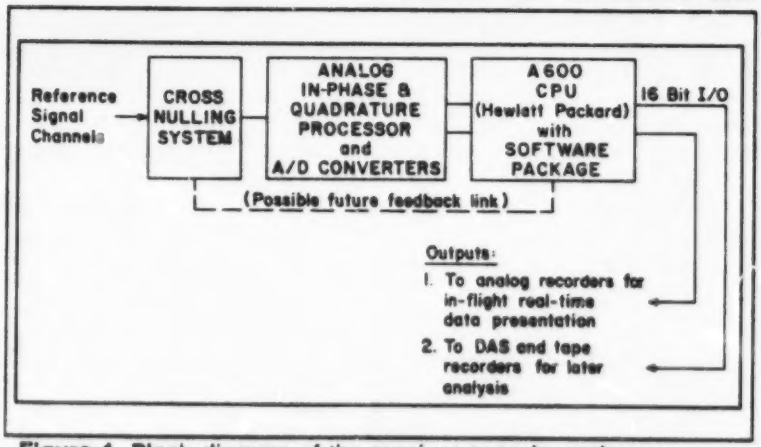
Reference Signal Channels
CROSS NULLING SYSTEM
ANALOG IN-PHASE & QUADRATURE PROCESSOR and A/D CONVERTERS
A600 CPU (Hewlett Packard) with SOFTWARE PACKAGE
16 Bit I/O
(Possible future feedback link)
Outputs:
1. To analog recorders for in-flight real-time data presentation
2. To DAS and tape recorders for later analysis

Figure 1. Block diagram of the receiver console package.

SYSTEM CONCEPT

After considering a number of options for the microprocessor-based receiver console package, the proposed block diagram, as shown in Figure 1, was prepared. The system consists of an analog in-phase and quadrature detection system similar to that which is now in existence. This basic detection unit is followed by a high speed digital processing unit. The digital processing unit, the A600 CPU, will manage all the data manipulation functions of the receiver.

The A600 will receive the raw output of the in-phase and quadrature system in digital form. The processing unit will then make all of the amplitude and phase correction adjustments. In addition, the A600 will be capable of spike-removal and of filtering the data in real-time. The design calls for sampling the output of the analog front end at a 100 Hz sample rate. The data would be processed and filtered, and transmitted to a data acquisition system at a rate of 10 samples per second.

Figure 2 illustrates the general concept of signal processing. The mode of operation of the receiver will be set by buttons or switches on the EM

analog processor front panel. Typical modes of operation will consist of run-stop, phase, calibration, and any other operations which are deemed necessary. The A600 will operate in an endless loop. It will read in the mode of operation as well as the sample data from the analog front-end processor. At this point, a decision is made as to whether this is a run operation or whether it is a calibration and set-up operation.

In a calibration or a phasing operation, the computer would acquire the information about the incoming signal and compute the exact phase error and DC level offsets which are to be applied to the subsequent data. This information will be stored in memory for utilization in the run mode operation. This loop is a selective one in the sense that it runs for as long as the operator desires and integrates the incoming data. In this way, spurious and noisy data can be processed to yield reliable amplitude and phasing corrections. It is also possible to send a signal out of the A600, back down the 16-bit parallel to the analog processor. Such a signal could be used to give a feedback signal to the operator to perform the manual adjustments which will have to be established initially. The setting of the phase detection correction will always be monitored as part of the incoming signal so that any changes made by the operator are recorded.

In run mode operation, the incoming signal will be systematically compared with the previous signal. In this way signal samples which had unacceptable variances with respect to past history data, would be detected. Threshold noise levels will be programmed into the software; any signals exceeding these thresholds would be rejected. The simplest ways to handle this are to either replace an incoming signal with the previous value or to delete it from the stacking. Once the signal coming in has been filtered, it will then be phase-rotated and amplitude-shifted as required. Following the corrections, the resulting data will be stacked until a 0.1 second sampling rate is achieved. The corrected data would then be output to the data acquisition system.

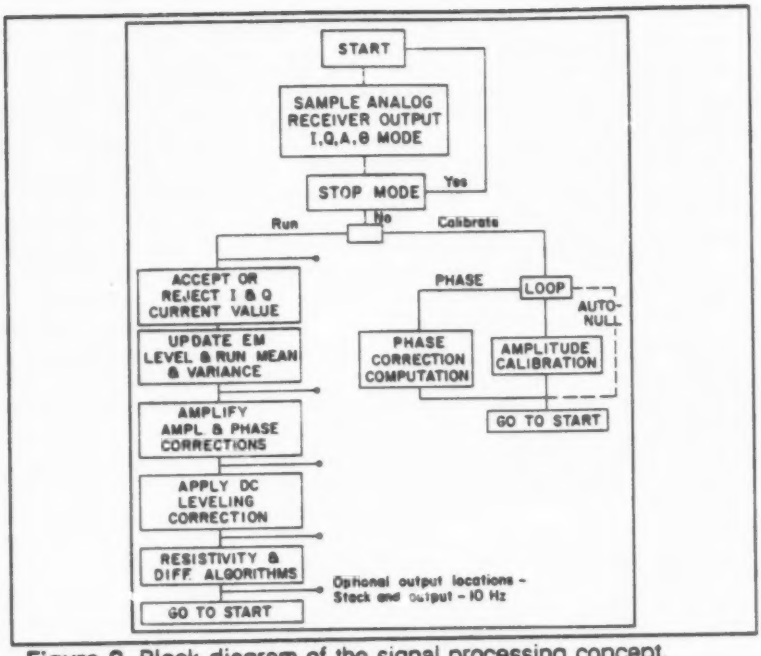

Figure 2. Block diagram of the signal processing concept.

A number of levels of operation will be carried out in the development phase of this receiver. In the early stages of operation, it is anticipated that only the raw sample data would be output to the data acquisition system. The only processing here would be stacking to obtain a 0.1 second sampling rate. As confidence in the receiver develops, various stages of processing could be inserted before the data are output to the data acquisition system. Two types of data can also be sent by the receiver to the data acquisition system; one is raw information, and the other is processed data which could then be displayed by the chart recorder to provide a real-time record. One major advantage to this approach is that by recording the raw in-phase and quadrature plus the reference and the phase setting adjustments, post-flight computer processing can be performed to allow more sophisticated corrections than would be practical for in-flight processing.

HARDWARE DESIGN

The overall architecture of the system utilizes a card set A600 CPU (Figure 3). In addition, all of the input/output (I/O)

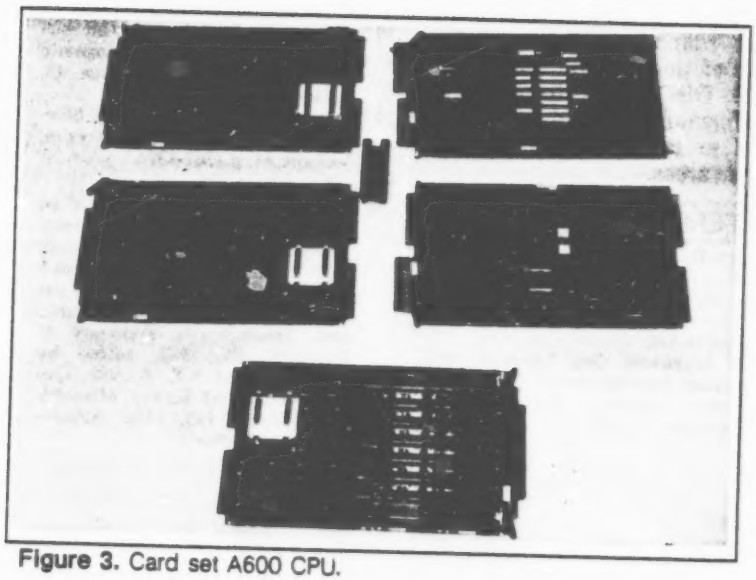

Figure 3. Card set A600 CPU.

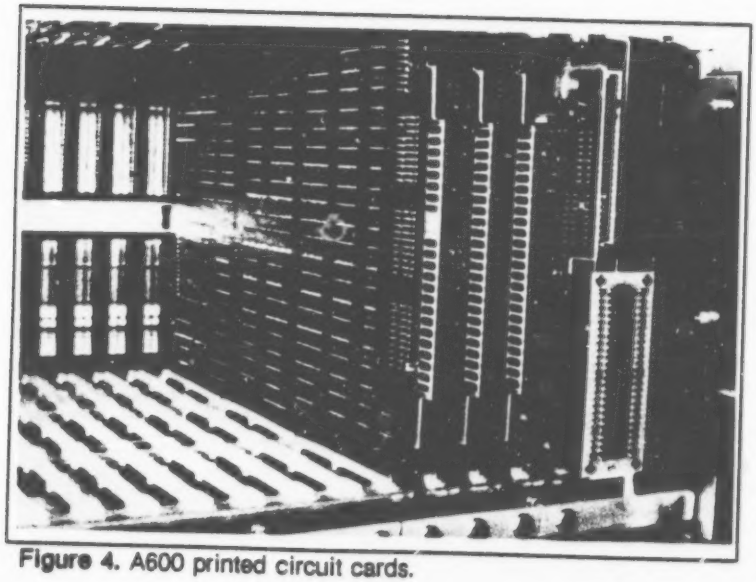

Figure 4. A600 printed circuit cards.

interfaces are standard hardware which is available from Hewlett-Packard. In this manner, the amount of customized hardware is minimized. This is extremely beneficial for field maintenance and maintaining backup spares. The A600 provides an optimum performance instrument for this type of application. It is an extremely robust unit which utilizes small printed circuit cards (Figure 4). Power consumption is reasonably moderate. The unit supports a multitasking real-time operating system which is extremely attractive for such real-time process control operations. The A600 is also a high speed computational machine for its size, weight, and power requirements. Typical computational rates of 50 000 floating point operations per second are achievable with this unit. Upgrading to even higher performance in the future can be achieved by adding a hardware arithmetics card.

FUTURE PLANS AND CONCLUSIONS

Grant 072 was awarded to Dighem Limited for the period of December 1, 1983 to March 31, 1984. During this time period, the overall system structure was defined and the overall design was finalized. All long term delivery items were ordered and detailed hardware design was commenced. Grant 072 was renewed for the period of April 1, 1984 to March 31, 1985. This grant renewal has allowed Dighem to proceed with the construction of both the analog front end and the A600 CPU.

The present time schedule should permit the first testing of the basic hardware and software package in September or October, 1984. The balance of

the time remaining during the period of the grant will be used to "debug" and improve upon both the hardware and software.

The use of digital technology and the application of a software controlled receiver package will allow greater flexibility in terms of system application. Dighem has, in the past, applied HEM technology in such diversified areas as mining, salt water encroachment, location of radio transmitter sites, and geothermal mapping. The introduction of this receiver should enable Dighem to improve its performance in these fields and to perhaps diversify into other areas.

REFERENCES

Fraser, D.C.
1972: A New Multicoil Aerial Electromagnetic Prospecting System; Geophysics. Volume 27, p.518-537.
1973: Magnetite Ore Tonnage Estimates from an Aerial Electromagnetic Survey; Geoexploration, Volume 11, p.97-106.
1978: Resistivity Mapping with an Airborne Multicoil Electromagnetic System; Geophysics. Volume 43, p.144-172.
1979: The Multicoil II Airborne Electromagnetic System; Geophysics. Volume 44, p.1367-1394.

Kilty, S.J.
1983: GR 025 The Development of an Omni-Directional Multi-Frequency Airborne EM System; p.99-103 *in* Exploration Technology Development Program of the Board of Industrial Leadership and Development, Summary of Research 1981-1983, edited by E.G. Pye and R.B. Barlow, Ontario Geological Survey, Miscellaneous Paper 115, 135p. Accompanied by 2 charts.

MAPS NOT

FILMED

CARTES

OMISES